TRAKYA UNIVERSITY
JOURNAL OF NATURAL SCIENCES

26 Volume 2 Number October 2025

TRAKYA UNIVERSITY JOURNAL OF NATURAL SCIENCES

TUJNS

Trakya Univ J Nat Sci
ISSN 2528-9691

Trakya University Journal of Natural Sciences
www.tujns.org
Volume: 26, Number: 2, October 2025

Trakya University Journal of Natural Sciences

Volume: 26 **Number: 2** **October** **2025**

Trakya Univ J Nat Sci

www.tujns.org
e-mail: tujns@trakya.edu.tr

ISSN 2528-9691

ISSN 2528-9691

Trakya University Journal of Natural Sciences
www.tujns.org
Volume: 26, Number: 2, October 2025

Owner
On behalf of Trakya University Rectorship, Graduate School of Natural and Applied Sciences
Doç. Dr. Filiz UMAROĞULLARI

Correspondence Address
Trakya Üniversitesi Fen Bilimleri Enstitüsü Binası, Balkan Yerleşkesi – 22030 Edirne / TÜRKİYE
e-mail: tujns@trakya.edu.tr
Tel: +90 284 2358230
Fax: +90 284 2358237

This journal is a peer-reviewed publication and is indexed in Biological Sciences, BIOSIS Previews, CAB Abstracts, DOAJ (Directory of Open Access Journals), ESCI (Emerging Sources Citation Index), Scopus, TÜBİTAK-ULAKBİM Life Sciences Database (Turkish Journal Index), and Zoological Record.

Publisher: www.galenos.com.tr • Publisher Certificate Number: 14521

TRAKYA UNIVERSITY JOURNAL OF NATURAL SCIENCES

Volume: 26 Number: 2 October 2025

REVIEWER LIST

ISSN 2528-9691

Trakya University Journal of Natural Sciences
www.tujns.org
Volume: 26, Number: 2, October 2025

Contents

Editorial

Research Article

Trakya University Journal of Natural Sciences, 26(2), 103–105, 2025
DOI: 10.23902/trkjnat.7102025
www.tujns.org

Editorial

Is ethology a neglected field within the scientific community in Türkiye?

Volkan Aksoy[1,2]

[1]*Trakya University, Faculty of Sciences, Department of Biology, Edirne, Türkiye*
[2]*Associate Editor, Trakya University Journal of Natural Sciences*

Cite this article as: Aksoy, V. (2025). Is ethology a neglected field within the scientific community in Türkiye? *Trakya University Journal of Natural Sciences, 26*(2), 103–105. https://doi.org/10.23902/trkjnat.7102025

The term "ethology," the scientific study of animal behavior, was coined by the French zoologist Isidore Geoffroy Saint-Hilaire in the nineteenth century, based on *ethos* meaning "character" and *logia* meaning "the study of," both from the Greek (Jaynes, 1969). The popularization of the term was propagated by the American myrmecologist Wheeler in 1902 (see Sleigh, 2007). The European school of ethology found its roots, in addition to other contributors, largely with Nikolaas Tinbergen (1907–1988), Konrad Lorenz (1903–1989), and Karl von Frisch (1886–1982), who was awarded the Nobel Prize for Physiology or Medicine in 1973. This event was a milestone for other later researchers who were greatly motivated by it, and data on different aspects of animal behavior on a wide variety of taxa started to accumulate with their studies. Readers are kindly asked to follow Fericean et al. (2015) for a plain and clear history of ethology in general and Taborsky (2010) for ethology in Europe in particular.

It is widely known that scientists who immigrated to Türkiye from Germany in the 1930s influenced the scientific advancement of the country with their contributions to the structuring of universities, providing new books or translations of existing ones, implementing new techniques, and contributing scientific journals (Ertan, 2016; Namal, 2012). I have no data to present the specific weight of any discipline relative to others in a temporal or spatial pattern throughout the country for the last century, but I wish to address the current state of ethology in Türkiye as a researcher in this field. The study by Gunay et al. (2013) provides important data about the progress of some basic science disciplines in Turkish universities for the period from 2007 to 2013. Among these, and in the same fluctuating manner as others, the number of active biology departments was 81 in 2007, reached 131 in 2010, but followed a gradual decline to 53 in 2013. This dramatic decrease also implies a decrease in the number of students placed in these departments across the country. This small-scale data set led me to conclude logically that, if we accept all graduates as potential researcher candidates, then we lose almost half of our future generation of researchers from the global scientific community. This makes sense not only for figures playing active roles in scientific development in Türkiye but also for me, as an ethologist, with my ongoing concern about the current state and future of the field in the country. The field of animal behavior is currently introduced to university students mostly in the biology departments and veterinary faculties of some state and foundation universities under courses with different names, such as Animal Behavior, Behavioral Biology, and Animal Behavior and Welfare. At this point, despite the abovementioned decreasing trends, we still have the option to guide junior researchers, as potential seniors of the future, to specializefor ethology. However, the current available data gives, at least for me, a feeling of pessimism. A quick search in the database of Web of Science (WOS) covering the period from 1900 to 2025 with the search terms "ethology" in all fields and "Türkiye" in the address field revealed 25 published items that included the term "ethology" at least once within the body text.

E-mail: *volkanaksoy@trakya.edu.tr*

The number was 44 when the search term was "animal behavior"[1] for the same period. There are other platforms in addition to WOS, which will increase these numbers via studies published in various journals, books, etc. that they indexed, but I am sure, based on my personal experience for the last 25 years in the field that, although studies in the field are more than I presented here, ethology is still in its infancy compared to other fields. Several explanations may be put forward for this disquieting picture, all of which will be speculation if they are included here to draw the reader's attention. I underline here the results of the influential study of Bueno-Guerra (2021), who analyzed the current state of ethology from the researchers' perspective using a questionnaire to gather data about discipline names and concepts, species, Umwelt, technology, data, networking, and the impact of sociocultural and ecological factors. The researchers completing the questionnaire represented ($n = 98$) different continents, educational backgrounds, age groups, professions, and target organisms. It is possible to discuss the data obtained individually, but some important points seem to arise, which can also be applied to the field of ethology in Türkiye. One important outcome is that there is still no consensus on a denomination for the discipline, since the answers obtained from the participants when asked for the discipline name were, in descending order, animal behavior, animal cognition, comparative psychology, primatology, and behavioral ecology. The level of consensus about theoretical concepts was highest for the theory of evolution, followed by Tinbergen's questions, associative learning, social learning, and so on. Can the theory of evolution be responsible for the minority of ethological studies in Türkiye? Several studies reported a poor acceptance of the theory of evolution in the country even among university students (Annaç & Bahçekapılı, 2012), biology teachers (Peker et al., 2010) and political and social circumstances, and religious influences have the potential to guide the public view on evolution (Burton, 2011), but I want to ignore any effect of it on ethology and find another scapegoat. The study by Bueno-Guerra (2021) seems to be a candidate for me to use. The responses of researchers in the study showed that "budget" was the main barrier to deploying more adequate technical devices currently in ethology. Similarly, participants were asked to score how much impact they attributed to different issues in ethology (Table 5 in the original study), and a high level of consensus appeared around a lack of funding.

At this point, I still cannot say "eureka" since I have no concrete data with which to blame funders for negligence of ethology in the country. If this were the case, then other disciplines would also be, at least in theory, expected to show a similar pattern. In Türkiye, the most powerful and generous source of scientific funds is the Scientific and Technological Council of Türkiye (TÜBİTAK), which offers a wide range of national and international research funds for all disciplines. Researchers or research groups that meet the required criteria have the option to request funding for their studies, for which they will be evaluated scientifically. TÜBİTAK recently announced the list of projects that were awarded funding in the first call of 2025. The list includes 473 research topics, but lacks details. I therefore consulted the list for the first call of 2024, which included project titles in the announcement. An analysis of these titles revealed the direct involvement of two projects on rat behavior and one project on human behavior, amounting to 1.11% of the total 269 funded projects (TÜBİTAK, 2024). Are behavioral studies really that rare? Do they exist somewhere without a need for a fund, or is it really hard to attract funding for such a study?

Despite this pessimistic picture I have presented, a quick literature search will show that the case may not be as alarming as I described. The WOS is not the only source to consult for scientific data, and more studies (but still comparatively not at a satisfactory level) on animal behavior will be found on other platforms with Turkish researchers as authors and/or co-authors. Trakya University Journal of Natural Sciences (TUJNS) is one of the scientific platforms in Türkiye which also welcomes studies in the field of ethology. I searched the last 5-year archive of the journal and could classify two studies in this field, with either direct or indirect evidence. In one study, Selçuk et al. (2021) report data on the feeding behavior of the Long-eared Owl *Asio otus* L. based on pellet analysis (directly related to ethology), and in the second one, Şakacı and Camlitepe (2022) evaluated the vectoral role of mosquitoes in the central district of Edirne province, Türkiye (indirectly related to ethology). Two studies on mice and rats were published more recently in the journal, but they addressed hepatotoxicity and apoptosis, excluding behavioral approaches (Cinar et al., 2024; Cerkezkayabekir et al., 2025).

In short, we (and TUJNS) have an important mission to guide junior scientists in the field of ethology by encouraging them with more popular fields related to ethology, particularly neuroscience (Korkmaz & Küçükali, 2024) and deep learning (Fazzari et al., 2025). This amounts to a difficult process, because the priority areas listed by TÜBİTAK and by the Council of Higher Education of Türkiye include areas related to agriculture, the automotive industry, chemistry, climate change, the defense industry, digital technologies, drugs, electronics, energy, food, health, and tourism-related topics and excludes ethology. We should keep in mind that the path that the Nobel Prize of Tinbergen, Lorenz, and von Frisch opened is still full of questions to be addressed, which will contribute to the consolidation of the field globally, as well as in Türkiye, with new concepts, theories, methodologies, discoveries, and inventions.

1 If the term "behavior" is used alone as the search term, the number of published items exceeds 80,000, but a considerable amount of time is needed to make a clear distinction for those related to animal behavior among others. I, therefore, only considered ethology and animal behavior here. In this context, 891 items are listed with the subject category Behavioral Sciences, 763 with veterinary sciences, 260 with psychology, 244 with biology, 233 with Zzoology, and 209 with ecology, all of which may be related to animal behavior, making up 3.25% of the total.

References

Annaç, E., & Bahçekapılı, H. (2012). Understanding and acceptance of evolutionary theory among Turkish university students. *Doğuş Üniversitesi Dergisi, 13*(1), 1–11. https://doi.org/10.31671/dogus.2018.111

Bueno-Guerra, N. (2021). Where is ethology heading? An invitation for collective metadisciplinary discussion. *Animals, 11*(9), 2520. https://doi.org/10.3390/ani11092520

Burton, E. K. (2011). Evolution and creationism in Middle Eastern education: A new perspective. *Evolution, 65*(1), 301–304. https://doi.org/10.1111/j.1558-5646.2010.01113.x

Cinar, I., Yayla, M., Toktay, E., & Binnetoğlu, D. (2024). Effects of gossypin on acetaminophen-induced hepatotoxicity in mice. *Trakya University Journal of Natural Sciences, 25*(1), 81–90. https://doi.org/10.23902/trkjnat.1410800

Cerkezkayabekir, A., Bakar, E., & Yence, D. Y. (2025). Brominated flame retardant BDE-99 promotes apoptosis by intrinsic mitochondrial pathway in rat liver. *Trakya University Journal of Natural Sciences, 25*(1), 29–37. https://doi.org/10.23902/trkjnat.1366842

Ertan, G. (2016). Nazi döneminde Almanya'dan kaçarak Türkiye'ye sığınan bilim adamları. *Trakya Üniversitesi Uluslararası İlişkiler Bölümü Öğrenci Dergisi, 10*(4).

Fazzari, E., Romano, D., Falchi, F., & Stefanini, C. (2025). Animal behavior analysis methods using deep learning: A survey. *Expert Systems with Applications, 256*, 128330. https://doi.org/10.1016/j.eswa.2025.128330

Fericean, M. L., Rada, O., & Badilita, M. (2015). The history and development of ethology. *Research Journal of Agricultural Science, 47*(2), 45–51.

Gunay, D., Günay, A., & Atatekin, E. (2013). Shake in the basic sciences in Turkey: The country's shake. *Journal of Higher Education and Science, 3*(2), 85–96. https://doi.org/10.5961/jhes.2013.063

Jaynes, J. (1969). The historical origins of "ethology" and "comparative psychology." *Animal Behaviour, 17*(4), 601–606. https://doi.org/10.1016/S0003-3472(69)80001-1

Korkmaz, H. Y., & Küçükali, C. İ. (2024). Animal behavior testing in neuroscience research. In N. Orhan, Z. Karakaş, & T. Demiralp (Eds.), *Current trends in neurosciences* (pp. 103–126). İstanbul University Press.

Namal, Y. (2012). Contributions of foreign scientists to the higher education between 1933–1950 years in Turkey. *Journal of Higher Education and Science, 2*(1), 14–19. https://doi.org/10.5961/jhes.2012.028

Peker, D., Cömert, G. S., & Kence, A. (2010). Three decades of anti-evolution campaign and its results: Turkish undergraduates' acceptance and understanding of the biological evolution theory. *Science & Education, 19*, 739–755. https://doi.org/10.1007/s11191-009-9199-1

Selçuk, A. Y., Özkoç, Ö. Ü., Bal, M., Yeltekin, O. Ö., & Güngör, U. (2021). Diet composition of the wintering *Asio otus* L. (Strigiformes: Strigidae) in two different habitat types in Turkey. *Trakya University Journal of Natural Sciences, 22*(1), 1–8. https://doi.org/10.23902/trkjnat.770526

Sleigh, C. (2007). *Six legs better: A cultural history of myrmecology.* Johns Hopkins University Press.

Şakacı, Z., & Çamlıtepe, Y. (2022). A mosquito survey of culicidae species at Edirne central district for disease vector. *Trakya University Journal of Natural Sciences, 23*(Special Issue: Biodiversity of Insect), 41-51.

Taborsky, M. (2010). Ethology in Europe. In *Encyclopedia of animal behavior* (Vol. 1, pp. 649–651). Elsevier. https://doi.org/10.1016/B978-0-08-045337-8.00203-5

TÜBİTAK. (2024, October 3). *TÜBİTAK-ARDEB 2024 yılı 1. dönem 1001 projelerinin bilimsel değerlendirme sonuçları açıklandı.* https://tubitak.gov.tr/tr/duyuru/tubitak-ardeb-2024-yili-1-donem-1001-projelerinin-bilimsel-degerlendirme-sonuclari-aciklandi

Trakya University Journal of Natural Sciences, 26(2), 106–117, 2025
DOI: 10.23902/trkjnat.1640957
www.tujns.org

Research Article

Expanding the diversity of *Genea* Vittad. (Ascomycota, Pezizales) in Türkiye: Morphological and molecular insights into newly recorded species

Eda Kumru[1], Gülce Ediş[1,2,3], Ergin Şahin[4,5], Emre Keskin[2,3,6], Ilgaz Akata[7]*

[1]*Ankara University, Graduate School of Natural and Applied Sciences, Ankara, Türkiye*
[2]*Ankara University, Faculty of Agriculture, Department of Fisheries and Aquaculture, Evolutionary Genetics Laboratory, Ankara, Türkiye*
[3]*AgriGenomics Hub Animal and Plant Genomics Research Innovation Centre, Ankara, Türkiye*
[4]*Dokuz Eylül University, Faculty of Science, Department of Biology, İzmir, Türkiye*
[5]*Dokuz Eylül University, Fauna and Flora Research and Application Center, İzmir, Türkiye*
[6]*Ankara University, Aquaculture Research and Application Center, Ankara, Türkiye*
[7]*Ankara University, Faculty of Science, Department of Biology, Ankara, Türkiye*

Cite this article as: Kumru, E., Ediş, G., Şahin, E., Keskin, E., & Akata, I. (2025). Expanding the diversity of *Genea* Vittad. (Ascomycota, Pezizales) in Türkiye: Morphological and molecular insights into newly recorded species. *Trakya University Journal of Natural Sciences, 26*(2), 106–117. https://doi.org/10.23902/trkjnat.1640957

Abstract

Despite their ecological significance, the diversity of *Genea* Vittad. species in Türkiye remains underexplored, highlighting the need for further research. The current study aims to expand the known distribution of *Genea* species in Türkiye by integrating morphological and molecular analyses of new collections. Fungal specimens were collected from Edirne and Kırklareli provinces between October and December 2022. Morphological characteristics were documented using light and scanning electron microscopy, and molecular phylogenetic analyses were conducted using nrITS (rDNA) sequences to confirm species identity. The studies identified the new Turkish collections as *Genea fragrans* (Wallroth) Saccardo, *Genea pseudobalsleyi* Agnello, Bratek & Cabero, *Genea pseudoverrucosa* Bratek, Konstant. & Van Vooren, and *Genea vagans* Mattir., each exhibiting over 99% sequence similarity. This study provides the first records of these species in Türkiye, offering detailed descriptions of their morphological features, habitats, and phylogenetic placement.

Özet

Ekolojik önemlerine rağmen, Türkiye'deki *Genea* Vittad. türlerinin çeşitliliği yeterince keşfedilmemiştir ve bu durum daha fazla araştırma yapılması gerektiğini vurgulamaktadır. Bu çalışma, morfolojik ve moleküler analizleri entegre ederek *Genea* türlerinin Türkiye'deki bilinen dağılımını genişletmeyi amaçlamaktadır. Mantar örnekleri Ekim ve Aralık 2022 tarihleri arasında Edirne ve Kırklareli illerinden toplanmıştır. Morfolojik özellikler ışık ve taramalı elektron mikroskobu kullanılarak belgelenirken, tür kimliğini doğrulamak için nrITS dizileri kullanılarak moleküler filogenetik analizler yapılmıştır. Çalışmalar, yeni Türk koleksiyonlarını *Genea fragrans* (Wallroth) Saccardo, *Genea pseudobalsleyi* Agnello, Bratek & Cabero, *Genea pseudoverrucosa* Bratek, Konstantinidis & Van Vooren ve *Genea vagans* Mattirolo olarak tanımladı ve her biri % 99'un üzerinde dizi benzerliği sergiledi. Bu çalışma, bu türlerin Türkiye'deki ilk kayıtlarını sunmakta ve morfolojik özellikleri, habitatları ve filogenetik yerleşimleri hakkında ayrıntılı tanımlar sunmaktadır.

Keywords: subterranean fungi, truffles, mycobiota, European part of Türkiye

Edited by: *Boris Assyov*

***Corresponding Author:** Ilgaz Akata, **E-mail:** akata@science.ankara.edu.tr*

***ORCID iDs of the authors:** EK. 0009-0000-7417-6197, GE. 0000-0001-7038-9865, EŞ. 0000-0003-1711-738X, EmK. 0000-0002-7279-313X0, IA. 0000-0002-1731-1302*

Received: 16 February 2025, **Accepted:** 14 May 2025, **Online First**: 18 May 2025, **Published:** 15 October 2025

Introduction

The genus *Genea* Vittad., established by Vittadini (1831), represents a group of subterranean fungi within the Ascomycota division. The name of the genus honours the distinguished zoologist Dr. Joseph Gené, with *G. verrucosa* Vittad. and *G. papillosa* Vittad. serving as the original taxa. While *Genea* is predominantly found throughout the Mediterranean region, it has not received the same scientific attention as the genus *Tuber* P. Micheli ex F.H. Wigg, which is widely recognised for its economically and gastronomically valuable truffles. It continues to dominate research priorities in mycology (Alvarado et al., 2014).

The taxonomic classification of *Genea* has undergone considerable revisions over time, reflecting advancements in understanding its phylogenetic relationships. Initially placed within the order Tuberales, the genus was reclassified under Pezizales by Trappe (1979), who retained its inclusion in the subterranean family Geneaceae due to unresolved connections with other taxa in the order. However, subsequent studies by Pfister (1984) highlighted shared structural and morphological features among *Genea* species, including similarities in excipulum architecture, pigmentation patterns, and spore ornamentation, which ultimately led to the dissolution of Geneaceae as a family and the reassignment of *Genea* to Pyronemataceae.

Morphologically, *Genea* species are characterized by hypogeous, hollow, spherical to subspherical ascomata, which are typically black, reddish-brown, or yellowish, often adorned with warts and featuring an apical opening (Læssøe & Hansen, 2007). The ascomata may possess surface hairs and typically exhibit a tuft of basal hyphae. The gleba is divided into chambers containing a ptycothecium arranged in a palisade and an epithecium formed by paraphyses at the peridial junction (Alvarado et al., 2016). Asci are hyaline, inamyloid, and contain eight uniseriate warted spores (Alvarado et al., 2014).

The genus exhibits broad ecological associations with a diverse array of host trees, including fir, larch, pine, oak, beech, birch, chestnut, hazel, hemlock, hornbeam, linden, rockrose, and Douglas fir (Zhang, 1991; Moreno-Arroyo et al., 1998; Smith, 2007; Guevara-Guerrero et al., 2012; Alvarado et al., 2014, 2016, 2021; Agnello et al., 2016; Paz et al., 2016, 2019; Ribes et al., 2016; Kaounas et al., 2016; Crous et al., 2021). Unlike specific, closely related genera, *Genea* has adapted to abandon the mechanism of active spore ejection, opting instead for dispersal facilitated by animals. The ripe ascomata emit volatile chemical signals to lure small mammals, including flying squirrels, voles, and mice. These animals consume the ascomata, and their digestive processes facilitate the effective distribution of the spores (Smith et al., 2006).

The genus exhibits broad ecological associations with a diverse array of host trees, including fir, larch, pine, oak, beech, birch, chestnut, hazel, hemlock, hornbeam, linden, rockrose, and Douglas fir (Zhang, 1991; Moreno-Arroyo et al., 1998; Smith, 2007; Guevara-Guerrero et al., 2012; Alvarado et al., 2014, 2016, 2021; Agnello et al., 2016; Paz et al., 2016, 2019; Ribes et al., 2016; Kaounas et al., 2016; Crous et al., 2021). Unlike specific, closely related genera, *Genea* has adapted to abandon the mechanism of active spore ejection, opting instead for dispersal facilitated by animals. The ripe ascomata emit volatile chemical signals to lure small mammals, including flying squirrels, voles, and mice. These animals consume the ascomata, and their digestive processes facilitate the effective distribution of the spores (Smith et al., 2006).

Currently, the genus includes 49 formally recognized species, described through contributions spanning nearly two centuries (Vittadini, 1831; Berkeley & Broome, 1846; Tulasne & Tulasne, 1851; Corda, 1854; Saccardo, 1889; Bresadola, 1893; Harkness, 1899; Mattirolo, 1900a, 1900b; Velenovský, 1922; Imai, 1933; Gilkey, 1939; Cribb, 1960; Trappe & Guzmán, 1971; Stewart & Heblack, 1979; Trappe, 1979; Zhang, 1991; Moreno-Arroyo et al., 1998; Smith et al., 2006; Smith, 2007; Guevara-Guerrero et al., 2012; Alvarado et al., 2014, 2016, 2021; Agnello et al., 2016; Kaounas et al., 2016; Paz et al., 2016, 2019; Crous et al., 2021). In Türkiye, five *Genea* species have been documented to date through morphological analyses carried out by various researchers. Specifically, *G. hispidula* Berk. ex Tul. & C. Tul. was reported from Trabzon, *G. klotzschii* Berk. & Broome from Samsun, *G. lobulata* (Mor.-Arr., J. Gómez & Calonge) P. Alvarado & Mor.-Arr. from Niğde, *G. sphaerica* Tul. & C. Tul. from İzmir, and *G. verrucosa* Vittad. from Muğla, with detailed descriptions provided in the studies by Uzun & Kaya (2019), Berber et al. (2019), and Türkoğlu & Castellano (2014). These findings were compiled and included in the Turkish truffles checklist by Akata et al. (2022).

The present study documents and characterizes these four newly recorded *Genea* species in Türkiye, thereby contributing to a deeper understanding of the genus diversity and distribution across the country.

Materials and Methods

Field Study

The *Genea* specimens were systematically collected from various forest habitats, including pine-dominated woodlands in the Uzunköprü district of Edirne and oak forests in the Demirköy and Pınarhisar districts of Kırklareli, employing trained *Lagotto Romagnolo* truffle dogs as part of the collection process (Figure 1). Extensive field investigations were conducted to document the macroscopic and ecological characteristics of the collected specimens, facilitating a detailed assessment of their morphological variability and environmental preferences. High-resolution imaging was performed using a Nikon D810 camera fitted with an AF-S NIKKOR 105 mm f/1.4E ED lens, ensuring the capture of intricate structural details essential for taxonomic analysis. Simultaneously, a comprehensive dataset was compiled, systematically recording vital metadata, including collection dates, precise geographical coordinates, habitat descriptions, and unique specimen identifiers.

Morphological Study

The samples were examined using light microscopy (LM) and scanning electron microscopy (SEM). For LM (Euromex Oxion), visualization was achieved with distilled water, 5% KOH, and Congo red. The dimensions of ascospores were assessed by measuring at least 30 randomly selected spores outside the asci, while the length-to-width ratio, noted as Q, was calculated independently of ornamentation. Spore sizes were reported without ornamentation, with the ornamentation width defined with the base of the warts. For SEM, sections of the gleba were affixed to stubs using double-sided tape and coated with gold particles to enhance conductivity. Imaging was conducted using a ZEISS EVO 40 SEM at an acceleration voltage of 20 kV. The specimens were then prepared for long-term preservation and stored in the Fungarium of the Faculty of Science at Ankara University (ANK).

Molecular Study

Determination of Internal Transcribed Spacer (ITS) rDNA Sequences

The nuclear ribosomal ITS (nrITS) rDNA region was amplified from genomic DNA isolated from *Genea* specimens using the polymerase chain reaction (PCR) method. This amplification strictly adhered to established and well-validated methodologies outlined in previous studies (Akata et al., 2023a, 2023b, 2024a, 2024b). These standardized protocols ensured the accuracy and reproducibility of the molecular data generated, thus providing a robust foundation for subsequent analyses.

Figure 1. (a–d) Collection areas; (e) truffle dogs (*Lagotto Romagnolo*).

Molecular Phylogenetic Analysis

The phylogenetic relationships among the fungal samples were meticulously analyzed with the MEGA-X software (Kumar et al., 2018), using nucleotide sequences obtained directly from the specimens. The reference sequences were selected from GenBank using a rigorous screening process that designates closely related taxa as the ingroup and more distantly related sequences as the outgroup, using NCBI BLAST searches. Multiple sequence alignment was performed with the MUSCLE algorithm (Edgar, 2004) to optimize accuracy and consistency. Following these alignments, K2+G+I was determined as the most suitable nucleotide substitution model to guide the construction of phylogenetic trees. The Neighbour-Joining method was employed to infer evolutionary relationships, and the robustness of the branching patterns was assessed with 1,000 bootstrap replicates. This analytical approach aligned with established methodologies outlined in previous research (Akata et al., 2024a, 2024b, 2024c, 2024d), ensuring methodological rigour and comparability.

Results

This study assessed the macroscopic and microscopic characteristics of the samples and evaluated their ribosomal DNA (rDNA) sequences using ITS sequencing.

Taxonomy

Phylum **ASCOMYCOTA** (Berk) Caval.-Sm.

Ordo **Pezizales** J. Schöt.

Family **Pezizaceae** Dumort.

Genus *Genea* **Vittad**.

Genea fragrans (Wallr.) Sacc. (1889), (Figures 2, 6a, and 6b). **Material examined:** Türkiye-Kırklareli, Pınarhisar, under oak, 350 m, 41°41′ N, 27°42′ E, 4 Oct. 2022, ANK Akata TT 098; ibid., 417 m, 41°41′ N, 27°38′ E, 18 Nov. 2022, ANK Akata TT 207.

Macroscopic and Microscopic Features

Ascomata 7–8 mm across, hypogeous, hollow, subglobose and lobed, with a peridium surface displaying a brownish-black hue and covered by tiny, blunt, inconspicuous dark warts; a small tuft of hyphae occupies the base. Peridium up to 150 µm thick, with an outer surface brownish-black and exhibiting small, blunt, inconspicuous dark warts, composed of a single layer of pseudoparenchymatous tissue, comprising hyaline to light brownish angular to subglobose cells measuring 15–35 µm in width. Internal chamber consists of unique, winding chambers leading to a gleba with a labyrinth-like configuration, and the chamber walls lined with a black epithecium, up to 70 µm, formed by brownish to dark brown angular cells

measuring 20–45 µm wide. Asci 240–300 × 25–30 µm, 8-spored, cylindrical, with a short peduncle. Paraphyses cylindrical, thread-like, 3–6 µm broad, septate, with some swollen cells. Ascospores (29)31–41(43) × (27)28–36(38) µm, (mean: 38 × 34), [(n = 30), Q = (1.02)1.06–1.22(1.31), Qav = 1.14], subglobose to broadly ellipsoid, hyaline to pale yellow, ornamented with truncated warts, measuring 1.5–4 × 2–4.5 µm, mixed with micro-warts.

Ecology and Distribution

Genea fragrans is typically found from September to December, mainly beneath deciduous trees like oak, beech, hornbeam, and common hazel, and less frequently associated with chestnut, poplar, willow, blackthorn, and European hop-hornbeam (Venturella et al., 2006; Riva, 2009; Zotti et al., 2010; Kajevska et al., 2013; Landi et al., 2015; Alvarado et al., 2016). Its known distribution covers Greece, Germany, Hungary, France, Italy, Macedonia, Serbia, Spain, and Morocco (Venturella et al., 2006; Diamandis & Perlerou, 2008; Saitta et al., 2008; Bratek et al., 2013; Kajevska et al., 2013; Alvarado et al., 2016, 2021; Savić et al., 2018).

Genea pseudobalsleyi Agnello, Bratek & J. Cabero (2014), (Figures 3, 6c, and 6d).

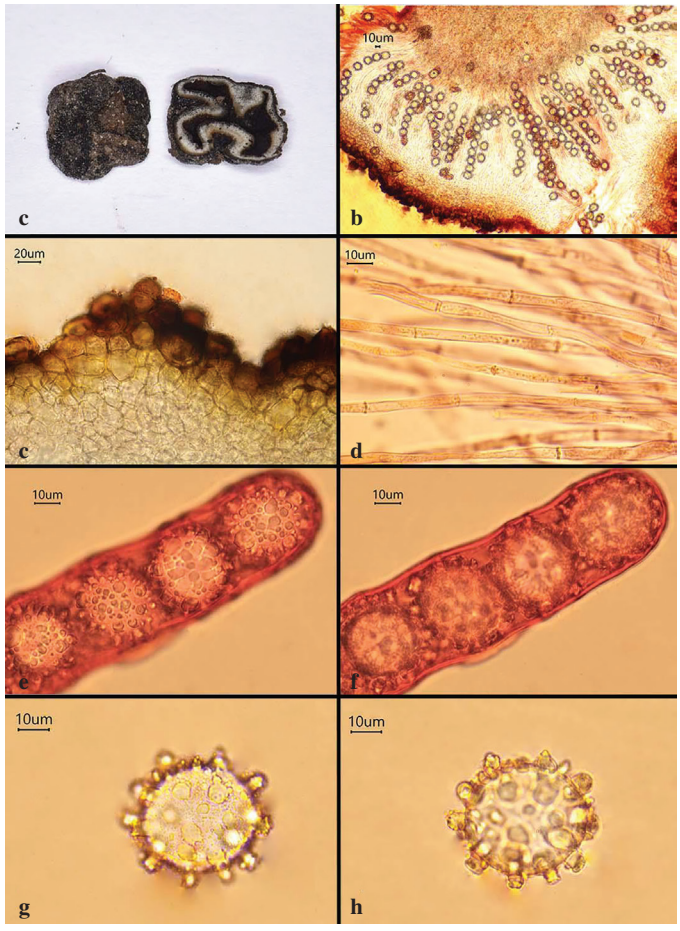

Figure 2. *Genea fragrans*. (a) ascomata; (b) microscopic cross-section of ascomata; (c) peridium; (d) septa of paraphyses; (e, f) spores contained within the ascus; (g, h) single ascospore.

Material examined: Türkiye- Kırklareli, Pınarhisar, under oak, 480 m, 41°44′ N, 27°34′ E, 5 Oct. 2022, ANK Akata TT 127; ibid., 312 m, 41°39′ N, 27°36′ E, 5 Dec. 2022, ANK Akata TT 281; Edirne, Uzunköprü, under pine, 106 m, 41°12′ N, 26°44′ E, 7 Dec. 2022, ANK Akata TT 350. Alvarado et al. (2014) offered a comprehensive overview of the type specimens from the original collection.

Macroscopic and Microscopic Features

Ascomata 7–9 mm across, hypogeous, hollow, subglobose to moderately lobed, with a uniformly warted peridium surface adorned with small polygonal black warts; a small tuft of hyphae occupies the base. Peridium consisting of a single layer of pseudoparenchymatic tissue up to 160 µm thick, composed of hyaline, subglobose cells measuring 15–45 µm in diam., transitioning towards the outer layer into angular cells with thicker, darker walls. Internal chamber displaying variability, ranging from a single chamber to multiple sinuous chambers formed by wall projections, producing a brain-like appearance; chamber walls lined with a blackish or brown-black epithecium up to 60 µm thick, comprising pseudoparenchymatous tissue with angular cells featuring thick, melanized walls measuring 15–40 µm in width. Asci 180–240 × 35–40 µm, eight-spored, somewhat cylindrical with a short peduncle. Paraphyses cylindrical, septate, 4–9 µm diam., with some cells appearing swollen. Ascospores (24)25–29 (31) × 23–26 µm, (mean: 28 × 24), [(n = 30), Q = 1.1–1.26, Qav = 1.18], spherical to broadly ellipsoid, pale yellow, containing prominent, unevenly positioned oil droplets; surface ornamented with truncated warts, occasionally featuring small digitations at the top, measuring 2–3.5 × 2–2.5 µm.

Ecology and Distribution

Genea pseudobalsleyi is primarily observed between June and December and is mainly associated with oak trees, particularly *Quercus ilex* L. and *Q. pyrenaica* Willd. Its geographical distribution encompasses France, Hungary, Italy, and Spain (Alvarado et al., 2014; Perez, 2024).

Genea pseudoverrucosa Bratek, Konstant. & Van Vooren (2014), (Figures 4, 6e, and 6f). Material examined: Türkiye-Kırklareli, Pınarhisar, under oak, 14 m, 41°44′ N, 27°34′ E, 5 Oct. 2022, ANK Akata TT 124. Alvarado et al. (2014) presented a thorough account of the type specimens from the original collection.

Macroscopic and Microscopic Features

Ascomata 10–12 mm across, hypogeous, hollow, spherical to extensively lobed, peridium surface black and adorned with tiny, rounded warts, with an inconspicuous basal tuft of dark hyphae. Peridium consisting of a single layer of pseudoparenchymatic tissue up to 200 µm thick, made up of light brownish angular cells measuring 18–35 µm in width. Internal chamber slightly partitioned yet primarily intact, coated with a dark epithecium resembling the peridium, epithecium structure pseudoparenchymatous made of isodiametric cells up to 160 µm. Asci 200–250 × 30–35 µm, 8-spored, somewhat cylindrical. Paraphyses 4–8 µm broad, cylindrical, septate, with some swollen cells. Ascospores (26–)28–

33 (–34) × (23–) 24–28(–29) µm, (mean: 31 × 26), [(n = 30), Q = (1.05)1.1–1.32 (1.4), Qav = 1.2], subglobose to broadly ellipsoid, hyaline, ornamented with conical-truncated to irregular warts, measuring 2–4 × 1.5–3 µm.

Ecology and Distribution

Genea pseudoverrucosa is typically found from July to January in temperate deciduous forests associated with oak, hornbeam, linden, and common hazel. It also thrives in Mediterranean habitats featuring oaks (*Quercus ilex* L. and *Q. coccifera* L.). Its distribution spans Greece, Hungary, France, Romania, and Morocco (Alvarado et al., 2014).

Genea vagans Mattir. (1900), (Figures 5, 6g, and 6h). Material examined: Türkiye-Kırklareli, Demirköy, under oak, 14 m, 41°51′ N, 27°56′ E, 8 Oct. 2022, ANK Akata TT 163.

Macroscopic and Microscopic Features

Ascomata 10–15 mm across, hypogeous, hollow, subglobose to moderately lobed, with an apical pore and a tuft of brownish hairs at the base, peridium black, finely verrucose, surface adorned with small polygonal black warts. Peridium consisting of a single layer of pseudoparenchymatic tissue up to 300 µm thick, composed of hyaline, angular cells measuring 25–50 µm in width. Internal chamber usually solitary, occasionally divided, coated with a dark epithecium, up to 150 µm thick, comprising pseudoparenchymatous tissue with angular cells measuring 20–40 µm wide. Asci 220–250 × 30–40 µm, 8-spored, somewhat cylindrical with a long peduncle. Paraphyses cylindrical, septate, 5–10 µm diam., with some swollen cells. Ascospores (29)31–38(39) × (25)27–30(31) µm, (mean: 35 × 29), [(n = 30), Q = (1.1)1.15–1.22(1.3), Qav = 1.18], broadly ellipsoid to ellipsoid, hyaline, ornamented with conical or conical-truncated warts, measuring 4–6 × 3–5 µm, sometimes showing single digitations at the top.

Ecology and Distribution

Genea vagans is typically observed in autumn, particularly beneath trees such as fir and beech, with a tentative association with chestnuts, as indicated in early studies (Mattirolo, 1900b). Recent research has documented its presence under oak, beech, alder, common hazel, and hornbeam (Alvarado et al., 2016, 2021; Savić et al., 2018). Geographically, the species is distributed across Italy, France, Spain, Russia, and Serbia, as evidenced by studies spanning over a century (Mattirolo, 1900a; Bucholtz, 1901; Ceruti, 1960; Vidal, 1997; Alvarado et al., 2014, 2016, 2018, 2021; Kaounas et al., 2016; Ribes et al., 2016; Savić et al., 2018).

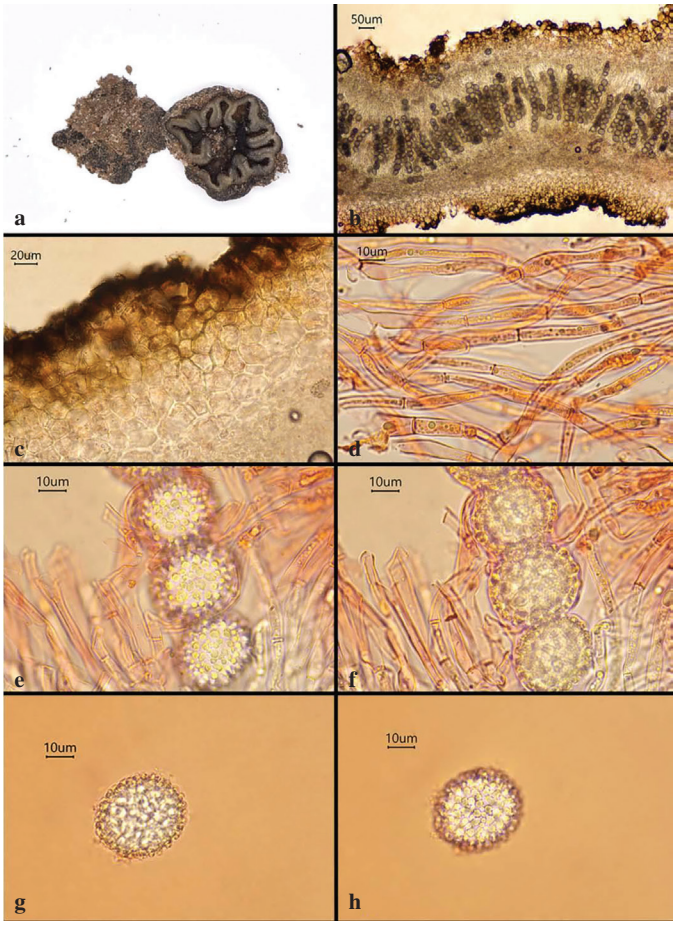

Figure 3. *Genea pseudobalsleyi*. (a) ascomata; (b) microscopic cross-section of ascomata; (c) peridium; (d) septa of paraphyses; (e, f) spores contained within the ascus; (g, h) single ascospore.

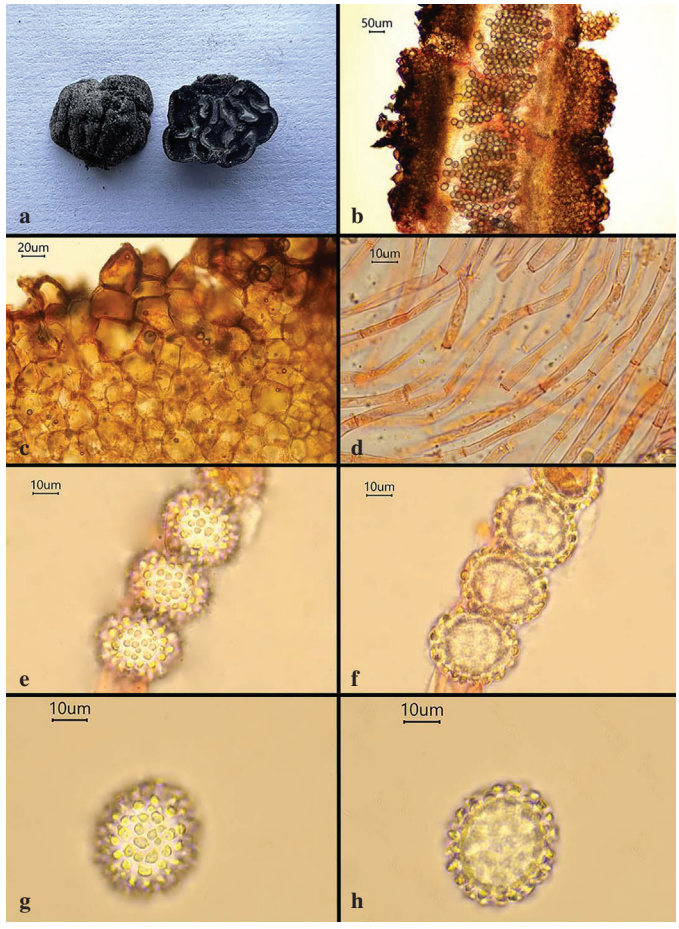

Figure 4. *Genea pseudoverrucosa*. (a) ascomata; (b) microscopic cross-section of ascomata; (c) peridium; (d) septa of paraphyses; (e, f) spores contained within the ascus; (g, h) single ascospore.

Evolutionary History of the Genea Specimens

The evolutionary lineages of the specimens ANK Akata TT 098, ANK Akata TT 124, ANK Akata TT 127, ANK Akata TT 163, ANK Akata TT 207, ANK Akata TT 281, and ANK Akata TT 350 were examined based on their nrITS rDNA sequences, which were obtained using standard molecular techniques and stored in the NCBI GenBank under the accession numbers provided in Table 1. To infer their evolutionary relationships, nrITS rDNA sequences from various members of *Genea* were selected for comparison, using a sequence of *Scutellinia verruculosa* M. Zeng, Q. Zhao & K.D. Hyde as outgroup. Our molecular phylogenetic analysis identified eight distinct clades (Figure 7). While Clade 1 comprised different isolates of *G. vagans* and the specimen ANK Akata TT 163, Clade 2 included an isolate of *G. pseudobalsleyi*, which clustered with the specimens ANK Akata TT 127, ANK Akata TT 281, and ANK Akata TT 350. In contrast, Clade 3 contained various isolates of *G. fragrans*, alongside the specimens ANK Akata TT 098 and ANK Akata TT 207. Lastly, the specimen ANK Akata TT 124 grouped with different isolates of *G. pseudoverrucosa* in a well-supported Clade 4. The remaining clades (Clades 5–8) incorporated other *Genea* species. Phylogenetic analyses confirmed the close relationship between our specimens and their associated *Genea* species, with high bootstrap branch support rates, thus validating their identity.

Discussion

Genea verrucosa, frequently compared with *G. fragrans*, is a darkly pigmented species characterized by significantly smaller ascospores and unique spore ornamentation (Bertolini, 2014). The ascospores of *G. verrucosa* measure 21–26 × 19–22 µm and exhibit conical warts approximately measuring 2 × 1.5–4.5 µm, which are smaller and less prominent than the larger and more distinct ornamentation observed in *G. fragrans* (Türkoğlu & Castellano, 2014; Alvarado et al., 2016). Despite similarities in macroscopic appearance, the ascospores and asci of *G. verrucosa* are generally smaller, with asci not exceeding 250 × 35 µm. Over time, the conical spore warts of *G. verrucosa* may develop into aculeate forms but remain less prominent than the ornamentation

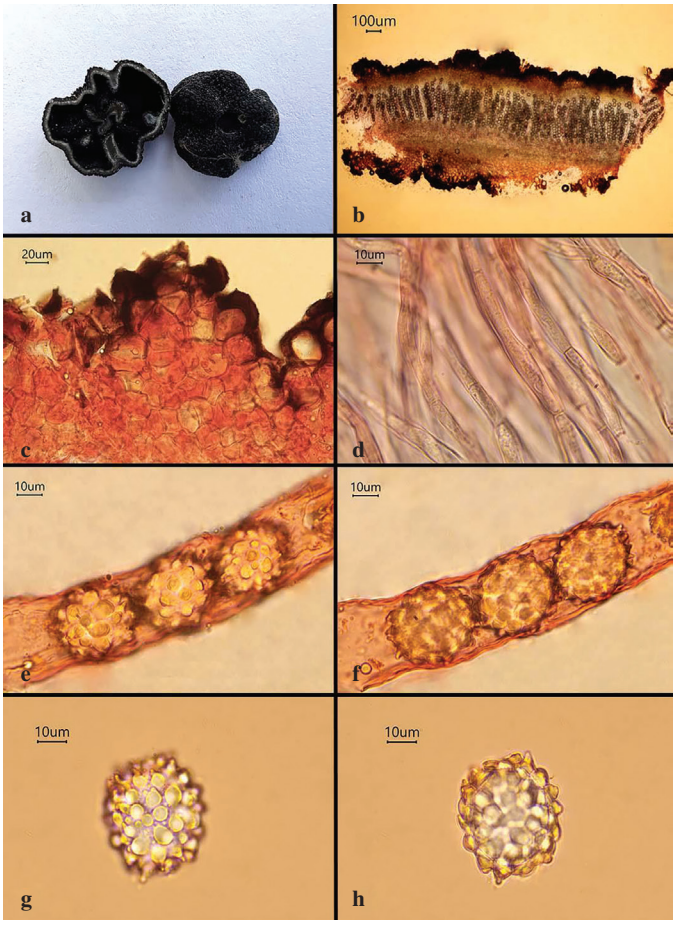

Figure 5. *Genea vagans*. (a) ascomata; (b) microscopic cross-section of ascomata; (c) peridium; (d) septa of paraphyses; (e, f) spores contained within the ascus; (g, h) single ascospore.

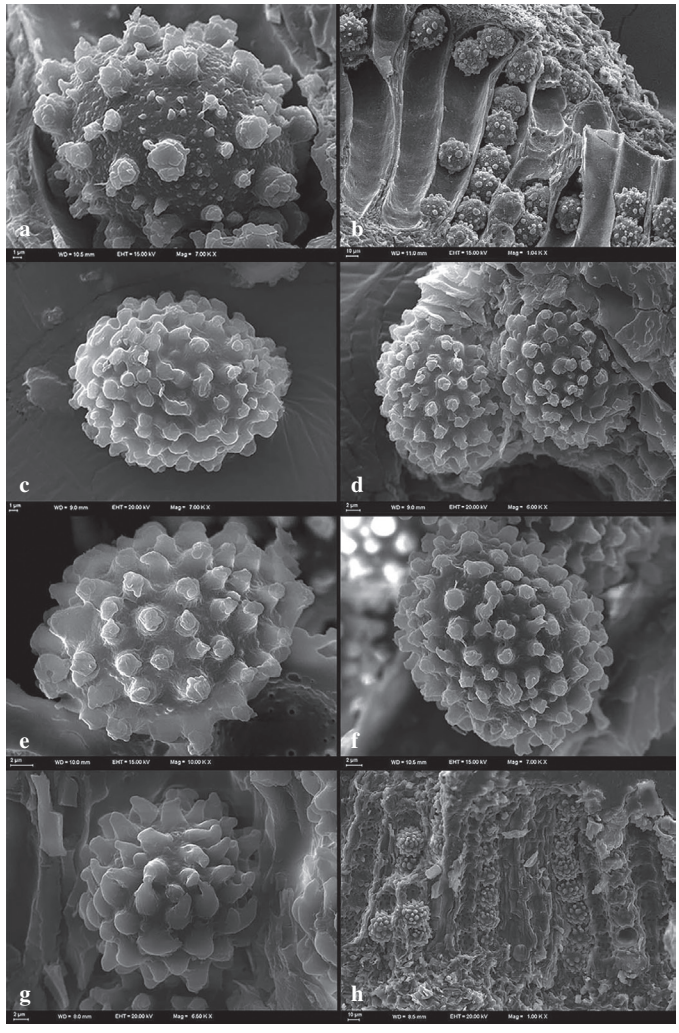

Figure 6. Scanning electron microscope micrographs. (a, b) *Genea fragrans*; (c, d) *Genea pseudobalsleyi*; (e, f) *Genea pseudoverrucosa*; (g, h) *Genea vagans*.

of *G. fragrans*. The ecological preferences of *G. verrucosa* further distinguish it, because it primarily associates with oak trees and is widely distributed across Europe, particularly in the Mediterranean region (Hollós, 1911; Diamandis & Perlerou, 2008; Alvarado et al., 2014; Bertolini, 2014).

Other species within the genus also display significant morphological and ecological distinctions: *G. brunneocarpa* G. Moreno, Cabero & Kaounas shares some similarities with *G. fragrans* but differs in ascospore size, measuring 28–31.5 × 19.5–24 µm, and by its ornamentation, which consists of truncate-conical warts that are occasionally nearly cubic, reaching 3.8–5.5 µm high. The brownish peridium and simpler internal chamber structure of *G. brunneocarpa* further set it apart. Unlike *G. fragrans*, this species is chiefly associated with holm oak and Aleppo pine, thriving on calcareous soils and fruiting between February and April. Its distribution is limited to Mediterranean regions, with records from Greece and Spain (Alvarado et al., 2014).

Similarly, *G. compressa* Merényi, Cabero & G. Moreno is a closely related species that can be distinguished by its smaller ascospores, measuring 23.5–30.5 × 18–25.5 µm, and ornamentation consisting of conical warts with digitate apices, up to 2.3–5.3 µm high. It is commonly associated with oak species and found in mixed habitats alongside common hornbeam or Atlas cedar, with a distribution spanning Hungary, Morocco, and Spain (Kaounas et al., 2016).

Another closely related species, *G. fageticola* Konstantin., Cabero & Faust. García shares overlapping spore dimensions with *G. fragrans*, 28–36.5 × 18–26 µm, but it is distinguishable by its

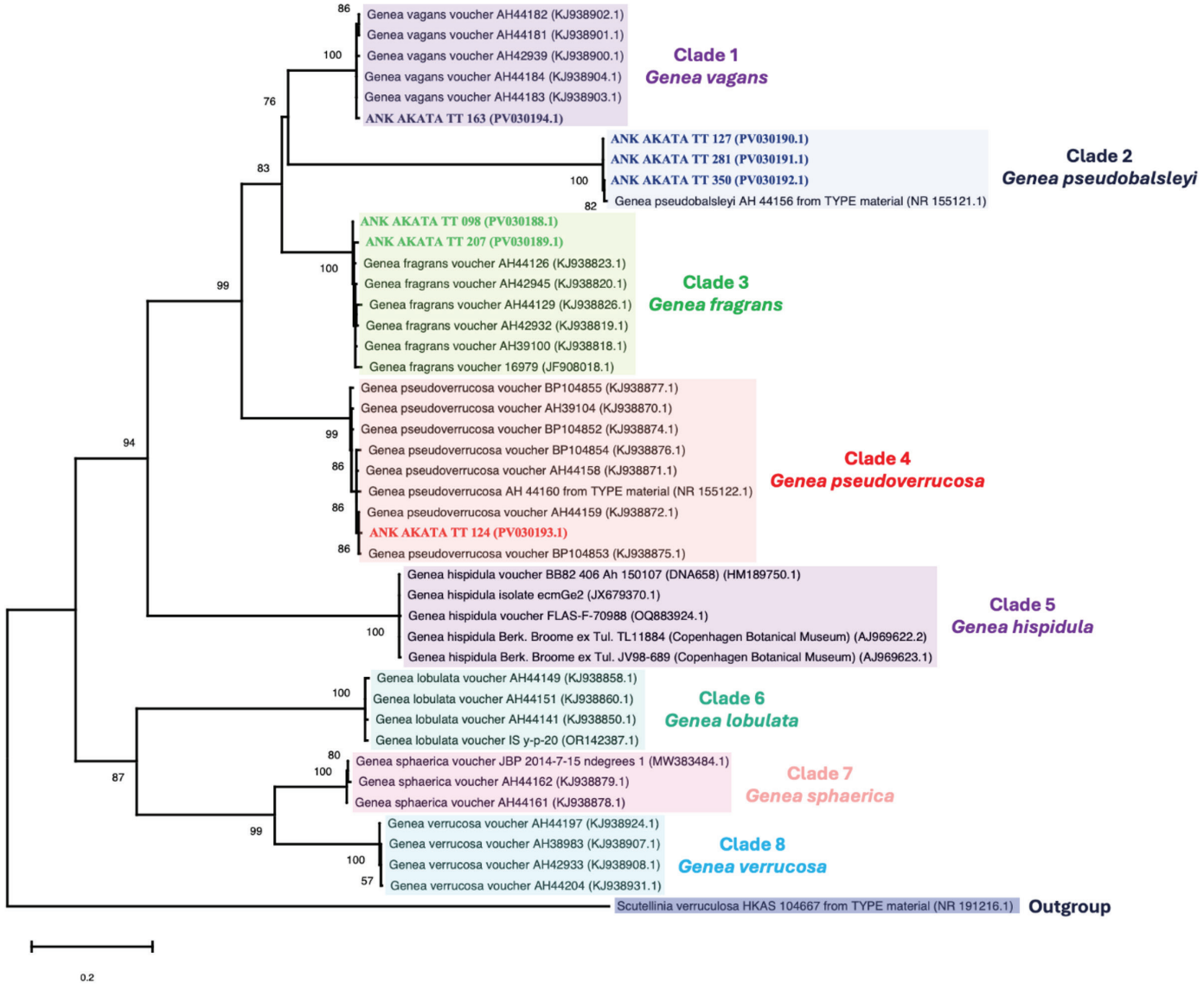

Figure 7. Phylogram of ML of a set of 44 *Genea* sequences based on the nrITS rDNA, rooted with *Scutellinia verruculosa* (outgroup). Nodes with ≥ 50% ML bootstrap support are annotated with their support values. Terminals that represent sequences obtained during this study are in bold. Each sequence is accompanied by its respective GenBank accession number, and a scale bar in the lower left corner indicates a genetic distance of 0.2. ML = maximum likelihood; nrITS = nuclear ribosomal internal transcribed spacer.

Table 1. GenBank accession numbers and collection sites of *Genea* specimens examined.

Species	Specimen voucher/isolate/ strain	nrITS GenBank Accession Number	Geographical origin	Reference
G. fragrans	ANK Akata TT 098	PV030188	Türkiye, Kırklareli, Pınarhisar	Current study
	ANK Akata TT 207	PV030189	Türkiye, Kırklareli, Pınarhisar	Current study
	AH44129	KJ938826	Spain, Zamora, Peleagonzalo	Alvarado et al., 2016
	AH42932	KJ938819	Spain, Madrid, Torrelaguna	Alvarado et al., 2016
	AH42945	KJ938820	Morocco, Chefchaouen	Alvarado et al., 2016
	AH39100	KJ938818	Morocco, Chefchaouen	Alvarado et al., 2016
	AH44126	KJ938823	Greece, Pigi Kilkis	Alvarado et al., 2016
	16979	JF908018	Italy	Osmundson et al., 2013
G. pseudobalsleyi	ANK Akata TT 127	PV030190	Türkiye, Kırklareli, Pınarhisar	Current study
	ANK Akata TT 281	PV030191	Türkiye, Kırklareli, Pınarhisar	Current study
	ANK Akata TT 350	PV030192	Türkiye, Edirne, Uzunköprü	Current study
	AH44156	NR_155121	Italy, Brindisi, Bosco Compare	Alvarado et al., 2016
G. vagans	ANK Akata TT 163	PV030194	Türkiye, Kırklareli, Demirköy	Current study
	AH44182	KJ938902	Spain, Zamora, Quintana de Sanabria	Alvarado et al., 2016
	AH44183	KJ938903	Spain, Zamora, Quintana de Sanabria	Alvarado et al., 2016
	AH44184	KJ938904	Spain, Girona, Campelles	Alvarado et al., 2016
	AH44181	KJ938901	Spain, Asturias, Pola de Somiedo	Alvarado et al., 2016
	AH42939	KJ938900	Spain, Guadalajara, El Ordial	Alvarado et al., 2016
G. pseudoverrucosa	ANK Akata TT 124	PV030193	Türkiye, Kırklareli, Pınarhisar	Current study
	AH44158	KJ938871	-	Alvarado et al., 2016
	AH44159	KJ938872	-	Alvarado et al., 2016
	AH44160	NR_155122	-	Alvarado et al., 2016
	AH39104	KJ938870	-	Alvarado et al., 2016
	BP104852	KJ938874	Hungary, Heves county, Bükk mountains, Szilvásvárad	Alvarado et al., 2016
	BP104853	KJ938875	Hungary, Pest county, Budapest	Alvarado et al., 2016
	BP104854	KJ938876	Hungary, Győr-Moson-Sopron, Fertőrákos	Alvarado et al., 2016
	BP104855	KJ938877	Romania, Harghita, Cristuru Secuiesc	Alvarado et al., 2016
G. verrucosa	AH42933	KJ938908	Spain, Guadalajara, Algora	Alvarado et al., 2016
	AH44204	KJ938931	Spain, La Rioja, Torrecilla en Cameros	Alvarado et al., 2016
	AH38983	KJ938907	Spain, Guadalajara, Valdearenas	Alvarado et al., 2016
	AH44197	KJ938924	Spain, Zamora, Peleagonzalo, Monte San Miguel	Alvarado et al., 2016
G. hispidula	FLAS-F-70988	OQ883924	USA: VT, Rutland Co.	Unpublished
	Berk. & Broome ex Tul. TL11884 (Copenhagen Botanical Museum)	AJ969622	Denmark: Broby Vesterskov, South Zealand	Tedersoo et al., 2006
	Berk. & Broome ex Tul. JV98-689 (Copenhagen Botanical Museum)	AJ969623	United Kingdom: Shropshire, Dudmaston Estate	Tedersoo et al., 2006
	BB82_406_Ah_150107 (DNA658)	HM189750	-	Unpublished
	ecmGe2	JX679370	Czech Republic	Unpublished

Table 1. Continued.

Species	Specimen voucher/isolate/ strain	nrITS GenBank Accession Number	Geographical origin	Reference
G. lobulata	AH44141	KJ938850	Cyprus	Alvarado et al., 2016
	AH44149	KJ938858	Greece, Attica, Parnitha	Alvarado et al., 2016
	AH44151	KJ938860	Greece, Attica, Parnitha	Alvarado et al., 2016
	IS_y-p-20	OR142387	Israel	Unpublished
G. sphaerica	AH44161	KJ938878	Germany, Grockstädt	Alvarado et al., 2016
	JBP 2014-7-15-1	MW383484	France: Sexey aux Forges Meurthe-et-Moselle	Unpublished
	AH44162	KJ938879	Germany, Leinefelde	Alvarado et al., 2016
Scutellinia verruculosa	HKAS:104667	NR_191216	China, Sichuan	Zeng et al., 2022

ANK = Ankara University; nrITS = nuclear ribosomal internal transcribed spacer.

spherical ascomata, the absence of labyrinthine hymenium folds, and the presence of small polygonal warts on its peridium instead of minute papillae. Additionally, *G. fageticola* has a brownish epithecium and a basal tuft of reddish or brownish hyphae, both absent in *G. fragrans*. This species, reported from Greece and Spain, associates with European beech and occasionally with sessile oak, emerging during late summer and winter (Alvarado et al., 2014; Kaounas et al., 2016).

Genea pseudobalsleyi exhibits notable morphological similarities with *G. balsleyi* M.E. Sm., primarily due to its black peridium surface, ascospore dimensions (24–30 × 20–25 µm), and ornamentation patterns (Alvarado et al., 2014). Nevertheless, it is distinguished by unique structural features, such as prominent projections on the peridium wall that create intricate, labyrinthine, chambered cavities absent in *G. balsleyi* (Smith, 2007). Geographic distribution further differentiates these species, as *G. balsleyi* is restricted to North America and typically associated with oak, while *G. pseudobalsleyi* is exclusively recorded in Europe (Smith, 2007; Alvarado et al., 2014). Additionally, *G. balsleyi* is characterized by a bilayered peridium structure, a feature not found in *G. pseudobalsleyi* (Alvarado et al., 2014).

In contrast, the rare American species *G. macrosiphon* Gilkey, while showing macroscopic resemblance to *G. pseudobalsleyi*, is distinct due to its significantly larger ascospore dimensions (36–40 × 24–28 µm) and highly inflated pseudoparenchymatous peridium cells (Gilkey, 1939; Alvarado et al., 2014).

Distinctive morphological features of *G. pseudobalsleyi* set it apart from closely related species. Compared to *G. verrucosa*, *G. pseudobalsleyi* is characterized by densely packed and truncated ascospore ornamentation, in stark contrast to the thinner, sharper, and more scattered ornamentation observed in *G. verrucosa* (Alvarado et al., 2014; Bertolini, 2014; Türkoğlu & Castellano, 2014). Furthermore, although *G. compressa* shares macroscopic similarities and identical ascospore dimensions, 23.5–30.5 × 18–25.5 µm, with *G. pseudobalsleyi*, it is readily distinguishable by its unique conical spore ornamentation. *Genea compressa* primarily grows in autumn under various host plants, including oak, and is distributed across regions such as Spain and Hungary (Alvarado et al., 2014).

Additional distinctions are evident in other closely related species. For instance, *G. fageticola* displays notably larger ascospores, measuring 28–36.5 × 18–26 µm, and unique ornamentation characterized by truncated or rounded warts measuring 2.1–6.5 × 2–6 µm (Alvarado et al., 2014). In contrast, *G. cephalonica* Kaounas, Agnello & P. Alvarado, which is exclusively associated with Greek fir (*Abies cephalonica* Loudon) in Greece, features slightly smaller ascospores, 24–35 × 15.5–26 µm, but it is distinguished by its distinct ornamentation, with warts reaching 3–6 µm in height (Kaounas et al., 2016).

The macroscopic features of *G. pseudoverrucosa* resemble *G. fragrans* but are often misidentified as *G. verrucosa* due to similarities in ascospore dimensions. Its spore ornamentation, characterized by truncate warts, is similar to that of *G. fragrans*; however, the warts in *G. pseudoverrucosa* are lower, denser, and more uniform. In contrast, *G. fragrans* has more prominent and scattered warts, often interspersed with smaller ones. *G. pseudoverrucosa* also shares similarities with *G. brunneocarpa*, yet the latter displays more irregularly scattered warts, necessitating ecological and macroscopic observations to separate them. Similarly, *G. pseudobalsleyi* features a black, warted peridium and comparable ascospores but it is distinguished by its thinner warts, 1.5–2 µm wide. The North American species *G. balsleyi* exhibits a bilayered peridium, a hollow inner cavity, and conical spore warts (Gilkey, 1939; Alvarado et al., 2014).

The original Italian collections of *G. vagans*, first described by Mattirolo (1900a), were subsequently detailed and illustrated by Ceruti (1960), who characterized the species as producing small, rounded ascomata with a black verrucose peridium. The ascospores were ellipsoidal, measuring 35–38 × 27–28 µm, and adorned with prominent conical warts that frequently coalesce at their bases.

Lawrynowicz (1988) reported nearly identical dimensions, with ascospores measuring 31–38 × 27–28 µm. However, Vidal (1997) and Montecchi and Sarasini (2000) documented significantly smaller ascospore sizes, ranging from 18–22 µm, highlighting variability in reported measurements. A later study by Ribes et al. (2016) aligned more closely with Ceruti (1960) and Lawrynowicz (1988), recording ascospore dimensions of 31.2–38.4 × 27.1–30.2 µm. Alvarado et al. (2016) further corroborated these findings, reporting ascospore sizes of 32–41 × 27–37 µm based on authentic material from Mattirolo and additional specimens. In our study, ascospore dimensions of 31–38 × 27–30 µm were observed, consistent with the findings of Lawrynowicz (1988) and Ribes et al. (2016), reinforcing the morphological variability within this species.

Genea vagans has often been misidentified due to its resemblance to other species, such as *G. anthracina* Heblack & Stewart, an American species. While both species share similar macroscopic features, including small, black fruiting bodies with a single basal cavity, *G. anthracina* is distinguishable by its smaller ascospores, which measure 22–26 × 18–20 µm and are ornamented with subglobose, irregular, and occasionally truncated warts (Stewart & Heblack, 1979). Confusion also arises with *G. pinicola* V. Kaounas, J. Cabero & F. García, a species that transitions from an initial yellowish hue to a yellowish-brown (Alvarado et al., 2014). Although typically associated with pine, collections of *G. pinicola* have also been documented under oak. This species has ascospores measuring 26–29 × 17–20 µm, with ornamentation made of small conical warts, 1–3 µm in height (Alvarado et al., 2014; Ribes et al., 2016). Externally, *G. vagans* also resembles *G. sphaerica* Tul. & C. Tul., sharing similarities in shape and colour (Vacek, 1951; Hawker, 1954). However, detailed microscopic analysis reveals key differences between the two species: *G. sphaerica* is characterized by broadly elliptical to sub-spherical ascospores, measuring 20–25 × 18–20 µm, densely ornamented with fine, truncated, or brush-like warts 0.5–1.5 µm in height (Alvarado et al., 2014, 2016). Additionally, *G. sphaerica* possesses a basal cavity with numerous folds, a feature absent in *G. vagans* (Ribes et al., 2016).

The genetic diversity among fungal species significantly surpasses their morphological appearance, necessitating the integration of genetic data with traditional morphological methods for species identification. Genetic markers, such as rRNA gene regions (nrITS, nuclear ribosomal small subunit, and nuclear ribosomal large subunit) and protein-coding gene sequences, have been employed in molecular systematics for decades (Raja et al., 2017). Among these, the ITS region is extensively used in fungal molecular taxonomy, providing valuable insights (White et al., 1990). Additionally, advancements in high-throughput sequencing and bioinformatics now enable whole-genome comparisons and phylogenomic analyses, which may soon surpass traditional molecular phylogenetic studies based on a limited number of marker genes (Marian et al., 2024).

In this study, nuclear ITS rDNA sequences were used to identify the fungal specimens ANK Akata TT 098, ANK Akata TT 124, ANK Akata TT 127, ANK Akata TT 163, ANK Akata TT 207, ANK Akata TT 281, and ANK Akata TT 350. This analysis demonstrated a genetic similarity of over 99% between the specimens and their related isolates of *Genea* (Table 1, Figure 6).

This study reports the first occurrence of *G. fragrans*, *G. pseudobalsleyi*, *G. pseudoverrucosa*, and *G. vagans* in Türkiye. The research achieved precise taxonomic identification using a combined approach of detailed morphological analyses and molecular phylogenetic methods focused on nrITS sequences. As a result, the number of documented *Genea* species known in Türkiye has increased to nine.

Ethics

Ethics Committee Approval: Since the article does not contain any studies with human or animal subject, its approval to the ethics committee was not required.

Data Sharing Statement: All data are available within the study.

Footnotes

Authorship Contributions: Conceptualization: E.K., G.D., and I.A.; Design/methodology: E.K., G.D., and I.A.; Execution/investigation: E.K., G.D., and I.A.; Resources/materials: E.K. and I.A.; Data acquisition: E.K., G.D., Em.K., and I.A.; Data analysis/interpretation: E.Ş., Em.K., and I.A.; Writing – original draft: E.Ş. and I.A.; Writing – review & editing/critical revision: I.A.

Conflict of Interest: No conflict of interest was declared by the authors.

Funding: The study was supported by the Turkish Scientific and Technological Research Council (TÜBİTAK) with project number 121Z924.

References

Agnello, C., Kaounas, V., & Alvarado, P. (2016). Genea gorii, una nuova specie descritta dall'Italia meridionale. *Rivista di Micologia, 59*(3), 195–202.

Akata, İ., Şen, İ., Sevindik, M., & Kabaktepe, Ş. (2022). Truffle checklist of Turkey II with a new record. *Turkish Journal of Agriculture-Food Science and Technology, 10*(10), 1913–1920. https://doi.org/10.24925/turjaf.v10i10.1913-1920.5482

Akata, İ., Şen, İ., Şahin, E., Çöl, B., & Keskin, E. (2023a). Delastria, a new genus of hypogeous fungi record for the Turkish mycobiota. *Trakya University Journal of Natural Sciences, 24*(2), 85–90. https://doi.org/10.23902/trkjnat.1331537

Akata, İ., Kumru, E., Ediş, G., Özbey, B. G., & Şahin, E. (2023b). Three new records for Turkish Agaricales inhabiting Ankara University Beşevler 10th Year Campus area. *Kastamonu University Journal of Forestry Faculty, 23*(3), 250–263. https://doi.org/10.17475/kastorman.1394933

Akata, İ., Kumru, E., Şahin, E., Acar, İ., & Kaya, E. (2024a). Amanita vidua: A new record for Turkish Amanita section Phalloideae based on morphological and molecular data. *Trakya University Journal of Natural Sciences, 25*(1), 97–110. https://doi.org/10.23902/trkjnat.1446327

Akata, İ., Ediş, G., Kumru, E., Acar, İ., & Şahin, E. (2024b). Initial report of Inocybe costinitii in Türkiye with morphological and molecular data. *Kahramanmaraş Sütçü İmam Üniversitesi Tarım ve Doğa Dergisi, 27*(6), 1304–1312. https://doi.org/10.18016/ksutarimdoga.vi.1467628

Akata, İ., Ediş, G., Kumru, E., Acar, İ., & Şahin, E. (2024c). Taxonomic studies on *Rhodocybe asyae* specimens discovered in a new location. *Kahramanmaraş Sütçü İmam Üniversitesi Tarım ve Doğa Dergisi, 27*(Suppl 1), 124–132. https://doi.org/10.18016/ksutarimdoga.vi.1507554

Akata, İ., Kumru, E., Ediş, G., Acar, İ., & Şahin, E. (2024d). Two newly reported Agaricales species from Türkiye with morphological and molecular data. *Kastamonu University Journal of Forestry Faculty, 24*(3), 260–280. https://doi.org/10.17475/kastorman.1599952

Alvarado, P., Cabero, J., Moreno, G., Bratek, Z., Van Vooren, N., Kaounas, V., Konstantinidis, G., Agnello, C., Merényi, Z., & Smith, M. E. (2014). Species diversity of *Genea* (Ascomycota, Pezizales) in Europe. *Ascomycete.org, 6*(3), 41–51. https://doi.org/10.25664/art-0098

Alvarado, P., Cabero, J., Moreno, G., Bratek, Z., Van Vooren, N., Kaounas, V., Konstantinidis, G., Agnello, C., Merényi, Z., Smith, M. E., Vizzini, A., & Trappe, J. M. (2016). Phylogenetic overview of the genus *Genea* (Pezizales, Ascomycota) with an emphasis on European taxa. *Mycologia, 108*(2), 441–456. https://doi.org/10.3852/15-199

Alvarado, P., Healy, R., Moreno, G., Cabero, J., Scholler, M., Schneider, A., Vizzini, A., Kaounas, V., Vidal, J. M., Hensel, G., Rubio, E., Mujic, A., & Smith, M. E. (2018). Phylogenetic studies in *Genabea, Myrmecocystis*, and related genera. *Mycologia, 110*(2), 401–418. https://doi.org/10.1080/00275514.2018.1451140

Alvarado, P., Pérez, J. B., van Vooren, N., Bernauer, T., Hensel, G., & Scholler, M. (2021). *Genea coronata* (Pyronemataceae, Pezizales), a cryptic new species in a highly polymorphic genus. *Sydowia, 73*, 1–12. https://doi.org/10.12905/0380.sydowia73-2020-0001

Berber, O., Uzun, Y., & Kaya, A. (2019). *Genea lobulata*, a new hypogeous ascomycete record for Turkish mycobiota. *Süleyman Demirel Üniversitesi Fen Bilimleri Enstitüsü Dergisi, 23*(3), 922–924. https://doi.org/10.19113/sdufenbed.563863

Berkeley, M. J., & Broome, C. E. (1846). Notices of British hypogaeous fungi. *Annals and Magazine of Natural History, 18*, 73–82. https://doi.org/10.1080/037454809496568

Bertolini, V. (2014). Funghi ipogei: uno sguardo alle Genea. *Bollettino del Circolo Micologico G. Carini, 67*, 21–40.

Bresadola, J. (1893). Mycetes australienses novi, ct emendanda ad Floram Mycologicam Australiae. *Hedwigia, 32*(3), 118–119.

Bratek, Z., Merényi, Z., & Varga, T. (2013). Changes of hypogeous funga in the Carpathian-Pannonian region in the past centuries. *Acta Mycologica, 48*(1), 33–39. https://doi.org/10.5586/am.2013.005

Bucholtz, F. (1901). Hypogaeen aus Russland. *Hedwigia, 40*, 304–322.

Ceruti, A. (1960). *Iconographia mycologica. Supplementum II, Elaphomycetales et Tuberales*. Museo Tridentino di Scienze Naturali.

Corda, A. C. I. (1854). *Icones fungorum hucusque cognitorum* (Vol. 6). F. Ehrlich.

Cribb, J. W. (1960). Two new species of subterranean Ascomycetes from Queensland. *Papers from the Department of Botany, the University of Queensland, 4*, 35–37.

Crous, P. W., Osieck, E. R., Jurjević, Ž., Boers, J., van Iperen, A. L., Starink-Willemse, M., ... & Groenewald, J. Z. (2021). Fungal Planet description sheets: 1284–1382. *Persoonia, 47*, 178–374. https://doi.org/10.3767/persoonia.2021.47.06

Diamandis, S., & Perlerou, C. (2008). Recent records of hypogeous fungi in Greece. *Acta Mycologica, 43*(2), 139–142. https://doi.org/10.5586/am.2008.017

Edgar, R. C. (2004). MUSCLE: multiple sequence alignment with high accuracy and high throughput. *Nucleic Acids Research, 32*(5), 1792–1797. https://doi.org/10.1093/nar/gkh340

Gilkey, H. M. (1939). *Tuberales of North America*. Oregon State Monographs. Studies in Botany, 1, 1–63.

Guevara-Guerrero, G., Stielow, B., Tamm, H., Cázares-Gonzalez, E., & Göker, M. (2012). *Genea mexicana*, sp. nov., and *Geopora tolucana*, sp. nov., new hypogeous Pyronemataceae from Mexico, and the taxonomy of Geopora reevaluated. *Mycological Progress, 11*, 711–724. https://doi.org/10.1007/s11557-011-0781-y

Harkness, H. W. (1899). California hypogaeous fungi. *Proceedings of the California Academy of Sciences, 1*(8), 241–264.

Hawker, L. E. (1954). British hypogeous fungi. *Philosophical Transactions of the Royal Society of London. Series B, Biological Sciences, 237*, 429–546. https://doi.org/10.1098/rstb.1954.0002

Hollós, L. (1911). *Magyarország földalatti gombái, szarvasgombafélei: Fungi hypogaei Hungariae*. K. M. Termeszettudomanyi Tarsulat.

Imai, S. (1933). On two new species of Tuberaceae. *Proceedings of the Imperial Academy of Japan, 9*, 182–184.

Kajevska, I., Rusevska, K., & Karadelev, M. (2013). The Family Pyronemataceae (Pezizales, Ascomycota) in the Republic of Macedonia. *Macedonian Journal of Ecology and Environment, 15*(1), 11–22. https://doi.org/10.59194/MJEE13151011k

Kaounas, V., Agnello, C., & Alvarado, P. (2016). *Genea cephalonicae* sp. nov. Ascomycota, Pezizales, a new hypogeous species from Greece. *Ascomycete.org, 8*(3), 105–110. https://doi.org/10.25664/art-0179

Kumar, S., Stecher, G., Li, M., Knyaz, C., & Tamura, K. (2018). MEGA X: Molecular Evolutionary Genetics Analysis across computing platforms. *Molecular Biology and Evolution, 35*, 1547–1549. https://doi.org/10.1093/molbev/msy096

Læssøe, T., & Hansen, K. (2007). Truffle trouble: What happened to the Tuberales? *Mycological Research, 111*(9), 1075–1099. https://doi.org/10.1016/j.mycres.2007.08.004

Landi, M., Salerni, E., Ambrosio, E., D'Aguanno, M., Nucci, A., Saveri, C., Perini, C., & Angiolini, C. (2015). Concordance between vascular plant and macrofungal community composition in broadleaf deciduous forests in central Italy. *iForest – Biogeosciences and Forestry, 8*(3), 279–286. https://doi.org/10.3832/ifor1199-008

Lawrynowicz, M. (1988). *Grzyby (Mycota) XVIII (Ascomycetes, Elaphomycetales, Tuberales)*. Polska Akademia Nauk.

Marian, I. M., Valdes, I. D., Hayes, R. D., La Butti, K., Duffy, K., Chovatia, M., ... & Ohm, R. A. (2024). High phenotypic and genotypic plasticity among strains of the mushroom-forming fungus *Schizophyllum commune*. *Fungal Genetics and Biology, 173*, 103913. https://doi.org/10.1016/j.fgb.2024.103913

Mattirolo, O. (1900a). Elenco dei "fungi hypogaei" raccolti nelle Foreste di Vallombrosa negli anni 1899–1900. *Malpighia, 14*, 1–24.

Mattirolo, O. (1900b). Gli ipogei di Sardegna e di Sicilia. *Malpighia, 14*, 39–110.

Montecchi, A., & Sarasini, M. (2000). *Funghi ipogei d'Europa*. Associazione Micologia Bresadola.

Moreno-Arroyo, B., Gómez, J., & Calonge, F. D. (1998). *Genea subbaetica*, sp. nov., encontrada en España. *Boletín de la Sociedad Micológica de Madrid, 23*, 85–89.

Osmundson, T. W., Robert, V. A., Schoch, C. L., Baker, L. J., Smith, A., Robich, G., Mizzan, L., & Garbelotto, M. M. (2013). Filling gaps in biodiversity knowledge for macrofungi: contributions and assessment of an herbarium collection DNA barcode sequencing project. *PLOS ONE, 8*(4), e62419. https://doi.org/10.1371/journal.pone.0062419

Paz, A., Chautrand, P., & Lavoise, C. (2016). *Genea amici* una especie nueva encontrada en Córcega. *Yesca, 28*, 139–150.

Paz, A., Chautrand, P., & Lavoise, C. (2019). *Genea darii* une nouvelle espèce du sud de l'Europe. *Bulletin de la Fédération des Associations Mycologiques Méditerranéennes, 55*, 3–14.

Perez, J. B. (2024). Catalogue d'Ascomycètes hypogés de la région Auvergne-Rhône-Alpes. *Bulletin Mycologique et Botanique Dauphiné-Savoie, 253*, 37–49.

Pfister, D. H. (1984). *Genea-Jafneadelphus*-a Tuberalean-Pezizalean connection. *Mycologia, 76*, 170–172. https://doi.org/10.1080/00275514.1984.12023823

Raja, H. A., Miller, A. N., Pearce, C. J., & Oberlies, N. H. (2017). Fungal identification using molecular tools: a primer for the natural products research community. *Journal of Natural Products, 80*(3), 756–770. https://doi.org/10.1021/acs.jnatprod.6b01085

Ribes, M. A., Hernanz, J., Tello, S., Campos, J. C., Paz, A., Sánchez, G., Pancorbo, F., & Serrano, F. (2016). Contribución al conocimiento de la biodiversidad fúngica del Parque Nacional de Ordesa y Monte Perdido I. *Pirineos, 171*, e021. https://doi.org/10.3989/Pirineos.2016.171005

Riva, A. (2009). Wakefieldia macrospora e *Genea fragrans*, due funghi ipogei nuovi per il Ticino. *Schweizerische Zeitschrift für Pilzkunde, 87*, 119–121.

Saccardo, P. A. (1889). *Sylloge Fungorum hucusque cognitorum* (Vol. 8). Patavii.

Saitta, A., Gargano, M. L., Morara, M., Ilice, M., & Venturella, G. (2008). The hypogeous fungi from Sicily (southern Italy): New additions. *Mycologia Balcanica, 5*, 147–152.

Savić, D., Kajevska, I., & Milosavljević, N. (2018). Checklist of Pezizomycetes from Serbia. *Bulletin of the Natural History Museum, 11*, 21–61. https://doi.org/10.5937/bnhmb1811021S

Smith, M. E. (2007). NATS truffle and truffle-like fungi 15: *Genea balsleyi* sp. nov. (Pyronemataceae), a new hypogeous ascomycete from New Jersey. *Mycotaxon, 99*, 239–244.

Smith, M. E., Trappe, J. M., & Rizzo, D. M. (2006). *Genea*, *Genabea*, and *Gilkeya* gen. nov.: Ascomata and ectomycorrhiza formation in a *Quercus* woodland. *Mycologia, 98*(5), 699–716. https://doi.org/10.1080/15572536.2006.11832642

Stewart, E. L., & Heblack, R. K. (1979). Hypogeous fungi of Minnesota: *Genea anthracina* sp. nov. *Mycotaxon, 9*, 451–458.

Tedersoo, L., Hansen, K., Perry, B. A., & Kjøller, R. (2006). Molecular and morphological diversity of pezizalean ectomycorrhiza. *New Phytologist, 170*(3), 581–596. https://doi.org/10.1111/j.1469-8137.2006.01678.x

Trappe, J. M. (1979). The order, families, and genera of hypogeous Ascomycotina (truffles and their relatives). *Mycotaxon, 9*, 297–340.

Trappe, J. M., & Guzmán, G. (1971). Notes on some hypogeous fungi from Mexico. *Mycologia, 63*(2), 317–332. https://doi.org/10.1080/00275514.1971.12019112

Tulasne, L. R., & Tulasne, C. (1851). *Fungi hypogaei: histoire et monographie des champignons hypogés*. F. Klincksieck.

Türkoğlu, A., & Castellano, M. A. (2014). New records of some ascomycete truffle fungi from Turkey. *Turkish Journal of Botany, 38*(2), 406–416. https://doi.org/10.3906/bot-1303-24

Uzun, Y., & Kaya, A. (2019). New additions to Turkish Pezizales from the Eastern Black Sea Region. *Turkish Journal of Botany, 43*, 262–270. https://doi.org/10.3906/bot-1802-34

Vacek, V. (1951). Zemnička kulovitá–*Genea sphaerica* Tul. *Česká Mykologie, 5*(1–2), 3–5.

Velenovský, J. (1922). *České Houby* (Vols. 4–5). České Botanické Společnosti.

Venturella, G., Pecorella, E., Saitta, A., Zambonelli, A., & Morara, M. (2006). Ecology and distribution of hypogeous fungi from Sicily (southern Italy). *Cryptogamie, Mycologie, 27*(3), 201–217.

Vidal, J. M. (1997). Algunos hongos hipogeos nuevos o poco citados de Cataluña (Zygomycotina, Ascomycotina y Basidiomycotina). *Revista Catalana de Micologia, 20*, 25–62.

Vittadini, C. (1831). *Monographia Tuberacearum*. Milano, Italia.

Wallroth, K. F. W. (1833). *Flora cryptogamica Germaniae* (Vol. 2). Nuremberg, Germany.

White, T. J., Bruns, T., Lee, S., & Taylor, J. W. (1990). Amplification and direct sequencing of fungal ribosomal RNA genes for phylogenetics. In M. A. Innis & D. H. Gelfand (Eds.), *PCR Protocols: A Guide to Methods and Applications* (pp. 315–322). Academic Press.

Zeng, M., Gentekaki, E., Zeng, X. Y., Hyde, K. D., Zhao, Q., & Tian, Q. (2022). Evolutionary relationships and allied species of Pyronemataceae, with segregation of the novel family Pyropyxidaceae. *Mycosphere, 13*(2), 207–280. https://doi.org/10.5943/mycosphere/si/1f/7

Zhang, B. C. (1991). Taxonomic status of *Genabea*, with two new species of *Genea* (Pezizales). *Mycological Research, 95*(8), 986–994. https://doi.org/10.1016/S0953-7562(09)80096-8

Zotti, M., Vizzini, A., Di Piazza, S., Pavarino, M., & Mariotti, M. G. (2010). Hypogeous fungi in Liguria (Italy): Distribution and ecology. *Cryptogamie, Mycologie, 31*(1), 47–57.

Trakya University Journal of Natural Sciences, 26(2), 118–126, 2025
DOI: 10.23902/trkjnat.54357889
www.tujns.org

Research Article

Antioxidant, antiradical properties, vitamin and trace element status of *Artemisia spicigera* C. Koch distributed in the Türkiye flora

Damla Yıldız[1], Ahmet Bakır[1]*, Suat Ekin[1], Fevzi Özgökçe[2]

[1]*Van Yüzüncü Yıl University, Faculty of Science, Department of Chemistry, Van, Türkiye*
[2]*Van Yüzüncü Yıl University, Faculty of Science, Department of Biology, Van, Türkiye*

Cite this article as: Yıldız, D., Bakır, A., Ekin, S., & Özgökçe, F. (2025). Antioxidant, antiradical properties, vitamin and trace element status of *Artemisia spicigera* C. Koch distributed in the Türkiye flora. *Trakya University Journal of Natural Sciences, 26*(2), 118–126. https://doi.org/10.23902/trkjnat.54357889

Abstract

It is known that the active substances present in plants contribute to many biochemical processes and provide the balance of organisms. This study aims to determine the antioxidant and antiradical properties of the methanol extract of *Artemisia spicigera (A. spicigera)* C. Koch leaves and to measure the levels of trace elements and vitamins E and K. Trace element analyses were performed by the inductively coupled plasma–optical emission spectroscopy dry ashing dry ashing and vitamin analyses were performed by the high performance liquid chromatography method. Vitamin C, total phenol and flavonoid contencts, antioxidant capacity, DPPH•, ABTS•$^{+}$, O_2•$^{-}$, H_2O_2 and OH• values were determined spectrophotometrically. Total phenolic and flavonoid contents and antioxidant capacity were determined as 18.45 ± 0.39 mgGA/g, 26.29 ± 1.64 mgQE/g and 44.08 ± 2.91 mMAA/g, respectively. Mn, Zn, Cu, α-tocopherol, phylloquinone and ascorbic acid levels were found as 287.32 ± 0.57, 104.36 ± 2.12, 37.40 ± 0.10, 10.28 ± 0.75, 0.149 ± 0.047 µmol/kg and 217.36 ± 29.20 mg/100g, respectively. *In vitro* antioxidant properties determined by DPPH•, ABTS•$^{+}$, H_2O_2 and OH• assays showed maximum inhibitory with respective IC_{50} values of 61.83 ± 0.68, 71.74 ± 0.79, 34.25 ± 0.74 and 77.91 ± 0.88 µg/mL. The IC_{50} values of these assays showed promising antioxidant power. The results obtained in this study showed that the plant leaves migth be a potential candidate for *in vivo* studies to be evaluated in the future. *A. spicigera* can be also used as a potential supplement or in the pharmaceutical industries as a source of natural antioxidants.

Özet

Bitki içeriklerinde bulunan aktif maddelerin pek çok biyokimyasal süreçteki katkıları ve canlı organizmanın dengesini sağladığı bilinmektedir. Bu çalışmada, *Artemisia spicigera (A. spicigera)* C. Koch yaprağının metanol ekstraktının antioksidanve antiradikal özelliklerinin belirlenmesi ve iz element ile vitamin seviyelerinin ölçülmesi amaçlanmıştır. İz element analizleri endüktif eşleştirilmiş plazma – optik emisyon spektroskopisi kuru külleme ile vitamin E ve K analizleri ise yüksek performanslı sıvı kromatografisi yöntemi ile belirlenmiştir. Vitamin C, toplam fenol ve flavonoid içerikleri, antioksidan kapasite, DPPH•, ABTS•$^{+}$, O_2•$^{-}$, H_2O_2 ve OH• değerleri spektrofotometrik olarak tespit edilmiştir. Toplam fenolik ve flavonoid içerik ile antioksidan kapasitesi sırasıyla 18,45 ± 0,39 mgGA/g, 26,29 ± 1,64 mgQE/g ve 44,08 ± 2,91 mMAA/g olarak belirlenmiştir. Mn, Zn, Cu, α-tokoferol, filokinon ve askorbik asit düzeyleri sırasıyla 287,32 ± 0,57, 104,36 ± 2,12, 37,40 ± 0,10, 10,28 ± 0,75, 0,149 ± 0,047 µmol/kg ve 217,36 ± 29,20 mg/100g olarak bulunmuştur. DPPH•, ABTS•$^{+}$, H_2O_2 ve OH• deneyleri ile belirlenen *in vitro* antioksidan özelliklerin, ilgili IC_{50} değerleri 61,83 ± 0,68, 71,74 ± 0,79, 34,25 ± 0,74 ve 77,91 ± 0,88 µg/mL ile maksimum inhibitör göstermiştir. Bu testlerin IC_{50} değerleri ümit verici antioksidan güç göstermiştir. Bu sonuçlar gelecekte değerlendirilecek *in vivo* çalışmalar için *A. spicigera* yaprağının potansiyel bir aday olabileceğini kapsamlı bir şekilde göstemiştir. *A. spicigera* aynı zamanda potansiyel bir takviye veya doğal antioksidan kaynağı olarak ilaç endüstrisinde de kullanılabilir.

Keywords: *Artemisia spicigera*, reactive oxygen species, metal, α-tocopherol, phylloquinone

Edited by: *Yeşim Sağ Açıkel*

***Corresponding Author:** Ahmet Bakır, **E-mail:** ahmetbakir@yyu.edu.tr*

***ORCID iDs of the authors:** DY. 0000-0002-9489-3860, AB. 0000-0003-0797-285X, SE. 0000-0002-6502-5028, FÖ. 0000-0002-3119-8561*

Received: 22 January 2025, **Accepted:** 09 May 2025, **Online First**: 07 July 2025, **Published:** 15 October 2025

Introduction

It has long been known that many traditional medicines originate from plants or plant-based sources. The use of plants as medicine is as old as human history and forms the basis of modern medicine (Maridass & De Britto, 2008). According to World Health Organisation data, 25% of the pharmaceutical drugs used today are obtained from plants used for medicinal purposes. Plants produce a large number of secondary metabolites to protect themselves from external attack. These plant-derived compounds pose less of a threat to human health, and with each passing day a new one is being added to the list of plant-derived compounds, providing an alternative to existing synthetic drugs (Boztaş et al., 2021). Recent studies showed that plant components scavenge free radicals formed by oxidative stress and give effective results in the treatment of many diseases occurring in metabolism. It has also been determined that these plant components have fewer side effects than existing drugs (Sen et al., 2010; Rolnik & Olas, 2021).

The health of humans and all other organisms is closely interconnected. Especially antioxidant-derived components obtained from plants offer important natural food support for the protection of health (Gülçin, 2025). It is supported by studies that these herbal supplements applied after oxidative stress-induced diseases (including cancer) are effective by interrupting oxidative chain reactions (Tao et al,. 2020). According to the International Agency for Research on Cancer, in addition to 9.7 million deaths from cancer worldwide, there were approximately 20 million new cancer cases in 2022, and cases are estimated to reach 29.9 million by 2040. For a long time, studies have been carried out to investigate plants to treat cancer naturally and these studies are still up to date (Bajpai et al., 2024). Natural components such as phenols, flavonoids, polysaccharides, which are bioactive components derived from plants and have antioxidant activity, as well as vitamins and elements contained in plants, have strong anticancer effects. Therefore, natural antioxidant drugs obtained from plants can strengthen specific or non-specific immune function. They can also inhibit the production of free radicals by directly preventing cellular tissue damage caused by free radicals (Chank et al., 2020).

The *Asteraceae* family is widely used in traditional medicine for therapeutic applications throughout the world due to its cosmopolitan distribution (Kljucevsek & Kreft, 2025). The presence of flavonoids in this family is remarkable. Members of this family show a wide range of anti-inflammatory, anti-microbial, antioxidant and hepatoprotective activities (Konovalov, 2014). The currently increasing need for natural medicine resources has increased scientific interest in the *Asteraceae* family. Most members of the family are used in traditional medicine both in Türkiye and around the world due to their essential oil production, phytochemical properties and biological activities (Petretto et al., 2013; Rolnik & Olas, 2021). *Asteraceae* is the richest of flowering plants in terms of genus and species diversity. In Türkiye, 133 genera and 1156 species are known to naturally grow, of which 430 are endemic for the flora of the country. In this respect, the endemism rate of the *Asteraceae* in Türkiye is as high as 38%. The genus *Artemisia* belonging to this family includes perennial and economically valuable plants distributed over a wide geographical area, and is represented by 23 species in the flora of Türkiye (Öztürkmen, 1996).

Some species of the *Asteraceae* family (e.g. *A. annua*) have been reported to be anti-bacterial and anti-malarial effects (Soni et al., 2024). To treat drug-resistant strains of the genus *Plasmodium*, either the drug group artemisinin or plants with fewer side effects are recommended (Xiao et al., 2016; Soni et al., 2024). The important phytochemical artemisinin is synthesised in the leaves and flowers of *Artemisia* species and is currently used in the treatment of malaria worldwide (Czechowski et al., 2018). This compound has been shown to be sensitive on some bacterial species such as *Escherichia coli, Staphylococcus aureus* and *Streptococcus faecalis*. Many scientists attach importance to the synthesis of this compound and its derivatives due to increasing drug costs (Peplow, 2018; Ekiert et al., 2022). *Artemisia spicigera (A. spicigera*) C. Koch [bozkır yavşanı (in Turkish)], the endemic used in the present study, is distributed in Armenia, Central Anatolia and Iran (Chehregani et al., 2013). The plant has antiseptic and stomachic properties and is traditionally recommended in Türkiye for the treatment of skin infections, as well as for skin diseases and ulcerative wounds (Abad et al., 2012; Ghorbani et al., 2021).

No study has investigated the relationship between *A. spicigera* and parameters such as antiradical ($DPPH^{\cdot}$, $ABTS^{\cdot+}$, H_2O_2, $OH^{\cdot}$ and $O_2^{\cdot-}$) properties, vitamin (α-tocopherol, phylloquinone and ascorbic acid) and trace element status (As, Be, Cd, Cr, Cu, Sr, Pb, Mo, Li, Mn, Ti, Co, Tl and Zn). However, total phenol, flavonoid contents and antioxidant capacity levels of *A. spicigera* and *A. splendens* plant species collected from Iran region were determined (Afshar et al., 2012).

This study aimed to investigate the free radical scavenging activity of methanol extract of *A. spicigera* leaves by using $DPPH\bullet$, $ABTS\bullet^{+}$, hydrogen peroxide (H_2O_2), hydroxyl ($OH\bullet$) and superoxide ($O_2\bullet$) antioxidant methods. Total phenol, flavonoid content, total antioxidant capacity, vitamins C, E, K and trace element values in dry leaf content were also determined.

Materials and Methods

Plant Materials

The leaves of *A. spicigera* (*Asteraceae)* have been collected in September 2019 in the Saray/Kazlıgöl district of Van city, Türkiye (38° 32' 38.63" N, 44° 12' 17.90" E, at an altitude 2206 m). *A. spicigera* was defined by Prof. Dr. Fevzi Özgökçe. The sample was deposited in Van YYU herbarium, Botany Department, VANF16271. The plant leaf was dried in the shade for a period of two weeks. After drying, the leaves were ground to a fine powder in a super mixer rotary stainless grinder (new nova industrial kitchen equipment, model: Inox SM 108) and stored in coloured glass bottles for analysis.

Leaf Extraction Process

The plant material was pulverized and weighed (20 g), and methanol (MeOH-80%) was added at room temperature (24°C). The plant-MeOH mixture (1:20, g/v) was subjected to the extraction process

for 48 hours to ensure that the pulverized plant dissolves at the highest rate in methanol. Then the mixture was centrifuged at 4.500 rpm for 15 minutes and filtered with a Whatman grade 1 filter paper. Methanol in the filtrate was extracted using a rotary evaporator at 45°C under reduced pressure and the filtrate was removed. The residue remaining in the volumetric flask was lyophilized at -65°C to ensure that the remaining extract was thoroughly removed. It was then dissolved in methanol and made ready for studies. All the steps in the above described procedure were adapted with slight modifications following the method of Cai et al. (2004).

Determination of Trace Elements

The experimental process for trace element determinations was carried out according to the study of Zurera et al. (1987). 1000 mg of the plant sample was placed in a porcelain crucible, in three replicates. 2.1 mL of ethyl alcohol-sulphuric acid solution was added to the samples. The oven was set at 250°C and kept at the same temperature for 1 hour. Then the temperature of the muffle furnace was increased by 50°C every one hour. This process continued until the temperature of the furnace was 550°C. The samples were kept overnight at the final temperature. 5 mL of hydrochloric acid solution was added and made up to 25 mL. The samples were kept for 5–6 hours and then filtered with filter paper and made ready for analysis. Elemental analyses were carried out using the ICP-OES (Thermo iCAP 6300 Due, England) device.

Measurement of Total Phenolic Content

The determination of the total phenol content of the methanol extract of *A. spicigera* leaves was performed using the Folin-Ciocelteu (FCR) indicator (Yi et al., 1997; Gamez-Meza et al., 1999). 300 µg of 2% sodium carbonate was added to the prepared samples, then 100 µL of FCR indicator was added and incubated for 2.5 hours at room temperature. The absorbance of the samples was read against the control sample at 765 nm. A standard curve was constructed using different concentrations of gallic acid solution. The total phenol content of the plant was reported in milligrams of gallic acid equivalent (GAE) per gram of dried extract (mg GAE/g).

Measurement of Total Flavonoid Content

The extract prepared for the determination of the total flavonoid content of *A. spicigera* was diluted with methanol and used. 500 µL of this diluted solution was taken and 100 µL potassium acetate, 100 µL aluminium nitrate and 4.6 mL ethanol were added and vortexed. The mixture was kept for 45 min at room temperature. The absorbance of the samples was read against the control sample at 415 nm (Lamaison et al., 1990). Flavonoid concentration was calculated by plotting quercetin and the total flavonoid content of the samples was reported as quercetin equivalent (mg QE/g).

Measurement of Total Antioxidant Capacity

The measurement of the total antioxidant capacity of *A. spicigera* was based on the study of Prieto et al. (1999). The prepared plant extract was diluted with methanol and 0.2 mL was taken for each sample. 2 mL of marker solution [0.6 M H_2SO_4 + 28 mM Na_2HPO_4 + 4 mM $(NH_4)_2MoO_4$] was added to the samples and kept in a 100°C water bath for 90 min. Samples were read against the control at the appropriate wavelength. A standard graph was drawn using ascorbic acid solution and used for total antioxidant capacity calculation. Total antioxidant capacity is given as mM ascorbic acid/g.

Scavenging Activity of DPPH• Free Radical

In this method, extracts of different concentrations were placed in test tubes. 5 mL of DPPH (0.004%) solution was added to 200 µL of sample and incubated in the dark for 30 minutes. The absorbance values of the samples were read against the control sample (DPPH) at 517 nm and recorded. The inhibition percentages of the samples were calculated by Equation 1. BHT was used as positive control value. The obtained % inhibition values were plotted against the concentration. Then, the 50% inhibition values (IC_{50}) of the plant extract against DPPH• radical was determined (Cuendet et al., 1997; Chen et al., 2009).

Equation 1

$$\text{Inhibition (\%)} = \left\{ \frac{A_{Blank} - A_{Sample}}{A_{Blank}} \right\} X\ 100$$

Scavenging Activity of Superoxide ($O_2^{\bullet -}$) Free Radical

This method is based on measuring the absorbance of NBT at 560 nm with a spectrophotometer (Zhishen et al., 1999). 0.05 M phosphate buffer (pH: 7.8) was prepared. 200 µL riboflavin, 0.2 mL L-methionine and 0.2 mL NBT were added to the samples. The samples were kept under fluorescent light for 40 minutes at room temperature. Absorbance was measured at 560 nm against the control sample and compared with BHT. The % inhibition values of the samples were determined using Equation 2.

Equation 2

$$\text{Inhibition (\%)} = \left\{ \frac{A_{Blank} - A_{Sample}}{A_{Blank}} \right\} X\ 100$$

Hydrogen Peroxide (H_2O_2) Radical Scavenging Activity

At 230 nm, the absorbance values of the samples were read against the control sample (Ruch, 1989). 43 mM H_2O_2 solution was prepared using phosphate buffer (pH: 7.4). Plant samples were taken at different concentrations. BHT solution was used as the standard antioxidant substance. The volume of the BHT solution was completed to 0.4 mL with buffer solution. Then 0.6 mL of H_2O_2 solution was added and the mixture was kept at room temperature for 10 minutes. After the waiting time, absorbance values were read and recorded at 230 nm against the control sample (buffer solution). Inhibition values were calculated according to Equation 3.

Equation 3

$$\text{Inhibition (\%)} = \left\{ \frac{A_{Blank} - A_{Sample}}{A_{Blank}} \right\} X\ 100$$

Hydroxyl Radical (OH•) Scavenging Activity

In this method, OH• radical was formed by EDTA/Fe^{+3}/ascorbate/H_2O_2 system and absorbance was measured at 532 nm with spectrophotometer by using the competitive reaction property of deoxyribose (Kunchandy & Rao, 1990).

Stock samples were added to solutions of 2.8 mM deoxyribose, 1 mM $FeCl_3$, 1 mM EDTA, 1 mM ascorbic acid and 1 mM H_2O_2. 20 mM phosphate buffer (pH: 7.4) was prepared. This phosphate buffer was added to the samples to a final volume of 1 mL. The samples were kept in an oven at 37°C for 1.5 hour. Then 1000 µL TBA and 1000 µL TCA were added and vortexed, and the mixture was kept in an oven at 100°C for 30 minutes. The absorbance values of the samples were read against the control sample at 532 nm and recorded. The % inhibition values were plotted and IC_{50} values were determined. The obtained data were compared with BHT and inhibition values were calculated according to Equation 4.

Equation 4

$$\text{Inhibition (\%)} = \left\{ \frac{A_{Blank} - A_{Sample}}{A_{Blank}} \right\} X\ 100$$

Scavenging Activity of ABTS•$^+$ Free Radical

The methanol extract of *A. spicigera* leaves was carried out according to the method of Pellegrini et al. (1999) with a slight modification. $ABTS^{-+}$ radical was prepared in 2.45 mM potassium persulfate and 2 mM ABTS phosphate buffered solution. These two solutions were then mixed and kept at room temperature in darkness for 12–16 hours to form $ABTS^{-+}$ cation radical. $ABTS^{-+}$ cation radical was diluted appropriately and its absorbance at 734 nm was adjusted to 0.70–0.75 and used in the experiment. The radical was then added to stock solutions prepared at different concentrations. Activity (%) was calculated using Equation 5. The plant's scavenging power against stable free radicals was performed with a synthetic antioxidant, trolox.

Equation 5

$$\text{Inhibition (\%)} = \left\{ \frac{A_{Blank} - A_{Sample}}{A_{Blank}} \right\} X\ 100$$

Vitamin C (Ascorbic Acid) Analysis of *A. spicigera* Extract

In order to determine the vitamin C content of *A. spicigera* leaves, vitamin C was measured at 521 nm wavelength using ultraviolet-visible spectrophotometric method. 500 mg of the plant sample was taken and placed in plastic tubes. The experiment was performed in three replicates. 2 mL of HPO_3 acid and 0.5% oxalic acid were added to the tubes and centrifuged at 5000 rpm for 5 min. 2 mL of the filtrate was taken and 0.05 mL thiourea and 0.5 mL 2,4 dinitrophenylhydrazine were added. The samples were then placed in a 90°C water bath for 6 minutes. Then 2 mL of sulphuric acid solution was slowly added to the samples placed in an ice bath. After reaching the appropriate temperature, the samples were vortexed and their absorbance was measured against the control sample. The recorded ascorbic acid concentration values were calculated from the calibration graph (Golubkina et al., 2018).

Vitamin E (α-tokoferol) and K (Phylloquinone) Analysis of *A. spicigera* Extract by High Performance Liquid Chromatography

For phylloquinone and α-tocopherol, a stock solution was prepared at 500 µg/mL, diluted with methanol as appropriate. Linear regression analysis of the peak area versus standard solution concentrations was used to calculate the calibration.

The amount of phylloquinone and α-tocopherol in *A. spicigera* leaves was determined according to the method described in the literature (Sahin et al., 2005; Al-Saleh et al., 2006). For the analysis, 300 mg of the plant was weighed. Hexane-ethanol (50:30) solution was added and kept overnight. The samples were filtered and taken into 1 mL tubes (this procedure was repeated three times). 0.01% BHT was added in each tube, the tubes were vortexed and kept in the dark for 25 hours. Then they were centrifuged at +4°C and 5000 rpm for 15 min. The supernatant was filtered using a filter paper and 500 µL n-hexane was added and dried at 37°C under nitrogen gas. After drying, the residue was dissolved in 500 µL MeOH + C_4H_8O (98%) and prepared for analysis.

Phylloquinone and α-tocopherol analyses were performed on a Gl Science C18 reversed phase HPLC column (250 x 4.6 mm ID), methanol (80 mL) + tetrahydrofuran (20 mL) mobile phase, 1500 µL/min flow rate at 24°C. HPLC (brand: Agillent, model: 1100) - applications were performed at 248 nm phylloquinone and 290 nm α-tocopherol in 0.1 mL volumes in dark bottles in a tray autosampler (-10°C) using a photodiode array detector. Chromatographic analysis was performed at 40°C by isocratic elution.

Statistical Analysis

Experiments were performed with three replicates of each treatment measurements. Means and standard errors of the data were shown as X ± SEM. Group plots were constructed by finding X ± scanning electron microscope. IC_{50} values were determined using nonlinear regression analysis. The statistical analysis were performed by the software SPSS v23 (Chicago, USA).

Results

Folin-Ciocalteu reducing capacity [Folin-Ciocalteu Reagent (FCR) Assay], flavonoid content, total antioxidant capacity, vitamins and trace elements were evaluated to determine the antioxidant properties of methanol extract of *A. spicigera* leaves and results are shown in Table 1. 1,1-diphenyl-2-picrylhydrazyl (DPPH•)

radical scavenging, 2,2¢-azinobis-(3-ethylbenzothiazoline-6-sulphonate) radical (ABTS•$^+$) scavenging, hydrogen peroxide (H_2O_2), superoxide radical anion (O_2•$^-$), hydroxyl radical (OH•) scavenging % inhibition and IC_{50} (µg/mL) values compared to the positive control (BHT and trolox) are presented in Table 2.

Total phenol, flavonoid content and total antioxidant capacity values of methanol extract of *A. spicigera* leaves are shown in Figure 1. The % inhibition and IC_{50} values of *A. spicigera* against DPPH•, ABTS•$^+$, H_2O_2, OH• and O_2•$^-$ radicals after comparison with standard antioxidant (BHT and trolox) are shown in Figures 2-6.

The levels of As, Be, Cd, Co, Mo, Pb and Tl and phylloquinone measured in the dry leaves of A. spicigera are shown in Figure 7, and of Cu, Mn, Li, Sr, Ti, Zn and Cr, α-tocopherol and ascorbic acid are shown in Figure 8.

Discussion

If there are too many free radicals in the cell or if the protection provided by antioxidants is low and inadequate, oxidative stress develops in a way that can lead to chronic and permanent damage (Abdollahi et al., 2004). In this case, oxidative stress causes tissue damage in the cell and as a result, many diseases such as cardiovascular and diabetes occur (Tao et al., 2020; Block et al., 2002).

Natural antioxidant compounds have pharmacological potential as they have little or no side effects. Plants are a source of natural antioxidants that prevent oxidative stress. The most important natural antioxidants are flavonoids, tocopherols and phenolic acids. This is why antioxidant-containing compounds can help prevent many diseases, especially those associated with ROS (Kafshboran et al., 2011). The important flavone compound of *A. spicigera* species is hispidulin. This compound is known as anti-cancer (Chaudhry et al., 2024).

α-Tocopherol, phylloquinone and vitamin C contents of *A. spicigera* were evaluated. α-tocopherol exhibits significant antioxidant activity. Considering that *A. spicigera* has not been examined in terms of vitamin parameters in any study conducted to date, these data will make a significant contribution to the literature. In addition, the FCR assay, flavonoid content and total antioxidant capacity of the plant leaf were measured (Table 1 and Figures 1, 7, 8).

In this study, the activity of methanolic extracts (40% MeOH-water) of *A. spicigera* and *A. splendens* growing in Iran was investigated and the total phenolic content of *A. spicigera* was determined as 33.69 ± 1.49 in mg/100 g, total flavonoid content as 96.41 ± 8.74 in mg/100 g, and antioxidant activity (RC_{50}) as 0.0121 ± 0.003 in mg/L. Kafshboran et al. (2011) investigated the radical scavenging activity of *A. spicigera* according to its flavonoid content and when the total phenol and flavonoid contents of *A. spicigera* plants collected from different regions were compared, it was found that *A. spicigera* plants collected from Sufian regions had higher total phenol and flavonoid contents. When the results are compared

Table 1. Vitamins E, C and K, and trace element (As, Be, Cd, Cr, Cu, Sr, Pb, Mo, Li, Mn, Ti, Co, Tl, Zn) levels, and total phenolic and flavonoid content, and antioxidant capacity in leaves of *Artemisia spicigera*.

Parameters	**$\bar{X}$ ± SEM**
α-tocopherol (µmol/kg) (y = + 2.3645 18.3313x; r^2 = 0.9949) Vitamin C (mg 100/g) (y = 0.1268 + 0.1267x; r^2 = 0.9889) Phylloquinone (µmol/kg) (y = + 16.093 101.33x; r^2 = 0.9783)	10.28 ± 0.75 217.36 ± 29.20 0.149 ± 0.047
Total phenolic content (mg GA/g)	18.45 ± 0.39
Total flavonoid content (mg QE/g)	26.29 ± 1.64
Total antioxidant capacity (mM AA/g)	44.08 ± 2.91
As (mmol/kg)	1.22 ± 0.01
Be (mmol/kg)	2.31 ± 0.12
Cd (mmol/kg)	0.47 ± 0.006
Cr (mmol/kg)	7.66 ± 0.21
Cu (mmol/kg)	37.40 ± 0.10
Sr (mmol/kg)	110.40 ± 0.66
Pb (mmol/kg)	1.74 ± 0.59
Mo (mmol/kg)	2.18 ± 0.035
Li (mmol/kg)	155.14 ± 0.49
Mn (mmol/kg)	287.32 ± 0.57
Ti (mmol/kg)	54.59 ± 0.83
Co (mmol/kg)	0.95 ± 0.008
Tl (mmol/kg)	0.31 ± 0.085
Zn (mmol/kg)	104.36 ± 2.12

GA = gallic asid; QE = quercetin; AA = ascorbic acid; SEM = standard error of the mean. Values are expressed as ± SEM). All values are mean ± standard deviation of three replicates.

Table 2. Values of % inhibition and IC_{50} (µg/mL) in methanol extract of leaf of *Artemisia spicigera* compared with a positive control.

	Control	**% inhibition ($\bar{X}$ ± SEM)**	**IC_{50} (µg /mL) ($\bar{X}$ ± SEM)**
DPPH•		89.55 ± 0.04	61.83 ± 0.68
	BHT	83.65 ± 0.29	49.58 ± 0.54
ABTS•$^+$		90.03 ± 1.85	71.74 ± 0.79
	Trolox	93.71 ± 0.04	26.23 ± 0.36
H_2O_2		53.93 ± 0.22	34.25 ± 0.74
	BHT	55.59 ± 0.24	19.92 ± 0.37
OH•		65.79 ± 0.33	77.91 ± 0.88
	BHT	77.12 ± 1.02	103.40 ± 234
O_2•$^-$		69.88 ± 0.43	
	BHT	63.11 ± 2.88	

SEM = standard error of the mean.

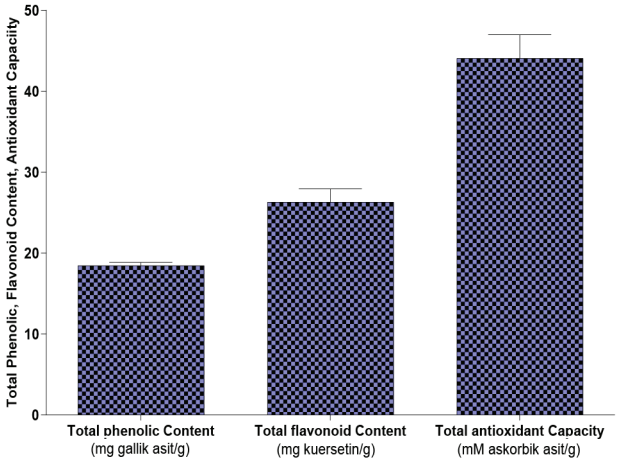

Figure 1. Total phenol, flavonoid content and total antioxidant capacity of *A. spicigera.*

as shown in Table 1, it was determined that the folin-ciocolteu reducing capacity and phenolic content values were lower in our study, but the total antioxidant capacity was very high (44.08 ± 2.91 mM AA/g). The level of active content of each plant may definitely differ depending on the family it is in, the soil structure where it grows, its geographical location, and the climate it is in.

The elemental composition of plants is an important quality parameter that shows the degree of safety of plants and the effect of mineral content on their biological activity. The elements present in the structure of the plant are also important as they will affect the drugs to be obtained from the plant (Golubkina et al., 2018; Chaachouay & Zidane, 2024).

In our current study, trace elements levels of *A. spicigera* were determined and the values found are shown in Table 1 and Figures 7, 8. When the results obtained were compared, it was observed that there was a degreasing relationship between Mn > Li > Sr > Zn > Ti > Cu > Cr > Be > Mo > Pb > As > Co > Cd > Tl. Golubkina et al. (2018) determined the presence of 26 elements in *A. abrotanum,*

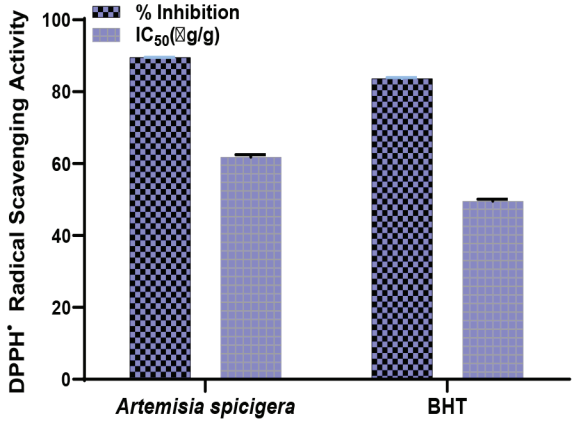

Figure 2. % inhibition of DPPH• radical and IC_{50} value for *A. spicigera* and standard antioxidant BHT.

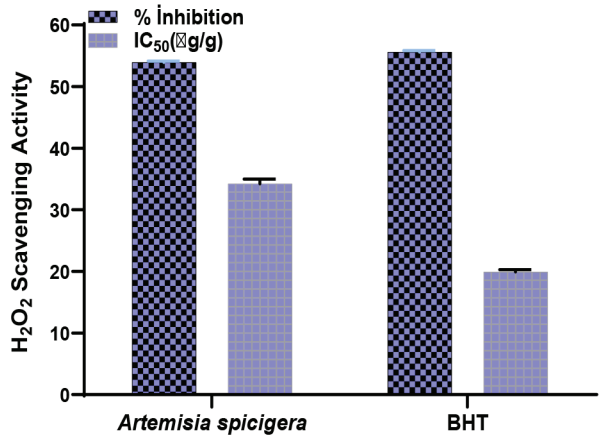

Figure 4. % inhibition of H_2O_2 radical and IC_{50} value for *A. spicigera* and BHT.

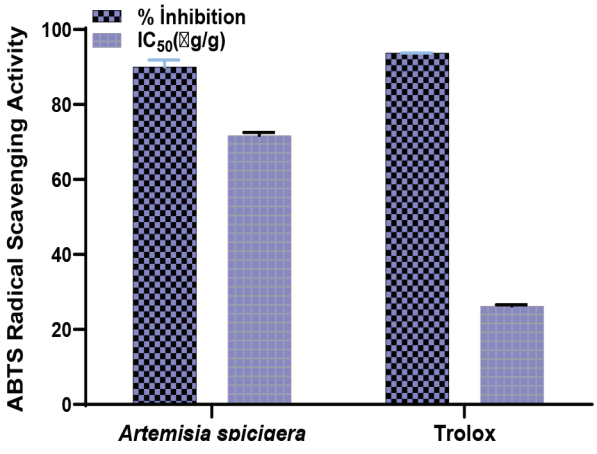

Figure 3. % inhibition of ABTS•$^+$ radical and IC_{50} value for *A. spicigera* and standard antioxidant trolox.

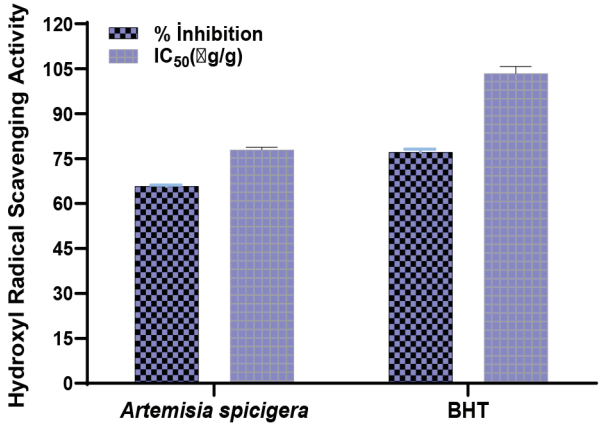

Figure 5. % inhibition of OH• radical and IC_{50} value for *A. spicigera* and BHT.

A. feddei, A. taurica willd, A. dranculucus, A. annua, A. santonica and *A. scoporia* by the ICP-MS method. The presence of Al, Cr, Pb, As and V as heavy metals in *A. scoparia* and Mn, I, Zn and Cu in *A. annua* were determined. In addition, a high Na content was determined in *A. santonica*. However, differently, the presence of trace elements such as Mo, Mn and Co was detected in *A. spicigera.*

In our study, the anti-radical capacity of *A. spicigera* was evaluated by measuring the DPPH• radical scavenging avtivity and the inhibition percentage and IC_{50} concentration results are given in Table 2 and Figure 2. The lower the IC_{50} value, the higher the anti-radical capacity. IC_{50} is the concentration of a substance required to inhibit a specific biological or biochemical function by 50%. On the other hand, this value gives us an idea of how effective a substance is at inhibiting a target and also allows us to compare biological activity between different compounds under the same conditions (Marinova & Batchvarov, 2011; Gülçin & Alwasel, 2023). According to our results, the methanolic extract of leaves of *A. spicigera* showed significant radical scavenging activity showing a value close to BHT (IC_{50} 61.83 µg/mL).

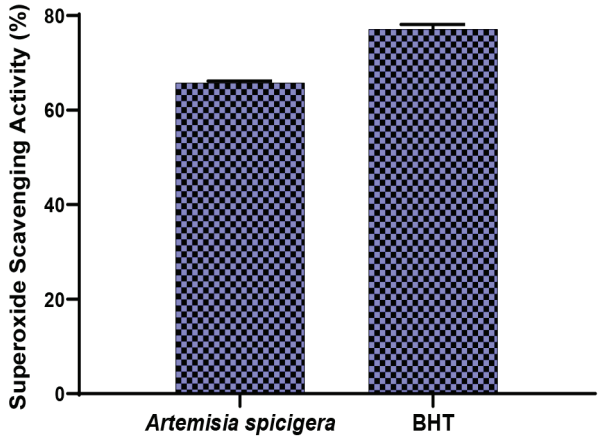

Figure 6. Values of % inhibition of $O_2\bullet^-$ radical for *A. spicigera* and BHT.

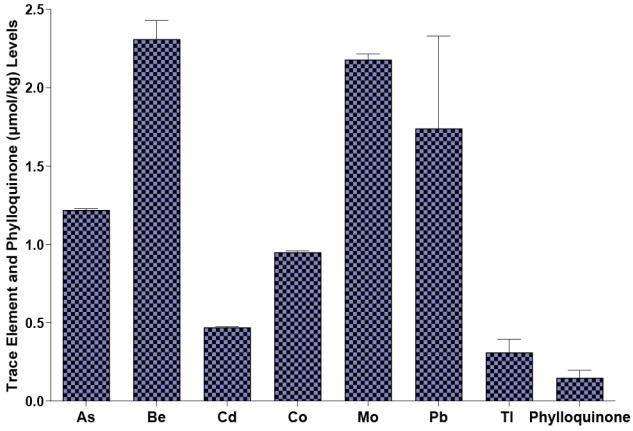

Figure 7. Trace element (As, Be, Cd, Co, Mo, Pb and Tl) and phylloquinone levels in the dry leaves of *A. spicigera.*

Lee et al. (2015) conducted a study on the measurement of DPPH• radical scavenging activity of *A. annua, A. feddei, A. apiacea, A. argyi, A. japonica, A. capillaris, A. gmelinii, A. japonica* ssp. *littoricola, A. keiskeana, A. montana, A. indica, A. rubripes, A. selengensis, A. sieversiana* and *A. stolonifera*. IC_{50} (µg/mL) values for these species were 190.54 ± 2.80, 71.70 ± 4.53, 36.32 ± 4.92, 33.05 ± 1.12, 46.41 ± 7.60, 448.15 ± 78.48, 71.41 ± 2.90, 59. 27 ± 1.51, 74.31 ± 6.42, 18.10 ± 2.04, 60.11 ± 4.67, 38.00 ± 1.27, 54.25 ± 0.96, 336.75 ± 18.34 and 6.64 ± 0.34, respectively. When the DPPH• radical scavenging activity of these species was compared with *A. spicigera,* it was observed that *A. spicigera* showed better radical scavenging activity than approximately 50% of the plants studied.

Kafshboran et al. (2011) investigated the DPPH• radical scavenging activity of *A. spicigera* collected from 5 different regions of East Azerbaijan. Compared to our study, *A. spicigera* (IC_{50} 61.83 ± 0.68) collected from Sufian (ASS, IC_{50} 32.18), Ahar (ASA, IC_{50} 29.74) and Khaje (ASK, IC_{50} 58.93) regions had lower DPPH• radical scavenging activity than the species collected from Dare-diz (ASD, IC_{50} 62.94) and Julfa (ASJ, IC_{50} 64.18) regions. In general, it was observed that there was a consistent with the plants collected in 3 regions and the region we collected.

In the presence of H_2O_2 and $O_2\bullet^-$ radicals OH• radical, which is highly reactive and harmful among free radicals, is formed (Tumilaar et al., 2024). The very short half-life of the OH• radical causes it to react rapidly with some molecules such as sugars, amino acids, nucleic acids, making this radical dangerous. So much so that it causes serious damage to proteins, carbohydrates, DNA and lipids (Sen et al., 2010).

In our study, H_2O_2, OH• scavenging and $O_2\bullet^-$ values in methanol extract of *A. spicigera* leaves were determined. High inhibition percentages and IC_{50} values of H_2O_2 and OH• are given in Table 2 and Figures 4 and 5. In addition, the inhibition percentage of $O_2\bullet^-$ radical anion is shown in Figure 6. The results showed that the H_2O_2 radical scavenging activity of *A. spicigera* was lower than that of BHT, while its OH• radical scavenging activity. The scavenging activity of the plant for $O_2\bullet^-$ radical was also more effective compared to BHT.

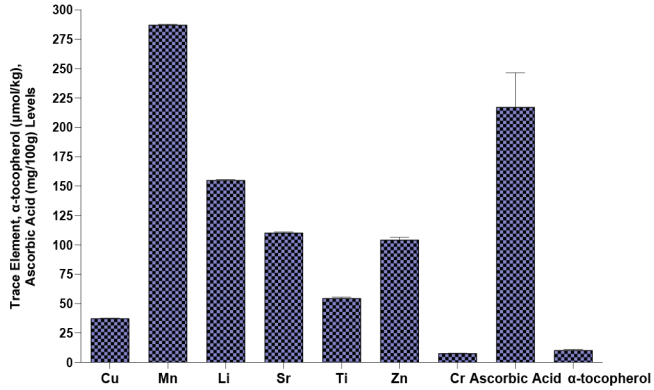

Figure 8. Trace element (Cu, Mn, Li, Sr, Ti, Zn and Cr) levels, ascorbic acid and α-tocopherol levels in the dry leaf of *A. spicigera.*

ABTS•$^+$ is not a radical but reacts with potassium persulfate or sodium persulfate to form ABTS•$^+$ radical. This radical is dark blue/green in colour and is quite stable. Through this radical, the antioxidant capacity of the solutions can be determined. In the presence of antioxidant, dark blue/green colour lightening occurs (Erel, 2004). We investigated the ABTS•$^+$ radical scavenging activity of *A. spicigera*. The highest inhibition percentage of the methanol extract was 90.03 ± 1.85, while it was 93.71 ± 0.04 for trolox. Fifty per cent inhibition of ABTS•$^+$ radical was determined as 71.74 ± 0.79 µg/mL for *A. spicigera* and 26.23 ± 0.36 µg/mL for trolox (Table 2 and Figure 3). When the results were examined, it was determined that the percentage inhibition values of the plant and trolox were very close to each other and the plant had a radical scavengingactivity. In the study conducted by Lee et al. (2015) on the measurement of ABTS•$^+$ radical scavenging activity of *A. annua, A. japonica ssp. littoricola, A. apiacea, A. argyi, A. capillaris, A. feddei, A. gmelinii, A. japonica, A. keiskeana, A. montana, A. indica, A. rubripes, A. selengensis, A. sieversiana* and *A. stolonifera* were determined as 74.46 ± 1.12, 38.27 ± 1.93, 19.22 ± 0.37, 11.93 ± 0.62, 115.80 ± 3.61, 46.59 ± 4.21, 60.34 ± 2.84, 28.55 ± 1.30, 44.99 ± 1.58, 12.75 ± 0.26, 35.86 ± 2.60, 29.82 ± 0.21, 27.50 ± 2.25, 232.39 ± 12.22 and 15.39 ± 0.24, respectively. When the studies were compared, it was observed that the ABTS•$^+$ radical scavenging activity of *A. spicigera* plant used in the study showed lower radical scavenging activity compared to other plant species.

Conclusion

The results obtained showed that the vitamin, total phenol, flavonoid and antioxidant capacity levels and trace element ratios of *A. spicigera* were at a significant level. The methanol extract of *A. spicigera* leaves showed a better antioxidant power compared to the synthetic antioxidant of OH• and O_2•$^-$ radicals. In the same way, it was observed that the plant extract had scavenging effects on DPPH• and ABTS•$^+$ radicals, but lower than the synthetic antioxidants used for comparison. The fact that *A. spicigera* is used as a spice in food and also as a natural remedy for many diseases develops the idea that this plant has antioxidant properties, and the data obtained here are in parallel with this idea. This plant can be also used as a potential supplement or in the pharmaceutical industries as a source of natural antioxidants.

Ethics

Ethics Committee Approval: Since the article does not contain any studies with human or animal subject, its approval to the ethics committee was not required.

Data Sharing Statement: All data are available within the study.

Footnotes

Author Contributions: Conceptualization: D.Y., A.B., and S.E.; Design/methodology: D.Y., A.B., and S.E.; Execution/investigation: D.Y., A.B., and S.E.; Resources/materials: D.Y., A.B., S.E., and F.Ö.; Data acquisition: D.Y., A.B., and S.E.; Data analysis/interpretation: D.Y., A.B., and S.E.; Writing – original draft: D.Y., A.B., and S.E.; Writing – review & editing/critical revision: D.Y., A.B., and S.E.

Conflict of Interest: The authors have no conflicts of interest to declare.

Funding: The study was supported by the Van Yüzüncü Yıl University Scientific Research Projects Coordination Unit with project number 2022 FDK-9894.

References

Abad, M. J., Bedova, L. M., Apaza, L., & Bermejo, P. (2012). The *Artemisia L.* genus: a review of bioactive essential oils. *Molecules, 17*, 2542–2566. https://doi.org/10.3390/molecules17032542

Abdollahi, M., Ranjbar, A., Shadnia, S., Nikfar, S., & Rezaie, A. (2004). Pesticides and oxidative stress: a review. *Medical Science Monitor, 10*(6), 141–147.

Afshar, F. H., Delazar, A., Nazemiyeh, H., Esnaashari, S., & Moghadam, S. B. (2012). Comparison of the total phenol, flavonoid contents and antioxidant activity of methanolic extracts of *Artemisia spicigera* and *A. splendens* growing in Iran. *Pharmaceutical Sciences, 18*(3), 165–170.

Al-Saleh, I. A., Billed, G., & El-Doush, I. I. (2006). Levels of selenium, dl α-tocopherol, dl-γ- tocopherol, all-trans-retinol, thymoquinone, and thymol in different brands of *Nigella sativa* seeds. *Journal of Food Composition and Analysis, 19*(2–3), 167–175. https://doi.org/10.1016/j.jfca.2005.04.011

Bajpai, P., Usmani, S., Kumar, R., & Prakash, O. (2024). Recent advances in anticancer approach of traditional medicinal plants: A novel strategy for cancer chemotherapy. *Intelligent Pharmacy, 2*(3), 291–304. https://doi.org/10.1016/j.ipha.2024.02.001

Block, G., Dietrich, M., Norkus, E. P., Morrow, J. D., Hudes, M., Caan, B., & Packer, L. (2002). Factors associated with oxidative stress in human populations. *American Journal of Epidemiology, 156(3), 274–285.* https://doi.org/10.1093/aje/kwf029

Boztaş, G., Avcı, A. B., Arabacı, O., & Bayram, E. (2021). Economic status of medicinal and aromatic plants in the world and in Türkiye. *Theoretical and Applied Forestry, 1*, 27–33.

Cai, Y., Luo, Q., Sun, M., & Corke, H. (2004). Antioxidant activity and phenolic compounds of 112 traditional Chinese medicinal plants associated with anticancer. *Life Sciences, 74*, 2157–2184. https://doi.org/10.1016/j.lfs.2003.09.047

Chaachouay, N., & Zidane, L. (2024). Plant-derived natural products: a source for drug discovery and development. *Drugs and Drug Candidates, 3*(1), 184–207. https://doi.org/10.3390/ddc3010011

Chank, X., Zhanq, T., Zhank, W., Zhao, Z., & Sun, J. (2020). Natural drugs as a treatment strategy for cardiovascular disease through the regulation of oxidative stress. *Oxidative Medicine and Cellular Longevity, 2020*, 5430407. https://doi.org/10.1155/2020/5430407

Chaudhry, G. E. S., Zeenia, Sharifi-Rad, J., & Calina, D. (2024). Hispidulin: a promising anticancer agent and mechanistic breakthrough for targeted cancer therapy. *Naunyn-Schmiedeberg's Archives of Pharmacology, 397*(4), 1919–1934. https://doi.org/10.1186/s12917-024-03983-3

Chehregani, A., Atri, M., Yousefi, S., Albooyeh, Z., & Mohsenzadeh, F. (2013). Essential oil variation in the populations of *Artemisia spicigera* from northwest of Iran: chemical composition and antibacterial activity. *Pharmaceutical Biology, 51*(2), 246–252. https://doi.org/10.3109/13880209.2012.717631

Chen, Y., Chang, H., Wang, C., & Cheng, F. (2009). Antioxidative activities of hydrolysates from duck egg white using enzymatic hydrolysis. *The Asian-Australasian Journal of Animal Sciences, 22*(11), 1587–1593.

Cuendet, M., Hostettmann, K., & Potterat, O. (1997). Iridoid glucosides with free radical scavenging properties from *Fagraea blumei. Helvetica Chimica Acta, 80*, 1144–1152.

Czechowski, T., Larson, T. R., Catania, T. M., Harvey, D., Wei, C., Essome, M., Brown, G. D., & Graham, I. A. (2018). Detailed phytochemical analysis of high-

and low artemisinin-producing chemotypes of *Artemisia annua*. *Frontiers in Plant Science, 9*, 641. https://doi.org/10.3389/fpls.2018.00641

Ekiert, H., Klimek-Szczykutowicz, M., Rzepiela, A., Klin, P., & Szopa, A. (2022). *Artemisia* species with high biological values as a potential source of medicinal and cosmetic raw materials. *Molecules, 27*(19), 6427. https://doi.org/10.3390/molecules27196427

Erel, O. (2004). A novel automated direct measurement method for total antioxidant capacity using a new generation, more stable ABTS radical cation. *Clinical Biochemistry, 37*(4), 277–285. https://doi.org/10.1016/j.clinbiochem.2003.11.015

Gamez-Meza, N., Noriega-Rodriguez, J. A., Medina-Juarez, L. A., Ortega-Garcia, J., Cazarez-Casanova, R., & Angulo-Guerrero, O. (1999). Antioxidant activity in soybean oil of extracts from Thompson grape bagasse. *Journal of the American Oil Chemists' Society, 76*, 1445–1447.

Ghorbani, S., Kosari Nasab, M., Mahjouri, S., Talebpour, A. H., Movafeghi, A., & Maggi, F. (2021). Enhancement of *in vitro* production of volatile organic compounds by shoot differentiation in *Artemisia spicigera*. *Plants, 10*, 208. https://doi.org/10.3390/plants10020208

Golubkina, N., Shevchuk, O., Logvinenko, L., Molchanova, A., & Plugatar, Y. V. (2018). Macro and trace element accumulation by species of genus *Artemisia* on the southern coast of the Crimea. *Acta Horticulturae, 1324*, 389–394. https://doi.org/10.17660/ActaHortic.2021.1324.60

Gülçin, İ. (2025). Antioxidants: a comprehensive review. *Archives of Toxicology, 99*, 1893–1997. https://doi.org/10.1007/s00204-025-03997-2

Gülçin, İ., & Alwasel, S. H. (2023). DPPH radical scavenging assay. *Processes, 11*(8), 2248. https://doi.org/10.3390/pr11082248

Kafshboran, H. R., Dehghan, G., & Aghdam, M. N. (2011, January 7–9). Investigation of radical scavenging potential of some populations of Artemisia spicigera in relation to their flavonoid content. In *Proceedings of International Conference on Life Science and Technology.* Mumbai, India.

Ključevšek, T., & Kreft, S. (2025). Allergic potential of medicinal plants from the Asteraceae family. *Health Science Reports, 8*(2), e70398. https://doi.org/10.1002/hsr2.70398

Konovalov, D. A. (2014). Polyacetylene compounds of plants of the Asteraceae family. *Pharmaceutical Chemistry Journal, 48*, 9. https://doi.org/10.1007/s11094-014-1159-7

Kunchandy, E., & Rao, M. N. A. (1990). Oxygen radical scavenging activity of curcumin. *International Journal of Pharmaceutics, 58*(3), 237–240. https://doi.org/10.1016/0378-5173(90)90201-E

Lamaison, J. L., Carnat, A., & Petitjean, C. (1990). Tannin content and inhibiting activity of elastase in Rosaceae. *Annales Pharmaceutiques Françaises, 48*(6), 335–340.

Lee, J. H., Lee, J. M., Lee, S. H., Kim, Y. G., Lee, S., Kim, S. M., & Cha, S. W. (2015). Comparison of artemisinin content and antioxidant activity from various organs of *Artemisia* species. *Horticulture, Environment, and Biotechnology, 56*, 697–703. https://doi.org/10.1007/s13580-015-0143-9

Maridass, M., & De Britto, A. J. (2008). Origins of plant derived medicines. *Ethnobotanical Leaflets, 12*(1), 373–387.

Marinova, G., & Batchvarov, V. (2011). Evaluation of the methods for determination of the free radical scavenging activity by DPPH. *Bulgarian Journal of Agricultural Science, 17*(1), 11–24.

Öztürkmen, L. (1996). *Pharmacognostical studies on Artemisia spicigera C. Koch* (PhD thesis). IU Health Sciences Institute, İstanbul, Türkiye.

Pellegrini, N., Re, R., Proteggente, A., Pannala, A., Yang, M., & Rice-Evans, C. (1999). Antioxidant activity applying an improved ABTS radical cation decolorization assay. *Free Radical Biology and Medicine, 26*(9–10), 1231–1237. https://doi.org/10.1016/S0891-5849(98)00315-3

Peplow, M. (2018). Looking for cheaper routes to malaria medicines. *Chemical Engineering News, 96*(11), 29–31. http://doi/abs/10.1021/op4003196

Petretto, G. L., Chessa, M., Piana, A., Masia, M. D., Foddai, M., Mangano, G., Culeddu, N., Afifi, F. U., & Pintore, G. (2013). Chemical and biological study on the essential oil of *Artemisia caerulescens* L. ssp. *densiflora* (Viv.). *Natural Product Research, 27*, 1709–1715. https://doi.org/10.1080/14786419.2012.749471

Prieto, P., Pineda, M., & Aguilar, M. (1999). Spectrophotometric quantitation of antioxidant capacity through the formation of a phosphomolybdenum complex: Specific application to the determination of vitamin E. *Analytical Biochemistry, 269*, 337–341. https://doi.org/10.1006/abio.1999.4019

Rolnik, A., & Olas, B. (2021). The plants of the Asteraceae family as agents in the protection of human health. *International Journal of Molecular Sciences, 22*(6), 3009. https://doi.org/10.3390/ijms22063009

Ruch, R. J., Cheng, S. R., & Klaunig, J. E. (1989). Prevention of cytotoxicity and inhibition of intercellular communication by antioxidant catechins isolated from Chinese green tea. *Carcinogenesis, 10*(6), 1003–1008. https://doi.org/10.1093/carcin/10.6.1003

Sahin, A., Kıran, Y., Karataş, F., & Sönmez, S. (2005). Vitamins A, C, and E and β-Carotene content in seeds of seven species of *Vicia* L. *Journal of Integrative Plant Biology, 47*(4), 487–493. https://doi.org/10.1111/j.1744-7909.2005.00083.x

Sen, S., Chakraborty, R., Sridhar, C., Reddy, Y. S. R., & De, B. (2010). Free radicals, antioxidants, diseases and phytomedicines: Current status and future prospect. *International Journal of Pharmaceutical Sciences Review and Research, 3*(1), 91–100.

Soni, R., Singh, A., & Gupta, V. (2024). Efficient in vitro regeneration of *Artemisia annua*: Effect of different combinations of plant growth regulators on various types of explants. *Plant Biosystems, 158*(1), 59–69. https://doi.org/10.1080/11263504.2023.2287538

Tao, G., Dagher, F., Moballegh, A., & Ghose, R. (2020). Role of oxidative stress in the efficacy and toxicity of herbal supplements. *Current Opinion in Toxicology, 20–21*, 36–40. https://doi.org/10.1016/j.cotox.2020.04.004

Tumilaar, S. G., Hardianto, A., Dohi, H., & Kurnia, D. (2024). A comprehensive review of free radicals, oxidative stress, and antioxidants: Overview, clinical applications, global perspectives, future directions, and mechanisms of antioxidant activity of flavonoid compounds. *Journal of Chemistry, 2024*(1), 5594386. https://doi.org/10.1155/2024/5594386

Xiao, L., Tan, H., & Zhang, L. (2016). *Artemisia annua* glandular secretory trichomes: The biofactory of antimalarial agent artemisinin. *Science Bulletin, 61*(1), 26–36. https://doi.org/10.1007/s11434-015-0980-z

Yi, O. S., Meyer, A. S., & Frankel, E. N. (1997). Antioxidant activity of grape extracts in a lecithin liposome system. *Journal of the American Oil Chemists' Society, 74*(10), 1301–1307.

Zhishen, J., Mengcheng, T., & Jianming, W. (1999). The determination of flavonoid contents in mulberry and their scavenging effects on superoxide radicals. *Food Chemistry, 64*, 555–559.

Zurera, G., Estrada, B., Rineon, F., & Pozo, R. (1987). Lead and cadmium contamination levels in edible vegetables. *Bulletin of Environmental Contamination and Toxicology, 38*, 805–812.

Trakya University Journal of Natural Sciences, 26(2), 127–134, 2025
DOI: 10.23902/trkjnat.5767632345
www.tujns.org

Research Article

Chemical composition of endemic *Hypericum bilgehan-bilgilii* Basköse & Savran essential oil and its α-glucosidase antidiabetic, anti-inflammatory, cytotoxic and antioxidant potentials

Hüseyin Servi[1], Timur Hakan Barak[2]*, Ali Şen[3], Simge Kara Ertekin[4], Hüseyin Türker[5], Bengü Türkyılmaz Ünal[5], Cemil İşlek[5]

[1]*İstanbul Yeni Yüzyıl University, Faculty of Pharmacy, Department of Pharmacognosy, İstanbul, Türkiye*
[2]*Acıbadem Mehmet Ali Aydınlar University, Faculty of Pharmacy, Department of Pharmacognosy, İstanbul, Türkiye*
[3]*Marmara University, Faculty of Pharmacy, Department of Pharmacognosy, İstanbul, Türkiye*
[4]*İstanbul Yeni Yüzyıl University, Faculty of Pharmacy, Department of Pharmaceutical Toxicology, İstanbul, Türkiye*
[5]*Niğde Ömer Halisdemir University, Faculty of Science, Department of Biotechnology, Niğde, Türkiye*

Cite this article as: Servi, H., Barak, TH., Şen, A., Kara Ertekin, S., Türker, H., Türkyılmaz Ünal, B., & İşlek, C. (2025). Chemical composition of endemic *Hypericum bilgehan-bilgilii* Basköse & Savran essential oil and its α-glucosidase antidiabetic, anti-inflammatory, cytotoxic and antioxidant potentials. *Trakya University Journal of Natural Sciences, 26*(2), 127–134. https://doi.org/10.23902/trkjnat.5767632345

Abstract

Hypericum L. is a significantly important genus for flora of Türkiye due to its richness in phytochemicals possessing medicinal and cosmetic benefits. The essential oil composition and biological activities of *Hypericum bilgehan-bilgilii* Basköse & Savran (HEO) were analysed for the first time in the present study. The volatile oil of the whole parts of *H. bilgehan-bilgilii* was obtained by hydrodistillation with Clevenger-type apparatus. The chemical composition was analyzed by GC-MS using non-polar column. α-glucosidase and 5-lipoxygenase inhibitory, cytotoxic, and DPPH radical scavenging activities were investigated. Forty-eight components were identified and represented 97.3% of the whole constituents. Interestingly, the major volatiles: 1-(2,4,5-trimethoxyphenyl)butan-1-one (27.7%) and 3-Methyl-1-(2,4,6-trihydroxyphenyl)butan-1-one (11.2%) were detected for the first time in *Hypericum* essential oils. The oil exhibited a significant activity against the 5-lipoxygenase enzyme with an IC_{50} value of 39 µg/mL. Cytotoxicity potential of HEO was investigated, at different concentrations, towards four cell lines and, IC_{50} values underlies mild cytotoxicity. These results indicated that *H. bilgehan-bilgilii* essential oil may be considered as a valuable source for bioactive ingredients and anti-inflammatory agents.

Özet

Hypericum cinsi, tıbbi ve kozmetik faydaları olan fitokimyasallar bakımından zengin olması nedeniyle Türkiye florası için önemli bir cinstir. *Hypericum bilgehan-bilgilii* Basköse & Savran'ın (HEO)'nin uçucu yağ bileşimi ve biyolojik aktiviteleri bu çalışmada ilk kez analiz edilmiştir. *Hypericum bilgehan-bilgilii* tüm kısımlarının uçucu yağı, Clevenger tipi aparatla hidrodistilasyon yoluyla elde edilmiştir. Kimyasal bileşim, polar olmayan kolon kullanılarak GC-MS ile analiz edilmiştir. α-glukozidaz ve 5-lipoksijenaz inhibitör, sitotoksik ve DPPH radikal süpürücü aktiviteleri araştırılmıştır. Kırk sekiz bileşen tanımlanmış ve tüm bileşenlerin %97,3'ünü temsil etmiştir. İlginç bir şekilde, majör uçucular: 1-(2,4,5-trimetoksifenil)bütan-1-on (%27,7) ve 3-Metil-1-(2,4,6-trihidroksifenil)bütan-1-on (%11,2) *Hypericum* uçucu yağlarında ilk kez tespit edilmiştir. Yağ, 39 µg/mL'lik bir IC_{50} değeriyle 5-lipoksijenaz enzimine karşı önemli bir aktivite göstermiştir. HEO'nun sitotoksisite potansiyeli, farklı konsantrasyonlarda, dört hücre hattına karşı araştırılmış ve IC_{50} değerleri hafif sitotoksisitenin varlığını göstermiştir. Bu sonuçlar, *H. bilgehan-bilgilii* uçucu yağının biyoaktif bileşenler ve anti-enflamatuvar ajanlar için değerli bir kaynak olarak kabul edilebileceğini göstermiştir.

Keywords: aromatherapy, gas chromatography-mass spectrometry, GC-FID, bioactivity, *Hypericum bilgehan-bilgilii*

Edited by: *Cem Vural*

***Corresponding Author:** Timur Hakan Barak, **E-mail:** timur.barak@acibadem.edu.tr*

***ORCID iDs of the authors:** HS. 0000-0002-4683-855X, THB. 0000-0002-7434-3175, AŞ. 0000-0002-2144-5741, SKE. 0000-0002-7976-7057, HT. 0000-0001-7309-9484, BTÜ. 0000-0003-4003-5200, CŞ. 0000-0002-6690-2846*

Received: 6 February 2025, **Accepted:** 13 June 2025, **Online First**: 10 July 2025, **Published:** 15 October 2025

Introduction

The genus *Hypericum* L. is a member of the Hypericaceae family and consists of more than 500 species all over the world. There are 109 taxa in 20 sections in the flora of Türkiye and 48 taxa of which are endemic (Duman & Cakir-Dündar, 2020). *Hypericum* species have been used as antidepressants, sedatives, diuretics, antiphlogistics, analgesics, astringents, and antipyretics in various parts of the world (Doğan et al., 2019; Ersoy et al., 2019; Galeotti, 2017; Kandilarov et al., 2018; Kurt-Celep et al., 2020; Marrelli et al., 2016; Velingkar et al., 2017; Wise et al., 2019; Zhang et al., 2020). The genus is a rich source of various secondary metabolites as naphthodianthrones, flavonoids, phloroglucinols, bioflavonoids, proanthocyanidins, and terpenes (Khorshidi et al. 2020; Semerdjieva et al., 2023). The results of extensive studies on phytochemical compositions and biological activities of *Hypericum* species have been reported. Notably, *H. perforatum* L., is prominent for many beneficial pharmacological properties such as antidepressant, antibacterial, antiviral, anti-inflammatory, antinociceptive, and analgesic (Galeotti, 2017).

As noteworthy utilities of *H. perforatum* in diminishing depressive symptoms have been highlighted, there has been an increasing attention to evaluate whether other *Hypericum* species have similar features. There are many reports on the essential oil composition of *Hypericum* species in the literature with significant amount of variation in their secondary metabolite profiles. The variation in essential oil composition of the *Hypericum* genus may be related to essential oil extraction type, phenological cycle, seasonal variation, plant part, and geographical area. Additionally, gland types (translucent and dark glands) may affect the essential oil composition of *Hypericum* species. Translucent and dark glands are found in different parts of the plants. For example, *H. androsaemum* had translucent glands, which were found on the leaf margin and lamina. (*E*)-2-hexenal (15.5%), hexadecanoic acid (14.7%), β-caryophyllene (11.2%), germacrene B (11.0%) and γ-himachalene (9.8%) were the major components of the lamina glands, whereas β-pinene (22.0%), limonene (17.6%), (*E*)-β-ocimene (6.1%), methyl linoleate (5.7%), terpinolene (5.4%), (*E*)-2-hexenal (4.9%) and α-pinene (4.1%) were the main compounds of the margin glands (Guedes et al., 2012). Due to the diversity of essential oils, *Hypericum* species display different biological activities such as antioxidant, antibacterial, antifungal, cytotoxic, insecticidal, neuroprotective, enzyme inhibitory, hepatoprotective, wound healing, etc. (Bertoli et al., 2011; Grafakou et al., 2022). This wide range of bioactivities of *Hypericum* essencial oils (EOs) has increased interest in novel candidates in the same genus. Although the genus *Hypericum* has many species, the biological activities and chemical composition of essential oils are known only in a few species, with the exception of *H. perforatum*. Due to this reason, studying the chemical composition and biological activities of the essential oils of *H. bilgehan-bilgilii*, which is an endemic perennial plant and was described as a new species in 2018, growing on calcareous rocks, chasmophyte, is of great importance. In light of this information, the *in vitro* α-glucosidase inhibitory, 5-lipoxygenase inhibitory, and DPPH radical scavenging activities of the essential oil of *H. bilgehan-bilgilii* (HEO) were investigated for the first time in the present study. Moreover, cytotoxic properties of HEO were evaluated towards four different cell lines (L929, A549, MCF-7 and CHO) for three different concentrations in order to determine possible toxic effects prior to medical utilizations.

Materials and Methods

Plant Material

Hypericum bilgehan-bilgilii was collected in the calcareous rocks (1600–2200 m, 37º 29’ 21.66’’N, 31º 19’ 35.81’’E) in Beyşehir district of Konya province, Türkiye, on August 2020 by Huseyin Turker and identified by Dr. Ahmet Savran (Baskose & Savran, 2018). Herbarium specimens of *H. bilgehan-bilgilii* was deposited in the Herbarium of Ankara University (Herbarium number: Savran-4600).

Hydrodistillation

The essential oil of dry whole parts (aerial parts and roots) of *Hypericum bilgehan-bilgilii* (HEO) was obtained by hydrodistillation method for 3 hours with Clevenger-type apparatus (Ertosun et al., 2023).

Gas Chromatography (GC-FID)

Gas chromatography analysis was performed on capillary column Innowax FSC (60 m × 0.25 mm, 0.25 m film thickness). Chromatographic conditions were as follows: helium was used as carrier gas at 1.0 mL min^{-1}; injector and detector temperature was 250ºC. Oven temperature was isothermal at 60ºC for 10 min, then increased to 220ºC, at a rate of 4ºC min^{-1}, isothermal at 220ºC for 10 min and increased to 240ºC, at a rate of 1ºC min^{-1}. Split ratio 1:25. The injection volume was 1 µL (Servi et al., 2023).

Gas Chromatography-mass Spectrometry (GC-MS)

The essential oil composition was determined by briefly used method of Barak et al. (2023b). The column type was DP-5 (5% diphenyl, 95% dimethyl polysiloxane; 30 m × 0.25 mm, 0.25 m film thickness). The GC-MS analysis parameters were: the oven temperature was 60ºC for 1 min, then raised at a rate of 3ºC min^{-1} to 246ºC. It was held at that temperature for 30 min. Helium was used as the carrier gas, and a flow rate of 0.9 mL min^{-1} was used. The essential oil components were determined by a comparison of relative retention indices obtained from a series of *n*-alkanes (C5 to C30) to the literature as the method used by Barak et al. (2025) and with mass spectra comparison to the in-house libraries (NIST14 and Wiley7).

In vitro Antioxidant Activity of *Hypericum bilgehan-bilgilii* Essential Oil

DPPH radical scavenging activity of essential oil was specified by briefly used method of Zou et al. (2011). 10 µL of essential oils (5000–9.77 µg/mL) or standard ascorbic acid (250–7.81 µg/mL) in dimethylsulfoxide (DMSO) at different concentrations were mixed with 190 µL of 0.1 mM DPPH solution in MeOH in a well of the 96-well plate. The mixture was kept in the dark at room

temperature for 30 min. The absorbance value was detected at 517 nm. The results are expressed as IC_{50} (mg/mL), the concentration of the sample that scavenges the radical by 50%. Each experiment was applied in triplicate.

In vitro Anti-inflammatory Activity Assay

The anti-inflammatory activity was determined with minor changes according to the method described by Phosrithong & Nuchtavorn (2016) was performed according to Yıldırım et al. (2019), with slight modifications, adapted to the 96-well microplate format. 10 µL of essential oils (250–9.77 µg/mL) or standard indomethacin (100–0.02 µg/mL) were added to 20 µL ethanol, 20 µL pure water, 25 µL of sodium borate buffer solution (0.1 M, pH 9) and 25 µL of type V soybean lipoxygenase solution in the buffer (pH 9, 20.000 U/mL). The mixture was pre-incubated at 25°C for 5 min. Then, 100 µL of 0.6 mM linoleic acid solution was added to solutions, mixed well and the change in absorbance at 234 nm was followed for 6 min. The results are expressed as IC_{50} value (mg/mL), the concentration of the sample that inhibits the activity of the enzyme by 50%. Each experiment was applied in triplicate.

In vitro Antidiabetic Activity Assay

The α-glucosidase inhibitor activity method suggested by Ramakrishna et al. (2017) was performed according to Sen et al. (2019) with some modifications. 10 µL of essential oils (5000–7.81 µg/mL) or standard acarbose (250–9.77 µg/mL), 40 µL of 0.1 M sodium phosphate buffer (pH 6.9), and 100 µL of a-glucosidase (obtained from *Saccharomyces cerevisiae*) were mixed in a well of the 96-well plate. After pre-incubation at 25°C for 10 min, 50 µL of 5 mM p-nitrophenyl-a-D-glucopyranoside (*p*NPG) to the solutions was added and re-incubated at 25°C for 5 min. The absorbance reading was taken before and after incubation at 405 nm using a microplate reader. The results are expressed as IC_{50} value (mg/mL), the concentration of the sample that inhibits the activity of the enzyme by 50%. Each experiment was applied in triplicate.

Evaluations for Cytotoxic Activity

To determine the cytotoxic effects, different concentrations (20, 100 and 250 µg/mL) of the essential oil of *H. bilgehan-bilgilii* were applied to A549 (human lung adenocarcinoma), MCF-7 (human breast carcinoma), L929 (mouse fibroblast), and CHO (Chinese hamster ovary) cell lines. These cell lines were obtained from ATCC and were cultured in DMEM-high glucose medium supplemented with 10% fetal bovine serum and 1% Penicillin-Streptomycin, under incubation conditions of 37°C with 5% CO_2.

Prior to the experiment, 5000 cells per well were seeded in 96-well culture plates and allowed to adhere overnight. Essential oil prepared at a concentration of 2.5 mg/100 mL in ethanol were applied at different concentrations for 48 hours. Following exposure, the effect on cell viability was assessed using an MTT solution (3-(4,5-Dimethylthiazol-2-yl)-2,5-diphenyltetrazolium bromide) prepared in PBS. The cells were incubated with the MTT reagent for 4 hours at 37°C in the dark to allow the formation of formazan crystals. The resulting formazan crystals were then dissolved in DMSO, and absorbance was measured at 570 nm using a microplate reader. The effect of the treatment groups on cell viability was determined in comparison to the control group, and the IC_{50} values (concentration that inhibits 50% of cell viability) were calculated using GraphPad Prism version 9.5.1 (Ustuner et al., 2023).

Statistical Analysis

All tests were performed at least three times. The results were expressed as mean ± standard deviation (SD). The statistical significance of the data was analysed using Student's t-test (for anti-lipoxygenase and α-glucosidase inhibitory assays) or ANOVA with post hoc comparison by Tukey (for DPPH radical scavenging assay). $p < 0.05$ was considered statistically significant.

Results and Discussion

The essential oil yield of *H. bilgehan-bilgilii* was calculated as 0.06 (v/w). Forty-eight constituents were identified in HEO, which was equal to 97.3% of its total ingredients (Table 1).

It was observed that there were three dominant groups in the HEO: phloroglucinol derivatives (40.1%), sesquiterpenes (23.6%), and oxygenated sesquiterpenes (21.1%). 1-(2,4,5-trimethoxyphenyl) butan-1-one (27.7%) and 3-Methyl-1-(2,4,6-trihydroxyphenyl) butan-1-one (11.2%) were the main compounds of the essential oil (Figure 1 and Table 1). It is well known that secondary metabolite profiles of plants are affected by various parameters

Table 1. Essential oil composition of whole parts of *Hypericum bilgehan-bilgilii.*

RT[1]	RRI[2]	RRI[3]	Compounds	(%)	IM[4]
6.328	933	939	α-Pinene	2.0	RI, MS
7.616	977	980	β-Pinene	1.7	RI, MS
8.034	991	991	β-Myrcene	0.2	RI, MS
9.367	1028	1031	Limonene	0.9	RI, MS
11.656	1089	1088	*p*-Mentha-1,4(8)-diene	0.2	RI, MS
12.107	1101	1098	Linalool	0.7	RI, MS
12.288	1105	1101	Nonanal	0.2	RI, MS
12.676	1114	1117	Fenchol	0.1	RI, MS

Table 1. Continued.

RT[1]	RRI[2]	RRI[3]	Compounds	(%)	IM[4]
13.729	1139	1137	*trans*-Pinocarveol	0.7	RI, MS
14.734	1163	1164	Pinocarvone	0.3	RI, MS
14.868	1166	1169	Endo-borneol	0.4	RI, MS
15.947	1191	1189	α-Terpineol	0.6	RI, MS
16.182	1197	1191	Myrtenol	0.7	RI, MS
21.327	1317	1314	(*E*,*E*)-2,4- Decadienol	0.5	RI, MS
23.845	1376	1376	Copaene	0.3	RI, MS
24.587	1394	1387	(*E*)-β-Elemene	4.4	RI, MS
25.654	1420	1418	Caryophyllene	0.6	RI, MS
26.448	1440	1440	Aromadendrene	0.6	RI, MS
27.046	1454	1455	α-Humulene	0.2	RI, MS
27.333	1461	1462	Alloaromadendrene	0.5	RI, MS
28.012	1478	1477	γ-Muurolene	1.1	RI, MS
28.205	1483	1480	Germacrene D	3.3	RI, MS
28.405	1488	1485	β-Selinene	2.5	RI, MS
28.848	**1499**	**1495**	**Bicyclogermacrene**	6.1	RI, MS
29.198	1508	1504	Eremophilene	3.1	RI, MS
29.490	1515	1513	γ-Cadinene	0.2	RI, MS
29.860	1525	1524	δ-Cadinene	0.7	RI, MS
31.727	1573	1570	*cis*-3-Hexenyl-benzoate	0.2	RI, MS
32.044	**1581**	**1576**	**Spathulenol**	5.8	RI, MS
32.223	1586	1584	Globulol	0.9	RI, MS
32.587	1595	1595	Salvial 4(14)-en-1-one	0.3	RI, MS
33.287	1614	1607	Eudesm-6-en-4 α-ol	0.5	RI, MS
33.671	1624	1613	Rosifoliol	0.3	RI, MS
33.935	1631	1638	Hinesol	1.2	RI, MS
34.011	1633	1630	γ-Eudesmol	0.7	RI, MS
34.288	1641	1645	α-Muurolol	1.2	RI, MS
34.737	1653	1649	β-Eudesmol	3.3	RI, MS
34.873	1657	1652	α-Eudesmol	4.9	RI, MS
36.019	1688	1686	Germacra-4(15),5,10(14)-trien-1α-ol	1.0	RI, MS
37.272	1723	1714	6-Isopropenyl-4,8a-dimethyl-1,2,3,5,6,7,8,8a-octahydro-naphthalen-2-ol	0.6	RI, MS
38.750	1765	1763	Benzyl benzoate	0.9	RI, MS
39.062	1774	1751	1-(2,4,5-Trimethoxyphenyl)propan-2-one	1.2	RI, MS
41.537	1846	1845	Hexahydrofarnesyl acetone	0.4	RI, MS
42.666	**1880**	**1891**	**1-(2,4,5-Trimethoxyphenyl)butan-1-one**	27.7	RI, MS
45.011	**1952**		**3-Methyl-1-(2,4,6-trihydroxyphenyl)butan-1-one**	11.2	MS
60.671	2500	2500	Pentacosane	0.2	RI, MS
65.956	2700	2700	Heptacosane	0.6	RI, MS
73.795	2901	2900	Nonacosane	1.4	RI, MS
			Oxygenated monoterpenes	3.7	
			Sesquiterpenes	23.6	
			Oxygenated sesquiterpenes	21.1	

Table 1. Continued.

RT[1]	RRI[2]	RRI[3]	Compounds	(%)	IM[4]
			Phloroglucinol derivatives	40.1	
			n-alkanes	2.2	
			Others	1.8	
			Total identified compounds	97.3	

[1]RT: Retention time.
[2]RRI: Experimental Relative retention indexes.
[3]RRI: Relative retention indexes from literature.
[4]IM: Identification method.

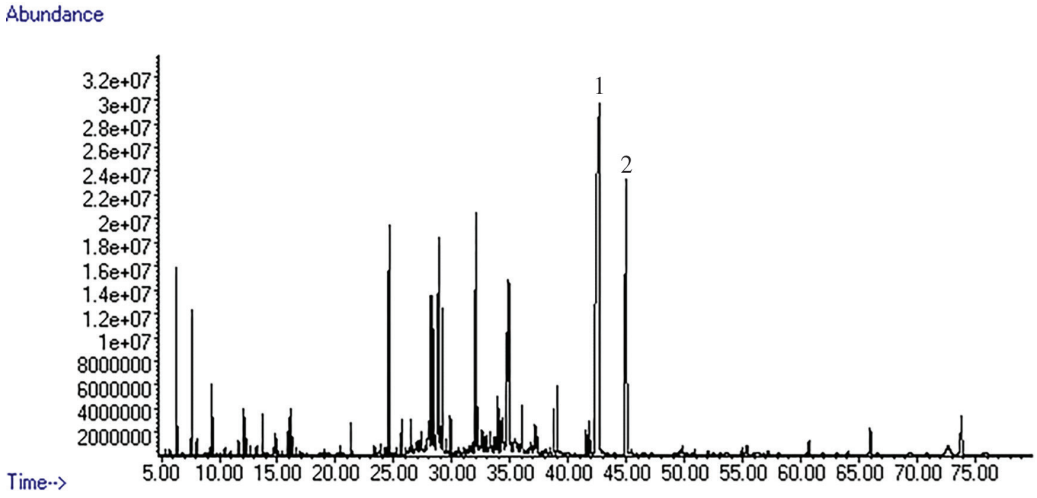

Figure 1. GC-MS chromatogram of essential oil of *H. bilgehan-bilgilii* whole part (1: 1-(2,4,5-Trimethoxyphenyl)butan-1-one; 2: 3-Methyl-1-(2,4,6-trihydroxyphenyl)butan-1-one).

such as climate, soil condition, genetic factors, etc. (Barak et al., 2023a; Sen et al., 2019; Barak et al., 2024). Correspondingly, these variations were reported for *Hypericum* species. Previous studies showed that increasing the sum of sunlight is correlated with higher amounts of hypericin, hyperforin, and pseudohypericin contents of *H. perforatum* (Odabas et al., 2008). On the contrary, warm winters negatively affect secondary metabolites of *H. perforatum* (Khorshidi et al., 2020). Consistently, relative humidity and annual rainfall increase hypericin content while augmented sunshine hours positively affect hyperforin content (Riazi et al., 2015).

Even though it is the first study that investigates the chemical composition of HEO, several reports have revealed the essential oil ingredients of *Hypericum* species. These previous studies demonstrated that essential oils of *Hypericum* species from Türkiye are rich in monoterpenes, sesquiterpenes, *n*-alkanes, and fatty acid derivatives. α-pinene (12.3–88.3%) was determined as the main monoterpene compound in the essential oils of *H. empetrifolium* Willd., *H. hircinum* L., *H. kotschyanum* Boiss., *H. lydium* Boiss., *H. microcalycinum* var. *microcalycinum* Boiss. & Heldr, *H. origanifolium* var. *depilatum* (Freyn & Bornm.) N.Robson, *H. scabrum* L., *H. thymopsis* Boiss., *H. triquetrifolium* Turra., and *H. uniglandulosum* Hausskn. ex Bornm. (Babacan & Bagci, 2017; Boga et al., 2021; Eroglu et al., 2013; Kıyan et al., 2014; Serbetci et al., 2012; Tabanca et al., 2015; Yuce & Bagci, 2012). Spathulenol (12.9%), iso-longifolene (11.2%), germacrene D (30.2%), allo-aromodendrene (24.7%), caryophyllene oxide (18.3%), α-eudesmol (11.3%), *α*-selinene (19.6 or 18.7%), and *β*-selinene (15.0-37.1%) were identified as main sesquiterpenes in the essential oils of *H. capitatum* Choisy, *H. saturejifolium* Trevir, *H. empetrifolium*, *H. lydium*, *H. orientale* Boiss, *H. origanifolium* Willd., and *H. pruinatum* Boiss. & Balansa (Bertoli et al., 2015; Boga et al., 2016; Boga et al., 2021; Cirak & Bertoli, 2013; Kıyan et al., 2014). Nonacosane (11.1-42.7%), 1-hexanal (18.8%), 3-methylnonane (12.5%), undecane (19.2%) were major *n*-alkane components of essential oils of *H. kotschyanum* Boiss., *H. salsugineum* N. Robson & Hub.-Mor., *H. triquetrifolium*, and *H. uniglandulosum* Hausskn. ex Bornm. (Babacan & Bagci, 2017; Eroglu et al., 2013; Yuce & Bagci, 2012). Hexadecanoic acid (17.7 and 23.2%) was found in high amounts in the essential oils of *H. salsugineum* and *H. scabroides* (Eroglu et al., 2013).

Fatty acid derivatives were not found in the essential oil of the present study. Additionally, there are quantitative differences in the main monoterpenes, sesquiterpenes, and *n*-alkanes. Even though there is a significant sesquiterpene amount in HEO, and the major ingredients were determined as phloroglucinol derivatives. More than 400 phloroglucinol derivatives have been identified in *Hypericum* crude extracts to date. Nevertheless,

these metabolites were not previously detected in the essential oils. To our knowledge, these compounds are considered as the main responsible principles for the therapeutic bioactivities of the genus (Bridi et al., 2018). The volatile oil composition of the current study displayed a different chemical profile from that of the volatile oils of other *Hypericum* species. This dissimilarity in the present study may be related to the plant's habitat conditions or genetic factors.

HEO showed a low DPPH free radical scavenging activity, having an IC_{50} value of 1.012 mg/mL compared to standards ($p < 0.05$, Table 2). Till date, no study is presented with the antioxidant capacity of *H. bilgehan-bilgilii* essential oil, however antioxidant activity studies were carried out on another species of *Hypericum*. In one of these studies, Kamila et al. (2018) indicated that essential oil obtained from the leaves and tender parts of *H. gaitii* Haines had an IC_{50} value of 105.12 µg/mL against DPPH radical. In another study, it was determined that the IC_{50} value of the essential oil of *H. perforatum* subsp. *veronense* aerial parts was 23.07 µg/mL against DPPH radical (Vuko et al., 2021).

DPPH radical scavenging activity of *H. bilgehan-bilgilii* essential oil in our present study was found to be lower than the results reported by other investigators. HEO presented a poor α-glucosidase inhibitory activity, having an IC_{50} value of 1.513 mg/mL compared with acarbose ($p < 0.05$, Table 2). There are no studies that have focused on the α-glucosidase inhibitory activity of not only the essential oil of *H. bilgehan-bilgilii* but also the essential oils of *Hypericum* species.

HEO exhibited a significant 5-lipoxygenase inhibitory activity with an IC_{50} value of 0.039 mg/mL when compared with indomethacin (0.022 mg/mL) used as the positive control ($p < 0.05$, Table 2). Similarly, no study in the literature analyzes the 5-lipoxygenase inhibitory activity of essential oils of any *Hypericum* species, including HEO. Hyperforin, a phloroglucinol derivative found in the *H. perforatum*, has been reported to have significant 5-LOX inhibitory activity (Albert et al., 2002). In another study, it was reported that different phloroglucinol derivative compounds (3-geranyl-1-[2′-methylpropanoyl] phloroglucinol and 3-geranyl-1-[2′-methylbutanoyl] phloroglucinol) found in *H. empetrifolium* have 5-LOX enzyme inhibitory activity (Crockett et al., 2008). Spathulenol, one of the major compounds of the essential oil of *H. bilgehan-bilgilii* has also been suggested to exhibit a good docking score against 5-LOX in an *in silico* studies (Fenanir et al., 2022). Therefore, phloroglucinol derivatives in particular, along with other compounds, may be responsible for the activity of the essential oil of the current study. Cytotoxic potential of HEO was likewise investigated in the current study. There are several studies in the literature that investigated the cytotoxic properties of different *Hypericum* species.

IC_{50} values of three different species of *Hypericum* were reported in a study conducted by Akdeniz et al. (2023). Results showed that *H. linarioides* Bosse had 26.39 µg/mL IC_{50} value while *H. lydium* Boiss. had 26.89, which indicates a significant difference. In addition, Vuko et al. (2021), investigated proliferation inhibition potentials of hydrosol obtained from *H. perforatum* subsp. *veronense* against three different cancer cell lines. Results demonstrated that the volatile content of hydrosol showed significant inhibitory potential against HeLa, HCT116, and U2OS cell lines. As literature stated, significant variations might be seen in cytotoxic properties of essential oils of *Hypericum* species. In this study, three different concentrations of HEO were investigated against four different cell lines (A549, L929, MCF-7, and CHO). Results showed that HEO exhibited notably low cytotoxicity, as none of the IC_{50} values fell within the tested concentration range (up to 250 µg/mL) (Table 3). This observation is further supported by the fact that all cell viability remained relatively unaffected, even at the highest concentration tested. These values are considerably higher than those reported for other *Hypericum* species with known cytotoxic or antiproliferative effects, such as *H. linarioides* and *H. lydium* (Akdeniz et al., 2023) or *H. perforatum* hydrosol (Vuko et al., 2021).

Taken together, the current findings indicate that HEO does not exhibit strong anticancer activity under the tested conditions. Rather, its low cytotoxicity profile may support its potential use in formulations where minimal toxicity is required, such as in dermatological or supportive therapeutic applications.

Table 2. Biological activity of *Hypericum bilgehan-bilgilii* essential oil.

HEO*/standards	**Antioxidant activity**	**Anti-inflammatory activity**	**Antidiabetic activity**
	DPPH radical scavenging activity	**Anti-lipoxygenase activity**	**α-glucosidae inhibitory activity**
	IC_{50} (mg/mL)		
HEO	1.012 ± 0.059[d]	0.039 ± 0.000[b]	1.513 ± 0.016[b]
Ascorbic acid	0.018 ± 0.000[a]		
Trolox	0.015 ± 0.000[a]		
Butylated hydroxyanisole	0.057 ± 0.000[b]		
Butylated hydroxytoluene	0.214 ± 0.015[c]		
Indomethacin		0.022 ± 0.000[a]	
Acarbose			0.192 ± 0.001[a]

*HEO shows essential oil of whole parts of *H. bilgehan-bilgilii*. **Each value in the table is represented as mean ± SD (n = 3). Different letter superscripts in the same column indicate significant differences ($p < 0.05$). ***Different letters in the same row indicate significance ($p < 0.05$).

Table 3. IC_{50} values (µg/mL) of HEO on different cell lines.

L929 (mouse fibroblast)	CHO (Chinese hamster ovary)	A549 (human adenocarcinoma)	MCF-7 (human breast carcinoma)
6112	374.9	367.9	720

Conclusion

The present study determined the chemical composition and biological activities of the essential oil of *H. bilgehan-bilgilii* as well as phloroglucinol derivatives were identified in the essential oil of *Hypericum* species for the first time. In the present study, 1-(2,4,5-trimethoxyphenyl)butan-1-one and 3-Methyl-1-(2,4,6-trihydroxyphenyl)butan-1-one were determined as the main compounds of HEO and this is the first report for this compounds in *Hypericum* essential oils, to our knowledge. In addition, it was displayed in this study that HEO is rich in sesquiterpenoid compounds which is parallel with literature. Results showed that phytochemical analysis of the HEO may be beneficial for enhanced perspective on its biochemical systematics and HEO might be a valuable source for medical purposes as a source of anti-inflammatory agents. HEO did not display antioxidant, cytotoxic, and antidiabetic activities.

Ethics

Ethics Committee Approval: The manuscript does not include any studies on human or animal topics. Ethics committee approval is not required.

Data Sharing Statement: Data can be shared upon reasonable request to authors.

Footnotes

Author Contributions: Conceptualization: H.S., Design/methodology: H.S., and H.T., Execution/investigation: H.S., T.H.B., A.Ş., and S.K.E., Resources/materials: H.T., B.T.Ü., and C.İ., Data acquisition: H.S., T.H.B., A.Ş., and S.K.E., Data analysis/interpretation: H.S., and S.K.E Writing – original draft: H.S., and T.H.B. Writing – review & editing/ critical revision: A.Ş., S.K.E., H.T., B.T.Ü., and C.İ.

Conflict of Interest: The authors have no conflicts of interest to declare.

Funding: No external funding acquired.

References

Akdeniz, M., Yener, I., Ertas, A., Dincel, D., Firat, M., Kocakaya, S. O., & Kolak, U. (2023). Essential Oil Contents of *Hypericum linarioides*, *H. helianthemoides*, and *H. lydium* with Their Biological Activities: Importance of *Hypericum* Genus in the Cosmeceutical and Pharmaceutical Industries. *Pharmaceutial Chemistry Journal*, *57*(9), 1460-1468. https://doi.org/10.1007/s11094-023-03011-y

Albert, D., Zündorf, I., Dingermann, T., Müller, W. E., Steinhilber, D., & Werz, O. (2002). Hyperforin is a dual inhibitor of cyclooxygenase-1 and 5-lipoxygenase. *Biochemical Pharmacology*, *64*(12), 1767-1775. https://doi.org/10.1016/s0006-2952(02)01387-4

Babacan, E. Y., & Bagci, E. (2017). Essential oil composition of *Hypericum uniglandulosum* Hausskn. ex Bornm. and *Hypericum lydium* Boiss. from Turkey. *International Journal of Nature and Life Sciences*, *1*(1), 12-16.

Barak, T. H., Bolukbas, E., & Bardakcı, H. (2023). Evaluation of marketed rosemary essential oils (*Rosmarinus officinalis* L.) in terms of European Pharmacopoeia 10.0 Criteria. *Turkish Journal of Pharmaceutical Sciences*, *20*(4), 253-260. https://doi.org/10.4274/tjps.galenos.2022.78010

Barak, T. H., Dogenci, İ., & Bardakcı, H. (2023). Evaluation of the essential oil samples that are sold as "Eucalyptus oil" on the market in Türkiye in terms of European Pharmacopoeia 10.0 criteria. *Journal of Research in Pharmacy*, *27*(4), 1463-1473. https://doi.org/10.29228/jrp.433

Barak, T. H., Gultekin, E., Senturk, T. B., & Ozdemir, K. (2024). Evaluation of commercial *Syzygium aromaticum* L. (clove) essential oil samples from market in accordance with the European Pharmacopoeia 10.0 criteria. *Journal of Research in Pharmacy*, *28*(4), 1088-1098. http://doi.org/10.29228/jrp.791

Barak, T.H., Eryilmaz, M., Karaca, B., Servi, H., Kara Ertekin, S., Dinc, M., & Ustuner, H. (2025). Antimicrobial, Anti-Biofilm, Anti-Quorum Sensing and Cytotoxic Activities of Thymbra spicata L. subsp. spicata Essential Oils. *Antibiotics*, *14*(2), 181. https://doi.org/10.3390/antibiotics14020181

Baskose, I., & Savran, A. (2018). A new species from southern Anatolia (Dedegöl Mountain Series-Çürük Mountain) in Turkey: *Hypericum bilgehan-bilgilii* (Hypericaceae). *Phytotaxa*, *374*(2), 110-118. https://doi.org/10.11646/phytotaxa.374.2.2

Bertoli, A., Cirak, C., & Silva J. D. (2011). *Hypericum* species as sources of valuable essential oils. *Medicinal and Aromatic Plant Science and Biotechnology*, *5*(1), 29-47.

Bertoli, A., Çirak, C., & Seyis, F. (2015). *Hypericum origanifolium* Willd.: The essential oil composition of a new valuable species. *Industrial Crops and Products*, 77, 676-679. https://doi.org/10.1016/j.indcrop.2015.08.014

Boga, M., Ertas, A., Eroglu-Ozkan, E., Kizil, M., Ceken, B., & Topcu, G. (2016). Phytochemical analysis, antioxidant, antimicrobial, anticholinesterase and DNA protective effects of *Hypericum capitatum* var. capitatum extracts. *South African Journal of Botany*, 104, 249-257. https://doi.org/10.1016/j.sajb.2016.02.204

Boga, M., Ersoy, E., Ozkan, E. E., Cinar, E., Kara, E. M., Canturk, Y. Y., & Zengin, G. (2021). Volatile and phenolic profiling of a traditional medicinal plant, *Hypericum empetrifolium* with *in vitro* biological activities. *Journal of Ethnopharmacology*, 272, 113933. https://doi.org/10.1016/j.jep.2021.113933

Bridi, H., de Carvalho Meirelles., G., & von Poser, G. L. (2018). Structural diversity and biological activities of phloroglucinol derivatives from *Hypericum* species. *Phytochemistry*, 155, 203-232. https://doi.org/10.1016/j.phytochem.2018.08.002.

Cirak, C., & Bertoli, A. (2013). Aromatic profiling of wild and rare species growing in Turkey: *Hypericum aviculariifolium* Jaub. and Spach subsp. *depilatum* (Freyn and Bornm.) Robson var. depilatum and Hypericum pruinatum Boiss. and Bal. *Natural Product Research*, *27*(2), 100-107. https://doi.org/10.1080/14786419.2012.660633

Crockett, S. L., Wenzig, E. M., Kunert, O., & Bauer R. (2008). Anti-inflammatory phloroglucinol derivatives from Hypericum empetrifolium. *Phytochemistry Letters*, *1*(1), 37-43. https://doi.org/10.1016/j.phytol.2007.12.003

Dogan, S., Gokalsın, B., Senkardes, I., Dogan, A., & Sesal, N. C. (2019). Anti-quorum sensing and anti-biofilm activities of *Hypericum perforatum* extracts against *Pseudomonas aeruginosa*. *Journal of Ethnopharmacology*, 235, 293-300. https://doi.org/10.1016/j.jep.2019.02.020

Duman, H., & Cakir-Dündar, E. G. (2020). Hypericum alacamdaglariense (Hypericaceae), a new species from Turkey. *Phytotaxa*, *470*(2), 176-185. https://doi.org/10.11646/PHYTOTAXA.470.2.6

Eroğlu Özkan, E., Demirci, B., Ünsal Gürer, Ç., Kültür, Ş., Mat, A., & Başer, K. H. C. (2013). Essential oil composition of five endemic *Hypericum* species from Turkey. *Organic Chemistry: Current Research*, *2*, 1. http://dx.doi.org/10.4172/2167-0412.1000121

Ersoy, E., Ozkan, E. E., Boga, M., Yilmaz, M. A., & Mat, A. (2019). Anti-aging potential and anti-tyrosinase activity of three *Hypericum* species with focus on phytochemical composition by LC–MS/MS. *Industrial Crops and Products*, 141, 111735. https://doi.org/10.1016/j.indcrop.2019.111735

Ertosun, G. B., Ergen, M., Bardakcı, H., Barak, T. H., & Suyen, G. (2023). Cholinergic cognitive enhancer effect of Salvia triloba L. essential oil inhalation in rats. *Marmara Medical Journal,* 36(3), 361-370. https://doi.org/10.5472/marumj.1368345

Fenanir, F., Semmeq, A., Benguerba, Y., Badawi, M., Dziurla, M. A., Amira, S., & Laouer, H. (2022). In silico investigations of some Cyperus rotundus compounds as potential anti-inflammatory inhibitors of 5-LO and LTA4H enzymes. *Journal of Biomolecular Structure and Dynamics,* 40(22), 11571-11586. https://doi.org/10.1080/07391102.2021.1960197

Galeotti, N. (2017). Hypericum perforatum (St John's wort) beyond depression: A therapeutic perspective for pain conditions. *Journal of Ethnopharmacology*, 200, 136-146. https://doi.org/10.1016/j.jep.2017.02.016

Grafakou, M. E., Barda, C., Karikas, G.A., & Skaltsa, H. (2022). *Hypericum* essential oils-composition and bioactivities: an update (2012–2022). *Molecules*, *27*(16), 5246. https://doi.org/10.3390/molecules27165246

Guedes, A. P., Franklin, G., & Fernandes-Ferreira, M. (2012). *Hypericum* sp.: essential oil composition and biological activities. *Phytochemistry Reviews*, 11, 127-152. https://doi.org/10.1007/s11101-012-9223-y

Khorshidi, J., Morshedloo, M. R., & Moradi, S. (2020). Essential oil composition of three Iranian *Hypericum* species collected from different habitat conditions. *Biocatalysis and Agricultural Biotechnology*, 28, 101755. https://doi.org/10.1016/j.bcab.2020.101755

Kıyan, H. T., Demirci, B., Başer, K. H. C., & Demirci, F. (2014). The *in vivo* evaluation of anti-angiogenic effects of *Hypericum* essential oils using the chorioallantoic membrane assay. *Pharmaceutical Biology*, *52*(1), 44-50. https://doi.org/10.3109/13880209.2013.810647

Kurt-Celep, İ., Celep, E., Akyüz, S., İnan, Y., Barak, T. H., Akaydın, G., & Yesilada, E. (2020). *Hypericum olympicum* L. recovers DNA damage and prevents MMP–9 activation induced by UVB in human dermal fibroblasts. *Journal of Ethnopharmacology*, 246, 112202. https://doi.org/ 10.1016/j.jep.2019.112202.

Kamila, P. K., Ray, A., Jena, S., Mohapatra, P. K., & Panda, P. C. (2018). Chemical composition and antioxidant activities of the essential oil of *Hypericum gaitii* Haines–an endemic species of Eastern India. *Natural Product Research*, *32*(6), 739-742. https://doi.org/10.1080/14786419.2017.1338283

Kandilarov, I. K., Zlatanova, H. I., Georgieva-Kotetarova, M. T., Kostadinova, I. I., Katsarova, M. N., Dimitrova, S. Z., & Sadakov, F. (2018). Antidepressant effect and recognition memory improvement of two novel plant extract combinations-Antistress I and anti-stress II on rats subjected to a model of mild chronic stress. *Folia Medica*, *60*(1), 110-116. https://doi.org/10.1515/folmed-2017-0073

Marrelli M., Statti G., Conforti F., & Menichini F. (2016). New potential pharmaceutical applications of *Hypericum* species. *Mini-Reviews in Medicinal Chemistry*, *16*(9), 710-720. https://doi.org/ 10.2174/1389557515666150709105844.

Odabas, M. S., Radusiene, J., Cirak, C., & Camas, N. (2008). Prediction models for the phenolic contents in some *Hypericum* species from Turkey. *Asian Journal of Chemistry*, *20*(6), 4792-4802.

Phosrithong, N., & Nuchtavorn, N. (2016). Antioxidant and anti-inflammatory activites of *Clerodendrum* leaf extracts collected in Thailand. *European Journal of Integrative Medicine*, *8*(3), 281-285. https://doi.org/10.1016/j.eujim.2015.10.002

Ramakrishna, R., Sarkar, D., Schwarz, P., & Shetty, K. (2017). Phenolic linked anti-hyperglycemic bioactives of barley (*Hordeum vulgare* L.) cultivars as nutraceuticals targeting type 2 diabetes. *Industrial Crops and Products*, 107, 509-517. https://doi.org/10.1016/j.indcrop.2017.03.033

Riazi, A., Hosseini, N. M., Badi, H. N., Naghavi, M. R., & Rezazadeh, S. (2015). Phytochemical characteristics evaluation of 25 *Hypericum perforatum* L. populations in Iran's natural habitats. *Iranian Journal of Medicinal and Aromatic Plants*, *31*(1), 63-79. https://doi.org/10.22092/ijmapr.2015.12611

Semerdjieva, I., Zheljazkov, V. D., Dincheva, I., Piperkova, N., Maneva, V., Cantrell, C. L., & Ivanova, T. (2023). Essential oil composition of seven Bulgarian *Hypericum* species and its potential as a biopesticide. *Plants*, *12*(4), 923. https://doi.org/10.3390/plants12040923

Sen, A., Kurkcuoglu, M., Senkardes, I., Bitis, L., & Baser, K. H. C. (2019). Chemical Composition, Antidiabetic, Anti-inflammatory and Antioxidant Activity of *Inula ensifolia* L. Essential Oil. *Journal of Essential Oil Bearing Plants*, *22*(4), 1048-1057. https://doi.org/10.1080/0972060X.2019.1662333

Servi, H., Demir, U., Servi, E. Y., Gundogdu, B., & Barak, T. H. (2023). Antiproliferative and Antibacterial Activities of Four Commercial Essential Oil Samples from Boswellia carteri, B. serrata and two chemotypes of Canarium luzonicum. *Journal of Essential Oil-Bearing Plants*, *26*(1), 79-94. doi: https://doi.org/10.1080/0972060X.2023.2165167

Şerbetçi, T., Özsoy, N., Demirci, B., Can, A., Kültür, Ş., & Başer, K. C. (2012). Chemical composition of the essential oil and antioxidant activity of methanolic extracts from fruits and flowers of Hypericum lydium Boiss. *Industrial crops and products*, *36*(1), 599-606. https://doi.org/10.1016/j.indcrop.2011.11.002

Tabanca, N., Demirci, B., Ali, A., Khan, S. I., Jacob, M. R., Aytac, Z., & Khan, I. A. (2015). Chemical composition, biting deterrent, antimalarial and antimicrobial activity of essential oil from *Hypericum scabrum* L. *Current Bioactive Compounds*, *11*(2), 62-72. https:// doi.org/ 10.2174/15734072110215 0820124215

Ustuner, H., Barak, T. H., Servi, H., Ertekin, S. K., Sen, A., Dinç, M., & Özkan, V. K. (2023). Anticancer, antidiabetic, and antioxidant activities of endemic *Stachys buttleri* Mill. and *Stachys pinardii* Boiss. essential oils. *Journal of Essential Oil-Bearing Plants*, *26*(6), 1502-1514. https://doi.org/10.1080/097206 0X.2023.2293960

Velingkar, V. S., Gupta, G. L., & Hegde, N. B. (2017). A current update on phytochemistry, pharmacology and herb–drug interactions of *Hypericum perforatum*. *Phytochemistry Reviews*, *16*(4), 725-744. https://doi.org/10.1007/s11101-017-9503-7

Vuko, E., Dunkić, V., Ruščić, M., Nazlić, M., Mandić, N., Soldo, B., & Fredotović, Ž. (2021). Chemical composition and new biological activities of essential oil and hydrosol of *Hypericum perforatum* L. ssp. *veronense* (Schrank) H. Lindb. *Plants*, *10*(5), 1014. https://doi.org/10.3390/plants10051014

Wise, K., Selby-Pham, S., Bennett, L., & Selby-Pham, J. (2019). Pharmacokinetic properties of phytochemicals in *Hypericum perforatum* influence efficacy of regulating oxidative stress. *Phytomedicine*, 59, 1-5. https://doi.org/10.1016/j.phymed.2018.11.023

Yıldırım, A., Sen, A., Dogan, A., & Bitis, L. (2019). Antioxidant and anti-inflammatory activity of capitula, leaf and stem extracts of *Tanacetum cilicicum* (Boiss.) Grierson. *Internatioal Journal of Secondary Metabolites*, *6*(2), 211-222. https://doi.org/10.21448/ijsm.510316

Yuce, E., & Bagci, E. (2012). The essential oils of the aerial parts of two *Hypericum* taxa (*Hypericum triquetrifolium* and *Hypericum avicularüifolium* subsp. *depilatum* var. *depilatum* (Clusiaceae)) from Turkey. *Natural Product Research*, *26*(21), 1985-1990. https://doi.org/10.1080/14786419.2011.636743

Zhang, R., Ji, Y., Zhang, X., Kennelly, E. J., & Long, C. (2020). Ethnopharmacology of *Hypericum* species in China: A comprehensive review on ethnobotany, phytochemistry and pharmacology. *Journal of Ethnopharmacology*, 254, 1-12. https://doi.org/10.1016/j.jep.2020.112686

Zou, Y., Chang, S. K. C., Gu, Y., & Qian, S. Y. (2011). Antioxidant activity and phenolic compositions of Lentil (*Lens culinaris* var. *morton*) extract and its fractions. *Journal of Agricultural and Food Chemistry*, *59*(6), 2268-2276. https://doi.org/10.1021/jf104640k

Trakya University Journal of Natural Sciences, 26(2), 135–142, 2025
DOI: 10.23902/trkjnat.524243354
www.tujns.org

Research Article

In silico analysis of molecular docking between nicotine and *GSTP1* gene in oral squamous cell carcinoma

Shashanka Thowdanahalli Munipapanna[1], Prabhudas Nelaturi[2]*

[1]*Chikkamagaluru Institute of Medical Sciences, Department of Biochemistry, Karnataka, India*
[2]*Saveetha University, Saveetha Medical College and Hospitals, Saveetha Institute of Medical and Technical Sciences, Department of Anatomy, Unit of Molecular Biology, Tamil Nadu, India*

Cite this article as: Munipapanna, S. T., & Nelaturi, P. (2025). *In silico* analysis of molecular docking between nicotine and *GSTP1* gene in oral squamous cell carcinoma. *Trakya University Journal of Natural Sciences, 26*(2), 135–142. https://doi.org/10.23902/trkjnat.524243354

Abstract

Oral squamous cell carcinoma (OSCC) is a predominant cancer strongly associated with risk factors like use of tobacco, viral infections, and genetic predispositions. Genetic risk factors often involve polymorphisms in genes that are critical for various biological pathways. Glutathione S-transferase pi 1 (*GSTP1*) is a gene involved in detoxifying oral carcinogens and the Ile105Val variant of *GSTP1* is associated with increased risk of cancer development including OSCC. Understanding the interaction between *GSTP1* and carcinogens such as nicotine offers valuable insights into OSCC progression. The study employed *in silico* screening with molecular docking technique in order to explore the binding affinity between nicotine and *GSTP1*. Methods included the use of canonical SMILES from PubChem for drug-likeness and pharmacokinetic assessments. Alongside toxicity evaluation through ToxiM platform, docking analysis revealed a strong binding affinity of -7.1 kcal/mol score. The interaction was stabilized by a Pi–sigma bond with TYR109 at 3.579 Å and Pi–alkyl bonds with PHE9, ARG14, and ILE105. These findings emphasize the crucial role of *GSTP1*, particularly the Ile105Val variant, in progression of OSCC. The study highlighted the involvement of *GSTP1* in carcinogen detoxification and contribute to a better understanding of OSCC's biochemical pathways.

Özet

Oral skuamöz hücreli karsinom (OSHK), tütün kullanımı, viral enfeksiyonlar ve genetik yatkınlıklar gibi risk faktörleriyle güçlü ilişkilide olan baskın bir kanser tipidir. Genetik risk faktörleri arasında genellikle çeşitli biyolojik yolaklar için kritik olan gen polimorfizmleri yer almaktadır. Glutatyon S-transferaz pi 1 (*GSTP1*), oral kanserojenlerin detoksifikasyonunda rol oynayan bir gendir ve *GSTP1*'in Ile105Val varyantı, OSHK dahil olmak üzere kanser gelişimi riskinin artmasıyla ilişkilidir. *GSTP1* ile nikotin gibi kanserojenler arasındaki etkileşimin anlaşılması, OSHK ilerlemesi konusunda değerli bilgiler sunmaktadır. Bu çalışmada, nikotin ve *GSTP1* arasındaki bağlanma afinitesini keşfetmek için moleküler yerleştirme tekniğiyle *in silico* tarama kullanılmıştır. İlaç benzerliği ve farmakokinetik değerlendirmeler için PubChem'den kanonik SMILES kullanılmıştır. ToxiM platformu aracılığıyla yapılan toksisite değerlendirmesinin yanı sıra, yerleştirme analizi -7,1 kcal/mol puanlık güçlü bir bağlanma afinitesi ortaya koymuştur. Etkileşim, 3,579 Å'da TYR109 ile bir Pi–sigma bağı ve PHE9, ARG14 ve ILE105 ile Pi-alkil bağları ile stabilize edilmiştir. Bu bulgular, GSTP1'in, özellikle Ile105Val varyantının OSHK ilerlemesindeki kritik rolünü vurgular niteliktedir. Sonuçlar, *GSTP1*'in kanserojen detoksifikasyonuna katılımını vurgulamış ve OSHK'nın biyokimyasal yollarının daha iyi anlaşılmasına katkıda bulunmuştur.

Keywords: toxicity prediction, cancer genetics, tobacco, gene-environment interactions, computational biology

Edited by: *Melike Sapmaz Metin*

***Corresponding Author:** Nelaturi Prabhudas, **E-mail:** prabhudasn.smc@saveetha.com*
***ORCID iDs of the authors:** STM. 0009-0003-7428-4202, PN. 0000-0002-0390-3235*

Received: 24 January 2025, **Accepted:** 10 June 2025, **Online First**: 11 July 2025, **Published:** 15 October 2025

Introduction

Oral squamous cell carcinoma (OSCC) is recognized as the thirteenth most predominant cancer in the world, accounting for approximately 15% of all cancer cases. Despite advances in medical science, the prognosis for OSCC remains challenging, with less than 60% of patients surviving beyond five years (Tan et al., 2023). OSCC affects the buccal mucosa followed by other oral sites, such as the alveolar surface, hard palate, anterior two-third of tongue and floor of mouth. The development of OSCC is strongly associated with several risk factors, including tobacco use, infection of human papillomavirus (HPV), and genetic predispositions (Ramalingam et al., 2023). Genetic risk factors often involve polymorphisms in genes that are critical for various biological pathways. These pathways include carcinogen detoxification, DNA repair, cell cycle regulation, extracellular matrix stability, immune response, and inflammation (Kay et al., 2019). The gene glutathione S-transferase pi 1 (*GSTP1*) plays crucial role as an enzyme essential for the detoxification of carcinogens, particularly in the oral mucosa. It controls cancer by forming conjugation between harmful substances with glutathione, which is a major cellular antioxidant. Elevated expression of *GSTP1* is frequently observed in OSCC and is associated in resistance to chemotherapy. Conversely, decreased *GSTP1* expression is associated with increased DNA damage when exposed to carcinogens (Schnekenburger et al., 2014).

The gene *GSTP1* is located on chromosome 11q13.2 and encodes for the *GSTP1* enzyme, a key player in detoxifying carcinogens in the oral mucosa. Genetic variations within the *GSTP1* gene, particularly single nucleotide polymorphisms (SNPs), can significantly impact its enzymatic activity and increases the risk of the developing cancer. The selected three variants, Arg187Trp (rs11549), Ala114Val (rs1138272), and lle105Val (rs1695), of the *GSTP1* gene were revealed to be linked to cancer susceptibility, clinical relevance, and roles in carcinogen detoxification. The lle105Val variant, which has been extensively studied is strongly associated with an increased risk of tobacco-related cancers and is known to reduce enzymatic actions. Although the Ala114Val polymorphism is less clearly linked to cancer risk, it is important due to its potential to alter ligand binding affinity and destabilize protein structure. The Arg187Trp variant was prioritized for its predicted harmful effect on protein function which may impair detoxification and the management of oxidative stress. One of the most studied SNPs in this gene is Ile105Val (c.313A>G; rs1695) (Mandal & Mittal, 2020). Polymorphism results in a replacement of isoleucine (Ile) with valine (Val) at codon 105, notably reducing the enzyme activity of approximately 21.8% of its normal function. The Ile105Val variant of *GSTP1* is associated with an increased risk of various cancers, including those of the head and neck, thyroid, breast, lung, stomach, liver, and prostate (Parl, 2005). The reduction in *GSTP1* activity caused by this polymorphism impair the ability of the enzyme thereby affect the detoxification of carcinogens. Accumulation of carcinogens can intensify cancer susceptibility in individuals carrying the Ile105Val (c.313A>G; rs1695) variant (Arja et al., 2014; Mandal & Mittal, 2020).

The present study aimed to investigate the binding interaction between nicotine and *GSTP1* through molecular docking analysis, with particular focus on the Ile105Val polymorphism. Previous studies have highlighted the association between *GSTP1* variants and increased OSCC risk, with evidence showing that the Ile105Val variant is linked to higher oral cancer susceptibility and altered detoxification capacity (Koh et al., 2011). Several investigations have emphasized the clinical relevance of *GSTP1* polymorphisms in carcinogenesis and their contribution to impaired detoxification of carcinogens such as areca-nut metabolites. Previous studies have demonstrated a significant association between *GSTP1* polymorphisms, particularly the Ile105Val variant, and cancer susceptibility, including OSCC (Li et al., 2013; Marshall et al., 2000). The Ile105Val substitution is known to alter GSTP1 enzymatic activity, leading to reduced detoxification efficiency and increased vulnerability to carcinogenic compounds (Mandal & Mittal, 2020). Numerous investigations have reported correlations between this polymorphism and OSCC risk, underscoring its involvement in oxidative stress modulation and xenobiotic metabolism (Yadav et al., 2020; Pandith et al., 2013; Sharma et al., 2014; Akkus & Kucuk Kurtulgan, 2025). Despite these findings, the mechanistic details of how nicotine interacts with *GSTP1* and its variants remain insufficiently characterized. This study addresses this gap by integrating molecular docking analysis to explore how nicotine binding may impair *GSTP1* function, offering new insights into potential role in OSCC pathogenesis.

Materials and Methods

Structure Retrieval

The Protein Data Bank (PDB) coordinates for the structural domain (17GS; UniProtID: P09211) of *GSTP1* was obtained from the PDB database. Nicotine compound (PubChemCID: 89594) (Figure 1), including L-nicotine (BS; ID: 349993228), were retrieved from the PubChem database.

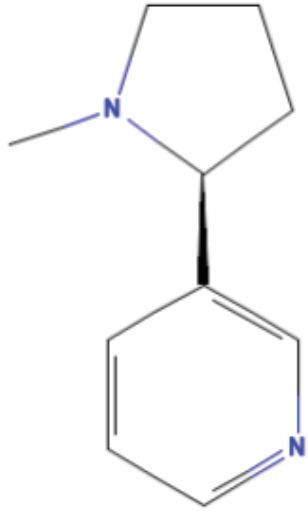

Figure 1. Nicotine PubChem Compound ID (CID: 89594).

Ligand Preparation

Ligands were prepared via Chimera software version 1.15, and protein preparation was performed via AutoDock Vina version 1.5.7. Energy minimization for both proteins and ligands was conducted via the YASARA minimization server. Water molecules and heteroatoms were removed, polar hydrogens were added, and nonpolar hydrogens were merged. Kollman and Gasteiger charges were added. Ligands, initially downloaded in SDF format from PubChem, were converted to PDB format via Open Babel. Ligand charges were neutralized, and Gasteiger charges were applied. Default torsion settings were retained.

Molecular Docking

Molecular docking was carried out via AutoDock Vina (SwissDock). Initial blind docking was followed by precision docking. The grid spacing was set to 1 Å, and the grid box was manually adjusted to include all active-site residues of the receptor. The grid box dimensions were set at X = 30, Y = 30, and Z = 30 and centered at X = 21.289, Y = 5.227, and Z = 21.348 for the 17GS protein. Docking was performed in triplicate, and exhaustiveness was adjusted to optimize the docking process. Docking experiments were also conducted via InstaDock for additional validation. For visualization of the protein–ligand interactions, Discovery Studio was utilized. Modifications to both proteins and ligands, including the addition of hydrogen atoms, removal of water molecules, and substitution of amino acids, were performed via Discovery Studio. AutoDock Tools version 1.5.6, was employed to explore the binding modes of the inhibitory compounds on the *GSTP1* enzyme (17GS). The protein and ligand files were saved in pdbqt format following preparation, and the grid box parameters were carefully set to cover the entire target enzyme. Binding interactions were analysed via PyMol for 3D visualization.

Visualization of Docking Poses

PyMol was used to visualize and analyse the docked poses and protein structures, as well as to render figures. Two–dimensional protein–ligand interactions were generated via LigPlot+ (version 2.2.5) and Discovery Studio Visualize. Cartoons of the protein–ligand interactions were produced to illustrate the docking results.

Validation Using the Database of Useful Decoys: Enhanced (DUDE. E)

To assess the docking method and minimize false positives, decoys with similar physical properties to the reference ligand were generated via DUDE. E database (http://decoys.docking.org). These decoys were compared with five target proteins available on the server.

ADMET Predictions

Pharmacokinetic properties, including absorption, distribution, metabolism, excretion, and toxicity (ADMET), were predicted via SwissADME. Canonical SMILES from PubChem was used to calculate drug-likeness and pharmacokinetic profiles.

Toxicity Prediction

Toxicity predictions were performed via ToxiM software. The PDB or SDF files of the desired compounds or their PubChem compound ID numbers were input into ToxiM to assess toxicity via various descriptors, fingerprints, and hybrid models.

Results

Selection and Preparation of Ligands

Eight flavonoid ligand compounds were selected for molecular docking analysis. These ligands were obtained in SDF format, and their 2D structures were retrieved from the PubChem database (Figure 1). The sole ligand specifically mentioned in this work is nicotine, found by PubChem Compound ID (CID: 89594). Although the section on methods notes that eight flavonoid ligands were chosen for molecular docking analysis, their names, IDs, or chemical structures were neither mentioned nor recorded in the results. The SDF files were converted to PDB format via Discovery Studio software to facilitate further analysis. The selected ligands, particularly nicotine, interact effectively with *GSTP1* with one ligand, 17GS, which strongly binds at the 105th position of the gene. Nicotine compounds were then analysed via the SWISS-ADME database for toxicity prediction, which revealed high permeability and significant absorption in human intestinal and lung tissues, suggesting enhanced bioavailability. Twenty nicotine derivatives docked against a target protein are shown in the image as a ribbon structure with their binding poses and docking scores. The docking scores of selected nicotine derivatives ranging from -6.4 to -7.6 kcal/mol indicate different levels of binding affinity, and each ligand is displayed in its predicted binding conformation. The strongest binding was notably shown by ligands 15 (-7.6 kcal/mol), 20 (-7.5 kcal/mol), and 8 (-7.5 kcal/mol), indicating a high potential for interaction with the protein's active site. The nicotine derivatives of ligands' moieties are aromatic and heterocyclic, which is consistent with scaffolds that resemble nicotine compounds, like pyridine and pyrrolidine rings (Figure 2).

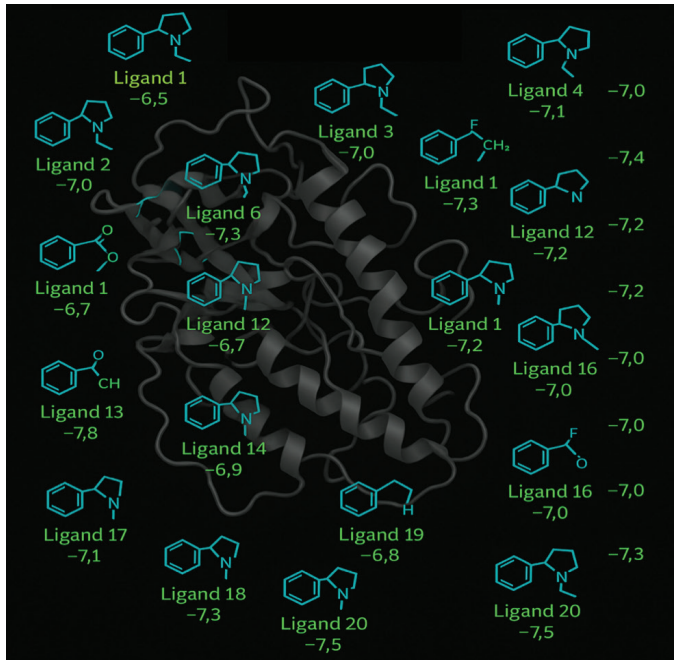

Figure 2. Schematic representation of binding poses and docking scores of nicotine derivatives (varies ligands) with the target *GSTP1*.

Molecular Docking Studies

The study primarily focused on the molecular docking of nicotine with *GSTP1* and its variants was the main focus of the study, which reported different docking scores and binding modes for each. With the wild-type *GSTP1*, nicotine showed a docking score of -7.1 kcal/mol. It interacted with TYR109 via a Pi–sigma bond and with PHE9, ARG14, and ILE105 via Pi–alkyl interactions. With a docking score of -9.8 kcal/mol, the Arg187Trp variant showed the highest binding affinity among the variants. It formed Pi–Pi stacking interactions with TRP104 and hydrogen bonds with GLU68, SER75, and CYS101. The Ile105Val variant had the lowest binding score of -4.5 kcal/mol with little effect from interactions, whereas the Ala114Val variant had a moderate binding score of -7.2 kcal/mol and interacted with CYS101 and SER108 through hydrogen bonds. The study focused on the in-depth examination of nicotine's interactions with *GSTP1* and its missense variants, rather than providing specific docking results for the eight flavonoid ligands that were initially mentioned.

Molecular docking between nicotine and *GSTP1* revealed a strong interaction with docking score of -7.1 kcal/mol, indicating a stable binding affinity (Table 1). The interaction of nicotine with specific amino acids, including TYR109, PHE9, ARG14, and ILE105, occurs primarily through hydrophobic interactions. TYR109 formed a Pi–sigma interaction at a short distance of 3.579 Å, contributing to the stability of the complex (Figure 3). PHE9 and ARG14 exhibited Pi–alkyl interactions with nicotine at distances of 5.138 Å and 5.252 Å, respectively, whereas ILE105 formed a Pi–alkyl interaction at 5.210 Å (Figure 4). These hydrophobic interactions suggest that nicotine stabilizes its binding within the GSTP1 enzyme, potentially affecting its detoxification function.

The *GSTP1* gene has role in detoxifying harmful compounds by making conjugation of glutathione with various substances. The strong binding of nicotine to *GSTP1* could modulate or inhibit the activity of the enzyme, affecting its detoxification role. This stable interaction suggest that nicotine may interfere with the function of *GSTP1* with possible implications for nicotine metabolism and toxicity. However, further studies are required to explore the specific effects of this binding on *GSTP1* activity.

Molecular Modelling of *GSTP1* Variants

In this study, molecular modelling was used to assess the impact of three *GSTP1* missense variants (Ile105Val, Ala114Val, and Arg187Trp) on the risk of oral squamous cell carcinoma. Molecular docking simulations focused on the binding interactions between *GSTP1* and its substrates to predict functional disruptions caused by these variants. Three clinically significant missense variations in the *GSTP1* gene -Arg187Trp (rs115494), Ala114Val (rs1138272),

Table 1. Screening of nicotine against the protein target *GSTP1*.

GSTP1 type	Docking score (kcal/mol)	Key interactions	Binding affinity
Wild-type	-7.1	Pi–sigma bond with TYR109; Pi–alkyl with PHE9, ARG14, ILE105	Moderate
Arg187Trp	-9.8	Hydrogen bonds with GLU68, SER75, CYS101; Pi–Pi stacking with TRP104	Strongest
Ala114Val	-7.2	Hydrogen bonds with CYS101, SER108	Moderate
Ile105Val	-4.5	Minimal interaction impact	Weakest

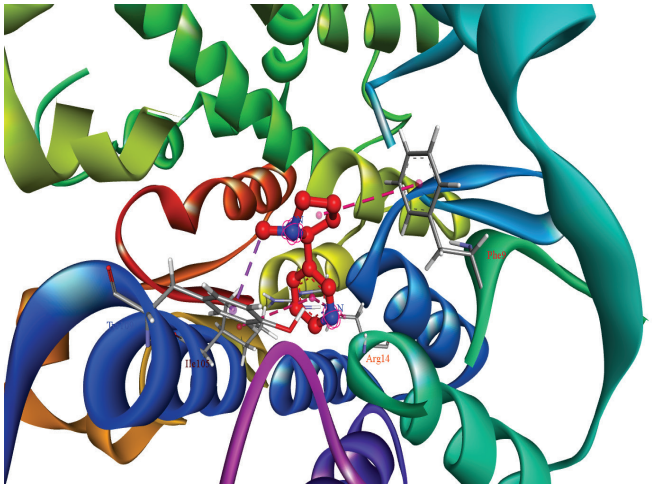

Figure 3. Structure of the treated protein target of the nicotine compound.

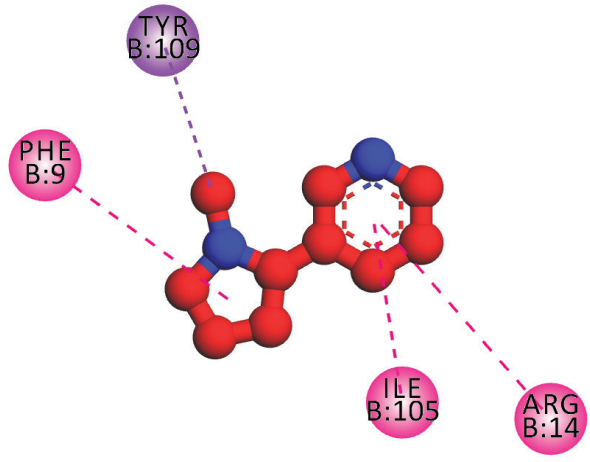

Figure 4. 2D interaction view of nicotine with target of the *GSTP1* gene's SNPs positions.

and Ile105Val (rs1695)- are the focus of the study. The genetic variations were selected because of their functional significance in carcinogen detoxification and their associations with cancer risk. Ile105Val was added because of its proven impact on detoxification effectiveness. Its association with decreased enzymatic activity and a higher risk of tobacco-related cancers, such as bladder, lung, and OSCC, has also been thoroughly studied. Because of its ability to generate ligand interactions that change protein structure, the Ala114Val variant was found to have a weaker association with the risk of oral cancer. Since it was expected that Arg187Trp would have a detrimental effect on protein function, detoxification, and the control of oxidative stress, it was given top priority because of its likely substantial functional effect. Bioinformatic docking studies were used to determine the genetic implications of these variations on *GSTP1*'s interaction with nicotine and their possible significance in the pathophysiology of OSCC. In South Asian groups, the allele frequencies were 0.31, 0.06, and 0.01 (Figure 5).

The Arg187Trp variant showed the highest docking score (-9.8 kcal/mol) that indicates a significant alteration in binding affinity and protein function. It forms strong hydrogen bonds with critical residues such as Glu68, Ser75, and Cys101 and pi–pi stacking interaction with Trp104. Findings suggest a compromised detoxification function, particularly in individuals exposed to carcinogens such as tobacco. The Ala114Val variant with a docking score of -7.2 kcal/mol, also showed significant interactions with Cys101 and Ser108, indicating moderate functional disruption. Conversely, the Ile105Val variant had a weaker docking score (-4.5 kcal/mol) and showed minimal impact on binding, aligning with its lower association with OSCC risk (Figure 6). The observed changes in docking scores for the Ala114Val and Arg187Trp variants imply the presence of possible allosteric effects, despite the fact that Ala114 and Arg187 are not found within the identified nicotine-binding pocket of *GSTP1*. By indirectly altering the structural and physicochemical properties of the ligand-binding site on a gene, missense mutations that arise far from the active binding pocket it may affect a protein's overall conformation, flexibility, and dynamic properties. The differences in expected binding affinities observed in the docking study of this particular gene in the Arg187Trp and Ala114Val variants could be explained by such allosteric effects.

Overall, these findings indicate that the Arg187Trp and Ala114Val variants are likely to impair the detoxification capacity of *GSTP1*, particularly in the context of carcinogen exposure. This reduced detoxification efficiency may lead to increased oxidative stress and DNA damage, contributing to the development of OSCC.

Discussion

Cancer is a major health risk associated with chewing tobacco, focusing specifically on its impact which differ from other smokeless tobacco products that cause seven disease outcomes examined about six i.e. esophageal cancer, lip and oral cavity cancer, laryngeal cancer, nasopharyngeal cancer, other pharyngeal cancers, and stroke have been found but less evidence related to tobacco use (Gil et al., 2024). This study conducted on the molecular interaction between nicotine and *GSTP1*, alongside three clinically relevant *GSTP1* variants of Ile105Val (rs1695),

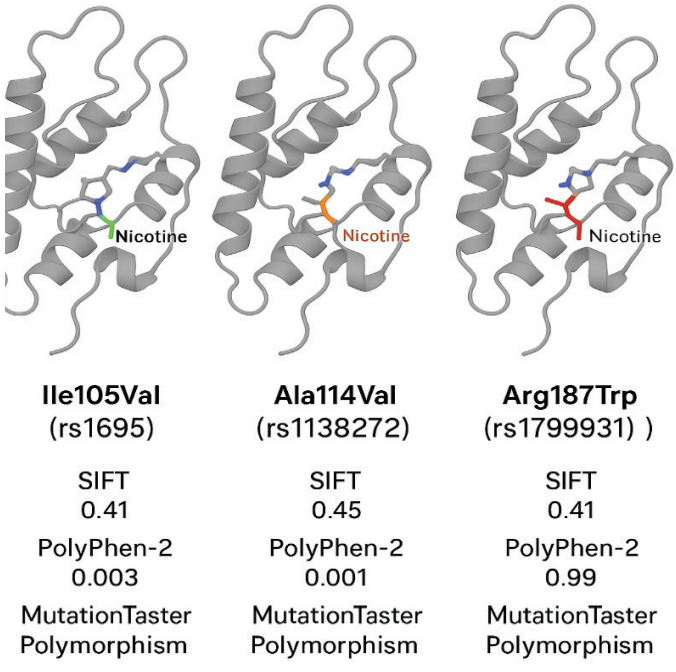

Figure 5. Molecular structural impact the Ile105Val, Ala114Val, and Arg187Trp variants with allele frequencies.

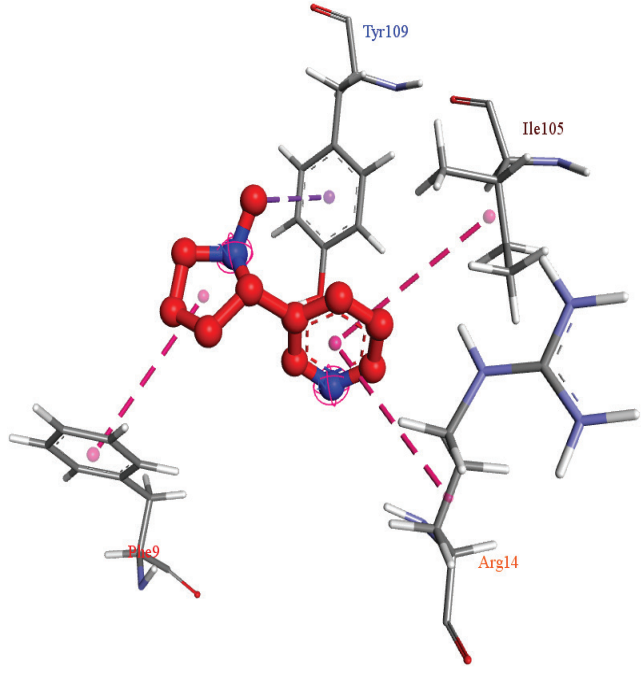

Figure 6. 3D interaction view of nicotine with target of interest 105 SNPs position in the *GSTP1* gene.

Ala114Val (rs1138272) and Arg187Trp (rs11549467) using *in silico* docking and modelling techniques. *GSTP1* plays an essential role in detoxifying electrophilic compounds, including those derived from tobacco and polymorphisms in this gene have been shown to influence cancer susceptibility (Awad et al., 2024; Vasconcelos & Gilbert, 2018). Docking analysis revealed that nicotine binds moderately to the wild-type *GSTP1* with a docking score of -7.1 kal/mol. This interaction was primarily stabilized by Pi–sigma and Pi–alkyl interactions involving TYR109, PHE9, ARG14 and ILE105 suggesting that nicotine could potentially occupy the enzyme's active site influencing its detoxification capacity. Menthol, a common flavour additive found to increase airflow sensation while it impairs respiratory reflex, enhancing lung exposure to harmful substances in both cigarettes and e-cigarettes (Kaur et al., 2018).

Among the studied variants the Arg187Trp mutation showed the highest binding affinity for nicotine (-9.8 kcal/mol) forming multiple hydrogen bonds and Pi–Pi stacking interactions with surrounding residues, including GLU68, SER75, CYS101 and TRP104. Although Arg187 is distant from the active site, this variant likely induces conformational changes that enhance ligand binding it a phenomenon consistent with allosteric modulation mechanism previously reported for GST enzymes. These findings emphasize the long-term effects of early nicotine exposure on genetic regulation (Blaskovic et al., 2022). The Ala114Val variant exhibited a moderate docking score of -7.2 kcal/mal, with hydrogen bonding observed CYS101 and SER108. Though not directly within the binding pocket Ala114 may subtly influence protein flexibility and the orientation of nearby residues, potentially affecting ligand accommodation. The process coupled with the regulation of growth factors, may contribute to cancer progression by promoting tumor growth (Barr et al., 2007). *GST* gene polymorphisms modify the effect of maternal smoking on offspring DNA methylation, showing sec-specific differences at certain CpG sites (Kheirkhah Rahimabad et al., 2023).

A study provided insights into nicotine metabolism, revealing a complex relationship between nicotine transport, protein expression, glycometabolism, and nitrogen metabolism with implications in various biochemical pathways (Mo et al., 2021). Another aspect of the study examined the Ile105Val SNP in the *GSTP1* gene in relation to OSCC in an Indian population. However, further investigation into additional *GSTP1* polymorphisms, such as Ala114Val and Arg187Trp revealed stronger associations with OSCC, suggested that other functional SNPs may play more critical role in disease pathogenicity. The *GSTP1* Ile105Val polymorphism (rs1695) is a genetic variation in the *GSTP1* gene that lead to an amino acid substitution from isoleucine (Ile) to valine (Val) at position 105 (Li et al., 2013). The Val105 variant has been associated with increased susceptibility to several cancers, including lung, breast, and oral cancers, particularly in individuals exposed to environmental toxins such as tobacco smoke (Marshall et al., 2000; Yadav et al., 2020). Due to its role in cancer risk, the *GSTP1* Ile105Val SNP is widely studied in cancer predisposition. Docking analysis can assess nicotine's binding to *GSTP1*, offering insight into how this interaction may affect the enzyme's detoxification function (Pandith et al., 2013). The consumption of tobaco major constituent of nicotine, the primary addictive component of tobacco, binds to nicotinic acetylcholine receptors (nAChRs), specifically the α7-nAChR subtype expressed in OSCC cells. This cellular intigrety will be stimulates intracellular signalling cascades, notably the PI3K/AKT pathway, which leads to increased production of synuclein gamma, a protein associated to cancer formation. Interestingly, the carcinogenic features connected to nicotine-induced expression are diminished when the AKT pathway or α7-nAChR is suppressed. Additionally, nicotine and its metabolites–particularly NNN and NNK–act as agonists on nAChRs, increasing the invasion, proliferation, and spread of oral cancer cells (Shen et al., 2024). The relative functional relevance of the Ile105Val, Ala114Val, and Arg187Trp variations of *GSTP1* may be better binding affinities and interaction residues based on our molecular docking research. The docking findings demonstrated a consistent binding energy of -7.1 kcal/mol between nicotine and the wild-type *GSTP1* protein, indicating that nicotine may impair *GSTP1*'s detoxifying function and promote carcinogen buildup. With the greatest binding affinity of -9.8 kcal/mol of the variations studied, Arg187Trp indicated a strong potential to interfere with detoxification operations. As previously reported, the Ile105Val variant, on the other hand, displayed a reduced binding affinity of -4.5 kcal/mol, suggesting its very minor influence on *GSTP1* enzymatic activity (Akkus & Kucuk Kurtulgan, 2025). The Ile105Val variant displayed the weakest binding affinity (-4.5 kcal/mol), likely due to steric alteration within the active site. Substituting isoleucine with valine slightly reduces the side chain volume, possibly disrupting the stability of ligand binding. This finding is consistent with experimental evidence indicating reduced enzymatic activity and substrate binding for the Ile105Val variant (Hollman et al., 2016). Interestingly, even though Ala114Val and Arg187Trp are situated outside the active binding region in our model, discrepancies in their docking scores suggest the potential of allosteric effects that might have an indirect influence on ligand interactions. Collectively, these findings suggest that *GSTP1* variants particularly Arg187Trp and Ala114Val may alter nicotine binding stability and potentially compromise detoxification efficiency with implications for tobacco-related cancer susceptibility. The study findings explore the function of the *GSTP1* Ile105Val (rs1695) and other functionally significant SNPs in the glutathione S-transferase family, connecting them to differences in detoxification ability and cancer susceptibility, specifically OSCC (Sharma et al., 2014). The mechanistic understanding of nicotine-related carcinogenesis by highlighting the interactions between nicotine and *GSTP1* may impair enzymatic function through docking analysis and proteomic insights. With significant ramifications for public health and tailored cancer prevention strategies, the work integrates epidemiological, toxicological, and molecular genetic evidence to enhance our understanding of tobacco-related disease risk.

Conclusion

OSCC poses significant public health challenges as its development is influenced by various genetic and environmental factors. The *GSTP1* enzyme, particularly its Ile105Val (rs1695) polymorphism, plays a crucial role in the detoxification of carcinogens and has been linked to cancer susceptibility. Understanding the interaction between nicotine and *GSTP1* through docking analysis could shed light on the biochemical mechanisms underlying cancer risk and provide valuable information for developing targeted interventions. By integrating molecular modelling, docking analysis, and proteomic data, the findings demonstrate how nicotine's interaction with variant *GSTP1* enzymes may impair detoxification capacity, contributing to carcinogenesis. The findings also underscore the broader impact of functionally significant SNPs within the *GSTP1* family on individual variability in cancer risk. These results have important public health implications, supporting the development of personalized prevention strategies and advancing our understanding of the molecular underpinnings of tobacco-related diseases.

Ethics

Ethics Committee Approval: Since the article does not contain any studies with human or animal subject, its approval to the ethics committee was not required.

Data Sharing Statement: All data are available within the study.

Footnotes

Author Contributions: Conceptualization: S.T.M., and P.N.; Design/methodology: S.T.M., and P.N.; Execution/investigation: S.T.M.; Resources/materials: S.T.M.; Data acquisition: S.T.M.; Data analysis/interpretation: S.T.M., and P.N.; Writing – original draft: S.T.M., and P.N.; Writing – review & editing/critical revision: S.T.M., and P.N.

Conflict of Interest: The authors have no conflicts of interest to declare.

Funding: No external funding acquired.

References

Akkus, N., & Kucuk Kurtulgan, H. (2025). Glutathione S-transferase polymorphisms and their role in recurrent pregnancy loss: A genetic risk assessment. *Turkish Journal of Obstetrics and Gynecology, 22*(1), 19-25. https://doi.org/10.4274/tjod.galenos.2025.57609

Arja, C., Ravuri, R. R., Pulamaghatta, V. N., Surapaneni, K. M., Raya, P., Adimoolam, C., & Kanala, K. R. (2014). Genetic determinants of chronic obstructive pulmonary disease in South Indian male smokers. *PLoS One, 9*(2), e89957. https://doi.org/10.1371/journal.pone.0089957

Awad, A. A., Itumalla, R., Gaidhane, A. M., Khatib, M. N., Ballal, S., Bansal, P., Srivastava, M., Arora, I., Kumar, M., Sinha, A., Pant, K., Serhan, H. A., & Shabil, M. (2024). Association of electronic cigarette use and suicidal behaviors: a systematic review and meta-analysis. *BMC Psychiatry, 24*(1), 608. https://doi.org/10.1186/s12888-024-06012-7

Barr, J., Sharma, C. S., Sarkar, S., Wise, K., Dong, L., Periyakaruppan, A., & Ramesh, G. T. (2007). Nicotine induces oxidative stress and activates nuclear transcription factor kappa B in rat mesencephalic cells. *Molecular and Cellular Biochemistry, 297*(1-2), 93-99. https://doi.org/10.1007/s11010-006-9333-1

Blaskovic, S., Donati, Y., Ruchonnet-Metrailler, I., Avila, Y., Schittny, D., Schlepütz, C. M., Schittny, J. C., & Barazzone-Argiroffo, C. (2022). Early life exposure to nicotine modifies lung gene response after elastase-induced emphysema. *Respiratory Research, 23*(1), 44. https://doi.org/10.1186/s12931-022-01956-4

Gil, G. F., Anderson, J. A., Aravkin, A., Bhangdia, K., Carr, S., Dai, X., Flor, L. S., Hay, S. I., Malloy, M. J., McLaughlin, S. A., Mullany, E. C., Murray, C. J. L., O'Connell, E. M., Okereke, C., Sorensen, R. J. D., Whisnant, J., Zheng, P., & Gakidou, E. (2024). Health effects associated with chewing tobacco: a Burden of Proof study. *Nature Communications, 15*(1), 1082. https://doi.org/10.1038/s41467-024-45074-9

Hollman, A. L., Tchounwou, P. B., & Huang, H.C. (2016). The Association between Gene-Environment Interactions and Diseases Involving the Human GST Superfamily with SNP Variants. *International Journal of Environmental Research and Public Health, 13*(4), 379. https://www.mdpi.com/1660-4601/13/4/379

Kaur, G., Muthumalage, T., & Rahman, I. (2018). Mechanisms of toxicity and biomarkers of flavoring and flavor enhancing chemicals in emerging tobacco and non-tobacco products. *Toxicology Letters, 288*, 143-155. https://doi.org/10.1016/j.toxlet.2018.02.025

Kay, J., Thadhani, E., Samson, L., & Engelward, B. (2019). Inflammation-induced DNA damage, mutations and cancer. *DNA Repair (Amst), 83*, 102673. https://doi.org/10.1016/j.dnarep.2019.102673

Kheirkhah Rahimabad, P., Jones, A. D., Zhang, H., Chen, S., Jiang, Y., Ewart, S., Holloway, J. W., Arshad, H., Eslamimehr, S., Bruce, R., & Karmaus, W. (2023). Polymorphisms in Glutathione S-Transferase (GST) Genes Modify the Effect of Exposure to Maternal Smoking Metabolites in Pregnancy and Offspring DNA Methylation. *Genes, 14*(8), 1644. https://doi.org/10.3390/genes14081644

Koh, W. P., Nelson, H. H., Yuan, J. M., Van den Berg, D., Jin, A., Wang, R., & Yu, M. C. (2011). Glutathione S-transferase (GST) gene polymorphisms, cigarette smoking and colorectal cancer risk among Chinese in Singapore. *Carcinogenesis, 32*(10), 1507-1511. https://doi.org/10.1093/carcin/bgr175

Li, W., Chen, J., & Liu, C. (2013). Glutathione S-transferase P1 Ile105Val polymorphism and oral cancer risk: a meta-analysis. *International Journal of Medical Sciences, 10*(4), 392-398. https://doi.org/10.7150/ijms.5770

Mandal, R. K., & Mittal, R. D. (2020). Glutathione S-Transferase P1 313 (A > G) Ile105Val Polymorphism Contributes to Cancer Susceptibility in Indian Population: a meta-analysis of 39 Case-Control Studies. *Indian Journal of Clinical Biochemistry, 35*(1), 8-19. https://doi.org/10.1007/s12291-018-0787-1

Marshall, S. E., Bordea, C., Haldar, N. A., Mullighan, C. G., Wojnarowska, F., Morris, P. J., & Welsh, K. I. (2000). Glutathione S-transferase polymorphisms and skin cancer after renal transplantation. *Kidney International, 58*(5), 2186-2193. https://doi.org/https://doi.org/10.1111/j.1523-1755.2000.00392.x

Mo, Z., Pu, Y., Zhou, J., Tian, Z., Teng, J., Chen, Q., Duan, L., & Liu, R. (2021). Effect of the over-dominant expression of proteins on nicotine heterosis via proteomic analysis. *Scientific Reports, 11*(1), 21063. https://doi.org/10.1038/s41598-021-00614-x

Pandith, A. A., Lateef, A., Shahnawaz, S., Hussain, A., Malla, T. M., Azad, N., Shehjar, F., Salim, M., & Shah, Z. A. (2013). GSTP1 gene Ile105Val polymorphism causes an elevated risk for bladder carcinogenesis in smokers. *Asian Pacific Journal of Cancer Prevention, 14*(11), 6375-6378. https://doi.org/10.7314/apjcp.2013.14.11.6375

Parl, F. F. (2005). Glutathione S-transferase genotypes and cancer risk. *Cancer Letters, 221*(2), 123-129. https://doi.org/https://doi.org/10.1016/j.canlet.2004.06.016

Ramalingam, K., Krishnan, M., Ramani, P., & Muthukrishnan, A. (2023). Quality of life assessment with european organisation for research and treatment of cancer questionnaire (head and neck module 43) and its clinicopathological correlation among patients treated for oral squamous cell carcinoma: an exploratory study. *Cureus, 15*(2), e34650. https://doi.org/10.7759/cureus.34650

Schnekenburger, M., Karius, T., & Diederich, M. (2014). Regulation of epigenetic traits of the glutathione S-transferase P1 gene: from detoxification toward cancer prevention and diagnosis. *Frontiers in Pharmacology, 5*, 170. https://doi.org/10.3389/fphar.2014.00170

Sharma, A., Pandey, A., Sharma, S., Chatterjee, I., Mehrotra, R., Sehgal, A., & Sharma, J. K. (2014). Genetic polymorphism of glutathione S-transferase P1 (GSTP1) in Delhi population and comparison with other global populations. *Meta Gene, 2*, 134-142. https://doi.org/10.1016/j.mgene.2013.12.003

Shen, Y., Huang, Q., Yuan, X., Gong, H., Xu, C., Du, H., Hsueh, C.-Y., & Zhou, L. (2024). Nicotine-induced activation of cholinergic receptor nicotinic alpha 5 subunit mediates the malignant behaviours of laryngeal squamous epithelial cells by interacting with RABL6. *Cell Death Discovery, 10*(1), 286. https://doi.org/10.1038/s41420-024-02051-x

Tan, Y., Wang, Z., Xu, M., Li, B., Huang, Z., Qin, S., Nice, E. C., Tang, J., & Huang, C. (2023). Oral squamous cell carcinomas: state of the field and emerging directions. *International Journal of Oral Science, 15*(1), 44. https://doi.org/10.1038/s41368-023-00249-w

Vasconcelos, V., & Gilbert, H. (2018). Smokers' knowledge and perception of electronic cigarettes (e-cigarettes): a qualitative study of non-quitting smokers in a North London general practice. *Primary Health Care Research & Development, 20*, e38. https://doi.org/10.1017/s1463423618000439

Yadav, P., Banerjee, A., Boruah, N., Singh, C. S., Chatterjee, P., Mukherjee, S., Dakhar, H., Nongrum, H. B., Bhattacharjee, A., & Chatterjee, A. (2020). Glutathione S-transferasesP1 AA (105Ile) allele increases oral cancer risk, interacts strongly with c-Jun kinase and weakly detoxifies areca-nut metabolites. *Scientific Reports, 10*(1), 6032. https://doi.org/10.1038/s41598-020-63034-3

Trakya University Journal of Natural Sciences, 26(2), 143–155, 2025
DOI: 10.23902/trkjnat.5877563254657
www.tujns.org

Research Article

Marine-derived *Penicillium oxalicum* M6A as a halotolerant biocatalyst for enzymatic biodegradation and detoxification of the azo dye Direct Red 75

Ugochukwu Okechukwu Ozojiofor*, Mohammed Sani Abdulsalami[1], Nkechi Eucharia Egbe, Ahmed Ali Haroun

Nigerian Defence Academy, Faculty of Science, Department of Biotechnology, Kaduna, Nigeria

Cite this article as: Ozojiofor, O. U., Abdulsalami, M. S., Egbe, N. E., & Haroun, A. A. (2025). Marine-derived Penicillium oxalicum M6A as a halotolerant biocatalyst for enzymatic biodegradation and detoxification of the azo dye Direct Red 75. *Trakya University Journal of Natural Sciences, 26*(2), 143–155. https://doi.org/10.23902/trkjnat.5877563254657

Abstract

The structural complexity and synthetic origin of azo dyes such as Direct Red 75 (DR75) make them environmentally persistent and challenging to remove from industrial effluents. In this study, *Penicillium oxalicum* M6A, a halotolerant marine-derived fungus isolated from the Nigerian coastline, was evaluated for its capacity to biodegrade and detoxify DR75. The influence of pH, temperature, salt, and dye concentration on degradation efficiency was assessed, along with enzymatic activity. Fourier-transform infrared (FTIR) spectroscopy and gas chromatography–mass spectrometry (GC–MS) analyses were employed to identify degradation products and predict metabolic pathways. Toxicity was determined using three bacterial strains and two crop plant seeds. Optimal degradation was achieved at a pH of 5 (90.37%), a temperature of 35°C (66.82%), a dye concentration of 50 mg/L (91.53%), and a NaCl concentration of 4% (67.08%). Enzymatic assays revealed significant upregulation of laccase (24.17 U/mL), azoreductase (13.14 U/mL), and lignin peroxidase (12.54 U/mL), indicating their involvement in dye breakdown**.** FTIR analysis confirmed the disappearance of characteristic azo and sulfonic peaks, while GC–MS identified key metabolites such as 2,3-dihydrobenzofuran, m-hydroquinone, and 6-ethoxy-6-methyl-2-cyclohexenone. Microtoxicity and phytotoxicity assessments revealed that the degradation products of DR75 by *P. oxalicum* M6A did not inhibit the bacterial strains and exhibited low toxicity to the seeds of the crop plants used. These findings establish that *P. oxalicum* M6A can effectively degrade and detoxify DR75, converting it into less toxic metabolites. These observations highlight

Özet

Direct Red 75 (DR75) gibi azo boyaların yapısal karmaşıklığı ve sentetik kökenleri, bunları çevreye kalıcı hale getirir ve endüstriyel atıklardan uzaklaştırılmasını zorlaştırır. Bu çalışmada, Nijerya kıyılarından izole edilen halotolerant deniz kaynaklı bir mantar olan *Penicillium oxalicum* M6A, DR75'i biyolojik olarak parçalama ve detoksifikasyon kapasitesi açısından değerlendirilmiştir. Enzimatik aktivite ile birlikte pH, sıcaklık, tuz ve boya konsantrasyonunun bozunma verimliliği üzerindeki etkisi değerlendirilmiştir. FTIR ve GC-MS analizleri, bozunma ürünlerini tanımlamak ve metabolik yolakları tahmin etmek için kullanılırken, toksisite üç bakteri suşu ve iki mahsul bitkisi tohumu kullanılarak değerlendirilmiştir. Optimum bozunma pH 5 (90,37%), 35°C (66,82%), 50 mg/L boya konsantrasyonu (91,53%) ve %4 NaCl (67,08%) değerlerinde elde edilmiştir. Enzimatik analizler, laccaz (24,17 U/mL), azoredüktaz (13,14 U/mL) ve lignin peroksidaz (12,54 U/mL) enzimlerinin önemli ölçüde yukarı regülasyonunu ortaya çıkarmış ve bunların boya parçalanmasında rol oynadığını göstermiştir**.** FTIR analizi, karakteristik azo ve sülfonik piklerin kaybolduğunu doğrularken, GC-MS, 2,3-dihidrobenzofuran, m-hidrokinon ve 6-etoksi-6-metil-2-sikloheksenon gibi önemli metabolitleri tanımladı. Mikrotoksisite ve fitotoksisite değerlendirmeleri, *P. oxalicum* M6A tarafından DR75'in bozunma ürünlerinin bakteri suşları üzerinde herhangi bir inhibisyon bölgesi göstermediğini ve kullanılan mahsul bitkilerinin tohumları için daha az toksik olduğunu göstermiştir. Bu sonuçlar, *P. oxalicum* M6A'nın DR75'i etkili bir şekilde bozunabileceğini ve detoksifiye edebileceğini, onu daha az toksik metabolitlere

Edited by: *Özkan Danış*

***Corresponding Author:** Ugochukwu Okechukwu Ozojiofor, **E-mail:** ozojiofor.uo@nda.edu.ng*

***ORCID iDs of the authors:** UOO. 0000-0001-7829-1045, MSA. 0009-0006-7350-2871, NEE. 0000-0003-0086-2172, AAH. 0009-0007-4689-9380.*

Received: 05 June 2025, **Accepted:** 17 July 2023, **Online First**: 08 August 2025, **Published:** 15 October 2025

the biocatalytic potential of *P. oxalicum* M6A for treating dye-contaminated saline wastewater and encourage further scale-up for environmental applications.

dönüştürebileceğini göstermektedir. Bu bulgular, boya ile kirlenmiş tuzlu atık suların arıtılmasında *P. oxalicum* M6A'nın biyokatalitik potansiyelini vurgulamakta ve çevresel uygulamalar için daha fazla ölçeklendirilmesini teşvik etmektedir.

Keywords: *Penicillium oxalicum M6A*, laccase, recalcitrant pollutants, peroxidase, synthetic dyes, ecotoxicity assessment

Introduction

Azo dyes are the largest group of dyes widely used in industries, including textiles, cosmetics, printing, paper, and pharmaceuticals (Vinodhkumar et al., 2013). In the textile industry, dyeing processes generate dye-rich wastewaters containing various functional groups. These dyes interfere with ecological processes such as photosynthesis, posing further environmental and health concerns owing to their carcinogenic and mutagenic properties (Gavril & Hodson, 2007; Basu & Kumar, 2014; Ben Mbarek et al., 2023). Azo dyes are synthetic dyes, and their complex intrinsic structural properties make them challenging to decolorize, especially in industries that utilize sewage systems to treat dyes. Their water solubility and colored, acidic, and reactive nature make these dyes highly resistant to degradation, and they remain unaffected during conventional treatment (Willmott et al., 1998). Biodegradation processes, which employ microbial enzyme transformation and the detoxification of pollutants, have been the subject of numerous investigations (Couto, 2007). Fungi are considered to be more resilient than bacteria and are able to withstand high concentrations of recalcitrant pollutants (Ellouze & Sayadi, 2016). Fungi utilize economical and environmentally benign processes to generate vast quantities of extracellular enzymes with significant industrial potential (Ellouze & Sayadi, 2016; Ozojiofor et al.; 2025). The majority of fungi investigated have been isolated from terrestrial environments such as forests and marshlands, and the diversity of marine fungi has not been extensively studied (Ben-Ali et al., 2020). However, various fungal species are present in marine environments, which are incredibly complex (Amend et al., 2019).

Fungi belonging to the phylum Ascomycota are recognized for their significant role in degrading aromatics and other recalcitrant organic pollutants (Singh et al., 2015). Of these, *Penicillium* spp. are particularly well known for their metabolic versatility, enabling them to colonize a wide range of habitats. This versatility allows them to thrive in some of the most extreme environments on earth, including deep-sea sediments, the poles, highly acidic habitats, and those with extreme temperatures (Frisvad & Samson, 2004). Though typically thought to be decomposers, *Penicillium* spp. possess high hydrocarbon-assimilating capacities with low cosubstrate demands and produce an enormous amount of bioactive metabolites (Houbraken et al., 2011). Their ability to utilize numerous carbon sources reflects their metabolic flexibility and the potential to break down a wide range of substrates. Several reports are available on the potential of *Penicillium oxalicum* to degrade complex compounds, such as textile dyes, food residues, lignocellulosic residues, and hydrocarbons (Singh et al., 2015), as well as detoxify xenobiotic chemicals into less mutagenic or toxic products (Zhang et al., 2013). Due to its halotolerance, *P. oxalicum* presents promising possibilities for treating textile industry wastewaters with high salt concentrations. Saroj et al. (2014) isolated SAR-3 *P. oxalicum*, which was able to degrade a broad spectrum of azo dyes, including Acid Red 183, Direct Blue 15, and Direct Red 75 (DR75).

This study aimed to characterize and detoxify an azo dye, DR75, using a halotolerant *P. oxalicum* M6A isolated from the marine habitat and to determine the degradation products and the toxicity of the dye and its products.

Materials and Methods

DR75, the textile dye used, as shown in Figure 1, was obtained from Glentham Life Science. Veratraldehyde, catechol quinone, 2,2′-azino-bis-(3-ethylbenzthiazoline-6-sulfonic acid) (ABTS), potato dextrose agar (PDA), Mueller–Hinton agar, and malt extract agar were purchased from Sigma–Aldrich. A 10,000 mg/L stock solution of the dye was prepared and sterilized via filtration through a 0.22 µm filter. The solution was then appropriately diluted to the desired concentration before use.

Isolation of Fungi

The fungal strain *P. oxalicum* M6A employed in this study was previously isolated from samples (woods immersed in seawater, seaweeds, marine plants, pieces of nets, and sands from sea shores) from the Lagos Atlantic Ocean shores (coordinates: 6° 27′ 55.5192″ N and 3° 24′ 23.2128″ E) by the authors Ozojiofor

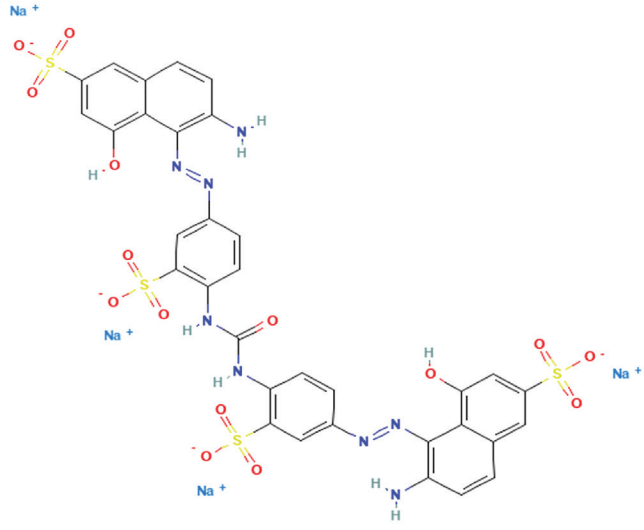

Figure 1. Structure of DR75. DR75 = Direct Red 75.

et al. (2025). The fungus was purified and maintained on 3.9% (w/v) PDA and 1.8% (w/v) malt extract supplemented with 3.4% (w/v) NaCl (Zouari-Mechichi et al., 2016). The gene sequence of *P. oxalicum* M6A can be found in the NCBI GenBank under the accession number PP077349.

Decolorization on Solid and Liquid Media

PDA plates supplemented with chloramphenicol (30 µg/mL) and 200 mg/L of DR75 were inoculated with mycelia placed in the center of each plate (Fernández-Remacha et al., 2022). The plates were incubated for 7 days at room temperature and then examined daily for the presence of halos corresponding to the areas in which the dye was degraded.

For further investigation in the liquid medium potato dextrose broth (PDB), the fungus was inoculated into 10 mL of preautoclaved medium supplemented with 200 mg/L of the dye at 25°C. After centrifuging the liquid medium containing the fungal mycelia for 10 min at 5,000 rpm, aliquots of the supernatant were transferred to fresh tubes and diluted as needed to obtain the desired absorbance. An untreated liquid medium was used as a control for each dye.

The standard curve of each dye was generated at its maximum absorbance wavelength, with concentrations ranging from 0 to 200 mg/L. The percentage of dye in the samples was calculated at different time intervals of 24 h for 5 days using the formula $D = \left(\frac{(AC\text{-}AT)}{AC}\right)$ x 100, where D represents the decolorization rate (%) and A_C and A_T represent the absorbance measured for the control and treated samples, respectively (Rosales et al., 2011).

Enzyme Assay

The decolorized DR75 sample pellet obtained via centrifugation was used to perform enzyme activity assays selected to substantiate the proposed dye degradation pathway. Azo-reductase activity was determined by assaying the decrease in color absorbance of methyl red at 430 nm, and veratryl alcohol oxidase activity by assaying the reduction in color absorbance of veratraldehyde at 310 nm (Phugare et al., 2011). Furthermore, tyrosinase activity was determined by observing the development of catechol quinone at 495 nm (Parshetti et al., 2007). The observation of an increase in absorbance at 420 nm, resulting from the oxidation of the ABTS compound, was used to detect laccase activity. Lignin peroxidase activity was assayed at 310 nm using veratryl alcohol as the substrate (Parshetti et al., 2007). Aldehyde dehydrogenase activity was assayed by monitoring the changes in absorbance owing to the formation of NADH at 340 nm (Murshid & Dhakshinamoorthy, 2021). Enzyme activity was measured spectrophotometrically at 25°C. One unit (U) of enzyme activity was defined as the amount of enzyme required to produce one micromole of the product per minute.

Growth Study of the Isolate at Different Dye Concentrations

The growth of P. oxalicum M6A at different concentrations of DR75 (0.4 g/L, 0.6 g/L, 0.8 g/L, and 1.0 g/L) in PDB supplemented with the textile dye was measured at 600 nm at intervals of 24 h during incubation for 5 days (Al-Tohamy et al., 2023).

Effects of Various Conditions on Dye Degradation by the Selected Isolates

The factors affecting dye decolorization were studied via single-factor optimization to investigate the dye decolorization capability of P. oxalicum M6A. The effects of dye concentrations, pH, salt, and temperature on the degradation of the dye by the fungus were examined. The ability of P. oxalicum M6A to decolorize different concentrations of the dye was analyzed using various initial dye concentrations (50, 100, 200, 300, and 400 mg/L). The dye-containing media were adjusted to different pH levels between 3 and 11 using either 0.1 M NaOH or 0.1 M HCl.

The effects of different temperatures (15–45°C, with an interval of 10°C) were tested in a thermostatic incubator (GEMTOP, ZSH-250 F, China). A range of salt concentrations, from 0% to 5% NaCl, was tested to assess the effects of salinity.

The decolorization efficiency of DR75 was studied, and during the investigation of a particular factor, all other variables were held constant as follows: 200 mg/L DR75, pH 7, 1% salinity, and a temperature of 25°C. The culture underwent static incubation for 120 h. Samples were withdrawn from the flasks at 24 h intervals. All the experiments were conducted in triplicate (Al-Tohamy et al., 2023).

Identification of the Metabolites of Dye Degradation

Extraction and chromatographic investigation of the metabolites were performed to fully understand the degradation pattern and metabolites from the decolorization of the dye. Multiple analytical methods were used, such as gas chromatography–mass spectrometry (GC–MS), Fourier-transform infrared (FTIR) spectroscopy, and ultraviolet–visible (UV–Vis) spectroscopy.

FTIR analysis was conducted at the National Research Institute for Chemical Technology (NARICT), Zaria, Kaduna, Nigeria, using an Agilent Technologies Cary 630 FTIR spectrophotometer to monitor the structural and distinctive changes in the dye.

Dye samples were subjected to FTIR analysis before (without the fungus) and after degradation (with the fungus). The fungus was incubated at 28°C in 25 mL of solution containing the dye and was grown for 7 days. The samples were carefully filtered after 7 days, and the resulting residues were washed three times with distilled water. To remove extra moisture from the test sample, it was held in a hot air oven set at 110°C for 30 min with the introduction of potassium bromide. For analysis, the materials were further ground at a 5:95 (w/w) ratio (Al-Tohamy et al., 2023). For a total of 16 scans, the sample data were recorded in the midinfrared range of 650–4,000 cm^{-1}.

GC–MS was employed to separate and identify the possible active constituents from the dye metabolites. GC–MS was performed at NARICT, Zaria, Kaduna State, using a Shimadzu GC–MS-QP2010 PLUS (Japan) machine.

Lyophilized samples were dissolved in GC-grade methanol and filtered through a syringe filter before being injected into the GC–MS column. One microliter of sample was taken for injection via a standard operating procedure based on the manufacturer's instructions (SHIMADZU GC–MS) (Klatte et al., 2017). Helium was used as the carrier gas. A comparison of the retention times, mass spectra obtained with GC–MS solution software, and fragmentation patterns was performed to identify the metabolites. The fragmentation method was used to determine the structures of the identified compounds, and mass spectrometry analysis provided the m/z values (Al-Tohamy et al., 2023).

Microtoxicity and Phytotoxicity Studies of Dyes and Their Degradation Products

The microtoxicity of the original dye and its degradation product, as determined using GC–MS analysis at a concentration of 200 mg/L, was assessed. The dye was extracted with dichloromethane and then dissolved in sterilized water, and it was tested against *Pseudomonas aeruginosa*, *Staphylococcus aureus,* and *Bacillus cereus.* The inhibition study was performed on Mueller–Hinton agar plates using the agar well diffusion method. Wells of 0.9 cm in diameter were carefully punched into the media and filled with 200 µL of control (sterilized water) and treated and untreated dye. The experimental study was conducted in triplicate, and the petri dishes were sealed with parafilm and incubated for 24 h at 30°C.

The zone of inhibition was calculated by subtracting the well diameter from the total zone of inhibition, and the results were recorded (Bagewadi et al., 2017; Yang et al., 2016).

The phytotoxicity of the original dye at a concentration of 200 mg/L and the products of dye degradation by the fungus were extracted with dichloromethane and then dissolved in sterilized water. These extracts were evaluated on the seeds of *Zea mays* (maize) and *Vigna unguiculata* (cowpea). The experiments were conducted at room temperature by placing 10 seeds of each crop on a bedded filter paper in a petri dish for germination and irrigating them daily with 10 mL solutions of the respective samples (original dye or treated dye) for 7 days. The control plants were irrigated with distilled water. The toxicity was assessed in terms of percentage germination (%), plumule length (cm), and radicle length (cm) (Bagewadi et al., 2017).

Statistical Analysis

The results were presented as the mean ± standard deviation of three determinations, which were subjected to one-way analysis of variance to compare the means of three or more groups and determine if at least one group was significantly different from the others. The Duncan multiple range test was used to determine which specific groups differed from each other, with a significance level of $p < 0.05$.

Results

The effects of DR75 concentration on the growth of *P. oxalicum* M6A were studied, as shown in Figure 2. The time course study of the impact of different concentrations (0.4, 0.6, 0.8, and 1.0 g/L) of DR75 on the growth of *P. oxalicum* M6A is presented in Figure 2. The maximum growth of *P. oxalicum* M6A was observed at a concentration of 0.8 g/L in DR75 after 5 days of incubation with the dye. The maximum absorption wavelength for DR75 was 520 nm.

The fungus *P. oxalicum* M6A degraded the dye optimally at a pH of 5, with > 70% degradation after 120 h (5 days). The degradation ability of the fungus was time dependent, and it degraded the dye better after 72–120 h (3–5 days) at pH 5–7, with a degradation percentage of > 80%, but degraded poorly at pH 3 and 11. The time course of dye degradation by *P. oxalicum* M6A at different pH values is presented in Figure 3.

P. oxalicum M6A degraded > 60% of DR75 at 35°C after 120 h (5 days) of incubation. The time course of the degradation of the dye by *P. oxalicum* M6A at different temperatures is shown in Figure 4.

The decolorization percentage of DR75 at various dye concentrations (ranging from 50 mg/L to 400 mg/L), as presented in Figure 5, showed that *P. oxalicum* M6A degraded > 90% of DR75 at 50 mg/L after 5 days of incubation, and the degradation percentage decreased with increasing dye concentration.

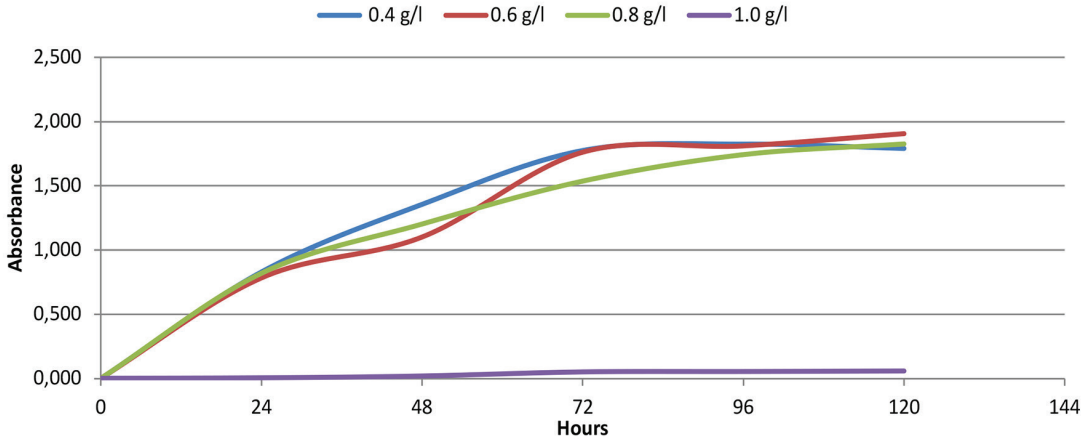

Figure 2. Effect of different concentrations of DR75 on the growth of *Penicillium oxalicum* M6A. DR75 = Direct Red 75.

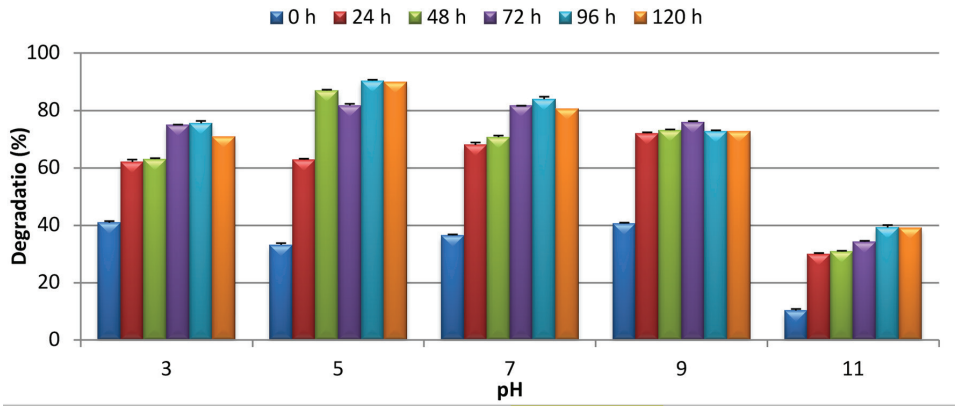

Figure 3. Effect of different pH values on the degradation of DR75 by *Penicillium oxalicum* M6A. Error bars represent the standard deviation of the degradation (%) at a given pH and time. DR75 = Direct Red 75.

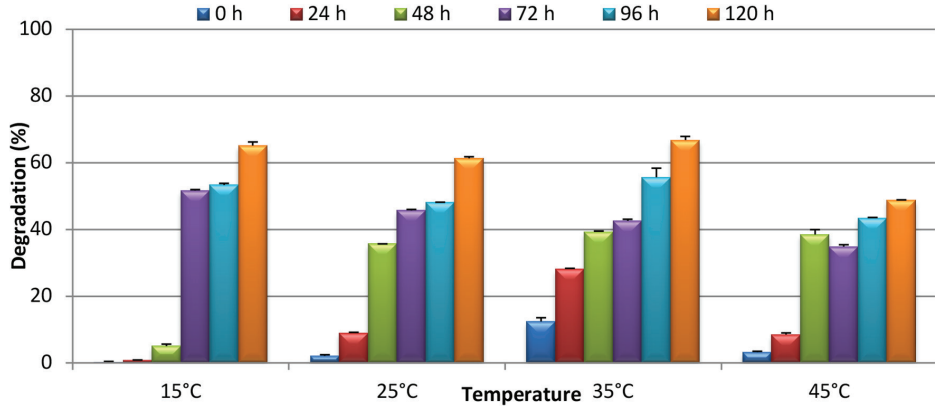

Figure 4. Effect of different temperatures on the degradation of DR75 by *Penicillium oxalicum* M6A. Error bars represent the standard deviation of the degradation (%) at a given temperature and time. DR75 = Direct Red 75.

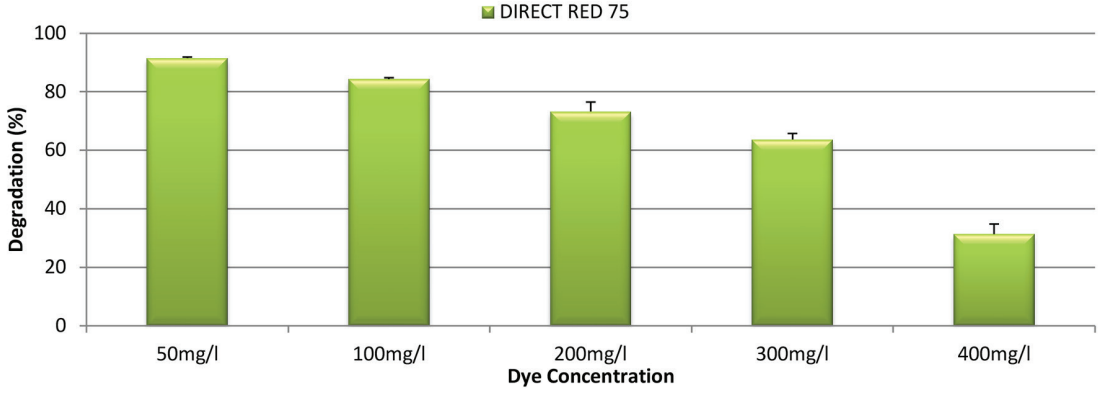

Figure 5. Effect of different dye concentrations on the degradation of DR75 by *Penicillium oxalicum* M6A. Error bars represent the standard deviation of the degradation (%) at a given dye concentration and time. DR75 = Direct Red 75.

The decolorization percentage of DR75 at various salt concentrations (1–5%) is presented in Figure 6. The maximum decolorization rate of *P. oxalicum* M6A for DR75 was 67% at a 4% salt concentration on Day 4 of incubation. The optimum salt concentration for the degradation of DR75 was 1% on Days 2–5.

The activities of different enzymes before and after degradation showed higher activities for laccase (24.17 ± 0.83), azo reductase (13.14 ± 0.87), and lignin peroxidase (12.54 ± 0.33), as presented in Table 1.

FTIR spectral peaks for the degraded and nondegraded DR75 are presented in Figure 7a and b. FTIR spectra of the untreated dye (Figure 7a) exhibited significant peaks corresponding to azo linkages (–N=N–), C=C aromatic stretching, and vibrations of sulfonic groups, indicative of the complicated structure of the azo dye.

The GC–MS revealed 17 peaks and 10 possible metabolites, namely, 2,3-dihydrobenzofuran, m-hydroquinone, n-phenylacetic acid, 1-pentadecanecarboxylic acid, cis-9-hexadecenal, 13-octadecenal,

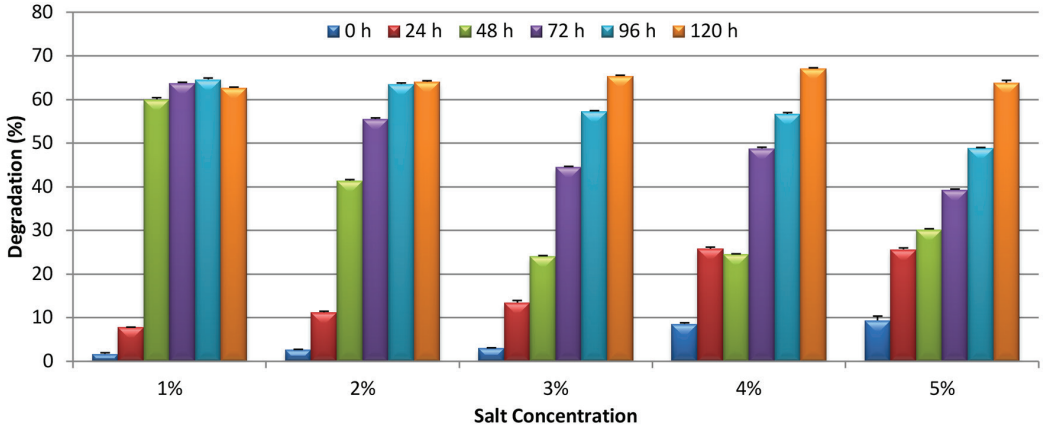

Figure 6. Effect of different salt concentrations on the degradation of DR75 by *Penicillium oxalicum* M6A. Error bars represent the standard deviation of the degradation (%) at a given salt concentration and time. DR75 = Direct Red 75.

Table 1. Enzyme activities before and after degradation of 50 mg/L of DR75 by *Penicillium oxalicum* M6A.

Enzyme	Activity before degradation (U/mL)	Activity after degradation (U/mL)	Negative control (U/mL)
Laccase	3.67 ± 0.18	24.17 ± 0.83	5.43 ± 0.22
Azo reductase	5.65 ± 0.67	13.14 ± 0.87	6.12 ± 0.38
Lignin peroxidase	2.34 ± 0.77	12.54 ± 0.33	3.56 ± 0.27
Veratryl alcohol oxidase	1.67 ± 0.06	2.43 ± 0.92	2.11 ± 0.23
Tyrosinase	1.34 ± 0.44	3.54 ± 0.61	2.50 ± 0.54
Aldehyde dehydrogenase	ND	3.20 ± 0.66	2.55 ± 0.17

DR = Direct Red 75, ND = not detected.

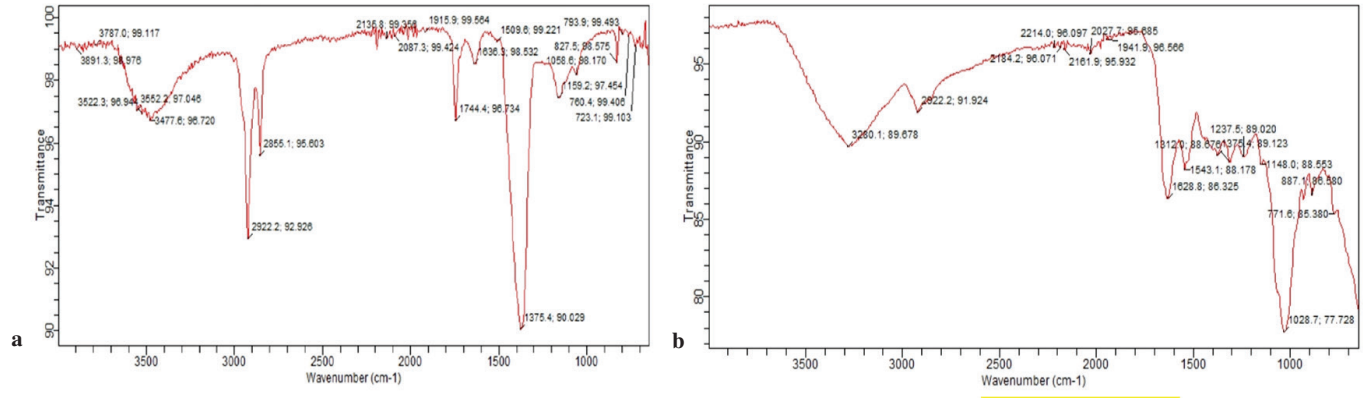

Figure 7. (a) FTIR spectrum of nondegraded DR75 (control); (b) FTIR spectrum of DR75 degraded by *Penicillium oxalicum* M6A. FTIR = Fourier-transform infrared spectroscopy; DR75 = Direct Red 75.

14-octadecenoic acid methyl ester, 9,17-octadecadienal, 13-docosenamide, and 6-ethoxy-6-methyl-2-cyclohexenone. The GC–MS peaks and spectra of the key metabolites of degraded DR75 are presented in Figures 8 and 9. The FTIR spectrum (Figure 7a and 7b) and GC–MS chromatogram (Figures 8 and 9) jointly validated the effective biodegradation of DR75 by *P. oxalicum* M6A. The degraded sample (Figure 7b) exhibited a loss of peaks corresponding to azo and sulfonic groups, along with the emergence of additional bands indicative of carbonyl (C=O) stretching (approximately 1,700 cm^{-1}), hydroxyl (–OH), and aliphatic C–H stretches, which signified dye degradation and the generation of simpler metabolites.

The microtoxicity results of the dye and its degradation products on *S. aureus*, *P. aeruginosa*, and *B. cereus* are presented in Table 2.

The results showed that the dye inhibited the growth of the bacteria used in this study more effectively than its degradation products by *P. oxalicum* M6A. The degradation products of DR75 by the fungus showed no zone of inhibition on the three bacterial strains. The phytotoxicity results of the dye and its degradation products on the seeds of *Z. mays* (Maize) and *V. unguiculata* (Cowpea) are presented in Table 3.

Discussion

Dye degradation results in the formation of new peaks, as Al-Tohamy et al. (2023) reported the appearance of new peaks during the decolorization of the reactive azo dye Reactive Black 5 (RB5) using the novel halotolerant yeast consortium HYCA, which comprised *Meyerozyma guilliermondii* (*M. guilliermondii)* SSA-

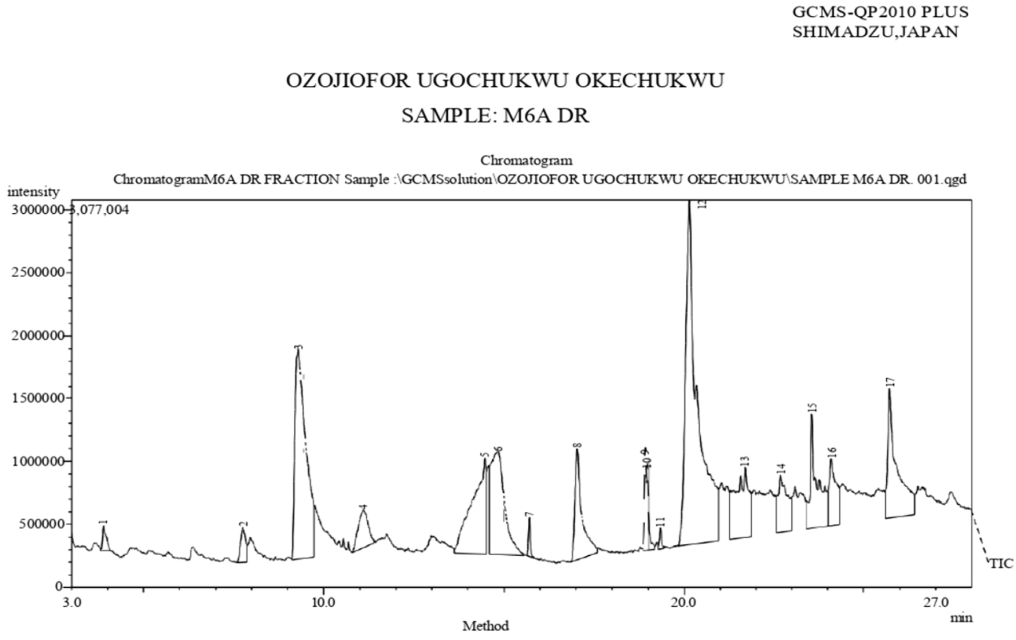

Figure 8. GC–MS chromatogram of DR75 degraded by *Penicillium oxalicum* M6A. GC–MS = gas chromatography–mass spectrometry.

Table 2. Zone of inhibition (cm) of DR75 and its products of degradation by *Penicillium oxalicum M6A* on certain bacterial strains.

Bacterial strain	Control	DR	DR-P
Staphylococcus aureus	-	0.6 ± 0.2	-
Pseudomonas aeruginosa	-	0.23 ± 0.1	-
Bacillus cereus	-	0.7 ± 0.3	-

DR = Direct Red 75; DR-P = Direct Red Product.

Table 3. Phytotoxicity assessment of DR75 and its products of degradation by *Penicillium oxalicum M6A* on *Vigna unguiculata* and *Zea mays.*

Parameters	*Vigna unguiculata*			*Zea mays*		
	Control	DR	Products	Control	DR	Products
Germination (%)	90 ± 16^{b}	43.3 ± 5.8^{a}	70.0 ± 0^{b}	100 ± 0^{c}	66.7 ± 5.8^{a}	90.0 ± 10^{b}
Plumule (cm)	4.4 ± 0.9^{b}	2.4 ± 1.0^{a}	4.4 ± 1.0^{b}	6.4 ± 0.9^{c}	2.0 ± 0.6^{a}	3.2 ± 0.8^{b}
Radicle (cm)	2.9 ± 0.7^{b}	1.2 ± 0.3^{a}	2.5 ± 0.9^{b}	2.5 ± 0.3^{c}	1.0 ± 0.3^{a}	1.5 ± 0.5^{b}

Superscript (a, b, c…) indicates significant difference across the rows at a 95% confidence interval. DR = Direct Red 75; DR-P = Direct Red Product.

1547 and *Sterigmatomyces halophilus* SSA-1575. Furthermore, Gharieb et al. (2020) documented the appearance of new peaks for DR75 (552–240 nm) and Reactive Red (534–244 nm), which were degraded by *M. guilliermondii* and *Naganishia diffluens,* respectively. The most common technique employed for assessing dye degradation is UV–Vis spectroscopy. There was an obvious association between dye degradation and the observed absorption peaks. If a dye's absorption peak disappears and a new peak appears in the UV–Vis range, it is indicative of dye degradation.

Fungal growth in media supplemented with dyes is strongly affected by the structure and concentration of the dye used. At low dye concentrations, some fungi may exhibit better growth because the enzymes involved in dye degradation can break down the dye more efficiently. However, at high concentrations, the dye becomes toxic to the fungi, inhibiting their growth in media supplemented with the dye by blocking the active sites of enzymes involved in the detoxification process (Li et al., 2019).

In a study on the growth of *Aspergillus niger* in Congo Red, maximum growth was observed at a concentration of 0.25 g/L. As the initial dye concentration increased to 1 g/L, the growth rate decreased significantly owing to exacerbated toxicity (Asses et al., 2018).

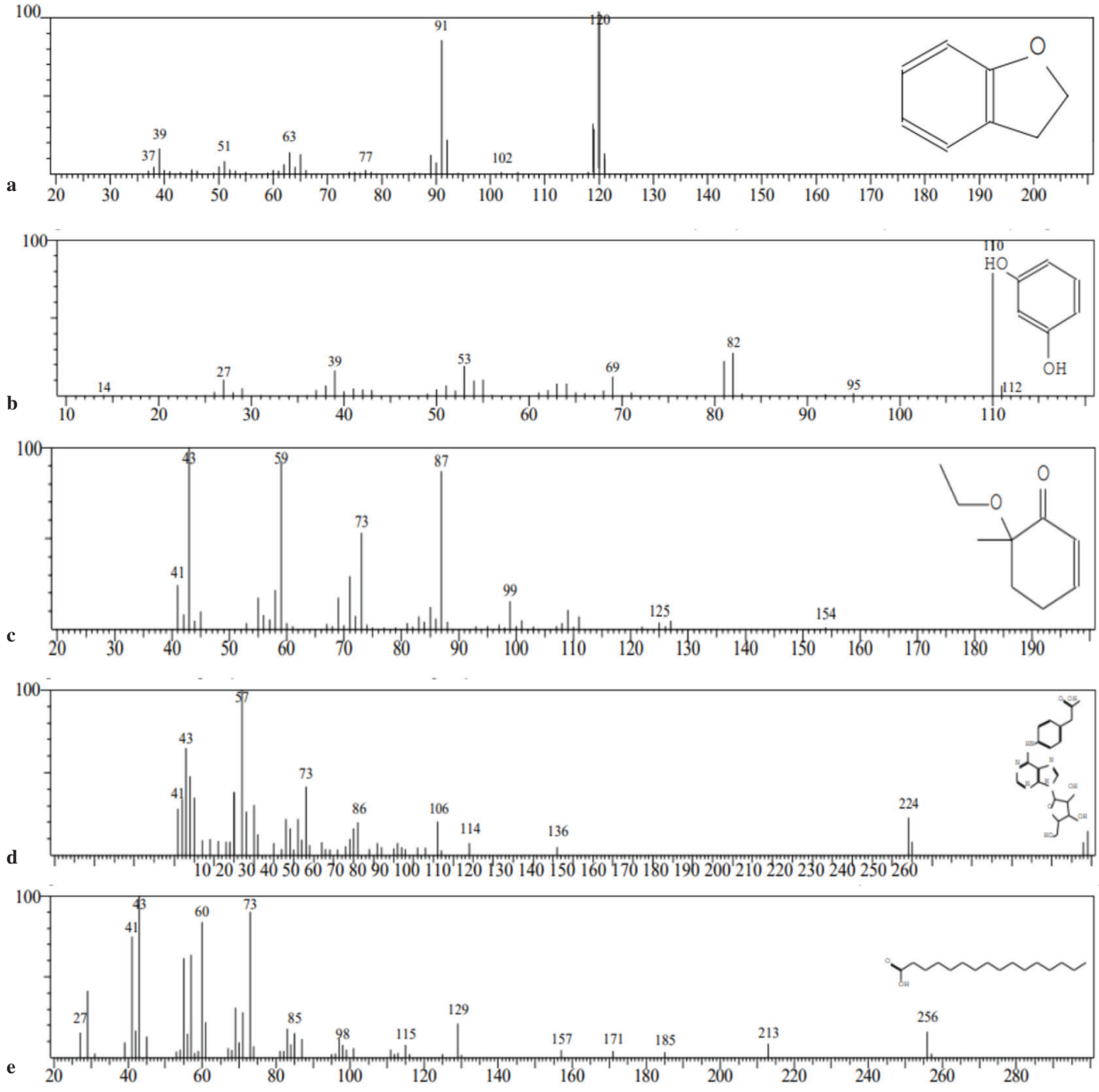

Figure 9. Identification of metabolites of DR75 via GC–MS. (a) 2,3-dihydrobenzofuran, mass peak (m/z) 120; (b) m-hydroquinone, mass peak (m/z) 110; (c) 6-ethoxy-6-methyl-2-cyclohexenone, mass peak (m/z) 154; (d) n-phenylacetic acid, mass peak (m/z) 401; (e) 1-pentadecanecarboxylic acid, mass peak (m/z) 256. DR75 = Direct Red 75; GC–MS = gas chromatography–mass spectrometry.

In a study by Wang et al. (2017) on the decolorization of Congo Red by *Ceriporia lacerate,* the authors reported maximum growth rate at a dye concentration of 0.5 g/L. These published works agree with the findings of this study. The observed growth rate decreased with increased dye concentration. Furthermore, as the number of dye molecules per unit volume increased, fungal growth declined because of increased stress, and the enzyme degradation ability decreased owing to a reduction in the amount of the enzyme (Cheng et al*.,* 2012; Yang et al*.,* 2012).

Erum and Ahmed (2011) reported maximum growth for *A. niger* SA1, *A. flavus* SA2, and *A. terreus* SA3 in media supplemented with Acid Red 151 at a dye concentration of 50 mg/L. Akdogan et al. (2014) obtained maximum growth for two fungi, *Coprinus plicatilis* and *Lentinus crinitus*, when incubated in media supplemented with Remazol Brilliant Blue R at concentrations of 0.05 g/L and 0.25 g/L, respectively. These reports are not in agreement with the present study, and this discrepancy could be attributed to the fact that the fungi used in the previous study were not derived from marine environments and could not grow at high dye concentrations.

pH is a crucial factor in the degradation of dyes as different enzymes work optimally at specific pH levels. The degradation of DR75 by *P. oxalicum* M6A was time dependent and decreased with increasing pH. Gharieb et al. (2020) documented the maximum decolorization percentage (80.3%) for DR75 degraded by *M. guilliermondii* at pH 5 and that of Reactive Red degraded by *N. diffluens* (70.8%) at pH 7, and their work agrees with the present study. In this investigation, the decolorization percentage for DR75 was the lowest at the two extremes of pH 3 and 11. In the decolorization activity of Direct Violet by *Aspergillus fumigatus*, the extremes of decolorization were observed from 94% at pH 5.5 to 47% at pH 3 (El-Sayeh, 2010). The extremes of pH observed in this study, at 3 and 11, may not favor the enzymes involved in dye degradation.

According to Trevizani et al. (2018), a slightly acidic pH has an impact on growth, resulting in a small increase in degradation activity, as observed in this study. This finding can be explained by the nature of the azo dye used in this research. Decolorization is slower at extreme pH values as dye cations are less able to interact owing to the massive accumulation of H^+ and OH^- ions. At slightly elevated pH values, the electrostatic attraction force between the negatively charged membrane surface of fungi and positively charged dye cations is strong, which enhances the transition of dye molecules through the cell membrane, thereby augmenting decolorization (Martorell et al., 2017). For DR75, the enzymatic activity peaked at a pH of 5, which might have facilitated improved binding of the enzyme's active site to the dye surface, leading to decolorization (Cheng et al*.,* 2012). The dye decolorization efficiency is largely influenced by pH, with the normal range of color removal typically between pH 6 and 10 (Kilic et al*.,* 2007).

The DR75 used in this study is an azo dye. The biological reduction of azo bonds has been reported to cause an increase in pH as microorganisms form aromatic amine metabolites, which are more alkaline than the original azo compound (Ikram et al., 2022), explaining the inability of *P. oxalicum* M6A employed in this study to degrade DR75 effectively at alkaline pH.

Temperature is a crucial factor that influences microbial growth, survival, and metabolism. Temperature considerably affects all microbial survival processes, including those involved in water and soil remediation. In this study, the optimum temperature for the degradation of DR75 by *P. oxalicum* M6A was 35°C. Al-Tohamy et al. (2023) observed that the optimum decolorization efficiency of the halotolerant consortium HYC in terms of temperature was 35°C (87%). Furthermore, Gharieb et al. (2020) stated that *M. guilliermondii* and *N. diffluens* decolorized DR75 and Reactive Red most effectively at 30°C, with 85.3% and 80.8% color reduction, respectively. Both of these studies agree with our work.

Feng et al. (2023) opined that the optimal temperature for the degradation of azo dye by the marine-derived fungus *M. guilliermondii* A4 was 35°C. In addition, Ren and Osborne (2020) demonstrated that *P. oxalicum* RJJ-2 degraded 84.88% of erythromycin after 96 h of incubation at 35°C, although this study focused on pharmaceuticals rather than dyes.

Based on the experimental findings, when the fungus was exposed to 50 mg/L of DR75, a degradation rate of 91% was achieved. During the same period, the degradation efficiency of the fungus decreased when the dye concentration was > 50 mg/L. At a dye concentration of 400 mg/L, the degradation rate was found to be the lowest at 31%.

The degradation rate of RB5 by a yeast consortium of *S. halophilus* and *M. guilliermondii* decreased with increasing dye concentration from 50 mg/L to 400 mg/L (Al-Tohamy et al., 2023). The observed decrease in degradation efficiency could be attributed to the toxicity of the dye, which might have inhibited the enzyme activities of the fungus by blocking the active sites of the enzymes involved in dye degradation (Ameenudeen et al., 2021). A study conducted by Kalyani et al. (2009) found that azo dyes at high concentrations significantly inhibited microbial growth owing to the presence of sulfonic acid (SO_3H) groups on the aromatic rings of the reactive groups.

In another study, Gharieb et al. (2020) identified that the biodegradation of DR75 by *M. guilliermondii* and *N. diffluens* decreased significantly with increasing dye concentration (up to 1,500 mg/L) and that increasing the dye concentration to > 50 mg/L resulted in a marked decline in biodegradation. Fetyan et al. (2016) reported that *Saccharomyces cerevisiae* was highly effective at decolorizing Direct Blue 71, reaching a maximum activity of 100%. The decolorization ability decreased at concentrations > 200 mg/L, which may be due to the toxicity of high dye concentrations on the yeast. Both studies agree with this work, and this observation could also be explained by the insufficient biomass concentration for the uptake of the dye by the organisms at higher concentrations (Sumathi & Manju, 2020).

The consortium of *S. halophilus* and *M. guilliermondii* HYC showed degradation rates for RB5 ranging from 88.1% to 9.2% at

salinity levels of 0–5% (Al-Tohamy et al., 2023). An increase in the salt level resulted in a considerable decrease in enzyme activity, eventually leading to total inactivation (Sarkar et al., 2020), as hypersalinity can cause plasmolysis and cellular inactivity (He et al., 2017). The decolorization of DR75 and Reactive Red decreased from 77.9% and 53.5% to 20.87% and 7.99%, respectively, when the concentration of NaCl was increased from 0.0% to 10.0% for the yeasts *M. guilliermondii* and *N. diffluens*, (Gharieb et al., 2020). This difference may be the result of elevated external osmotic pressure, as suggested by Jafari et al. (2014), and these studies agree with this work.

During the degradation of DR75 by *P. oxalicum* M6A, a considerable increase was noted in the activities of enzymes such as laccase, azoreductase, and lignin peroxidase, indicating their prominent roles in the cleavage of azo bonds and aromatic rings. Minimal increases in tyrosinase and veratryl alcohol oxidase activity were observed, suggesting their involvement in hydroxylation and other oxidation reactions. Aldehyde dehydrogenase, which was previously undetectable owing to degradation, became active after degradation, facilitating the detoxification of aldehyde intermediates. Such enzymatic activity supports the proposed degradation pathway and underscores the robust bioremediation capacity of *P. oxalicum* M6A.

FTIR analysis served as a powerful tool to confirm the structural alterations in DR75 before and after biodegradation by *P. oxalicum* M6A. In this study, a spectral comparison of the control (Figure 7a) and the degraded dye (Figure 7b) revealed certain key changes in functional groups, indicating chemical alterations upon fungal treatment. In the FTIR spectrum of the nondegraded DR75, bands were observed at approximately 1,620–1,640 cm^{-1}, which could be attributed to C=C stretching vibrations of the aromatic rings. Moreover, the peaks at 1,500–1,530 cm^{-1} correspond to azo (–N=N–) stretching, which is characteristic of azo dyes and agrees with the work of Saratale et al. (2011). The maxima at the region 1,020–1,080 cm^{-1} results from S=O stretching of the sulfonic acid groups, accounting for the solubility of the dyes (Saratale et al., 2009). In addition, the broad band at 3,400 cm^{-1} indicates O–H or N–H stretching from phenolic or amine groups. Upon the degradation of *P. oxalicum* M6A, the FTIR spectrum demonstrated notable depletion or disappearance of the azo bond peak (approximately 1,500 cm^{-1}), suggesting successful cleavage of the bond, which is often the initial step of azo dye decolorization, as reported by Rai et al. (2005). Attenuation of the C=C aromatic peaks and the appearance of new peaks at 1,700–1,740 cm^{-1} owing to C=O stretching suggests oxidative cleavage of the aromatic ring and the formation of carboxylic acid or aldehyde functional groups (Kalyani et al., 2009; Parshetti et al., 2007). This finding supports the activity of ligninolytic enzymes, such as laccases and lignin peroxidases, which have been documented to catalyze aromatic ring degradation and oxidative decoupling (Pointing, 2001).

In addition, the reduction in S=O stretching peaks at approximately 1,050 cm^{-1} of the degraded sample implies desulfonation, which is a necessary step to alleviate the toxicity of the dye and enhance its biodegradability (Ali et al., 2009). The broadening of the band at 3,400 cm^{-1} may also justify the formation of hydroxylated or aminated intermediates by microbial degradation (Singh et al., 2015).

These shifts observed via FTIR spectroscopy agree with the identification of numerous metabolites via GC–MS. 2,3-dihydrobenzofuran and m-hydroquinone are oxygenated aromatic derivatives, indicating oxidative cleavage of the aromatic rings of the dye. These metabolites possess hydroxyl groups in their structures and conform to the FTIR-determined –OH and aromatic C–O stretching bands (1,220–1,260 cm^{-1}), confirming partial ring opening and functionalization (Singh et al., 2015). For 6-ethoxy-6-methyl-2-cyclohexenone, the presence of ketone (C=O) and ether (C–O–C) functional groups in the compound is evidenced by FTIR bands at approximately 1,710 cm^{-1} and 1,050–1,150 cm^{-1}, reflecting carbonyl group formation upon dye degradation. N-phenylacetic acid, a carboxylic acid derivative with an aromatic ring, follows aromatic cleavage after oxidation, consistent with FTIR peaks for carboxylic functionality, and is indicative of oxidative process–mediated degradation. Long-chain fatty acid derivatives, such as 1-pentadecanecarboxylic acid, cis-9-hexadecenal, 13-octadecenal, and 14-octadecenoic acid methyl ester, signify the formation of aliphatic products, reflected in FTIR spectroscopy as broad C–H stretches (2,850–2,950 cm^{-1}) and C=O stretches of esters and aldehydes (1,700–1,740 cm^{-1}). These metabolites suggest extensive structural fragmentation and probable catabolism of fungal lipids during dye degradation (Rai et al., 2005; Kaushik & Malik, 2009). 9,17-Octadecadienal and 13-docosenamide are aliphatic amides and aldehydes containing unsaturation, and their presence indicates the cleavage of complex dye molecules into long-chain intermediates, as inferred from FTIR peaks for C=N and C=O bonds. m-Hydroquinone and 2,3-dihydrobenzofuran are of immense significance as they are known to be low-toxicity aromatic intermediates obtained via microbial azo bond cleavage and aromatic amines, which agrees with the findings of Telke et al. (2010).

The spectral alterations and GC–MS results confirm that *P. oxalicum* M6A decolorized DR75 via azo bond cleavage, aromatic ring biodegradation, and modification of side-chain substituents, thereby validating the detoxification potential of the fungus. These findings concur with earlier observations on fungal dye degradation (Revankar & Lele, 2007; Kaushik & Malik, 2009).

In this study, a possible degradation pathway was proposed based on the GC–MS metabolites and enzymes identified, as presented in Figure 10.

The results of the microtoxicity assessment showed that the degradation products of DR5 had no inhibitory effect on any of the three bacterial strains tested. The nondegraded dye exhibited the smallest zone of inhibition, measuring 0.23 cm, against *P. aeruginosa*. This finding indicates that the fungus was able to break down the dye into less toxic products. An apparent zone was not seen outside the wells containing the degraded dye or the control as the test microorganisms were able to withstand the reduced toxicity of the dye products. Zubbair et al. (2020) reported the

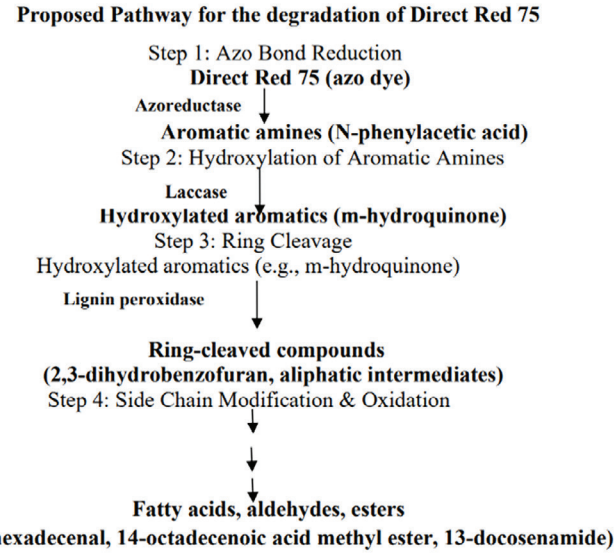

Figure 10. Proposed pathway for the degradation of DR75 (azo dye). DR75 = Direct Red 75.

microtoxicity of reactive black to *P. aeruginosa, Escherichia coli*, and *Klebsiella pneumoniae*. The results showed that *P. aeruginosa* and *E. coli* grew within clear zones measuring 6 mm and 3 mm, respectively; in contrast, *K. pneumoniae* demonstrated resistance to dye toxicity.

Phytotoxicity evaluation revealed that the percentage germination of the plant seeds of the two crops was highest for seeds irrigated with the control (sterilized water) (100%), followed by the degradation products of the dye by the fungus. In contrast, the percentage of germinated seeds was lowest for the dye. The rate of germination was highest for the seeds of *Z. mays* irrigated with the degradation product of DR75 (90 ± 10). The plumule and radicle lengths of the plant seeds of *Z. mays* and *V. unguiculata* irrigated with the degradation products of the dye were statistically significant and higher than those of the seeds irrigated with the nondegraded dye.

These findings demonstrate that the dye was detoxified and that the phytotoxicity of industrial effluents containing these dyes can be reduced by treating them with the fungus. In the study by Bagewadi et al. (2017), a phytotoxicity assessment of MG, Congo Red, Methylene Blue, and their degradation products revealed that the original dye significantly inhibited the germination of *P. mungo* seeds compared with its degradation products and the control treatment (sterilized water). This finding is consistent with the results of this research. In this investigation, seeds irrigated with the products of dye degradation exhibited better germination than those irrigated with the original dye. As azo dye is complex and robust, it exerted a greater inhibitory effect on *V. unguiculata*, as demonstrated by the greater toxicity of DR75. When Reactive Black dye was broken down by *Ganoderma tsugae,* the untreated dye prevented maize and bean seeds from sprouting. In contrast, the degraded dye did not, due to its reduced toxicity (Zubbair et al., 2020).

Conclusion

This study confirms the potent biocatalytic capacity of the marine-derived, halotolerant fungus *P. oxalicum* M6A in degrading and detoxifying the recalcitrant azo dye DR75. The fungus effectively reduced the dye concentration under saline conditions, driven by elevated activities of key oxidative enzymes, particularly of laccase, azoreductase, and lignin peroxidase, which resulted in azo bond cleavage and disruption of aromatic structure. Confirmation via spectroscopic (FTIR) and chromatographic (GC–MS) analyses revealed extensive structural modification of the dye, resulting in the formation of low-toxicity intermediates. Ecotoxicological assessments further established the environmental compatibility of this bioprocess. These results position *P. oxalicum* M6A as a promising candidate for the bioremediation of dye-laden saline wastewater. Future work should focus on pilot-scale validation with wastewater systems, genome-level elucidation of enzyme pathways, and optimization of continuous flow systems for industrial applications.

Acknowledgments

The authors are grateful to the Department of Biotechnology, Faculty of Science, Nigerian Defence Academy, and the National Research Institute for Chemical Technology, Zaria, for carrying out the research and analysis in their laboratories. Also, the authors extend their appreciation to the Tertiary Education Trust Fund-Institutional Based Research for providing the grant for the study.

Ethics

Ethics Committee Approval: Since the article does not contain any studies with human or animal subject, its approval to the ethics committee was not required.

Data Sharing Statement: All data are available within the study.

Footnotes

Author Contributions: Conceptualization: U.O.O., and M.S.A.; Design/methodology: U.O.O., and N.E.E.; Execution/investigation: U.O.O., N.E.E., and A.A.H.; Resources/materials: U.O.O.; Data acquisition: U.O.O., and N.E.E.; Data analysis/interpretation: U.O.O., and M.S.A.; Writing – original draft: U.O.O., and M.S.A.; Writing – review & editing/critical revision: M.S.A., N.E.E., and A.A.H.

Conflict of Interest: The authors have no conflicts of interest to declare.

Funding: The authors declared that this study has received no financial support.

References

Akdogan, H. A., Topuz, M. C., & Urhan, A. A. (2014). Studies on decolorization of reactive blue 19 textile dye by *Coprinus plicatilis*. *Journal of Environmental Health Science and Engineering, 12*, 49–56.

Ali, N., Hameed, A., Ahmed, S., & Haque, A. (2009). Decolorization and degradation of textile azo dye by *Bacillus subtilis*. *Environmental Technology, 30*(10), 1103–1110.

Al-Tohamy, R., Ali, S. S., Xie, R., Schagerl, M., Khalil, M. A., & Sun, J. (2023). Decolorization of reactive azo dye using novel halotolerant yeast consortium HYC and proposed degradation pathway. *Ecotoxicology and Environmental Safety, 263*, 115436.

Ameenudeen, S., Unnikrishnan, S., & Ramalingam, K. (2021). Statistical optimization for the efficacious degradation of reactive azo dye using *Acinetobacter baumannii* JC359. *Journal of Environmental Management, 279*, 111512.

Amend, A., Burgaud, G., Cunliffe, M., Edgcomb, V. P., Ettinger, C. L., & Gutiérrez, M. H. (2019). Fungi in the marine environment: Open questions and unsolved problems. *mBio, 10*(3), e01189-18. https://doi.org/10.1128/mBio.01189-18

Asses, N., Ayed, L., Hkiri, N., & Hamdi, M. (2018). Congo red decolorization and detoxification by *Aspergillus niger*: Removal mechanisms and dye degradation pathway. *BioMed Research International, 2018*, 7148537. https://doi.org/10.1155/2018/7148537

Bagewadi, Z. K., Sikandar, I. M., & Harichandra, Z. N. (2017). Purification and immobilization of laccase from *Trichoderma harzianum* strain HZN10 and its application in dye decolorization. *Journal of Genetic Engineering and Biotechnology, 15*, 139–150.

Basu, A., & Kumar, G. S. (2014). Targeting proteins with toxic azo dyes: A microcalorimetric characterization of the interaction of the food colorant amaranth with serum proteins. *Journal of Agricultural and Food Chemistry, 62*, 7955–7962.

Ben Mbarek, W., Issa, M., Salvadó, V., Escoda, L., Khitouni, M., & Suñol, J. J. (2023). Degradation of azo dye solutions by a nanocrystalline Fe-based alloy and the adsorption of their by-products by cork. *Materials, 16*(18), 7612.

Ben-Ali, W., Delphine, C., David, N., Christian, L., Annick, T. D., Emmanuel, B., Craig, B. F., Guiliano, S., Laurence, L. M., Eric, R., & Tahar, M. (2020). Screening of five marine-derived fungal strains for their potential to produce oxidases with laccase activities suitable for biotechnological applications. *BMC Biotechnology, 20*, 27. https://doi.org/10.1186/s12896-020-00637-1

Cheng, Z. Z., Yang, Z. P., Jing, D. J., & Chen, H. P. (2012). Decolorization of 12 kinds of dye by the mycelium pellets of *Trametes gallica* under nonsterile condition. *Mycosystema, 31*(6), 878–889. Cab Digital Library+13ResearchGate+13IIPSeries+13

Couto, S. R. (2007). Decolouration of industrial azo dye by crude laccase from *Trametes hirsuta*. *Journal of Hazardous Materials, 148*(3), 768–770. https://doi.org/10.1016/j.jhazmat.2007.06.123 Wiley Online Library+7PubMed+7ResearchGate+7

Ellouze, M., & Sayadi, S. (2016). Whiterot fungi and their enzymes as a biotechnological tool for xenobiotic bioremediation. *Intech*, 17, 103–120.

ElSayeh, I. (2010). Fungal biodegradation of textile dye. *Egyptian Journal of Chemistry, 62*(10), 1799–1813.

Erum, S., & Ahmed, S. (2011). Comparison of dye decolorization efficiencies of indigenous fungal isolates. *African Journal of Biotechnology, 10*(17), 3399–3411.

Feng, Y., Cui, J., Xu, B., Jiang, Y., Fu, C., & Tan, L. (2023). A potentially practicable halotolerant yeast *Meyerozyma guilliermondii* A4 for decolorizing and detoxifying azo dye and its possible halotolerance mechanisms. *Journal of Fungi, 9*, 851.

Fernández-Remacha, D., GonzálezRiancho, C., Osua, M. L., Arce, G. G., Montánchez, I., GarcíaLobo, J. M., EstradaTejedor, R., & Kaberdin, V. R. (2022). Analysis of laccase like enzymes secreted by fungi isolated from a cave in northern Spain. *MicrobiologyOpen, 11*, e1279. https://doi.org/10.1002/mbo3.1279

Fetyan, N. A. H., Abdelazeiz, A. Z., Ismail, I. M., & Shaban, S. A. (2016). Oxidative decolorization of direct blue 71 azo dye by *Saccharomyces cerevisiae* catalyzed by nano zerovalent iron. *Annual Research & Review in Biology, 11*(11), 1–12.

Frisvad, J. C., & Samson, R. A. (2004). Polyphasic taxonomy of *Penicillium* subgenus *Penicillium*—A guide to identification of food and airborne terverticillate *Penicillia* and their mycotoxins. *Studies in Mycology, 49*, 1–173.

Gavril, M., & Hodson, M. (2007). Investigation of the toxicity of the products of decoloration of amaranth by *Trametes versicolor*. *Journal of Environmental Quality, 36*, 1591–1598.

Gharieb, M. M., Soliman, A. M., & Hassan, E. M. (2020). Biodegradation of the azo dye DR75 81 and reactive brilliant red X-3B by wild strains of yeasts *Meyerozyma guilliermondii* and *Naganishia diffluens*. *International Journal of Current Microbiology and Applied Sciences, 9*(3), 1243–1260.

He, H., Chen, Y., Li, X., Cheng, Y., Yang, C., & Zeng, G. (2017). Influence of salinity on microorganisms in activated sludge processes: A review. *International Biodeterioration & Biodegradation, 119*, 520–527.

Houbraken, J., Frisvad, J. C., & Samson, R. A. (2011). Taxonomy of *Penicillium* section *Citrina*. *Studies in Mycology, 70*, 53–138.

Ikram, M., Naeem, M., & Zahoor, M. (2022). Biological degradation of the azo dye basic orange 2 by *Escherichia coli*: A sustainable and ecofriendly approach for the treatment of textile wastewater. *Water, 14*, 2043.

Jafari, N., Soudi, M. R., & Kasra-Kermanshahi, R. (2014). Biodegradation perspectives of azo dye by yeasts. *Microbiology, 83*, 484–497.

Kalyani, D. C., Telke, A. A., Dhanve, R. S., & Jadhav, J. P. (2009). Ecofriendly biodegradation and detoxification of reactive red 2 textile dye by newly isolated *Pseudomonas* sp. SUK1. *Journal of Hazardous Materials, 163*, 735–742.

Kaushik, P., & Malik, A. (2009). Fungal dye decolorization: Recent advances and future potential. *Environment International, 35*(1), 127–141.

Kilic, N. K., Nielsen, J. L., Yuce, M., & Donmez, G. (2007). Characterization of a simple bacterial consortium for effective treatment of wastewaters with reactive dye and Cr (VI). *Chemosphere, 67*, 826–831.

Klatte, S., Schaefer, H., & Hempel, M. (2017). Pharmaceuticals in the environment – A short review on options to minimize the exposure of humans, animals and ecosystems. *Sustainable Chemistry and Pharmacy, 5*, 61–66.

Li, N., Chen, G., Zhao, J., Yan, B., Cheng, Z., Meng, L., & Chen, V. (2019). Self-cleaning PDA/ZIF-67@PP membrane for dye wastewater remediation with

peroxymonosulfate and visible light activation. *Journal of Membrane Science, 591*, 117341.

Martorell, M. M., Ruberto, L. A. M., Fernández, P. M., Figueroa, L. I. C., & MacCormack, W. P. (2017). Bioprospection of cold-adapted yeasts with biotechnological potential from Antarctica. *Journal of Basic Microbiology, 57*(6), 504–516.

Murshid, S., & Dhakshinamoorthy, G. P. (2021). Application of an immobilized microbial consortium for the treatment of pharmaceutical wastewater: Batch-wise and continuous studies. *Chinese Journal of Chemical Engineering, 29*, 391–400.

Ozojiofor, U. O., Abdulsalami, M. S., Egbe, N. E., & Haroun, A. I. (2025). Biotechnological potential of marine-derived fungi for textile dye degradation via laccase-like activity. *Suan Sunandha Science and Technology Journal, 12*(2), 26-43.

Ozojiofor, U. O., Abdulsalami, M. S., Egbe, N. E., Haroun, A. I., Hassan, A. U., & Onuh, K. (2025). Molecular docking of laccase from *Trametes versicolor* with ligand substrates from textile dyes and antibiotics impacting the environment. *Science & Technology Asia, 30*(2), 268–281.

Parshetti, G. K., Kalme, S. D., Saratale, G. D., & Govindwar, S. P. (2007). Biodegradation of malachite green by *Kocuria rosea* MTCC 1532. *Acta Chimica Slovenica, 54*(4), 792–798.

Phugare, S. S., Kalyani, D. C., Surwase, S. N., & Jadhav, J. P. (2011). Ecofriendly degradation, decolorization and detoxification of textile effluent by a developed bacterial consortium. *Ecotoxicology and Environmental Safety, 74*, 1288–1296.

Pointing, S. B. (2001). Feasibility of bioremediation by white-rot fungi. *Applied Microbiology and Biotechnology, 57*(1–2), 20–33.

Rai, H., Bhattacharyya, M. S., Singh, J., Bansal, T. K., Vats, P., & Banerjee, U. C. (2005). Removal of dyes from the effluent of textile and dyestuff manufacturing industry: A review of emerging techniques with reference to biological treatment. *Critical Reviews in Environmental Science and Technology, 35*(3), 219–238.

Ren, S., & Osborne, W. (2020). Heavy metal determination and aquatic toxicity evaluation of textile dye and effluents using *Artemia salina*. *Biocatalysis and Agricultural Biotechnology, 25*, 101621.

Revankar, M. S., & Lele, S. S. (2007). Synthetic dye decolorization by white rot fungus, *Ganoderma* sp. WR-1. *Bioresource Technology, 98*(4), 775–780.

Rosales, E., Pazos, M., & Sanromán, M. A. (2011). Comparative efficiencies of the decolorization of leather dye by enzymatic and electrochemical treatments. *Desalination, 278*(3), 312–317.

Saratale, R. G., Saratale, G. D., Chang, J. S., & Govindwar, S. P. (2011). Bacterial decolorization and degradation of azo dyes: A review. *Journal of the Taiwan Institute of Chemical Engineers, 42*(1), 138–157.

Saratale, R. G., Saratale, G. D., Kalyani, D. C., Chang, J. S., & Govindwar, S. P. (2009). Enhanced decolorization and biodegradation of textile azo dye Scarlet R by using developed microbial consortium-GR. *Bioresource Technology, 100*(9), 2493–2500.

Sarkar, S., Banerjee, A., Chakraborty, N., Soren, K., Chakraborty, P., & Bandopadhyay, R. (2020). Structural-functional analyses of textile dye degrading azoreductase, laccase and peroxidase: A comparative *in silico* study. *Electronic Journal of Biotechnology, 43*, 48–54.

Saroj, S., Kumar, A., & Dastidar, M. G. (2014). Biodegradation of azo dyes by *Penicillium oxalicum* SAR-3 in aquatic environment. *Environmental Technology, 35*(13–16), 1636–1645.

Singh, R. L., Singh, P. K., & Singh, R. P. (2015). Enzymatic decolorization and degradation of azo dyes – A review. *International Biodeterioration & Biodegradation, 104*, 21–31.

Sumathi, S., & Manju, B. (2000). Uptake of reactive textile dye by *Aspergillus foetidus*. *Enzyme and Microbial Technology, 27*, 347–355.

Telke, A. A., Kalyani, D. C., Jadhav, S. U., & Govindwar, S. P. (2010). Kinetics and mechanism of Reactive Red 141 degradation by a bacterial isolate *Rhodococcus pyridinivorans* NT2. *Journal of Hazardous Materials, 186*(1), 748–755.

Trevizani, J. L. B., Nagalli, A., Passig, F. H., Carvalho, K. Q., Schiavon, G. J., & Model, A. N. L. (2018). Influence of pH and concentration on the decolorization and degradation of BR red azo dye by ozonization. *Acta Scientiarum. Technology, 40*(1), e35436.

Vinodhkumar, T., Shamalaa, L. F., Maithilia, S. S., Ramanathan, V., & Sudhakar, S. (2013). Antibacterial properties of secondary metabolites from the endophytic marine algal bacterial population against chicken meat microbial pathogen. *International Journal of Current Science, 5*, 35–40.

Wang, N., Chu, Y., Wu, F., Zhao, Z., & Xu, X. (2017). Decolorization and degradation of Congo red by a newly isolated white rot fungus, *Ceriporia lacerata*, from decayed mulberry branches. *International Biodeterioration & Biodegradation, 117*, 236–244.

Willmott, N., Guthrie, J., & Nelson, G. (1998). The biotechnology approach to color removal from textile effluent. *Review of Progress in Coloration and Related Topics, 114*(2), 38–41.

Yang, B., Feng, L. D., & Zhang, L. Y. (2012). Decolorization of wastewater containing reactive brilliant blue dye by laccase. *Chinese Journal of Environmental Engineering, 6*(10), 3514–3518.

Yang, P., Shi, W., & Wang, H. (2016). Screening of freshwater fungi for decolorizing multiple synthetic dye. *Brazilian Journal of Microbiology, 47*, 828–834.

Zhang, W., Zhang, D., Ling, H., & Liu, Y. (2013). Biodegradation of synthetic dyes by *Penicillium oxalicum* strain DSYD05. *Environmental Science and Pollution Research, 20*(7), 4601–4610.

Zouari-Mechichi, H., Mechichi, T., Dhouib, A., Sayadi, S., Martínez, A. T., & Martínez, M. J. (2016). Laccase purification and characterization from *Trametes trogii* isolated in Tunisia: Decolourization of textile dye by the purified enzyme. *Enzyme and Microbial Technology, 39*, 141–148.

Zubbair, N. A., Ajao, A. T., Adeyemo, E. O., & Adeniyi, D. O. (2020). Biodegradation of malachite green by white-rot fungus, *Pleurotus pulminarious*. *Egyptian Academic Journal of Biological Sciences, 12*(1), 79–90.

Trakya University Journal of Natural Sciences, 26(2), 156–173, 2025
DOI: 10.23902/trkjnat.565464764
www.tujns.org

Research Article

Indoor air quality of academia-related workshops based on health complaints

Abdel Hameed Awad*, Safaa El-Gendy, Yuosra Saeed, Salwa Kamal

Air Pollution Research Department, Environment and Climate Change Research Institute, National Research Centre, Giza, Egypt

Cite this article as: Awad, A. H., El-Gendy, S., Saeed, Y., & Kamal, S. (2025). Indoor air quality of academia-related workshops based on health complaints. *Trakya University Journal of Natural Sciences, 26*(2), 156–173. https://doi.org/10.23902/trkjnat.565464764

Abstract

Indoor Air Quality (IAQ) is a result of the interaction between micro-environmental conditions, location, and building characteristics. IAQ directly affects human health, comfort, productivity, and performance. However, very little attention has been paid to the IAQ of nonindustrial workshops.

This cross-sectional survey aimed to determine the IAQ of academia-related workshops based on the factors such as the microbial load (including bacteria, fungi, and actinomycetes), particulate matter (PM) content, presence of chemical pollutants (such as ammonia [NH_3], volatile organic compounds [VOCs], and formaldehyde [HCHO]), and physical conditions (such as temperature [T°C], relative humidity [RH%], light intensity, noise, dewpoint and air speed). Moreover, the perception weights of IAQ factors affecting the indoor comfort condition were also examined.

A two-stage viable, Andersen cascade impactor, was used by suctioning air onto the selective culture media. The PM content was determined by using a preweighted membrane filter. Portable air quality monitors were used to estimate the chemical and physical factors. A questionnaire survey was employed to assess the health complaints and the participants' perception weights on the indoor environmental parameters (such as thermal, acoustic, visual environment, and air quality).

The concentrations of mesophilic bacteria, fungi, and actinomycetes were found to be higher indoors than outdoors, with indoor/outdoor (I/O) values of 3.13, 1.56, and 1.53, respectively. The Global Index of Microbial Contamination/m^3 exceeded 7,000 colony forming units/m^3 in approximately 46% of the workshop areas. The I/O ratios of PM, VOCs, HCHO, and NH_3 were 1.69, 1.52, 0.65, and 0.6, respectively. T°C and RH% values ranged 18–35°C and 40–56%, respectively.

Özet

İç Hava Kalitesi (IAQ), mikro çevre koşulları, konum ve bina özellikleri arasındaki etkileşimin bir sonucu olup, insan performansını ve sağlığını etkiler. Endüstriyel olmayan atölyelerin IAQ çok az dikkat edilmiştir. IAQ, insan sağlığını, konforunu ve üretkenliğini doğrudan etkiler.

Akademi ile ilgili atölyelerde IAQ faktörlerini belirlemek için kesitsel bir araştırma yapılmıştır. IAQ faktörleri mikrobiyal (bakteriler, mantarlar ve aktinomisetler), partikül madde (PM), kimyasal [amonyak (NH_3), uçucu organik bileşikler (VOC) ve formaldehit (HCHO)] ve fiziksel (sıcaklık [T°C], bağıl nem [%RH], ışık yoğunluğu, gürültü, çiğlenme noktası ve hava hızı) düzeyleri açısından incelenmiş ve iç mekan konforunu etkileyen IAQ faktörlerinin algılama ağırlıkları değerlendirilmiştir.

Seçici kültür ortamlarına hava emerek iki aşamalı Andersen numune alıcı kullanılmıştır. PM, önceden tartılmış membran filtre kullanılarak ölçülmüştür. Kimyasal ve fiziksel faktörleri ölçmek için taşınabilir hava kalitesi monitörleri kullanılmıştır. Sağlık şikayetlerini ve katılımcıların iç ortam parametrelerine (termal, akustik, görsel ortam ve hava kalitesi) ilişkin algı ağırlıklarını belirlemek için bir anket kullanılmıştır.

İç mekanlarda dış mekanlara göre mezofilik bakteriler mantar ve aktinomisetlerin konsantrasyonlarının daha yüksek olduğunu ortaya koymuştur. İç mekan/dış mekan (I/O) değerleri sırasıyla 3,13, 1,56 ve 1,53 olarak ölçülmüştür. Mikrobiyal Kontaminasyon Küresel Endeksi/m^3 atölyelerin yaklaşık %46'sında 7000 koloni oluşturan birim/m^3'yi aşmıştır. PM, VOCs, HCHO ve NH_3'ün I/O oranları sırasıyla 1,69; 1,52; 0,65 ve 0,6 olarak ölçülmüştür. T°C ve %RH değerleri sırasıyla 18-35°C ve 40-56% arasında değişmiştir. Gürültü değerleri iç ve dış ortamda 70 desibel (dBA) değerini aşmıştır. Işık yoğunluğu

Edited by: *Mustafa Yamaç*
***Corresponding Author:** Abdel Hameed Awad, **E-mail:** abed196498@yahoo.com*
***ORCID iDs of the authors:** AHA. 0000-0003-0784-9835, SE-G. 0000-0003-1100-5985, YS. 0000-0002-5183-4342, SK. 0000-0001-8087-1268.*

Received: 01 March 2025, **Accepted:** 16 July 2025, **Online First**: 19 August 2025, **Published:** 15 October 2025

Noise values exceeded 70 dBA in both the indoor and outdoor environments. Light intensity was also unacceptable (≤ 300 lux) at 84.6% of the workshop areas. VOCs and dewpoint revealed significant positive and negative effects on microbial viability, differing with regard to the microbial type. Fatigue (45.5%), allergies (38.6%), and headache (35.2%) were the common complaints of the occupants. All of the tested IAQ parameters influenced the workplace environment, with noise ranking as the main factor (40.9%).

Microbial air quality is differently associated with the indoor environmental factors. The IAQ in the workshops was poor and potentially affected the occupant's well-being. The perception of comfort varied among the occupants under the same IAQ factors. Thus, corrective actions based on comparative analysis should be implemented to promote the indoor quality of even nonindustrial and academia-related workplaces.

atölyelerin %84,6'sında kabul edilemez düzeyde (≤ 300 lux) idi. VOC'ler ve çiğlenme noktası, mikrobiyal canlılık üzerinde önemli pozitif ve negatif etkiler göstermiş, mikrobiyal türe göre farklılık göstermiştir. Yorgunluk (%45,5), alerji (%38,6) ve baş ağrısı (%35,2) katılımcılar arasında en sık görülen sağlık şikayetleriydi. Tüm IAQ parametreleri işyeri ortamını etkilemiş olup, gürültü katılımcıların konforunu etkileyen ana faktör (%40,9) olarak sıralanmıştır.

Mikrobiyal hava kalitesi, iç ortam faktörleriyle farklı şekilde ilişkiliydi. Atölyelerde IAQ kötüydü ve katılımcıların' refahını potansiyel olarak etkiledi. Aynı IAQ faktörleri altında katılımcılar arasında konfor algısı farklılık gösterdi. Karşılaştırmalı analiz yoluyla, işyerlerinin iç ortam kalitesini iyileştirmek için düzeltici önlemler alınmalıdır.

Keywords: indoor air quality, nonindustrial workshops, deposited dust, particulate morphology, microorganisms, VOCs, noise, lighting, health complaint, satisfaction

Introduction

Indoor Air Quality (IAQ) is influenced by multiple interrelated factors, including building activities and materials, ventilation efficiency, emission sources, and both geographical and microclimatic conditions (Apte & Salvi, 2016; Tran et al., 2020; Chawla et al., 2023). Air pollutants, thermal comfort, illumination level, and noise pollution are the key factors that significantly impact IAQ (Tang et al., 2020; Roumi et al., 2022; Wu et al., 2023). Indoor air pollution levels are often reported to be 2–5 times higher than outdoor (United States Environmental Protection Agency [U.S. EPA], 2025a), with indoor environments emitting wide array of hazardous pollutants such as volatile organic compounds (VOCs), particulate matter (PM), and microorganisms (Kumar & Imam, 2013).

Among these pollutants, microorganisms are pervasive in indoor environments, and present substantial public health risks (DiCarlo et al., 2016; U.S. EPA, 2025b). Numerous studies have evaluated microbial air quality across both industrial (Gilbert & Duchaine, 2009; Mackiewicz et al., 2015; Thorne, 2019; Quintana et al., 2020; Quintanilla-Martinez et al., 2022; Tyagi & Srivastava, 2023) and public (Shiferaw et al., 2016; Osman et al., 2017; Abdel Hameed et al., 2018; Pyrri et al., 2020; Nath et al., 2023) settings. The diversity and concentration of microbial populations in indoor air are shaped by geographical location, weather conditions, and human activities (Rai et al., 2021). Inhalation exposure to airborne microbes can trigger respiratory infections, allergic reactions, hospital-acquired (nosocomial) diseases, and symptoms associated with sick building syndrome (SBS) (Dyląg, 2017). Furthermore, microbial contamination contributes to the biodeterioration of structural materials (Kadaifciler, 2017; Lippai et al., 2024).

PM, one of the most critical indoor pollutants, is composed of both primary particles (emitted directly from anthropogenic or natural sources) and secondary particles (formed through complex chemical reactions in the atmosphere) (Juda-Rezler et al., 2020). Indoor PM concentrations are influenced by external air quality, building envelope characteristics, ventilation rates, material composition, and human activities (Cheng, 2017; Melymuk et al., 2020). Elevated PM levels have been documented in specific workplaces, including metal and wood working facilities (Abdel Hameed et al., 2000; Insley et al., 2019, Buljat et al., 2024). The shape, size, and chemical composition of PM vary significantly, which determines its toxicity and surface-soiling potential (DiBernardino et al., 2021; Park et al., 2018). Therefore, both the mass concentration and chemical composition of PM should be analyzed to understand its full impact on human health.

VOCs are another critical group of indoor air contaminants, consistently found in higher concentrations indoors compared to outdoor (Nurmatov et al., 2015; Spinazzè et al., 2020). VOCs, including formaldehyde (HCHO), are released from a range of sources such as building materials, insulation foams, cleaning agents, furnishings, and human activities (Mangotra & Singh, 2024). Building materials alone can contribute up to 40% of total indoor VOCs emissions, depending on the building's age, type, and prevailing temperature and humidity conditions (Missia et al., 2010; Zhu et al., 2024). Notably, newly constructed or recently renovated buildings exhibit significantly higher VOC levels than older structures (Holøs et al., 2018). In Chinese residential, educational, and office buildings, median HCHO concentrations ranged between 94–163 μg/m³, with 46–91% of sampled buildings, exceeding the standard threshold of 100 μg/m³ (Fang et al., 2022). Formaldehyde is classified as a Group 1 human carcinogen by the International Agency for Research on Cancer IARC, 2006).

Ammonia (NH_3) is a dominant basic gas present in both indoor and outdoor environments (Li et al., 2020). Emissions originate from various sources, including livestock, decomposition of organic matter, industrial and vehicular emissions, combustion activities, building materials, paints, and even human metabolism and exhaled breath (Li et al., 2022; Lefferts & Castell, 2022). NH_3 also plays a critical role in atmospheric chemistry, particularly in the formation of secondary PM (Wyer et al., 2022). Studies from Chinese college dormitories reported mean NH_3 concentrations of 0.59 mg/m³, exceeding the national standard threshold (GB/T

18883–2002). Chronic exposure to NH_3 has been linked to neurophysiological disturbances, mucous membrane irritation, and headache (California Office of Environmental Health Hazard Assessment, 1999; Pacharra et al., 2016; Sun et al., 2024).

Physical parameters, including thermal conditions, directly affect both IAQ and occupant well-being (Asadi et al., 2017). Thermal discomfort, particularly temperatures > 26°C, has been shown to negatively impact productivity (Lan et al., 2011), whereas uncontrolled fluctuations in temperature and humidity can damage building materials (Camuffo, 2019). High temperatures, low air exchange, elevated humidity, excessive light intensity, and poor air quality are commonly associated with SBS symptoms (Akova et al., 2022).

A prior assessment of academia workshop environments categorized their indoor environmental quality (IEQ) as Class D (IIEQ score of 10–32.5), indicating a high-risk classification according to the IEQ Index model (Abdel Hameed et al., 2023). Walkthrough inspections of these workshops revealed several concerns, including high humidity levels, visible dust and dirt accumulation, inadequate ventilation, fungal growth, and musty odors. Occupants also reported health-related complaints potentially linked to these environmental deficiencies.

Given these observations, the present study aims to investigate IAQ-related factors within academic workshop settings; examine the influence of micro-environmental parameters on airborne microbial composition; identify the prevalence and extent of indoor fungal contamination; and determine the perception weightage of various IAQ factors to pinpoint the primary contributors to occupant satisfaction. The findings are intended to draw attention to potential IAQ hazards in nonindustrial academic and public workshop settings, and support the development of threshold guidance values tailored for such environments.

Materials and Methods

IAQ Factors and Sampling Workshops

A cross-sectional survey of IAQ (including microbial, PM, chemical, and physical) factors was conducted in 13 workshops related to academia building. The workshops are namely "wood, alumina, glass, painting, plumbing, welding, car garage & maintenance, scientific equipment maintenance, cooling, oil extraction, marble and granite test, water pump station, and electricity station." These workshops cannot be classified as the same as industrial workshops despite performing technical/or professional tasks related to public building activities. The workshops are located in different buildings and differ in their total area (range: 40–187 m^2), height above the ground level (–3 m to + 6 m), number of occupants (range: 3–22 persons/location), and ventilation mode. Poor ventilation rate, dampness, musty odor, and crowding are the common characteristics of the workshops. Natural ventilation (openings) is the main ventilation type; however, mechanical ventilation (fans/no air conditioner) is operated in some workshops. The academic building is located in the Dokki district, Giza governorate. This district is an urban area characterized by heavy anthropogenic activities, high traffic, commercial activities, hospitals, offices, and numerous educational facilities, with rare and permanent vegetation cover. The description of the sampling sites and timetable schedule for the IAQ measurements has been presented in Table 1.

Sampling Campaign

A total of 28 samples (a minimum of 2 event/workshop) and 6 samples (at least one sample/month) were collected from inside and outside the workshops, respectively. The sampler/monitor was placed at approximately 1.5–2 m height on a flat surface, approximately 1–2 m away from the openings and disturbance of direct obstacles. The outdoor sampling was conducted approximately 3–4 m outside of the main building, away from any distinct emission sources. The indoor and outdoor samples were almost collected in parallel.

The measurements of the chemical and physical parameters were performed at the beginning and the end of each sampling event (approximately 2 readings/event), except for the PM, with one PM sample collected at every sampling event. The air samples were collected during the normal working days, which lasted approximately 4–5 h, during 10:00 and 15:00 hours, which is the period of full capacity of the work activity. The sampling was conducted on Mondays through Thursdays of the last weeks of each month, during the period between May and December 2022.

Sampling of the Airborne Microorganisms

A two-stage viable particle sampler (TE-10-160, Tisch Environmental Cleves, OH, USA) was used to collect airborne microorganisms (National Institute for Occupational Safety and Health, 1998). This device separates particles into fine (≤ 2.5 μm) and coarse (≥ 7 μm) size ranges and operates at the recommended flow rate of 28.3 L/min for 5 min; it was run in duplicate. Trypticase soya agar supplemented with 0.25% cycloheximide, malt extract agar supplemented with 0.01% chloramphenicol, and starch casein agar media were used to culture bacteria, fungi, and actinomycetes, respectively. The culture plates of fungi and actinomycetes were incubated at 28°C ± 2°C for 5 and 7–14 days, respectively, whereas those of environmental and mesophilic (human-related) bacteria were incubated at 30°C ± 2°C for 48 h and at 37°C for 48–72 h, respectively. Positive hole correction was applied to the raw colony forming unit (CFU) recorded on each plate and by using the CFU with sampling time and flow rate; the concentration was calculated and expressed as CFU/m^3 of air (Andersen, 1958).

Fungal isolates were identified through direct observation of micro- and macro-morphological features by reverse and surface coloration of colonies on Sabouraud's dextrose agar, Czapek dox agar, potato dextrose agar (Difco, Detroit, MI) and malt extract agar media (Hi-media laboratories, Mumbai, India) with the use of keys for taxonomic literature (Ellis, 1971; Raper & Fennell, 1977; Barnett & Hunter, 1999; Pitt & Hocking, 2009).

Table 1. Description of the sampling sites and sampling timescale for the IAQ tests.

Number	Workshop	Building floor	Ventilation type/ quality*	Area (m^2)	Average number of occupants	Measurement timescale (day/ month)
1	Wood	Separated building/ ground floor	Natural/bad	184	22	28/9; 29/9 & 18/10
2	Alumital	Separated building/ ground floor	Natural/moderate	110	8	15/11 & 22/11
3	Glass	2nd floor	Natural/moderate	95	8	28/9 & 19/12
4	Painting	Basement	Natural/bad	97	12	18/10 & 25/10
5	Plumbing	Basement	Natural/bad	112	9	11/10 & 25/10
6	Welding	Ground floor	Natural/bad	120	3	22/11 & 15/11
7	Car garage & maintenance	Ground floor	Natural/moderate	150	17	24/5 & 21/9
8	Scientific equipment maintenance	2nd floor	Natural/bad	30	6	24/5 & 22/6
9	Cooling	Ground floor	Natural/bad	62	6	14/9 & 20/9
10	Oil extraction	Basement	Natural/moderate	40	3	14/9, 12/12 & 19/12
11	Marble and granite test	Basement	Natural/bad	40	4	15/11 & 12/12
12	Water pump station	Ground floor	Natural/moderate	176	3	18/10 & 15/11
13	Electricity station	Ground floor	Natural/moderate	28	3	20/9 & 18/10
14	Outdoor air	External environment/ outside main buildings	-	-	-	24/5, 22/6, 21/9; 18/10, 22/11 & 12/12

IAQ = indoor air quality.

Suspended and Deposited Particulates

Suspended PM was collected on a preweighed cellulose nitrate membrane filter (25 mm-diameter, 0.45 μm-pore size) using an open face filter holder and a vacuum pump calibrated to draw 15 L/min for 4–5 h. The PM mass concentration was calculated and expressed as microgram per cubic meter of air ($\mu g/m^3$). The shape (morphology) of the PM collected from some workshops was analyzed with the high-resolution scanning electron microscope (SEM; Quanta FEG 250, FEL Company, Netherlands, Electron Unit of Microscopy, NRC). The chemical species of the PM sample collected from the auto-mechanic (car maintenance) workshop were only examined by using an energy-dispersive X-ray analyzer (EDAX) attached to the electron microscope.

The deposited (settled) dust was determined using a passive collector (170-mm height, 80-mm diameter) by positioning the collector approximately 2–3 m above the floor surface in the center of the workshop. The dust collectors were harvested after 3 months of exposure, and the deposited dust was carefully transferred to dry-sterilized preweighted beakers. The dust rate was then calculated and expressed as milligram per square meter per day ($mg/m^2/day$).

Chemical Pollutants (i.e., VOCs, HCHO & NH_3)

A portable digital Aeroqual-Series 200 detector (Auckland, New Zealand) was used to measure the levels of VOCs and NH_3. Moreover, a portable air quality monitor (Yvelines air quality monitor, Model: HTO-131, USA) was used to measure the HCHO levels. The levels of the chemical pollutants were expressed as milligram per cubic meter of air (mg/m^3) for VOCs and as microgram per cubic meter of air ($\mu g/m^3$) for HCHO and NH_3.

Physical Factors (i.e., Noise, T°C, Relative Humidity [RH%], Light and Air Speed)

The noise levels were determined by using a sound level meter (model RO-1350, Taiwan) positioned approximately 1.5 m above the ground surface level, no closer than 3 m to any reflecting surface, and expressed as decibel-A (dBA). The light intensity was measured at nearly 4 points/location with a light meter (Light meter-TM-201, Taiwan) and expressed as lux. T°C and RH% were measured using a thermo-hygrometer (Sato-PC 5,000, China) (ASTM 2015). The air velocity (m/s) was measured using an anemometer (ABH-4225, Taiwan). The physical parameters were

measured at the start time (10:00 – 11:00 AM) and at the end time (2:00 – 3:00 PM) of each sampling event.

Survey of the Complaints Related to the Indoor Environment

A questionnaire survey was administered to 88 randomly selected subjects, with no inclusion or exclusion criteria. The survey items were general questions based on the frequent occurrence of the health symptoms for 3 days per week in the past 4 weeks before the survey. These symptoms appeared daily or nearly every working day and disappeared/or got better when the employee left the workplace. The questionnaire listed the following general symptoms: shortness of breath, wheezing, cough, sneezing, stuffy nose, throat irritation, allergy, watering eyes, dry eyes, irritation of the eyes, headache, fatigue, dizziness, and nausea (Mendell et al., 2003; Azuma et al., 2022). Moreover, the weighting of four IAQ factors (i.e., temperature, light intensity, noise, and air quality [ventilation/odor]) that affected the occupant's satisfaction was analyzed with reference to the questionnaire-based survey so as to determine the major IAQ factor affecting the worker's comfort.

Statistical Analysis

Descriptive (i.e., range, mean, standard deviation (SD), and 95% confidence intervals) and nonparametric statistics were employed to analyze the obtained data. Spearman's rank-correlation test was performed to determine the relationships between the chemical and physical factors with the microbial load. $p \leq 0.05$ was considered to indicate statistical significance.

QA/QC

QA/QC was applied using duplicate samples in each sampling event for the determination of the microbial load and the presence of physical and chemical parameters. A blank membrane filter and culture media were maintained to standardize the PM and microbial pollutants, respectively. The sampling devices were verified against the calibrated reference equipment. Statistical analysis was performed to interpret the obtained data. The outdoor samples were collected on the same days for IAQ assessments.

Results and Discussion

Microbial Air Quality

Indoor microbial air quality depends on the shear force, microbial type, indoor sources, outdoor air quality, occupant's intensity, nature of work, and the ventilation mode (Romano 2023). The summary of the indoor and outdoor microbial air quality is presented in Table 2 and Figure 1. The airborne microbial concentrations varied with regard to the workshops. The concentrations of environmental bacteria, mesophilic bacteria, fungi, and actinomycetes averaged 4,646 CFU/m^3 (95% confidence interval [CI] 2,308–6,984 CFU/m^3), 1,931 CFU/m^3 (95% CI 1,186–2,677 CFU/m^3), 825 CFU/m^3 (95% CI 490–1,159 CFU/m^3) and 532 CFU/m^3 (95% CI 153–862 CFU/m^3), respectively. The indoor/outdoor (I/O) ratios were 0.95, 3.13, 1.56, and 1.53 for the corresponding microbial indicators, respectively. The highest concentration of mesophilic bacteria (4,531 CFU/m^3) was recorded in the cooling workshop. The highest loads of fungi (2,841 CFU/m^3) and actinomycetes (2,254 CFU/m^3) were detected in the water pump workshop. Environmental bacteria (19,378 CFU/m^3) were detected in the highest concentration in the marble and granite test workshop (Figure 1), suggesting that the dust-raising activities increased the bacterial counts relative to the fungal counts.

Table 2. Range, mean, and 95% CI of indoor/outdoor microbial parameters in the workshops.

Parameter	Indoor environment (Range) [mean ± SD]	95% CI	Outdoor environment (Range) [mean ± SD]	95% CI
Environmental bacteria–CFU/m³	(1,594–19,378) [4,646 ± 4,464]	2,308–6,984	(1,366–11,081) [4,867 ± 4,383]	571.7–9,162
Mesophilic bacteria–CFU/m³	(524–4,531) [1,931 ± 1,423]	1,186–2,677	(71–1,021) [617 ± 396.4]	228–1,005
Fungi–CFU/m³	(362–2,841) [825 ± 638.7]	490–1,159	(387.5–692.6) [527 ± 144]	385–668
Actinomycetes–CFU/m³	(59–2,254) [532 ± 667]	153–862	(131–674) [348 ± 231]	122–574

CFU = colony-forming unit; CI = confidence interval; SD = standard deviation.

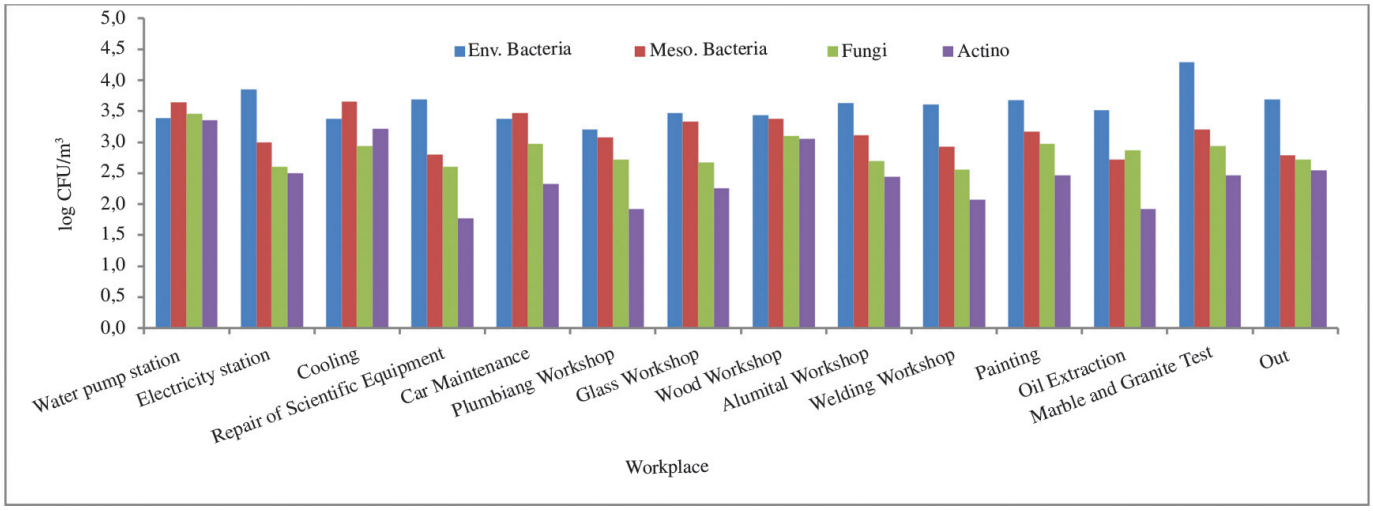

Figure 1. Log concentrations of airborne microbial parameters in the workshops.

Airborne microorganisms are randomly transmitted between the indoor and outdoor environments. Indoor microorganisms originate from indoor sources and natural/or anthropogenic surrounding activities. The I/O ratios of microbial air parameters indicated that the indoor environment was the main contributor of mesophilic bacteria, fungi, and actinomycetes, whereas the outdoor environment was the main contributor of environmental bacteria. I/O value > 1 indicates that biocontamination originates from the indoor environment (Roshan et al., 2019; Jabeen et al., 2023). Overcrowding, poor ventilation, and adequate moisture facilitate the emission of bacteria and fungi indoors (Crawford et al., 2015). Actinomycetes are not normal indoor microbial flora, and their presence has been associated with abnormal situations such as presence of dampness and mold (Nevalainen et al., 1991). Actinomycetes are associated with the complaints of odor in buildings (Nevalainen et al., 1990). The low counts of actinomycetes may be attributed to their complex natural aerosolization mechanism, considering that they have small spore sizes approximately ≤ 1 μm, which requires high air current to release them into the air (Reponen et al., 1998).

Natural ventilation, through openings, is the main ventilation mode in most workshops. The studied workshops had inadequate and bad ventilation (air velocity ≤ 0.15 m/s), which directly affected microbial concentrations and types. I/O ratio, a relative standard, was applied to establish the presence or absence of indoor biologically derived sources and the outdoor infiltration factor. Natural ventilation increases the fungal counts and mechanical ventilation reduces their counts (MacIntosh et al., 2006), and infiltration brings exogenous microbes to the indoor environment (Zhong et al., 2016). Mechanical ventilation (rarely operated at these workshops) has higher air exchange rates compared to natural ventilation, which consequently reduces the indoor microbial content (Langer & Bekö, 2013).

Indices of Biocontamination

An assessment of the contamination levels was performed using three evaluation indices for microbiological pollution, namely "Global Index of Microbial Contamination per cubic meter of air (GIMC/m^3), amplification index (AI), and the index of microbial contamination (IMC), (Dacarro et al., 2005). GIMC/m^3 was calculated as the sum of the total counts of microbial parameters in each workshop. IMC was determined by calculating the ratio of the CFU/m^3, as measured for mesophilic and environmental bacteria at the same sampling site. AI is calculated as the ratio between the GICM/m^3 values measured indoors and outdoors, and it is an indicator of microbial accumulation indoors (Grisoli et al., 2019).

The summary of the biocontamination indices in the workshops is depicted in Table 3 and Figure 2. The GIMC/m^3 index values ranged between 10^3 CFU/m^3 and 10^4 CFU/m^3 and exceeded 7,000 CFU/m^3 at nearly 46% of the total workshops. The greatest GIMC/m^3 was detected in the marble and granite test workshop (22,110 CFU/m^3) and the lowest in the plumbing workshop (3,373 CFU/m^3) (Figure 2a). The values of the AI and IMC indices were ≥ 1 at 61.5% and 15% of the total workshops, respectively. GIMC/m^3, IMC, and AI achieved the highest values in the marble and granite test, water station, and cooling workshops, respectively (Figure 2a and b). The GMIC/m^3 values profile was in the following sequence: marble and granite test > water pump > cooling > electricity > wood > painting > car maintenance > alumital > repair of scientific equipment > glass > welding > oil extraction> plumbing. The workshops had higher microbial air loads (GIMC/m^3 ≥ 7,000 CFU/m^3) when compared to other public buildings, such as hospitals, libraries, schools, and child daycares in Egypt (Abdel Hameed et al., 2018).

Fungal Diversity

The identification of airborne fungal spores is a critical issue to determine their sources, health problems, and proactive steps so as to reduce the exposure. A total of 25 fungal taxa were identified at all workshops, including *Absidia*, *Acremonium*, *Alternaria*, *Aspergillus flavus (A. flavus)*, *Aspergillus niger*, *Aspergillus ochraceus*, *Aspergillus terreus*, *Aspergillus versicolor (A. versicolor)*, *Aspergillus fumigatus (A. fumigatus)*, other *Aspergillus*, *Aureobasidium*, *Cladosporium*, *Curvularia, Drechslera, Emericella, Epicoccum, Fusarium, Monilia,*

Table 3. Range, mean, and 95% CI of biocontamination indices at the workshops.

Biocontamination index	Air environment			
	Indoor		Outdoor	
	(Range) [mean ± SD]	95% CI	(Range) [mean ± SD]	95% CI
GIMC/m³	(3,374–22,111) [7.909 ± 4,662]	5,467–10,351	(2,713–12,331) [6,358.5 ± 4,324]	2,120.8–10,596
AI	(0.4–3.22) [1.45 ± 0.92]	0.95–1.95	–	–
IMC	(0.1–1.92) [0.64 ± 0.59]	0.32–0.96	–	–

GIMC = global index of microbial contamination; AI = amplification index; IMC = index of microbial contamination; CFU = colony-forming unit; CI = confidence interval; SD = standard deviation.

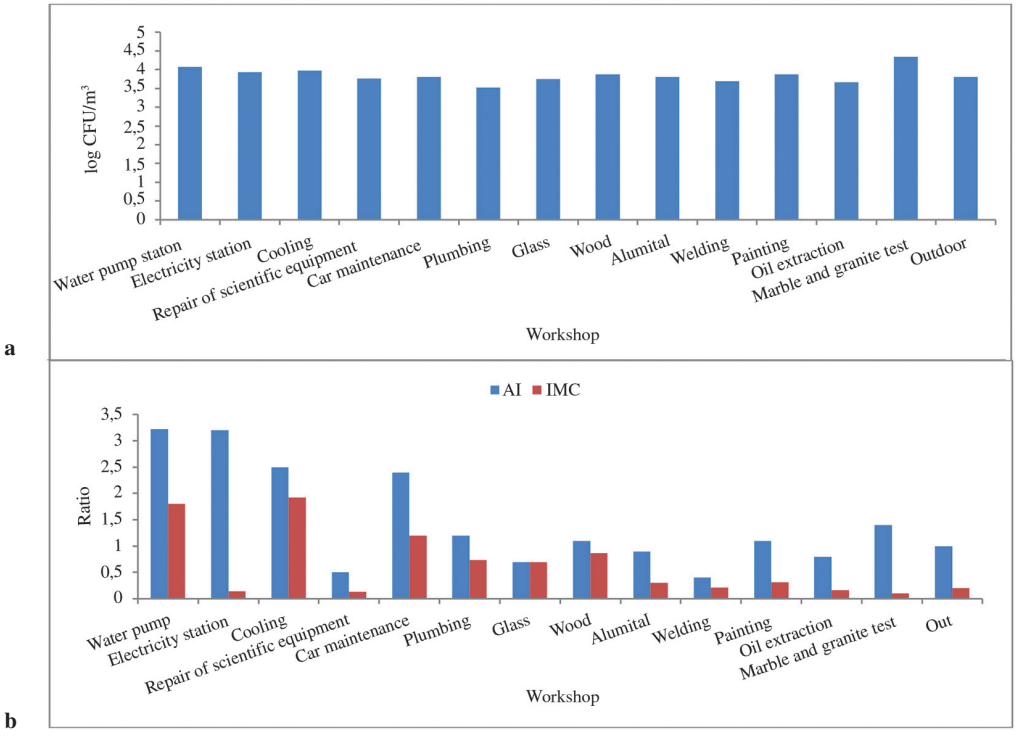

Figure 2. Air biocontamination indices at different workshops (a: GIMC/m³; b: AI and IMC). CFU = colony-forming unit; GIMC = global index of microbial contamination; AI = amplification index; IMC = index of microbial contamination.

Nigrospora, Penicillium, Rhizopus, sterile hyphae, *Trichoderma*, *Trichothecium,* and yeast.

Aspergillus (57.9%), *Penicillium* (9.34%), *Cladosporium* (4.84%), and *Alternaria* (3.42%) were the dominant fungal taxa. Fungal diversity was the highest at the wood workshop (13/ 25,~52%) and lowest at the plumbing workshop (6 /25, ~24%). *Aspergillus* constituted the largest counts, with 36–2,699 CFU/m³, at almost all the workshops. The highest counts of *Aspergillus*, *Alternaria*, *Cladosporium*, and *Penicillium* were detected in the water pump station, painting, granite and marble test, and oil extraction workshops, respectively (Figure 3). The secondary (*Alternaria*, *Cladosporium*, *A. flavus*, *A. versicolor*, *Penicillium,* and *Emericella*) and tertiary (*A. fumigatus*, *Nigrospora*, *Aureobasidium*, *Fusarium*, *Trichoderma*, *Monilia,* yeast, and sterile hyphae) fungal colonizers grew well at moderate and high water activities, respectively.

Generally, the characteristics of the surrounding environment and buildings, human activity, ventilation rate, and microclimatic conditions affect fungal counts and diversity (Hoekstra et al., 1994; Loukou et al., 2024). The dominance of primary fungal colonizers can be attributed to the fact that they are easily liberated into the air when disturbed, can adapt to atmospheric transport, and grow well in diverse habitats with minimal nutrients. Globally, *Aspergillus* and

Penicillium species are dominant in different climatic conditions (Mousavi et al., 2016), colonize damp materials (Horner, 2006), and prefer air humidity (Wilkie et al., 2023). The phyloplane taxa, *Alternaria*, *Cladosporium, Epicoccum,* and *Drechsler*a (naturally grow on leaves and other plant surfaces) dominate the outdoor environment (Levetin & Dorsey, 2006). *Penicillium*, a soil fungus, predominates in most regions and is replaced by *Aspergillus* in humid environments (Lacey et al., 1991). The tertiary fungal colonizers grow on most building materials in the presence of adequate moisture, with at least 0.65 water activity required for growth (Lacey & Dutkiewicz, 1994). The presence of primary, secondary, and tertiary fungal colonies indicates the fluctuation and stratification of microclimatic conditions, which warrants intervention to control dampness and dust.

Monitoring of microbial air quality is important as a regulatory compliance as well as for biological risk assessment. Although it is difficult to establish a dose–response relationship on the basis of the existing epidemiological data, the numbers and types of microorganisms detected can offer a useful index for evaluating IAQ (Grisoli et al., 2019).

Universally, there are no acceptable/official permissible values for airborne microorganisms. The Commission of the European Communities suggests < 500 CFU/m^3 and ≥ 2,000 CFU/m^3 as intermediate and high biocontamination, respectively, in a nonindustrial environment (Commission of the European Communities, 1993). Microbial counts > 1,000 CFU/m^3 indicates biocontamination (Occupational Safety and Health Administration [OSHA], 1992). Concentrations of bacteria > 3,000 CFU/m^3, fungi > 10,000 CFU/m^3, and actinomycetes > 100 are suggested as strongly microbial contaminated air (Polish Standard/PN-89/Z-04111/03, 1989). Fungal count ≥ 100 CFU/m^3 indicates the presence of an indoor source (Ohgke et al., 1987) and an abnormal condition when the count exceeds 500 CFU/m^3 (Reynolds et al., 1990). In Sweden, the concentration of *Aspergillus* species should be < 50 CFU/m^3 (Holmberg, 1987).

Actinomycetes count ≥ 100 CFU/m^3 indicates a damp environment and high microbial pollution (Breza–Boruta & Paluszak, 2007). Miller et al. (1988) reported that toxigenic and pathogenic fungi are unacceptable in indoor air, and if one of the counts of fungal species is > 50 CFU/m^3, indoor air is acceptable if the mixture of fungal species is < 150 CFU/m^3 and phylloplane fungi is < 300 CFU/m^3. The World Health Organization (WHO) expert group on the assessment of the health risks of biological agents in the indoor environment suggests that the $l0^3$ microorganisms/m^3 is generally considered the maximum safety level (Macher et al., 1995). Microbial air counts at the academia workshops exceeded some of the previously recommended limit values.

Suspended and Deposited PM

The concentrations of the suspended and deposited dust in the workshops are presented in Table 4. The concentrations of PM were 83–536 µg/m^3, with a mean of 287 µg/m^3 (95% CI 172–366 µg/m^3) in the indoor environment and 169 µg/m^3 (95% CI 112–226 µg/m^3) in the outdoor environment. The I/O ratio of PM was 1.69, indicating that indoor activities were the main contributor of particulates. Heavy dust contamination ≥ 400 µg/m^3) was detected in the welding, glass, car maintenance, wood, marble, and granite test workshops. The greatest PM concentration (536 µg/m^3) was detected in the welding workshop, as the nature and composition of the PM affected its mass concentration.

The deposited dust rate averaged 71.9 mg/m^2/day (95% CI 33.5–110.3 mg/m^2/day) inside the workshops. The highest and lowest deposited dust rates were detected in the wood (258 mg/m^2/day) and oil extraction (1.75 mg/m^2/day) workshops, respectively. Dust deposition inside the workshops widely varied, depending on the nature and capacity of the work and the infiltration factor. The calculation of the particle size is of great concern to determine the removal process and exposure risks. The particle sizes ranged between ≤ 5 and ≥ 20 µm. The deposition velocity is computed from the deposited dust rate (µg/m^2/h) and volumetric concentration (µg/m^3), and it is determined by the size, air turbulence, RH, thermal

Table 4. Range, mean, and 95% CI concentrations of indoor/outdoor particulates and chemical pollutants at the workshops.

Parameter	Indoor environment		Outdoor environment	
	(Range) [mean ± SD]	**95% CI**	**(Range) [mean ± SD]**	**95% CI**
PM-µg/m^3	(83–536) [287 ± 218]	172–366	(111–250) [169 ± 58.5]	112–226
Deposited dust-mg/m^2/day	(1.75–258) [72 ± 70.6]	33.5–110	–	–
HCHO-µg/m^3	(123.8–316) [226 ± 61]	193–259	(230–541) [343 ± 105]	258–427
NH_3-µg/m^3	(45.6–395) [157 ± 123]	90–224	(0.0–658) [258 ± 273]	38–478
VOCs- mg/m^3	(0.47–8.57) [2.5 ± 2.27]	0.96–3.74	(0.36–3.7) [1.65 ± 1.14]	0.37–2.57

CI = confidence interval; PM = particulate matter; HCHO = formaldehyde; NH_3 = ammonia; VOCs = volatile organic compounds.

gradient, and eddy diffusion (Lai & Nazaroff, 2000). In this study, the lowest deposition velocity (1.3E02 cm/s) was detected in the oil extraction workshop and the highest (1.13 cm/s) in the plumbing one. Particle sizes ≤ 5 μm were detected in the oil extraction, repair of scientific equipment, and water pump workshops.

The mass concentration, composition, size, and shape of the PM vary with the dust origin and the formation process (Morawska & Salthammer, 2003; Dong et al., 2019; Zhang et al., 2022). The study of the physical properties of suspended particles helped understand their behavior and removal process. Figure 4 depicts the SEM images and EDAX analytical approach of PM. The shape of the particles varied from being fairly simple and regular to irregular/or complex ones. The shapes are varied within rounded and smooth surfaces, crystalline, and small and elongated fibers. This variation confirmed that the particles had various contributors such as fly ash, diesel soot, fossil fuel burning, and organic origin. The regular fibrous/elongated shape was detected in the wood workshop, whereas small agglomerate spherical particles were detected in the auto mechanic workshop (Figure 3). Tiwar et al. (2024) reported that quartz (rock particles) and tapered fibers dominated in the glass workshop, spherical particles (Si, Al, and Fe-rich) produced from combustion, and irregular blocky particles (Fe, Si, Ca, and Mg-rich) produced by mechanical processes.

Chemical Air Pollutants

The average values of indoor HCHO, NH_3, and VOCs were 226 μg/m^3 (95% CI 193–259 μg/m^3), 157 μg/m^3 (95% CI 90–224 μg/m^3), and 2.52 mg/m^3 (95% CI 0.96–3.74 mg/m^3), respectively (Table 4). The highest values of the corresponding air chemical pollutants were measured at the electricity station (316 μg/m^3), car garage and maintenance (395 μg/m^3), and oil extraction (8.57 mg/m^3) workplaces, respectively. The I/O ratios of HCHO, NH_3, and VOCs were 0.65, 0.6, and 1.5, respectively. The indoor environment was the main contributor of VOCs. The VOCs and HCHO are generally linked and emitted from a variety of natural and human-caused sources (Hansen, 1999; Kumar et al., 2021; Dehghani et al., 2024). Surprisingly, the HCHO values were higher outdoors than indoors. HCHO is formed through the atmospheric oxidation of VOCs and the reaction among O_3, alkenes, and terpenes (Liu et al., 2023) and anthropogenic sources of industrial and vehicle emissions and vegetation. HCHO values were higher in the ambient air, especially in the urban environment (Salthammer et al., 2010).

Although VOCs are the main pollutants affecting the IAQ, there are no global/local limits on them. Some countries have recommended permissible limits, such as 200 μg/m^3 by Belgium, 1,000 μg/m^3 by South Korea (International Society of Indoor Air Quality and Climate, n.d.), and 3,000 μg/m^3 by Finland (Tuomi & Vainiotalo, 2016). The value of 500 μg/m^3 is recommended as a background level for VOCs (Bluyssen et al., 2005). VOCs were detected in high values, exceeding the recommended permissible limit of 3 mg/m^3 at 30% of the workshop areas (such as glass, aluminum, oil extraction, and painting workshops). However, the American Conference of Government Industrial Hygienists (ACGIH, 2012), the Occupational Safety and Health Administration (OSHA, 1992), the World Health Organization (WHO, 2000), and Danish guidelines (Nazaroff & Weschler, 2004) have recommended HCHO limit values of 370 μg/m^3/8 h, 920 μg/m^3/8 h, 100 μg/m^3, and 100 μg/m^3, respectively. HCHO values exceeding the limits have been set by the Danish guidelines and the WHO (100 μg/m^3) in all workshops under investigation.

NH_3 values varied at 45.6–395 μg/m^3 inside the workshops, with an overall average of 157 μg/m^3. The average value of NH_3 was within the recommended limits of 0.2 mg/m^3 (Standardization Administration of China, 2002) and 17 mg/m^3 (Health and Safety Executive, 2018). NH_3 values exceeded the threshold limits of 0.2 mg/m^3 in 30.7% of the total studied workshops (including water pump, car maintenance, plumbing and cooling workshops). The present results are compatible with those reported for residences (0.21 mg/m^3), offices (0.26 mg/m^3), and school buildings (0.15 mg/m^3) in China (Sun et al., 2021).

Physical Parameters

A summary of the levels of physical parameters at the workshops is presented in Table 5. Indoor and outdoor noise levels ranged at 54–87 dBA. The noise levels averaged 71 dBA (95% CI 66–76 dBA) inside and 74 dBA (95% CI 70.8–77 dBA) outside the workshops. The noise level was ≥ 70 dB in 53% of the total workshops. The noise level exceeded the minimum comfort level in the public buildings (60 dBA) in almost all the workshops, except at the oil extraction workshop (54 dBA). The highest noise level (87 dBA) was recorded at the wood workshop, exceeding the Egyptian permissible limit level of 85 dBA for the industrial sector (Egyptian Environmental Affairs Agency, 1994). The light intensity levels varied at 41–317 lux, with an average level of 176 lux (95% CI 132–222 lux). Light intensity was detected at very low levels at the welding and plumbing workshops (41–54 lux). The light intensity ranges (41–317 lux) were below the acceptable minimum level of 300 lux (NP 061, 2002) at 84.6% of the total workshops.

The temperature, RH, and dew point measurements averaged 28.4°C (95% CI 25.1°C–31.7°C), 48.8% (95% CI 46–53.7%), and 17.2°C (95%CI 14.3°C–20.1°C), respectively (Table 5). The highest reading of T°C (35°C) was determined at the glass workshop. The highest readings of RH% (58%) and dew point (21.4°C) were detected at the car maintenance workshop. The readings of temperature ≥ 30°C and RH ≥ 50% were, respectively, measured at 69.2% and 46.2% of the total workshops. The mean value of the RH was intermediate (48.8%), and temperature (28.4ºC) did not comply with the comfortable condition. The OSHA provides guidance for air temperature and RH ranges within 20°C–24.4°C and 20–60%, respectively (OSHA, n.d.). The dew point values exceeded the upper limit of 16.8°C (ASHRAE Standard 55, 2010) at 61.5% of the total workshops. The measurements of air velocity were below the recommended limit of 0.15–0.50 m/s (Sulaiman et al., 2013). Low air velocity causes air stagnation and, consequently, poor ventilation, helping accumulate pollutants.

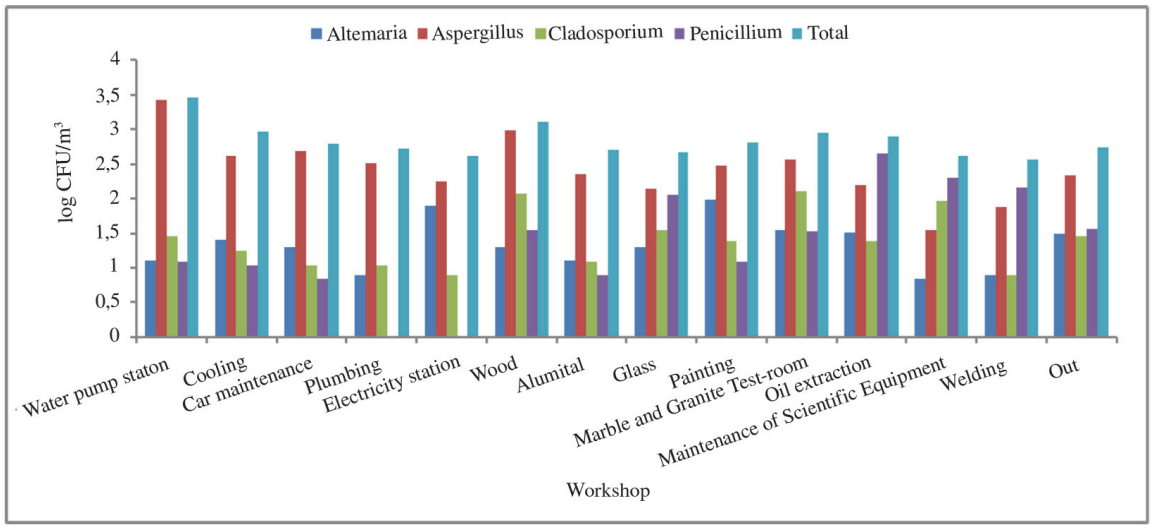

Figure 3. Log counts of the total and dominant fungal taxa in different workshops.

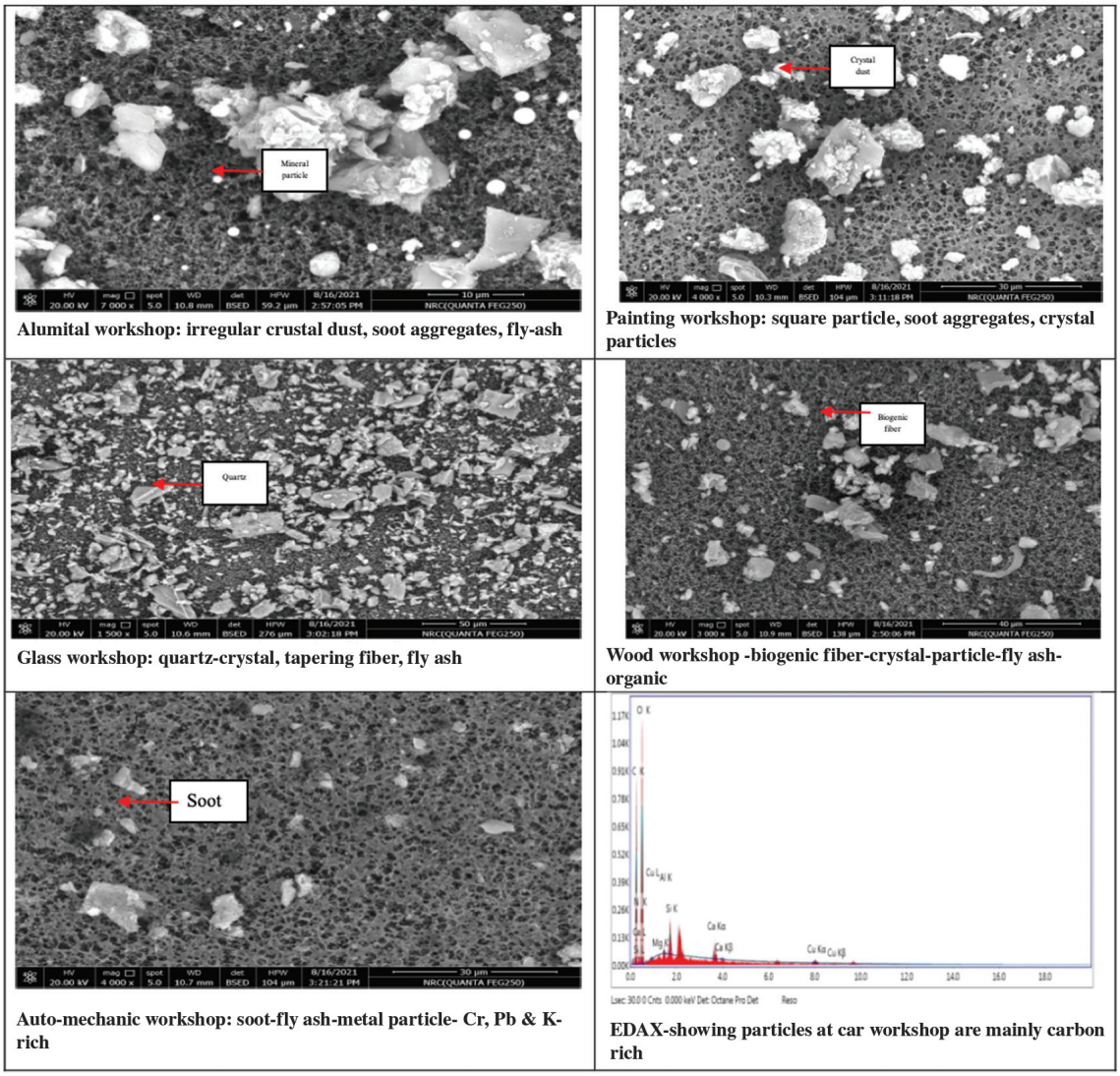

Figure 4. SEM images and EDAX analytical approach of PM samples from different workshops. SEM = scanning electron microscopy; EDAX = energy-dispersive X-ray analysis; PM = particulate matter.

Relationships Between Air Microorganisms and Environmental Stressors

The correlations between microbial air quality and environmental factors are shown in Table 6. A wide range of correlations were detected, depending on the microbial type and environmental factors. PM, HCHO, and VOCs showed similar correlation pattern with airborne microorganisms. They were negatively correlated with mesophilic bacteria, fungi, and actinomycetes and positively correlated with environmental bacteria. The VOCs and HCHO values adversely affected the bacterial and fungal viabilities. VOCs react with O_2 to form open air factor, inactivating microorganisms by damaging enzymes and DNA (Donaldson & Ferris, 1975). It has been suggested that indoor activities and indoor conditions are the main contributors of VOCs, HCHO, PM, mesophilic bacteria, fungi, and actinomycetes. PM positively and negatively correlated with the microbial parameters, confirming that PM had diverse contributors. The environmental bacteria may be associated with the outdoor infiltrated PM. Mesophilic bacteria, fungi, and actinomycetes may be emitted directly from the indoor environment, independent of the PM contributors. Indoor PM has small sizes (≤ 20 μm) and a more toxic chemical composition, which may negatively affect microbial viability (Sillanpää et al., 2005). PM has detrimental/or supportive effects on microbial viability (Matthias-Maser, 1998), depending on its composition and tenacity. Moreover, PM acts as a carrier/or niche of nutrients for microorganisms and affects their behavior in the air environment (Alghamdi et al., 2014; Soleimani et al., 2022).

T°C and RH% differently affected microbial viability. T°C displayed a considerable influence on microbial viability relative to RH% (Table 5). The dew point significantly supported the survival of actinomycetes (r = 0.66, $p \leq 0.05$), mesophilic bacteria (r = 0.67, $p \leq 0.05$), and fungi (r = 0.42) (Table 5). Environmental bacteria significantly correlated with the dew point (r = -0.53, $p \leq 0.05$), NH_3 (r = -0.53, $p \leq 0.05$), and VOCs (r = 0.53, $p \leq 0.05$). Several studies have reported contradictory associations between airborne microorganisms and environmental factors. Dennis and Lee (1988) reported the best survival of aerosolized *Legionella* at 90% RH%, which was intermediate at 30% and poor at 60%. However, Hambletonet et al. (1983) found the best survival of *Legionella* at 65% and the worst at 90% and 30%. Frohlich-Nowoisky et al. (2014) concluded that high RH (70–80%) promoted airborne microbial survivability. The death rates of some gram-positive and gram-negative bacteria showed an increase at intermediate RH% (50–70%) to high (70–90%) (Won & Ross, 1969; Hatch et al., 1970). RH% ≤ 65% had a negative effect on the survival of airborne bacteria and fungi (Karbowska-Berent et al., 2011). Temperature ≥ 24°C decreased the survival of airborne bacteria (Tang, 2009), whereas higher temperatures increased their survival (Smets et al., 2016).

Table 5. Range, mean, and 95% CI values of indoor/outdoor physical parameters at the workshops.

Parameter	Indoor environment		Outdoor environment	
	(Range) [mean ± SD]	**95% CI**	**(Range) [mean ± SD]**	**95% CI**
T°C	(18–35) [28.4 ± 6.1]	25.1–31.7	(18–35) [29.8 ± 7.7]	22.2–37
RH%	(40–56) [48.8 ± 5.3]	46–53.7	(37–46) [42 ± 4]	39.6–44.6
Dew point-T°C	(7.1–22.7) [17.2 ± 5.6]	14.3–20.1	(6.4–19.8) [16 ± 6.5]	12.5–19.5
Noise-dB	(54–87) [71 ± 9.1]	66–76	(68–79) [74 ± 6]	70.8–77
Lighting-lux	(41–317) [176.4 ± 83]	132–222	–	–

CI = confidence interval; SD = standard deviation; T°C = temperature in degrees Celsius; RH% = relative humidity.

Table 6. Spearman's rank correlations between air microorganisms and indoor environmental stressors.

Microorganism	Chemical pollutant				Physical factors				
	PM	**HCHO**	**NH_3**	**VOCs**	**T°C**	**RH%**	**Dewpoint**	**Noise**	**Lighting**
Environmental bacteria	0.10	0.29	–0.53*	0.53*	–0.19	–0.34	–0.53*	–0.09	0.02
Mesophilic bacteria	–0.02	–0.38	0.17	–0.68	0.51	0.00	0.67*	0.07	0.05
Fungi	–0.21	–0.20	0.12	–0.19	0.29	0.05	0.42	0.08	0.40
Actinomycetes	–0.13	–0.30	0.07	–0.60*	0.57*	–0.06	0.66*	0.24	–0.06

*$p \leq 0.05$. PM = particulate matter; HCHO = formaldehyde; NH_3 = ammonia; VOCs = volatile organic compounds; T°C = temperature in degrees Celsius; RH% = relative humidity.

Insignificant correlations were detected between bacteria and temperature, RH, and dust level (Cho et al., 2019). Fungal concentrations were higher with high RH values (Rodriguez-Rajo et al., 2005; Erkara et al., 2008), although some researchers have reported the opposite (Sabariego et al., 2000). No correlations were detected between temperature and RH with the counts of airborne bacteria and fungi (Andriana et al., 2023). The RH negatively affects microbial viability due to the changes in the lipid bilayers of the cell membrane, which affect the cell surface protein configuration (Hurst et al., 2007).

Noise and light intensity did not affect the viability of airborne microorganisms. Light intensity and noise were positively correlated with mesophilic bacteria and fungi, and negatively with actinomycetes and environmental bacteria, respectively (Table 5). Human activity and its intensity probably raise the noise level and increase the load of resuspended microorganisms. Light has a lethal effect on microbial viability, as it produces air ions that accelerate the physical decay rate of microorganisms through attraction/agglomeration (Krueger et al., 1969; Krinsky, 1976). The positive ions cause the physical decay of microorganisms (through inactivation of the surface protein) and the negative ions exhibit physical and biological effects on DNA (Pepper & Greba, 2015). The agglomeration of bioparticles increases aerosol mass and enhances their deposition (Murdoch et al., 2013). Environmental factors synergistically affect the integrity/biological activity of microorganisms (Verreault et al., 2014). Therefore, understanding the effect of environmental factors on the survival of airborne microorganisms is critical to address their transmission and fate and design corrective actions.

Building-Related Complaints

Figure 5 shows the frequency of the health complaints related to IAQ among the workshop's occupants. The prevalence of symptoms varied among occupants, with fatigue (45.5%), allergies (38.6%), and headache (35.2%) being the most common ones. Stuffy nose and nausea (9.1% each) were the lowest prevailing symptoms among the occupants. Little attention has been paid to optimal IAQ for public and nonindustrial settings. Fatigue and headache were the most prevalent symptoms among the Egyptian office workers, who were influenced by physical and psychosocial work conditions (Abdel-Hamid et al., 2013). Air quality, temperature, noise, ventilation rate, and lighting condition were found to affect occupants' satisfaction (Felgueiras et al., 2023). Temperature ≥ 23°C led to thermal discomfort (Norbäck, 2009), and low RH% (≤ 50%) was related to upper respiratory symptoms (Wolkoff, 2008). The SBS symptoms were noted to intensify with temperature of 30°C relative to that at 22°C (Lan et al., 2011). Exposure to air pollutants (such as VOCs, HCHO, PM) has been related to SBS and irritation to the eyes and upper respiratory system (WHO, 2010; Kim et al., 2015; Chai et al., 2019). The occurrence of actinomycetes was associated with abnormal and hazardous situations such as moisture damage of the building (Rintala, 2011). Exposure to actinobacteria can cause infections, allergic reactions, and lung inflammation (Lacey & Crook ,1988; Schäffer et al., 2009). Occupants living in damp and moldy buildings report more symptoms of nausea, blocked nose, and fainting compared to those living in dry buildings (Platt et al., 1989).

Figure 6 displays the perception weights of satisfaction related to the four IAQ factors. The opinions of the occupants were ranked as noise (40.9%), lighting (25%), air quality (18.2%), and temperature (15.9%). There was a discrepancy between the perceptions of IAQ factors. The perception of comfort differs among people under the same IAQ. Perception is a combination of IAQ factors (WHO, 2001) and varies with respect to the threshold of IAQ factors and individual health conditions. Although temperature condition is the key factor affecting satisfaction globally, it had the least perception weight in this survey, attributable to the interaction of other factors (e.g., RH%, dew point, climatic condition, and wind speed) that enhance the comfort effect.

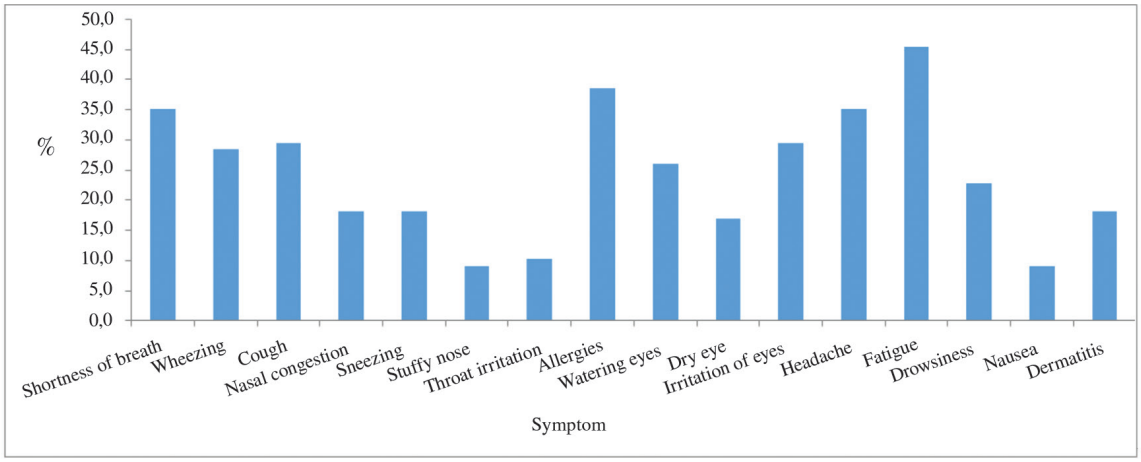

Figure 5. The prevalence of health complaints among the of workshop's occupants.

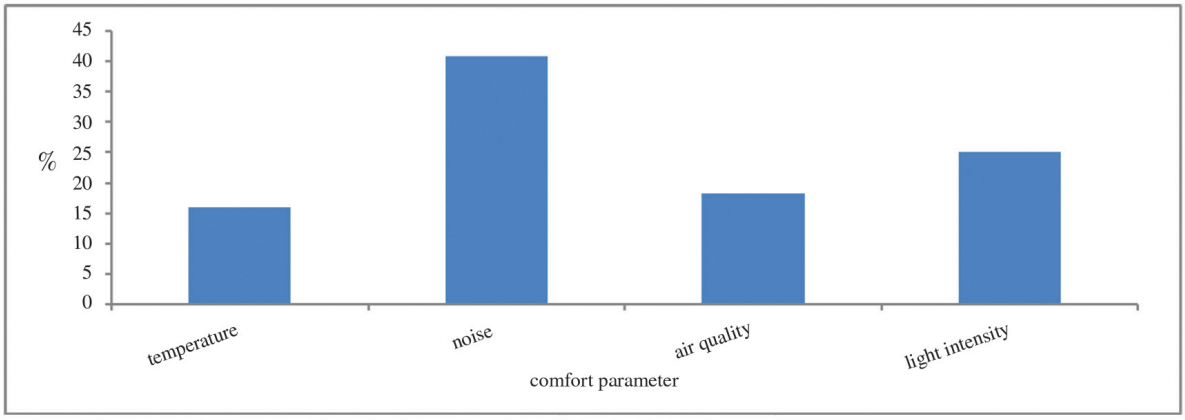

Figure 6. The prevalence of health complaints among the workshop's occupants.

Finally, there is a knowledge gap in relation to workshops associated with complex public buildings and academia. The main limitations of this comparative analysis are as follows: 1) the workshops carry out tasks similar to industry settings, but they cannot be considered as a real industrial sector, which raises confusion about the applicable guidance limits, 2) low numbers of sampling events and the wide variations among the workshop types, 3) no seasonal changes were considered (which play an important role in the perception of comfort), and 4) there was uncertainty of health complaints data due to confusion between workplace-related complaints and the existing health status of the occupants.

Conclusion

The evaluation of IAQ in workshop environments is inherently complex, influenced by microenvironmental conditions, microbial composition, and the behavior of airborne pollutants. Most IAQ parameters assessed in this study failed to comply with recommended threshold values. Airborne microbial concentrations were consistently higher indoors compared to outdoor (background). Notably, the upper bound of the 95% CI for the GIMC/m³ exceeded 7,000 CFU/m³ in approximately 46% of the workshops. The detection of actinomycete counts at or above 100 CFU/m³ further indicated abnormal, potentially hazardous conditions. PM varied significantly in terms of concentration, chemical composition, size, and morphology, largely depending on the nature of workshop activities. The presence and accumulation of deposited dust pose both health risks and potential material damage. Morphological characterization of PM using SEM imaging proved useful for understanding particle behavior and identifying pollution sources. VOCs exceeded the recommended limit of 3 mg/m³ in 30% of the workshops, whereas the noise levels surpassed the 60 dBA comfort threshold in most settings. Indoor temperatures (95% CI = 25.1°C–31.7°C) were above the optimal range of 20–24°C, although RH remained within acceptable limits (20–60%). Light intensity was found to be inadequate (≤ 300 lux) in nearly 80% of the workshops surveyed. Environmental parameters variably influenced microbial viability. VOC concentrations and dew point showed significant effects, whereas PM appeared to support the viability of environmental bacteria. These results suggest that poor IAQ may contribute to occupant health complaints, with noise being identified as the primary factor impacting occupant satisfaction. The findings underscore the urgent need for targeted IAQ management strategies, including moisture control, ventilation improvements, dust suppression, and optimized lighting conditions. Furthermore, this study highlights the necessity of establishing tailored IAQ guidelines for workshops associated with public buildings, where unique environmental and occupational conditions prevail.

Ethics

Ethics Committee Approval: Since the article does not contain any studies with human or animal subject, its approval to the ethics committee was not required.

Data Sharing Statement: All data are available within the study.

Footnotes

Authorship Contributions: Conceptualization: A.H.A.; Resources/materials: S.E.G., Y.S., and S.K.; Data acquisition: S.E.G., Y.S., and S.K.; Data analysis/interpretation: S.E.G., Y.S., and S.K.; Writing – original draft: A.H.A.; Writing – review & editing/critical revision: A.H.A.

Conflict of Interest: The author declares no competing interests.

Funding: This work was funded by the National Research Centre (NRC), Dokki, Giza, Egypt.

Editor-in-Chief's Note: Abdel Hameed Awad is a member of the editorial board of the Trakya University Journal of Natural Sciences. He was not involved in the editorial evaluation or decision-making process for this manuscript.

References

Abdel Hameed, A., Khoder, M., & Farag, S. (2000). Organic dust and gaseous contaminants at wood working shops. *Journal of Environmental Monitoring, 2*(1), 73–76. https://doi.org/10.1039/A907102D

Abdel Hameed, A., Saeed, Y., El-Gendy, S. A., & Hassan, S. K. (2023). Chemical, physical and microbial parameters inside a research building environment. *Egyptian Journal of Chemistry, 66*(13), 1489–1498. https://doi.org/10.21608/EJCHEM.2023.201245.7755

Abdel Hameed, A., Saeed, Y., Hassan, Y., Fawzy, Y., & Osman, M. (2018). Air microbial quality in certain public buildings, Egypt: A comparative study. *Atmospheric Pollution Research, 9*(4), 617–626. https://doi.org/10.1016/j.apr.2017.12.014

Abdel-Hamid, M. A., Hakim, A. S., Elokda, S., & Mostafa, S. N. (2013). Prevalence and risk factors of sick building syndrome among office workers. *Journal of the Egyptian Public Health Association, 88*(2), 109–114. https://doi.org/10.1097/01.EPX.0000431629.28378.c0

American Conference of Governmental Industrial Hygienists (ACGIH). (2012). *Threshold limit values for chemical substances and physical agents and biological exposure indices*. ACGIH.

Akova, İ., Kılıç, E., Sümer, H., & Keklikçi, T. (2022). Prevalence of sick building syndrome in hospital staff and its relationship with indoor environmental quality. *International Journal of Environmental Health Research, 32*(6), 1204–1219. https://doi.org/10.1080/09603123.2020.1862067

Alghamdi, A. M., Shamy, M., Redal, M. A., Khoder, M., Abdel Hameed, A., & Elserougy, S. (2014). Microorganisms associated particulate matter: A preliminary study. *Science of The Total Environment, 479–480*, 109–116. https://doi.org/10.1016/j.scitotenv.2014.02.006

Andersen, A. A. (1958). New sampler for the collection, sizing and enumeration of viable airborne particles. *Journal of Bacteriology, 76*(5), 471–484. https://doi.org/10.1128/jb.76.5.471-484.1958

Andriana, Y., Widodo, A. D. W., & Endraswari, P. D. (2023). A correlation between the number of airborne bacteria and fungi using the settle plate method with temperature and relative humidity at the clinical microbiology laboratory of Dr. Soetomo Regional General Hospital Surabaya, Indonesia. *Journal of Pure and Applied Microbiology, 17*(2), 942–950. https://doi.org/10.22207/JPAM.17.2.24

Apte, K., & Salvi, S. (2016). Household air pollution and its effects on health. *F1000Research, 5*, F1000 Faculty Rev-2593. https://doi.org/10.12688/f1000research.7552.1

Asadi, I., Mahyuddin, N., & Shafigh, P. (2017). A review on indoor environmental quality (IEQ) and energy consumption in building based on occupant behavior. *Facilities, 35*(11/12), 684–695. https://doi.org/10.1108/F-06-2016-0062

American Society of Heating, Refrigerating and Air-Conditioning Engineers (ASHRAE). (2010). *Standard 55-2010: Thermal environmental conditions for human occupancy*. ASHRAE.

ASTM International. (2015). *Standard test method for measuring humidity with a psychrometer (E337–15)*. ASTM International.

Azuma, K., Kagi, N., Yanagi, U., Kim, H., & Osawa, H. (2022). A longitudinal study on the effects of hygro-thermal conditions and indoor air pollutants on building-related symptoms in office buildings. *Indoor Air, 32*, e13164. https://doi.org/10.1111/ina.13164

Barnett, H. L., & Hunter, B. B. (1999). *Illustrated genera of imperfect fungi* (4th ed.). The American Phytopathological Society.

Bluyssen, P., de Oliveira Fernandes, E., Fanger, P. O., Groes, L., Clausen, G., Roulet, C. A., Bernhard, C. A., & Valbjørn, Ø. (2005). European audit project to optimise indoor air quality and energy consumption in office buildings. *TNO Report*. https://www.researchgate.net/publication/37460762

Breza–Boruta, B., & Paluszak, Z. (2007). Influence of water treatment plant on microbiological composition of air bioaerosols. *Polish Journal of Environmental Studies, 16*(5), 663–670.

Buljat, A., Čargonja, M., & Mekterović, D. (2024). Source apportionment of particulate matter in a metal workshop. *International Journal of Environmental Research and Public Health, 21*(6), 768. https://doi.org/10.3390/ijerph21060768

Camuffo, D. (2019). *Microclimate for cultural heritage: Measurement, risk assessment, conservation, restoration, and maintenance of indoor and outdoor monuments* (2nd ed.). Elsevier.

California Office of Environmental Health Hazard Assessment. (1999). *Ammonia, Appendix D.2: Chronic RELs and toxicity summaries*. https://oehha.ca.gov/media/downloads/crnr/appendixd2final.pdf

Commission of the European Communities. (1993). *Report No. 12: Biological particles in indoor environments*. Luxembourg.

Chai, G., He, H., Sha, Y., Zhai, G., & Zong, S. (2019). Effect of PM2.5 on daily outpatient visits for respiratory diseases in Lanzhou, China. *Science of The Total Environment, 649*, 1563–1572. https://doi.org/10.1016/j.scitotenv.2018.08.384

Chawla, H., Anand, P., Garg, K., Bhagat, N., Varmani, S. G., Bansal, T., McBain, A. J., & Marwah, R. G. (2023). A comprehensive review of microbial contamination in the indoor environment: Sources, sampling, health risks, and mitigation strategies. *Frontiers in Public Health, 11*. https://doi.org/10.3389/fpubh.2023.1285393

Cheng, Y.-H. (2017). Measuring indoor particulate matter concentrations and size distributions at different time periods to identify potential sources in an office building in Taipei City. *Building and Environment, 123*, 446–457. https://doi.org/10.1016/j.buildenv.2017.07.025

Cho, E. M., Hong, H. J., Park, S. H., Yoon, D. K., Goung, S. J. N., & Lee, C. M. (2019). Distribution and influencing factors of airborne bacteria in public facilities used by pollution-sensitive population: A meta-analysis. *International Journal of Environmental Research and Public Health, 16*, 1483. https://doi.org/10.3390/ijerph16091483

Cox, C. S. (1998). The microbiology of air. In L. Collier, A. Balows, & M. Sussman (Eds.), *Topley & Wilson's microbiology and microbial infections* (9th ed., pp. 339–350). Arnold, Oxford University Press.

Crawford, J. A., Rosenbaum, P. F., Anagnost, S. E., Hunt, A., & Abraham, J. L. (2015). Indicators of airborne fungal concentrations in urban homes: Understanding the conditions that affect indoor fungal exposures. *Science of The Total Environment, 517*, 113–124. https://doi.org/10.1016/j.scitotenv.2015.02.060

Dacarro, C., Grisoli, P., Del, F. G., Villani, S., Grignani, E., & Cotta, D. (2005). Microorganisms and dust exposure in an Italian grain-mill. *Journal of Applied Microbiology, 98*(1), 163–171. https://doi.org/10.1111/j.1365-2672.2004.02437.x

Dehghani, M. H., Bashardoust, P., Zirrahi, F., Ajami, B., Ghalhari, M. R., & others. (2024). Environmental and health effects due to volatile organic compounds. In M. H. Dehghani, R. R. Karri, T. Vera, & S. K. M. Hassan (Eds.), *Health effects of indoor air pollution* (pp. 191–221). Academic Press. https://doi.org/10.1016/B978-0-443-16090-5.00003-9

Dennis, P. J., & Lee, J. V. (1988). Differences in aerosol survival between pathogenic and non-pathogenic strains of *Legionella pneumophila* serogroup 1. *Journal of Applied Bacteriology, 65*, 135–141. https://doi.org/10.1111/j.1365-2672.1988.tb01501.x

DiBernardino, A., Iannarelli, A. M., Casadio, S., Perrino, C., Barnaba, F., Tofful, L., & others. (2021). Impact of synoptic meteorological conditions on air quality in three different case studies in Rome, Italy. *Atmospheric Pollution Research, 12*(4), 76–88. https://doi.org/10.1016/j.apr.2021.02.019

DiCarlo, E., Chisesi, R., Barresi, G., Barbaro, S., Lombardo, G., Rotolo, V., Sebastianelli, M., Travagliato, G., & Palla, F. (2016). Fungi and bacteria in indoor cultural heritage environments: Microbial-related risks for artworks and human health. *Environment and Ecology Research, 4*(5), 257–264. https://doi.org/10.13189/eer.2016.040504

Donaldson, A. I., & Ferris, N. P. (1975). Survival of foot-and-mouth disease virus in open air conditions. *The Journal of Hygiene, 74*(3), 409–416. https://doi.org/10.1017/s002217240004691x

Dong, T., Zhang, Y., Jia, S., Shang, H., Fang, W., Chen, D., & Fang, M. (2019). Human indoor exposome of chemicals in dust and risk prioritization using EPA's ToxCast database. *Environmental Science & Technology, 53*(12), 7045–7054. https://doi.org/10.1021/acs.est.9b00280

Dylag, M. (2017). Fungi present in home and their impact on human health-A short review. *Insights in Biology and Medicine, 1*(1), 016 -025. https://doi.org/10.29328/journal.hjbm.1001003

Egyptian Environmental Affairs Agency (EEAA). (1994). *Law No. 4/1994 Promulgating the Environment Law and its Executive Regulation*. Presidential Decree (4), 130. http://extwprlegs1.fao.org/docs/pdf/egy4984E.pdf

Ellis, M. B. (1971). *Dematiaceous hyphomycetes* (p. 608). The Western Press Ltd.

Erkara, I. P., Asan, A., Yilmaz, V., Pehlivan, S., & Okten, S. S. (2008). Airborne *Alternaria* and *Cladosporium* species and relationship with meteorological conditions in Eskisehir City, Turkey. *Environmental Monitoring and Assessment, 144*, 31–41. https://doi.org/10.1007/s10661-007-9939-0

Fang, L., Liu, N., Liu, W., Mo, J., Zhao, Z., Kan, H., Deng, F., Huang, C., Zhao, B., & others. (2022). Indoor formaldehyde levels in residences, schools, and offices in China in the past 30 years: A systematic review. *Indoor Air, 32*(10), e13141. https://doi.org/10.1111/ina.13141

Felgueiras, F., Mourão, Z., Moreira, A., & Fonseca-Gabriel, M. (2023). Indoor environmental quality in offices and risk of health and productivity complaints at work: A literature review. *Journal of Hazardous Materials Advances, 10*, 100314. https://doi.org/10.1016/j.hazadv.2023.100314

Frohlich-Nowoisky, J., Nespoli, C. R., Pickersgill, D. A., Galand, P. E., Muller-Germann, I., Nunes, T., Cardoso, J. G., Almeida, S. M., Pio, C., & others. (2014). Diversity and seasonal dynamics of airborne archaea. *Biogeosciences, 11*, 6067–6079. https://doi.org/10.5194/bg-11-6067-2014

GB/T 18883. (2002). *Indoor air quality standard*. National Standard of China. https://www.chinesestandard.net/PDF.aspx/GBT18883-2002

Gilbert, Y., & Duchaine, C. (2009). Bioaerosols in industrial environments: A review. *Canadian Journal of Civil Engineering, 36*(12), 1873–1886. https://doi.org/10.1139/L09-117

Grisoli, P., Albertoni, M., & Rodolfi, M. (2019). Application of airborne microorganism indexes in offices, gyms, and libraries. *Applied Sciences, 9*(6), 1101. https://doi.org/10.3390/app9061101

Hambleton, P., Broster, M., Dennis, P., Henstridge, R., Fitzgeorge, R., & Conlan, J. (1983). Survival of virulent *Legionella pneumophila* in aerosols. *Journal of Hygiene, 90*(3), 451–460. https://doi.org/10.1017/s0022172400029090

Hansen, D. L. (1999). *Indoor air quality issues*. Taylor and Francis.

Hatch, M. T., Wright, D. N., & Bailey, G. D. (1970). Response of airborne *Mycoplasma pneumoniae* to abrupt changes in relative humidity. *Applied Microbiology, 19*(2), 232–238. https://doi.org/10.1128/am.19.2.232-238.1970

Hoekstra, E. S., Samson, R. A., & Verhoeff, A. P. (1994). Fungal propagules in house dust: A qualitative analysis. In *Health implications of fungi in indoor environments* (pp. 169–177). Elsevier Science B.V.

Holmberg, K. (1987). Indoor mould exposure and health effects. In B. Seifen, H. Esdorn, M. Fischer, H. Ruden, & J. Wegner (Eds.), *Proceedings of Indoor Air '87* (Vol. 1, pp. 637–642). Institute of Water, Soil and Air Hygiene.

Holøs, S. B., Yang, A., Lind, M., Thunshelle, K., Schild, P., & Mysen, M. (2018). VOC emission rates in newly built and renovated buildings, and the influence of ventilation – A review and meta-analysis. *International Journal of Ventilation, 18*(3), 153–166. https://doi.org/10.1080/14733315.2018.1435026

Horner, W. E. (2006). Managing building-related *Aspergillus* exposure. *Medical Mycology, 44*(1), S33–S38. https://doi.org/10.1080/13693780600925194

Health and Safety Executive (HSE). (2018). *Workplace exposure limits: EH40/2005 (3rd ed.)*. HSE Books.

Hurst, C. I., Knudsen, G. T., McInerney, M. J., Stetzenbach, L. D., & Walter, M. V. (2007). *Manual of environmental microbiology* (pp. 661–663). ASM Press.

Insley, A. L., Maskrey, J. R., Hallett, L. A., Reid, R. C., Hynds, E. S., Winter, C., & Panko, J. M. (2019). Occupational survey of airborne metal exposures to welders, metalworkers, and bystanders in small fabrication shops. *Journal of Occupational and Environmental Hygiene, 16*(6), 410–421. https://doi.org/10.1080/15459624.2019.1603389

International Agency for Research on Cancer (IARC). (2006). *Formaldehyde, 2-butoxyethanol and 1-tert-butoxypropan-2-ol* (IARC monographs on the evaluation of carcinogenic risks to humans, Vol. 88).

International Society of Indoor Air Quality and Climate, Scientific and Technical Committee 34. (2025). *Indoor environmental quality guidelines database*. https://ieqguidelines.org/

Jabeen, R., Kizhisseri, M. I., Mayanaik, S. N., & Mohamed, M. M. (2023). Bioaerosol assessment in indoor and outdoor environments: A case study from India. *Scientific Reports, 13*, Article 18066. https://doi.org/10.1038/s41598-023-44315-z

Juda-Rezler, K., Reizer, M., Maciejewska, K., Błaszczak, B., & Klejnowski, K. (2020). Characterization of atmospheric PM2.5 sources at a Central European urban background site. *Science of The Total Environment, 713*, 136729. https://doi.org/10.1016/j.scitotenv.2020.136729

Kadaifciler, D. G. (2017). Bioaerosols assessment in the library of Istanbul University and fungal flora associated with paper deterioration. *Aerobiologia, 33*(1), 151–166. https://doi.org/10.1007/s10453-016-9457-z

Kang, S., Ou, D., & Mak, C. M. (2017). The impact of indoor environmental quality on work productivity in university open-plan research offices. *Building and Environment, 124*, 78–89. https://doi.org/10.1016/j.buildenv.2017.07.003

Karbowska-Berent, J., Górny, R. L., Strzelczyk, A. B., & Wlazło, A. (2011). Airborne and dust borne microorganisms in selected Polish libraries and archives. *Building and Environment, 46*(10), 1872–1879. https://doi.org/10.1016/j.buildenv.2011.03.007

Kim, K.-H., Kabir, E., & Kabir, S. (2015). A review on the human health impact of airborne particulate matter. *Environment International, 74*, 136–143. https://doi.org/10.1016/j.envint.2014.10.005

Krinsky, N. I. (1976). Cellular damage initiated by visible light. In *The survival of vegetative microbes: Symposium of the Society for General Microbiology* (Vol. 26, pp. 209–239). [Google Scholar]

Krueger, A. P., Kotaka, S., & Andriese, P. C. (1969). Atmospheric ions and aerosols. In R. I. Dimmick & A. B. Akers (Eds.), *An introduction to experimental aerobiology* (pp. 100–112). Wiley Interscience.

Kumar, P., & Imam, B. (2013). Footprints of air pollution and changing environment on the sustainability of built infrastructure. *Science of The Total Environment, 444*, 85–101. https://doi.org/10.1016/j.scitotenv.2012.11.056

Kumar, P., Kausar, A. M., Singh, A. B., & Singh, R. (2021). Biological contaminants in the indoor air environment and their impacts on human health. *Air Quality, Atmosphere & Health, 14*(11), 1723–1736. https://doi.org/10.1007/s11869-021-00978-z

Lacey, J., & Crook, B. (1988). Fungal and actinomycete spores as pollutants of the workplace and occupational allergens. *Annals of Occupational Hygiene, 32*, 515–533. https://doi.org/10.1093/annhyg/32.4.515

Lacey, J., & Dutkiewicz, J. (1994). Bioaerosols and occupational lung disease. *Journal of Aerosol Science, 25*(8), 1371–1404. https://doi.org/10.1016/0021-8502(94)90215-1

Lacey, J., Ramakrishna, N., Hamer, A., Magan, N., & Marfleet, I. (1991). Grain fungi. In D. K. Arora, K. G. Mukerji, & E. H. Marth (Eds.), *Handbook of Applied Mycology* (Vol. 3, pp. 121–177). Marcel Dekker.

Lai, A. C. K., & Nazaroff, W. W. (2000). Modeling indoor particle deposition from turbulent flow onto smooth surfaces. *Journal of Aerosol Science, 31*(4), 463–476. https://doi.org/10.1016/S0021-8502(99)00536-4

Lan, L., Wargocki, D. P., Wyon, D. P., & Lian, Z. (2011). Effects of thermal discomfort in an office on perceived air quality, SBS symptoms, physiological responses, and human performance. *Indoor Air, 21*(5), 376–390. https://doi.org/10.1111/j.1600-0668.2011.00714.x

Langer, S., & Bekö, G. (2013). Indoor air quality in the Swedish housing stock and its dependence on building characteristics. *Building and Environment, 69*, 44–54. https://doi.org/10.1016/j.buildenv.2013.07.013

Lefferts, M. J., & Castell, M. R. (2022). Ammonia breath analysis. *Sensors and Diagnostics, 1*, 955–967. https://doi.org/10.1039/D2SD00089J

Levetin, E., & Dorsey, K. (2006). Contribution of leaf surface fungi to the air spora. *Aerobiologia, 22*, 3–12. https://doi.org/10.1007/s10453-005-9012-9

Li, M., Weschler, C. J., Bekö, G., Wargocki, P., Lucic, G., & Williams, J. (2020). Human ammonia emission rates under various indoor environmental conditions. *Environmental Science & Technology, 54*(9), 5419–5428. https://doi.org/10.1021/acs.est.0c00094

Li, J., Xu, W., You, B., & Sun, Y. (2022). Dynamic variations of ammonia in various life spaces and seasons and the influences of human activities. *Building and Environment, 212*, 108820. https://doi.org/10.1016/j.buildenv.2022.108820

Lighthart, B., & Shaffer, B. T. (1997). Increased airborne bacterial survival as a function of particle content and size. *Aerosol Science and Technology, 27*, 439–446. https://doi.org/10.1080/02786829708965483

Lippai, A., Leelőssy, Á., & Magyar, D. (2024). Indoor and outdoor air microbial contamination during different reconstruction methods of historic buildings. *Pathogens, 13*(12), 1048. https://doi.org/10.3390/pathogens13121048

Liu, T., Lin, Y., Chen, J., Chen, G., Yang, C., Xu, L., Li, M., Fan, X., Zhang, F., & Hong, Y. (2023). Pollution mechanisms and photochemical effects of atmospheric HCHO in a coastal city of southeast China. *Science of The Total Environment, 859*(Part 1), 160210. https://doi.org/10.1016/j.scitotenv.2022.160210

Loukou, E., Jensen, N. F., Rohde, L., & Andersen, B. (2024). Damp buildings: Associated fungi and how to find them. *Journal of Fungi, 10*(2), 108. https://doi.org/10.3390/jof10020108

Macher, J. M., et al. (1995). Sampling airborne microorganisms and aeroallergens. In B. S. Cohen & S. V. Hering (Eds.), *Air sampling instruments for evaluation of atmospheric contaminants* (8th ed., pp. 589–617). ACGIH.

MacIntosh, D. L., Brightman, H. S., Baker, B. J., Myatt, T. A., Stewart, J. H., & McCarthy, J. F. (2006). Airborne fungal spores in a cross-sectional study of office buildings. *Journal of Occupational and Environmental Hygiene, 3*(7), 379–389. https://doi.org/10.1080/10543400600760438

Mackiewicz, B., Skórska, C., & Dutkiewicz, J. (2015). Relationship between concentrations of microbiological agents in the air of agricultural settings and occurrence of work-related symptoms in exposed persons. *Annals of Agricultural and Environmental Medicine, 22*(3), 473–477. https://doi.org/10.5604/12321966.1167717

Mangotra, A., & Singh, S. K. (2024). Volatile organic compounds: A threat to the environment and health hazards to living organisms – A review. *Journal of Biotechnology, 382*, 51–69. https://doi.org/10.1016/j.jbiotec.2023.12.013

Matthias-Maser, S. (1998). Primary biological aerosol particles: Their significance, sources, sampling methods, and size distribution in the atmosphere. In R. M. Harrison & R. E. Van Grieken (Eds.), *Environmental particles* (pp. 349–369). Wiley.

Melymuk, L., Demirtepe, H., & Rozárka Jílková, S. (2020). Indoor dust and associated chemical exposures. *Current Opinion in Environmental Science & Health, 15*, 1–6. https://doi.org/10.1016/j.coesh.2020.01.005

Mendell, M. J., Naco, G. M., Wilcox, T. G., & Sieber, W. K. (2003). Environmental risk factors and work-related lower respiratory symptoms in 80 office buildings: An exploratory analysis of NIOSH data. *American Journal of Industrial Medicine, 43*(6), 630–641. https://doi.org/10.1002/ajim.10211

Miller, J. D., Laflamme, A. M., Sobol, Y., Lafontaine, P., & Greenhalgh, R. (1988). Fungi and fungal products in some Canadian houses. *International Biodeterioration, 24*(2), 103–120. https://doi.org/10.1016/0265-3036(88)90053-X

Missia, D., Demetriou, E., Michael, N., Tolis, E. I., & Bartzis, J. G. (2010). Indoor exposure from building materials: A field study. *Atmospheric Environment, 44*(35), 4388–4395. https://doi.org/10.1016/j.atmosenv.2010.07.049

Morawska, L., & Salthammer, T. (2003). Fundamentals of indoor particles and settled dust. In L. Morawska & T. Salthammer (Eds.), *Indoor environment* (pp. 1–36). Wiley-VCH.

Mousavi, B., Hedayati, M. T., Hedayati, N., Ilkit, M., & Syedmousavi, S. (2016). *Aspergillus* species in indoor environments and their possible occupational and public health hazards. *Current Medical Mycology, 2*(1), 36–42. https://doi.org/10.18869/acadpub.cmm.2.1.36

Murdoch, L. E., McKenzie, K., Maclean, M., MacGregor, S. J., & Anderson, J. G. (2013). Lethal effects of high-intensity violet 405-nm light on *Saccharomyces cerevisiae*, *Candida albicans*, and on dormant and germinating spores of *Aspergillus niger*. *Fungal Biology, 117*(7), 519–527. https://doi.org/10.1016/j.funbio.2013.05.004

Nath, A., Baruah, N., Nonglait, M. L., et al. (2023). Biological contaminants in indoor environments of educational institutions. *Aerobiologia, 39*, 1–20. https://doi.org/10.1007/s10453-022-09771-6

Nazaroff, W. W., & Weschler, C. J. (2004). Cleaning products and air fresheners; Exposure to primary and secondary air pollutants. *Atmospheric Environment, 38*(18), 2841–2865. https://doi.org/10.1016/j.atmosenv.2004.02.040

Nevalainen, A., Pasanen, A.-L., Niininen, M., Reponen, T., Jantunen, M. J., & Kalliokoski, P. (1991). The indoor air quality in Finnish homes with mold problems. *Environment International, 17*, 299–302. https://doi.org/10.1016/0160-4120(91)90015-I

Nevalainen, A., Heinonen-Tanski, H., & Savolainen, R. (1990). Indoor and outdoor occurrence of *Pseudomonas* bacteria. In *Indoor Air '90: Proceedings of the Fifth International Conference on Indoor Air Quality and Climate* (Vol. 2, pp. 51–53). Canada Mortgage and Housing Corporation.

National Institute for Occupational Safety and Health. (1998). *NIOSH method 0800: NIOSH manual of analytical methods*.

Norbäck, D. (2009). An update on sick building syndrome. *Current Opinion in Allergy and Clinical Immunology, 9*(1), 55–59. https://doi.org/10.1097/ACI.0b013e32831f8f08

NP 061. (2002). *Normativ pentru proiectarea şi executarea sistemelor de iluminat artificial din clădiri*.

Nurmatov, U. B., Tagiyeva, N., Semple, S., Devereux, G., & Sheikh, A. (2015). Volatile organic compounds and risk of asthma and allergy: A systematic review. *European Respiratory Review, 24*(135), 92–101. https://doi.org/10.1183/09059180.00000714

Ohgke, H., Geers, A., & Beckert, J. (1987). Fungal load of indoor air in historical and newly constructed buildings used by public services. In *Proceedings of the 4th International Conference on Indoor Air Quality and Climate* (Vol. 1, pp. 681–684).

Occupational Safety and Health Administration (OSHA). (n.d.). *Reiteration of existing OSHA policy on indoor air quality: Office temperature/humidity and environmental tobacco smoke*. https://www.osha.gov (Accessed February 24, 2025)

Occupational Safety and Health Administration. (1992). *Technical manual*. U.S. Department of Labor.

Osman, M. E., Abdel Hameed, A. A., Ibrahim, H. Y., Yousef, F., Abo Elnasr, A. A., & Saeed, Y. (2017). Air microbial contamination and factors affecting its occurrence in certain book libraries in Egypt. *Egyptian Journal of Botany, 57*(1), 93–118. https://doi.org/10.21608/ejbo.2016.277.1007

Pacharra, M., Kleinbeck, S., Schäper, M., et al. (2016). Multidimensional assessment of self-reported chemical intolerance and its impact on chemosensory effects during ammonia exposure. *International Archives of Occupational and Environmental Health, 89*, 947–959. https://doi.org/10.1007/s00420-016-1134-6

Park, M., Joo, H. S., Lee, K., Jang, M., Kim, S. D., Kim, I., Borlaza, L. J. S., Lim, H., Shin, H., Chung, K. H., Choi, Y. H., Park, S. G., Bae, M. S., Lee, J., Song, H., & Park, K. (2018). Differential toxicities of fine particulate matters from various sources. *Scientific Reports, 8*(1), 17007. https://doi.org/10.1038/s41598-018-35398-0

Pepper, I. L., & Gerba, C. P. (2015). Aeromicrobiology. In *Environmental microbiology* (pp. 89–110). https://doi.org/10.1016/B978-0-12-394626-3.00005-3

Pitt, I. J., & Hocking, A. (2009). *Fungi and food spoilage*. Springer. https://doi.org/10.1007/978-0-387-92207-2

Platt, S. D., Martin, C. J., Hunt, S. M., & Lewis, C. W. (1989). Damp housing, mould growth and symptomatic health state. *British Medical Journal, 298*, 1673–1678. https://doi.org/10.1136/bmj.298.6689.1673

Polish Standards. (1989). *PN-89/Z-04111/03 Protection of air cleanness – Enumeration of microscopic fungi in atmospheric air* (in Polish).

Pyrri, I., Zoma, A., Barmparesos, N., Assimakopoulos, M. N., Assimakopoulos, V. D., & Kapsanaki-Gotsi, E. (2020). Impact of a green roof system on indoor fungal aerosol in a primary school in Greece. *Science of The Total Environment, 719*, 137447. https://doi.org/10.1016/j.scitotenv.2020.137447

Quintana, Á. R., Seseña, S., Garzón, A., & Arias, R. (2020). Factors affecting levels of airborne bacteria in dairy farms: A review. *Animals, 10*(3), 526. https://doi.org/10.3390/ani10030526

Quintanilla-Martinez, A., Aguirre-Gutron, L., Espinosa-Chaurand, L., Diaz-Ramirez, M., & Cortes-Sánchez, A. (2022). Microbiological analysis of the air in a popular fish processing and marketing area. *Applied Biosciences, 1*(3), 299–314. https://doi.org/10.3390/applbiosci1030019

Rai, S., Singh, D. K., & Kumar, A. (2021). Microbial, environmental and anthropogenic factors influencing the indoor microbiome of the built environment. *Journal of Basic Microbiology, 61*(4), 265–361. https://doi.org/10.1002/jobm.202000575

Raper, K. B., & Fennell, D. I. (1977). *The genus Aspergillus*. R. E. Krieger Publishing Company.

Reponen, T. A., Gazenko, S. V., Grinshpun, S. A., Willeke, K., & Cole, E. C. (1998). Characteristics of airborne actinomycete spores. *Applied and Environmental Microbiology, 64*(10), 3807–3812. https://doi.org/10.1128/AEM.64.10.3807-3812.1998

Reynolds, S. J., Streifel, A. J., & McJilton, C. E. (1990). Elevated airborne concentrations of fungi in residential and office environments. *American Industrial Hygiene Association Journal, 51*(11), 601–604. https://doi.org/10.1080/15298669091370185

Rintala, H. (2011). Actinobacteria in indoor environments: Exposures and respiratory health effects. *Frontiers in Bioscience-Scholar, 3*(1), 1273–1284. https://doi.org/10.2741/225

Rodriguez-Rajo, F. J., Iglesias, I., & Jato, V. (2005). Variation assessment of airborne *Alternaria* and *Cladosporium* spores at different bioclimatical conditions. *Mycological Research, 109*(Pt. 4), 497–507. https://doi.org/10.1017/S0953756204001777

Romano, S. (2023). Bioaerosols: Composition, meteorological impact and transport. *Atmosphere, 14*(3), 590. https://doi.org/10.3390/atmos14030590

Roshan, S. K., Godini, H., Nikmanesh, B., Bakhshi, H., & Charsizadeh, A. (2019). Study on the relationship between the concentration and type of fungal bioaerosols at indoor and outdoor air in the children's medical center, Tehran, Iran. *Environmental Monitoring and Assessment, 191*(2), 48. https://doi.org/10.1007/s10661-018-7183-4

Roumi, S., Zhang, F., Stewart, R. A., & Santamouris, M. (2022). Commercial building indoor environmental quality models: A critical review. *Energy and Buildings, 263*(3), 112033. https://doi.org/10.1016/j.enbuild.2022.112033

Sabariego, S., Díaz de la Guardia, C., & Alba, F. (2000). The effect of meteorological factors on the daily variation of air-borne fungal spores in Granada (southern Spain). *International Journal of Biometeorology, 44*, 1–5. https://doi.org/10.1007/s004840050131

Salthammer, T., Mentese, S., & Marutzky, R. (2010). Formaldehyde in the indoor environment. *Chemical Reviews, 110*(4), 2536–2572. https://doi.org/10.1021/cr800399g

Schäffer, J., Trautman, C., Dill, I., Fischer, G., et al. (2009). Actinomycetes in indoor environments. *Gefahrstoffe Reinhaltung der Luft, 69*(9), 335–341.

Shiferaw, T., Gebre-Silasse, L., Mulisa, G., Zewidu, A., Belachew, F., Muleta, D., & Zemene, E. (2016). Bacterial indoor-air load and its implications for healthcare-acquired infections in a teaching hospital in Ethiopia. *International Journal of Infection Control, 12*(1). https://doi.org/10.3396/ijic.v12i1.15808

Sillanpää, M., Saarikoski, S., Hillamo, R., Pennanen, A., Makkonen, U., Spolnik, Z., Van Grieken, R., Koskentalo, T., & Salonen, R. O. (2005). Chemical composition, mass size distribution and source analysis of long-range transported wildfire smokes in Helsinki. *Science of The Total Environment, 350*(1–3), 119–135. https://doi.org/10.1016/j.scitotenv.2005.01.024

Smets, W., Moretti, S., Denys, S., & Lebeer, S. (2016). Airborne bacteria in the atmosphere: Presence, purpose, and potential. *Atmospheric Environment, 139*, 214–221. https://doi.org/10.1016/j.atmosenv.2016.05.038

Soleimani, M., Shiran, F., Amir, S., & Jalali, H. (2022). Spatial and temporal variation of bacterial population in ambient air particulate matters (PM2.5, PM10 and TSP) of Isfahan city, Iran. *Journal of Air Pollution and Health, 7*(3), 261–274. https://doi.org/10.18502/japh.v7i3.10540

Spinazzè, A., Campagnolo, D., Cattaneo, A., Urso, P., Sakellaris, I. A., Saraga, D. E., Mandin, C., et al. (2020). Indoor gaseous air pollutants determinants in office buildings – The OFFICAIR project. *Indoor Air, 30*, 76–87. https://doi.org/10.1111/ina.12609

Sulaiman, M. A., Wan Yusoff, W. Z., & Wan Kamarudin, W. N. (2013). Evaluation of indoor environmental quality (IEQ) on dense academia Universiti Tun Hussein Onn Malaysia. *International Journal of Scientific and Research Publications, 3*(1), 1–5. https://www.ijsrp.org/research-paper-1301.php?rp=P13622

Sun, C., Cai, Y., Chen, J., Li, J., Su, C., Zou, Z., & Huang, C. (2024). Indoor ammonia concentrations in college dormitories and the health effects. *Journal of Building Engineering, 84*, 108556. https://doi.org/10.1016/j.jobe.2024.108556

Sun, C., Hong, S., Cai, G., Zhang, Y., Kan, H., Zhao, Z., Deng, F., Zhao, B., Zeng, X., Sun, Y., Qian, H., Liu, W., Mo, J., Guo, J., Zheng, X., Su, C., Zou, Z., Li, H., & Huang, C. (2021). Indoor exposure levels of ammonia in residences, schools, and offices in China from 1980 to 2019: A systematic review. *Indoor Air, 31*(6), 1691–1706. https://doi.org/10.1111/ina.12864

Tang, J. W. (2009). The effect of environmental parameters on the survival of airborne infectious agents. *Journal of the Royal Society Interface, 6*(6), S737–S746. https://doi.org/10.1098/rsif.2009.0227.focus

Tang, H., Ding, Y., & Singer, B. (2020). Interactions and comprehensive effect of indoor environmental quality factors on occupant satisfaction. *Building and Environment, 167*, 106462. https://doi.org/10.1016/j.buildenv.2019.106462

Tiwari, A., Pandey, M., Tirkey, A., Tiwari, A., Dubey, R., & Pandey, S. K. (2024). Image-based analytical approaches for study of particulate matter (PM) in air. *Frontiers in Environmental Science, 12*, 1362422. https://doi.org/10.3389/fenvs.2024.1362422

Thorne, P. S. (2019). Industrial livestock production facilities: Airborne emissions. In J. Nriagu (Ed.), *Encyclopedia of Environmental Health* (2nd ed., pp. 652–660). https://doi.org/10.1016/B978-0-12-409548-9.11862-7

Tran, V. V., Park, D., & Lee, Y. C. (2020). Indoor air pollution, related human diseases, and recent trends in the control and improvement of indoor air. *International Journal of Environmental Research and Public Health, 17*(8), 2927. https://doi.org/10.3390/ijerph17082927

Tuomi, T., & Vainiotalo, S. (2016). The guideline and target values for total volatile organic compound concentrations in industrial indoor environments in Finland. *Indoor and Built Environment, 25*(2), 424–434. https://doi.org/10.1177/1420326X14554270

Tyagi, S., & Srivastava, A. (2023). Characterization of size-segregated fungal bioaerosols in and around a sugar mill of Western Uttar Pradesh, India. *Research Square*. https://doi.org/10.21203/rs.3.rs-2407544/v1

U.S. Environmental Protection Agency (U.S. EPA). (2025a). *Indoor air quality (IAQ)*. https://www.epa.gov/indoor-air-quality-iaq (Accessed January 2025)

U.S. Environmental Protection Agency (U.S. EPA). (2025b). *Biological pollutants' impact on indoor air quality*. https://www.epa.gov/indoor-air-quality-iaq/biological-pollutants-impact-indoor-air-quality (Accessed January 2025)

Verreault, D., Duchaine, C., Marcoux-Voiselle, M., Turgeon, N., & Roy, C. J. (2014). Design of an environmentally controlled rotating chamber for bioaerosol aging studies. *Inhalation Toxicology, 26*(9), 554–558. https://doi.org/10.3109/08958378.2014.928763

Wilkie, A. D., Venz, L., & Letters, S. (2023). Outdoor airborne fungal spores in Queensland, Australia. *Journal of Bacteriology & Mycology: Open Access, 11*(1), 24–32. https://doi.org/10.15406/jbmoa.2023.11.00339

World Health Organization. (2000). *Air quality guidelines for Europe* (2nd ed.). WHO Regional Publications, European Series No. 91.

World Health Organization. (2001). *International classification of functioning, disability and health* (pp. 1–303). World Health Organization.

World Health Organization. (2010). *Guidelines for indoor air quality: Selected pollutants*. Geneva: WHO.

Wolkoff, P. (2008). "Healthy eye" in office-like environments. *Environment International, 34*(8), 1204–1214. https://doi.org/10.1016/j.envint.2008.04.005

Won, E., & Ross, H. (1969). Reaction of airborne *Rhizobium meliloti* to some environmental factors. *Applied Microbiology, 18*, 555–557. https://doi.org/10.1128/am.18.4.555-557.1969

Wu, Q., Li, N., Cai, X., He, Y., & Du, Y. (2023). Impact of indoor environmental quality (IEQ) factors on occupants' environmental perception and satisfaction in hospital wards. *Building and Environment, 245*, 110918. https://doi.org/10.1016/j.buildenv.2023.110918

Wyer, E. K., Kelleghan, B. D., Blanes-Vidal, V., Schauberger, G., & Curran, P. T. (2022). Ammonia emissions from agriculture and their contribution to fine particulate matter: A review of implications for human health. *Journal of Environmental Management, 323*, 116285. https://doi.org/10.1016/j.jenvman.2022.116285

Zhang, H., Sun, W., Li, W., & Wang, Y. (2022). Physical and chemical characterization of fugitive particulate matter emissions of the iron and steel industry. *Atmospheric Pollution Research, 13*(1), 101272. https://doi.org/10.1016/j.apr.2021.101272

Zhong, X., Qi, J. H., Li, H. T., Dong, L. J., & Gao, D. M. (2016). Seasonal distribution of microbial activity in bioaerosols in the outdoor environment of the Qingdao coastal region. *Atmospheric Environment, 140*(Suppl. 1), 506–513. https://doi.org/10.1016/j.atmosenv.2016.06.034

Zhu, Y., Guo, S., & Liang, W. (2024). A literature review investigating the impact of temperature and humidity on volatile organic compound emissions from building materials. *Building and Environment, 262*, 111845. https://doi.org/10.1016/j.buildenv.2024.111845

Trakya University Journal of Natural Sciences, 26(2), 174–181, 2025
DOI: 10.23902/trkjnat.554289774
www.tujns.org

Research Article

Assessment of the lead, cadmium, mercury, and arsenic adsorption capacities of EDTA-modified and umodified cellulose fibres from elephant grass *(Pennisetum purpureum)*

Innocent Izuchukwu Ujah*, Onuabuchi Nnenna Ani, Emmanuel Obiora Nneji

Enugu State University of Science and Technology, Faculty of Applied Natural Sciences, Department of Applied Biochemistry, Enugu State, Nigeria

Cite this article as: Ujah, I. I., Ani, O. N., & Nneji E. O. (2025). Assessment of the lead, cadmium, mercury, and arsenic adsorption capacities of EDTA-modified and umodified cellulose fibres from elephant grass *(Pennisetum purpureum). Trakya University Journal of Natural Sciences, 26*(2), 174–181. https://doi.org/10.23902/trkjnat.554289774

Abstract

Heavy metal pollution of water caused by various anthropogenic activities remains a significant global challenge, threatening the supply of clean water. Conventional water remediation approaches are costly with potential environmental risks. Thus, the development of cost-effective and biodegradable remediation methods is imperative. This study assessed the heavy metal adsorption capacities of native and EDTA-modified elephant grass (*Pennisetum purpureum*) cellulose. Elephant grass was collected from Enugu, Nigeria. The samples were washed and shade-dried. Cellulose was extracted via alkali treatment and bleaching, and then modified with EDTA to enhance its adsorptive properties. Batch adsorption experiments were designed to evaluate the capacities of unmodified and modified cellulose fibers to adsorb heavy metals from aqueous solutions under controlled conditions. The metal ion concentrations before and after adsorption were measured using flame atomic absorption spectrophotometry, and the adsorption capacities were calculated. The unmodified and modified cellulose exhibited the highest affinity for Hg(II) and Cd(II), respectively. Both types effectively removed ~70% of the Hg and Cd ions from solution. These results indicated that the unmodified cellulose was particularly effective for Hg removal, while the modified cellulose excelled in adsorbing Cd. They suggest the potential of these materials for the targeted remediation of specific contaminants and also identify them as cost-effective and biodegradable solutions for remediating heavy metal pollution.

Özet

Çeşitli antropojenik faaliyetler sonucu ağır metallerin neden olduğu su kirliliği, temiz su kaynaklarını tehdit eden önemli bir küresel sorun olmaya devam etmektedir. Geleneksel su arıtma yöntemleri maliyetli olup, potansiyel çevresel dezavantajları da bulunmaktadır. Bu nedenle, uygun maliyetli ve biyolojik olarak parçalanabilir arıtma tekniklerinin geliştirilmesi zorunludur. Bu çalışmada, sudan ağır metallerin uzaklaştırılması için fil otundan (*Pennisetum purpureum*) elde edilen modifiye edilmemiş ve EDTA ile modifiye edilmiş selülozun adsorpsiyon kapasiteleri değerlendirilmiştir. Fil otu Enugu, Nijerya'dan toplanmıştır. Örnekler yıkanmış ve gölgede kurutulmuştur. Alkali işlem ve ağartma yoluyla selüloz ekstraksiyonu yapılan selüloz, adsorpsiyon özelliklerini geliştirmek için EDTA ile modifiye edilmiştir. Modifiye edilmemiş ve EDTA ile modifiye edilmiş selüloz liflerinin sulu çözeltilerden ağır metalleri adsorbe etme kapasitelerini değerlendirmek için kontrollü koşullar altında toplu adsorpsiyon deneyleri gerçekleştirilmiştir. Adsorpsiyon öncesi ve sonrası metal iyon konsantrasyonları alev atom absorpsiyon spektrofotometresi kullanılarak ölçülmüş ve adsorpsiyon kapasiteleri buna göre hesaplanmıştır. Modifiye edilmemiş ve edilmiş selüloz en yüksek afiniteyi sırasıyla Hg(II) ve Cd(II) için göstermiştir. Her iki selüloz tipi çözeltilerden yaklaşık %70 oranında Hg ve Cd iyonlarını etkili bir şekilde uzaklaştırmıştır. Bulgular, modifiye edilmemiş selülozun Hg gideriminde özellikle etkili olduğunu, modifiye selülozun ise Cd adsorpsiyonunda üstün olduğunu göstermiştir. Bu sonuçlar, her iki tip selülozun belirli kirleticilere karşı hedefli arıtma potansiyeline sahip olduğunu düşündürmektedir. Sonuçlar bu maddelerin ağır metal arıtımı için uygun maliyetli ve biyolojik olarak parçalanabilir çözümler olarak ele alınabileceklerine işaret etmektedir.

Keywords: cellulose, heavy metals, biodegradable, remediation, adsorption

Edited by: *Bülent Yorulmaz*

***Corresponding Author:** Innocent Izuchukwu Ujah, **E-mail:** innocent.ujah@esut.edu.ng*

***ORCID iDs of the authors:** IIU. 0000-0003-4461-4031, ONA. 0000-0001-6533-0869, EON. 0009-0004-4334-8493*

Received: 28 March 2025, **Accepted:** 11 August 2025, **Online First**: 16 September 2025, **Published:** 15 October 2025

Introduction

Groundwater, a crucial natural resource supporting human health and socio-economic development, as well as ecosystems, has recently faced escalating contamination issues. The global reliance on groundwater for drinking needs has grown significantly, with ~2.5 billion people depending solely on this resource (Grönwall et al., 2020). Water, as an indispensable element for sustaining life on Earth, plays a pivotal role in socio-economic growth and sustainable development (Okudo et al., 2023). The impacts of water resource mismanagement are further compounded by a range of human activities, posing a severe threat to water quality worldwide (Ighalo & Adeniyi, 2020; Akhtar et al., 2021).

The contamination of water resources by heavy metals, originating from natural sources and human activities, has emerged as a global concern of prominence (Egbueri et al., 2020). Heavy metal pollution of water is a significant environmental issue due to its potential ecological and human health-associated repercussions. Heavy metals, characterized by high atomic weights and densities, can cause toxicity even at low concentrations due to their environmental persistence and cumulative nature (Kumar et al., 2021). These metals, including lead (Pb), mercury (Hg), cadmium (Cd), chromium (Cr), arsenic (As), and nickel (Ni), common in industrial effluents, can disrupt aquatic ecosystems and bioaccumulate in the food chain, thereby threatening aquatic organisms and humans (Ali et al., 2020; Abd Elnabi et al., 2023; Pugazhendhi, 2024).

The water bodies are contaminated by heavy metals from diverse sources, including industrial discharge, agricultural runoff, and geological processes (Aziz et al., 2023). They exert detrimental effects on environmental stability and human well-being, potentially leading to physical, muscular, and neurological disorders (Saha et al., 2019; Ali et al., 2020). Consequently, an in-depth understanding of the quality and evolution of groundwater, as well as the associated drivers, is imperative for ensuring long-term water sustainability (Obasi et al., 2020).

The remediation of polluted water involves a process that aims to restore water quality by removing or neutralizing undesirable elements (Hashim et al., 2011). Various techniques and strategies with a focus on mitigating the adverse environmental and health issues stemming from water pollution have been employed (Asefon, 2025). These methods comprise a spectrum of approaches, encompassing physical, chemical, and biological treatments, as well as engineered technologies, all applied together to enhance the safety and quality of water (Trifirò & Zanirato, 2024). Heavy metals, a prominent type of wastewater-derived contaminants, can be effectively eliminated through established techniques such as adsorption, nanofiltration, reverse osmosis, solvent extraction, chemical precipitation, flotation, coagulation, flocculation, membrane filtration, and ion exchange (Gupta et al., 2015). These encompass renewable and non-renewable sources, are adaptable, and utilize a range of chemicals, synthetic and biomaterials, as well as their modified forms (Biswal & Balasubramanian, 2023). Conventional water remediation methods often pose high costs and potential environmental drawbacks (Elbasiouny et al., 2021). Chemical water treatment, though effective, may lead to hazardous leaching (Srivastava, 2021). Especially, biomaterials exhibit considerable potential applicability across various domains, including energy generation, material production, and waste treatment (Chowdhury et al., 2025). In particular, they hold promise for use in environmentally friendly wastewater treatment methods, like adsorption. Agricultural by-products and plant biomass, either modified or not, have demonstrated significant efficacy when harnessed for adsorption. Emerging biosorbents hold potential for metal recovery, cost-effectivity, and minimal secondary waste generation (Bilal et al., 2021). Various materials of crop origin, such as hemicelluloses, cellulose (modified or unmodified), pectin, lignin, and proteins, possess adsorption capabilities, particularly cellulose (Fomina et al., 2014). While certain operational challenges arise with these materials, their modification can overcome such limitations, increasing their adsorption capacity and mitigating issues such as color leaching (Aziz et al., 2024). Therefore, the demand for non-toxic, degradable, cost-efficient, and highly efficient biomaterials has grown, positioning cellulose as a superior alternative (Oyewo et al., 2020). Cellulose, a biodegradable and non-toxic polysaccharide prevalent in various natural resources and agricultural residues, demonstrates applicability in varied water treatment techniques, particularly in removing toxic metals and dyes (Rehman et al., 2020).

Elephant grass (*Pennisetum purpureum*) is a rapidly growing and high-biomass source of cellulose (Yuan et al., 2024). This study investigated the adsorption capacity of unmodified and EDTA-modified cellulose from elephant grass for different concentrations of lead (Pb), cadmium (Cd), arsenic (As), and mercury (Hg) under constant temperature and pH. The objectives were (i) to extract cellulose from elephant grass and chemically modify it with EDTA to improve its heavy metal adsorption capacity; (ii) to investigate and quantify the adsorption capacities of both unmodified and modified cellulose for Pb, Cd, As, and Hg, using batch experiments; (iii) to compare the metal adsorption efficiencies of the unmodified and modified cellulose samples and determine if EDTA modification yields statistically significant improvements in absorption capacity; (iv) evaluate the degree of heavy metal extraction achieved by both forms of cellulose; and (v) assess the overall effect of EDTA modification on their metal-binding performance.

Materials and Methods

Collection of Grass Samples

The elephant grass used was obtained from the Lomalinda Estate, Enugu, Nigeria, where it grows widely during the dry season. The samples were collected by cutting the stems near the base with scissors (Lailaty et al., 2024). Their identity was confirmed by Prof. C. S. Eze of the Department of Applied Biology, Enugu State University, Nigeria. The samples were washed repeatedly with water to remove the extraneous impurities. Subsequently,

they were shade-dried to reduce the moisture content, a step that is crucial for preserving cellulose fiber quality (Kaur et al., 2018).

Cellulose Extraction

The dried elephant grass samples were ground; 114 g of each was soaked in 5% NaOH and mechanically stirred for 2 h at 70℃. Then, the suspension was filtered, and the solid fraction was rinsed with water until a neutral pH was achieved. It was then dried at 100℃ for 12 h and bleached by manual stirring with 30% H_2O_2 for 1 h at 90℃. The solid obtained after bleaching was rinsed and dried for 12 h at 100℃ (de Morais Teixeira et al., 2011).

EDTA Modification

The cellulose fibres were divided into two portions, and one was EDTA-modified (Igwe et al., 2005). For this, 17 g of the fibres was refluxed in a mixture of 300 mL pyridine and 56.7 g EDTA for 3 h at 70℃. The mixture was cooled, diluted with 300 mL of deionized water, and filtered. The filtered and EDTA-modified fibres were washed copiously with deionized water and dried at 50℃ for 12 h. The dried and modified adsorbent was then analyzed. The other portion was left unmodified and also analyzed.

Batch Adsorption Experiments

Equilibrium sorption of selected metal ions onto the cellulose fibres was assessed using 100 mL of each metal ion solution with concentrations varying from 200–1000 mg/L. A constant metal ion–substrate contact period of 1 h, at 29℃, and a pH of 6.7 was applied. Then, 0.2 g samples of the cellulose fiber were added to 20 mL of each solution with a specific concentration of metal ions. The setup was arranged in a rotary shaker at a moderate speed to equilibrate the mixture. After the allotted time, the mixture was rapidly filtered. The metal ion concentration of the filtrate was determined with a flame atomic absorption spectrophotometer. The difference between the initial and final ion concentrations of the solutions was considered the quantity of metal ions adsorbed by the fibres, both unmodified and modified ones.

The heavy metal adsorption capacity of cellulose was determined using Equation 1.

$$\text{Adsorption Capacity } (q) = \frac{(C_0 - C_f) \times V}{m} \qquad \text{(Equation 1)}$$

Where: C_0 = Initial concentration of metal ions in solution before adsorption, C_f = Final concentration of metal ions in solution after adsorption, V = Volume of the metal ion solution, and m = Mass of the cellulose used. The adsorption capacity is typically expressed in mg/g or µg/g, indicating the amount of metal ions adsorbed per unit mass of cellulose.

$$\text{Fraction of amount adsorbed} = \frac{C_t}{C_0} \qquad \text{(Equation 2)}$$

Where, C_t is the amount of metal ions adsorbed at any time "t;" $C_t = C_0 - C_f$.

The degree of extraction "α" was determined as follows (Nikiforova et al., 2023).

$$\alpha = \frac{C_0 - C_f}{C_0} \times 100\% \qquad \text{(Equation 3)}$$

Statistical Analysis

The statistical significance of the findings was comprehensively assessed using Excel 2016 (Microsoft, WA, USA) and Matplotlib 3.7.0 (https://matplotlib.org/3.7.0/) on Jupyter Notebook 6.5.4 (https://jupyter-notebook.readthedocs.io/en/v6.5.4/). Mean and standard deviations were computed as descriptive statistics for all the measured parameters.

Method Validation

A standard was spiked, run as a sample, and the resulting concentration was determined. The % recovery was then calculated, with values > 90% confirming equipment accuracy, thereby validating the results obtained (Table 1).

$$\%\ \text{recovery} = \text{spiked} - \text{unspiked} \times 10 \qquad \text{(Equation 4)}$$

Results

Heavy Metal Adsorption Capacity of the Unmodified and Modified Cellulose

The average adsorption capacity of the unmodified cellulose was highest with Hg, followed by Pb, Cd, and As; that of the modified cellulose was highest with Cd, followed by Hg, Pb, and As (Table 2).

Table 1. % recovery calculated using calibration.

Samples	As (ppm)		Hg (ppm)		Lead (ppm)		Cd (ppm)	
	1st	2nd	1st	2nd	1st	2nd	1st	2nd
Spike sample (ppm)	9.09	9.08	9.07	9.07	9.28	9.47	10.67	10.72
Unspike sample (ppm)	0.24	0.29	0.22	0.25	0.298	0.280	0.987	0.955
Original conc spiked (ppm)	10.00	10.00	10.00	10.00	10.00	10.00	10.00	10.00
% recovery	88.5	87.9	88.5	88.2	89.82	91.9	96.83	97.65

Amount injected (standard). All the tested metal ions fell within acceptable recovery limits, indicating that flame atomic absorption spectrophotometer could accurately quantify the heavy metals analyzed.

Table 2. Heavy metal adsorption capacities of the unmodified and modified cellulose.

Metal	Mean adsorption capacity (mg/g) ± standard deviation		
	Unmodified cellulose	Modified cellulose	*p*-value
Pb	42.40 ± 1.31	39.93 ± 16.46	0.754
Cd	35.50 ± 28.03	46.27 ± 19.16	0.436
As	19.77 ± 13.98	18.37 ± 7.73	0.828
Hg	53.63 ± 5.92	44.67 ± 11.14	0.165

No statistically significant differences were observed in the heavy metal adsorption capacities of the modified and unmodified cellulose. However, modification may still benefit other properties, such as improving physical stability or increasing the adsorption capacity for non-heavy metals. Though the mean adsorption capacity for Pb slightly decreased with modification, the large standard deviation in the capacities between the modified and unmodified samples suggests high variability in Pb uptake between the two. EDTA modification resulted in a higher average adsorption capacity for Cd, but a reduction in variability. However, very little difference was observed between the unmodiafied and modified cellulose in terms of As adsorption capacity. The unmodified cellulose performed better than EDTA-modified cellulose with Hg(II), having a greater mean adsorption and lower variability.

Fractions of Heavy Metals Adsorbed by the Unmodified and Modified Cellulose

The unmodified cellulose had the highest fraction of adsorbed Hg at 1000 mg/L, while the modified one had the maximal fraction of adsorbed Cd at 2000 mg/L.

There was no statistically significant difference in metal adsorption ability between the modified and unmodified cellulose for most of the heavy metals and concentrations tested. However, the *p*-value for 1500 mg/L Cd was marginally significant at 0.051, suggesting that modification might influence Cd adsorption at this concentration. EDTA modification did not consistently improve Pb adsorption, unlike Cd, especially at 1500 mg/L. The adsorption of As varied inconsistently with modification. Unmodified cellulose demonstrated better Hg adsorption, especially at lower concentrations.

Fraction of Pb Adsorbed by the Unmodified and Modified Cellulose

Figure 1 suggests that the highest fraction of Pb adsorbed was by the modified cellulose, but not the unmodified one.

Fraction of Cd Adsorbed by the Unmodified and Modified Cellulose

Figure 2 indicates that the greatest fraction of Cd adsorbed was by the modified cellulose rather than the unmodified one.

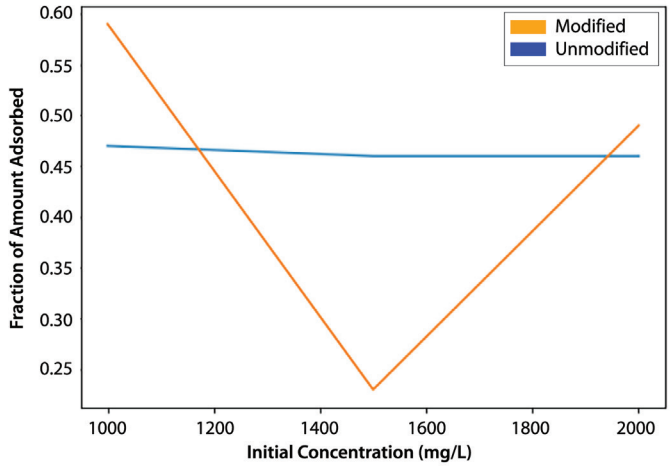

Figure 1. Fraction of Pb adsorbed by the unmodified and modified cellulose.

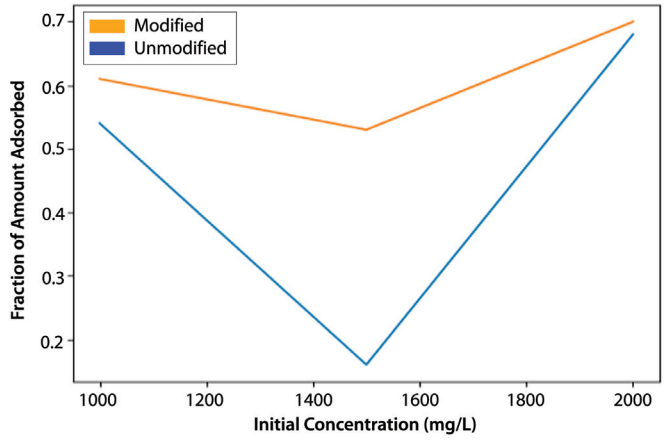

Figure 2. Fraction of the amounts of Cd adsorbed by the unmodified and modified cellulose.

Fraction of As Adsorbed by the Unmodified and Modified Cellulose

Figure 3 suggests that the highest fraction of As adsorbed was by the modified cellulose, but not by the unmodified one.

Fraction of Hg Adsorbed by the Unmodified and Modified Cellulose

Figure 4 shows that the highest fraction of Hg adsorbed was by the unmodified cellulose rather than the modified one.

Degree of Heavy Metal Extraction by the Unmodified and Modified Cellulose

The highest percentage of heavy metals extracted by the unmodified cellulose was with Hg, while that by the modified cellulose was with Cd (Table 4).

Statistically significant variations in heavy metal adsorption capabilities of the modified and unmodified cellulose were observed

for Pb at 1500 mg/L, Cd at 1500 mg/L, and As at 2000 mg/L. These results suggest that cellulose modification may have a metal-type and concentration-dependent effect on the adsorptive ability. At 1500 mg/L, Pb adsorption dropped from 46% (unmodified) to 23 % (modified), with a marked *p*-value of 0.046. However, at 1000 and 2000 mg/L, the differences were statistically insignificant, indicating no consistent enhancement with modification. At 1500 mg/L, Cd adsorption improved remarkably from 16% to 53% ($p = 0.027$), but not at 1000 and 2000 mg/L, which may be due to a saturation or equilibrium effect at higher doses. At 2000 mg/L, As adsorption declined significantly from 57% (unmodified) to 3% (modified) ($p = 0.043$), but increased insignificantly from 9% to 27% at 1500 mg/L. However, a general trend toward improved adsorption was observed, suggesting concentration sensitivity. E.g., unmodified cellulose demonstrated higher Hg adsorption consistently across all concentrations.

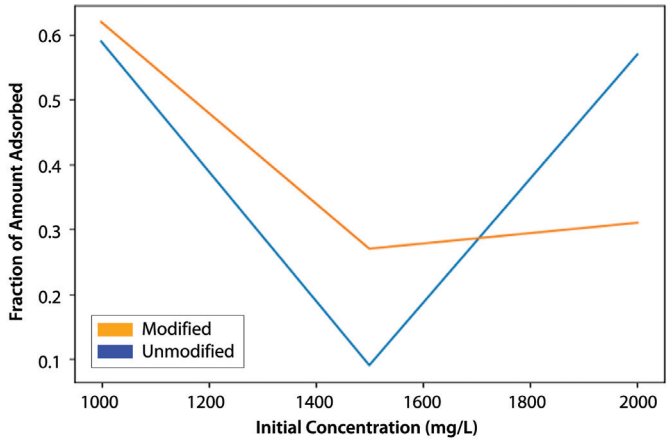

Figure 3. Fraction of As adsorbed by the unmodified and modified cellulose.

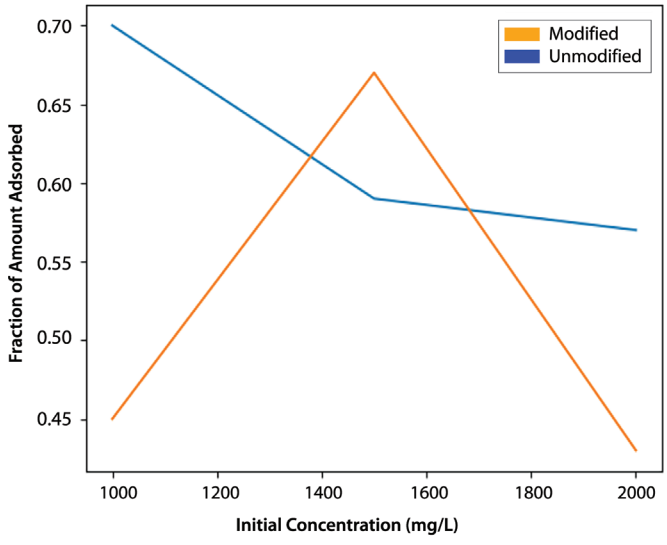

Figure 4. Fraction of Hg adsorbed by the unmodified and modified cellulose.

Table 3. Fractions of heavy metals adsorbed by the unmodified and modified cellulose.

Metal	Fraction of adsorbed amount		*p*-value
	Unmodified	Modified	
Pb			
1000 mg/L	0.466	0.589	0.345
1500 mg/L	0.456	0.229	0.151
2000 mg/L	0.463	0.491	0.836
Cd			
1000 mg/L	0.544	0.609	0.636
1500 mg/L	0.159	0.528	0.051
2000 mg/L	0.680	0.697	0.851
As			
1000 mg/L	0.585	0.615	0.834
1500 mg/L	0.085	0.269	0.272
2000 mg/L	0.574	0.308	0.144
Hg			
1000 mg/L	0.702	0.453	0.234
1500 mg/L	0.593	0.667	0.624
2000 mg/L	0.572	0.434	0.432

Table 4. Degree of heavy metal extraction by unmodified and modified cellulose.

Metal	Degree of extraction (%)		*p*-value
	Unmodified	Modified	
Pb			
1000 mg/L	47	59	0.345
1500 mg/L	46	23	0.046
2000 mg/L	46	49	0.836
Cd			
1000 mg/L	54	61	0.636
1500 mg/L	16	53	0.027
2000 mg/L	68	70	0.851
As			
1000 mg/L	59	62	0.834
1500 mg/L	9	27	0.161
2000 mg/L	57	31	0.043
Hg			
1000 mg/L	70	45	0.057
1500 mg/L	59	67	0.524
2000 mg/L	57	43	0.176

Discussion

The mean adsorption capacities indicated that modified cellulose adsorbed Cd the highest, but As the least, across all concentrations. In contrast, unmodified cellulose had the maximum adsorption

capacity for Hg, while the least for As at all concentrations (Table 2). EDTA modification of the cellulose fibers modestly enhanced the Cd adsorption capacity, supporting the role of the chelating groups of cellulose in improving Cd(II) uptake (Fujita et al., 2025). The adsorption of Pb and As was not markedly affected by the modification, suggesting that these metals may interact equally well with both native and functionalized cellulose (Motloung et al., 2023). Conversely, Hg adsorption capacity was greater in the unmodified cellulose, indicating that EDTA modification may introduce functional groups that are less favorable to Hg(II) binding (Riccardi et al., 2013). The adsorption mechanisms of cellulosic materials could explain these patterns. Intrinsic adsorption and columbic interaction are the two primary concepts that may be used to describe the adsorption of metal ions on cellulosic materials (Darmenbayeva et al., 2024). The electrostatic energy of the bonds between the adsorbents and adsorbates produces Coulombic interactions. The interaction intensity mostly depends on the charge of each substrate. The surface areas of the materials dictate intrinsic adsorption. Additionally, surface and microporous adsorptions can be simultaneous (Shi et al., 2022).

The variations in Pb, Cd, As, and Hg ion adsorption are represented as fractions of the adsorbed amount (C_t) vs. the initial concentration (C_o). C_t represents the quantity of metal ions adsorbed at any given time "t." Modified cellulose demonstrated the highest adsorption capacity for Pb, Cd, and As ions, indicating that EDTA modification improved adsorption. The adsorption fractions demonstrate an enhancement in Cd uptake by the EDTA-modified cellulose, particularly at 1500 mg/L Cd, indicating effective chelation (Table 3). Pb and As absorption showed inconsistent responses, with EDTA-functionalization reducing the adsorption efficiency of cellulose with certain concentrations of ions. Hg exhibited a stronger affinity for the unmodified cellulose, suggesting that EDTA ligands may not offer favorable coordination sites for the Hg(II) ions. These findings underscore the importance of matching adsorbent functional groups to the specific chemistry of each metal ion. An enhancement in the adsorption capacity of cellulose post-modification was reported by Kaur et al. (2022), who comprehensively reviewed modified cellulose adsorbents—including EDTA functionalized ones, and their adsorption capacities for Pb, Cd, and Cu. They noted that chemical modifications, like adding EDTA groups, significantly enhanced the adsorption capacity and binding affinity of the unmodified cellulose.

The adsorption abilities revealed a clear metal- and concentration-dependent behavior of cellulose modification (Table 4). EDTA-functionalization significantly improved the removal of Cd at 1500 mg/L, most likely due to robust chelation, while reducing the adsorption of Pb and As at specific concentrations, possibly due to steric effects or changes in surface chemistry. Hg showed a higher affinity for unmodified cellulose, which may be due to the metal-binding limitations of EDTA. These findings signify that certain modifications of adsorbents are suitable for specific contaminants and their expected concentrations. A comparison of Figures 1–4 suggested that modified cellulose had the maximum adsorption capacity for Cd ions, followed by Hg, As, and Pb. In general, this result indicates that Cd(II) > Hg(II) > As(III) > Pb(II) is the pattern of adsorption onto the modified cellulose. A comparison of the adsorption capabilities of unmodified cellulose for various concentrations of heavy metals indicated a maximum adsorption for Hg(II) at 1000 mg/L. Furthermore, Figures 1–4 demonstrate that unmodified cellulose had the maximum adsorption capacity for Hg ions, followed by those of Cd, As, and Pb. Thus, the general trend of adsorption onto unmodified cellulose is Hg(II) > Cd(II) > As(III) > Pb(II). Gupta et al. (2021) reported a similar trend in their review. In contrast, Kenawy et al. (2018) demonstrated a different trend: Cu(II) > Zn(II) > Cd (II) > Pb > Hg, which was consistent with both the modified and unmodified maize husks.

These findings demonstrate that the type of metal ion, the concentration of the metal ion in solution, and the type of adsorbent modification affect the amounts of metal ions bound by cellulose (Chen et al., 2019). The nature and distribution of the substrate active groups, the type of metal ion–substrate interaction, and size differences in the metal ions can explain the variations in their uptake levels (Wang et al., 2023). The ionic radii were As^{3+}: 0.46 Å, Cd^{2+}: 0.97 Å, Hg^{2+}: 1.02 Å, and Pb^{2+}: 1.20 Å. The adsorption rate is inversely proportional to the ionic diameter (Sasan et al., 2023). Similarly, in this study, the ion with the largest radius, Pb(II), had the lowest adsorption. However, the next in size, As(III), went against the trend. This inconsistency can be explained by the surface adsorption of component groups on substrates being more vital for adsorption capacity than microporous adsorption in such cases, which is especially true for Cd(II) and Hg(II) than As(III) ions (Abdelhamid & Mathew, 2021; Aguayo-Villarreal et al., 2024). As a result, compared to As(III), the adsorption of Cd(II) and Hg(II) ions was greater. Statistical analyses unraveled key trends in the adsorption behavior of the unmodified and EDTA-modified cellulose fibers toward heavy metals. While there were no statistically significant differences in the adsorption capacities for Pb, Cd, As, and Hg between the two cellulose types, EDTA modification enhanced Cd adsorption, particularly at its high concentrations. These results suggest that EDTA modification enhances Cd extraction, especially at 1500 mg/L, but may hinder that of Pb and As at certain concentrations. Hg was consistently adsorbed more by unmodified cellulose, indicating unfavorable interactions with the donor O_2 atoms of EDTA.

Conclusion

This study investigated the adsorption capacities of unmodified and EDTA-modified cellulose fibres derived from elephant grass for four toxic heavy metals—Pb, Cd, Hg, and As—from aqueous solutions. The results indicated that both cellulose types possessed considerable potential as biosorbents. However, their affinities varied based on the metal ion involved and the type of chemical modification. The unmodified cellulose demonstrated the highest adsorption capacity for Hg, particularly at its lower concentrations, suggesting a strong inherent affinity for Hg(II) ions. In contrast, EDTA-modified cellulose exhibited significantly improved adsorption for Cd, indicating that EDTA functionalization

increased metal binding, especially for Cd(II). These findings support the hypothesis that EDTA grafting introduces functional groups that facilitate chelation and complexation with specific metal ions. Although the differences in adsorption capacities were not always statistically significant at $p < 0.05$, modification did enhance the average adsorption and extraction percentages for certain metals—especially Cd at higher concentrations. The adsorption trends observed were Hg(II) > Cd(II) > As(III) > Pb(II) and Cd(II) > Hg(II) > As(III) > Pb(II) for the unmodified and modified cellulose, respectively. The results also suggest that surface adsorption by functional groups may play a more major role than microporous adsorption, particularly for Cd(II) and Hg(II) ions.

In conclusion, both unmodified and modified elephant grass cellulose fibres present biodegradable, cost-effective, and environmentally friendly options for the remediation of heavy metal-contaminated water. In particular, EDTA-modified and unmodified cellulose show promise for the targeted removal of Cd and Hg, respectively.

Ethics

Ethics Committee Approval: Since the article does not contain any studies with human or animal subject, its approval to the ethics committee was not required.

Data Sharing Statement: All data are available within the study.

Footnotes

Author Contributions: Conceptualization: I.I.U., O.N.A., and E.O.N.; Design/methodology: I.I.U., O.N.A., and E.O.N.; Execution/investigation: I.I.U., O.N.A., and E.O.N.; Resources/materials: I.I.U., O.N.A., and E.O.N.; Data acquisition: I.I.U., O.N.A., and E.O.N.; Data analysis/interpretation: I.I.U., O.N.A., and E.O.N.; Writing – original draft: I.I.U., O.N.A., and E.O.N.; Writing – review & editing/critical revision: I.I.U., O.N.A., and E.O.N.

Conflict of Interest: The authors have no conflicts of interest to declare.

Funding: The authors declared that this study has received no financial support.

References

Abd Elnabi, M. K., Elkaliny, N. E., Elyazied, M. M., Azab, S. H., Elkhalifa, S. A., Elmasry, S., Mouhamed, M. S., Shalamesh, E. M., Alhorieny, N. A., Abd Elaty, A. E., Elgendy, I. M., Etman, A. E., Saad, K. E., Tsigkou, K., Ali, S. S., Kornaros, M., & Mahmoud, Y. A.-G. (2023). Toxicity of heavy metals and recent advances in their removal: A review. *Toxics, 11*(7), 580. https://doi.org/10.3390/toxics11070580

Abdelhamid, H. N., & Mathew, A. P. (2021). Cellulose-based materials for water remediation: Adsorption, catalysis, and antifouling. *Frontiers in Chemical Engineering, 3*, 790314. https://doi.org/10.3389/fceng.2021.790314

Akhtar, N., Syakir Ishak, M. I., Bhawani, S. A., & Umar, K. (2021). Various natural and anthropogenic factors responsible for water quality degradation: A review. *Water, 13*(19), 2660. https://doi.org/10.3390/w13192660

Ali, M. M., Ali, M. L., Proshad, R., Islam, S., Rahman, Z., Tusher, T. R., Kormoker, T., & Al, M. A. (2020). Heavy metal concentrations in commercially valuable fishes with health hazard inference from Karnaphuli River, Bangladesh. *Human and Ecological Risk Assessment, 26*(10), 2646–2662. https://doi.org/10.1080/10807039.2019.1676635

Asefon, T. (2025). Mitigating water pollution through synergistic chemical and ecological approaches. *SSRN Electronic Journal*. https://ssrn.com/abstract=5175491

Aziz, K. H. H., Mustafa, F. S., Omer, K. M., Hama, S., Hamarawf, R. F., & Rahman, K. O. (2023). Heavy metal pollution in the aquatic environment: Efficient and low-cost removal approaches to eliminate their toxicity: A review. *RSC Advances, 13*(26), 17595–17610. https://doi.org/10.1039/D3RA00723E

Bilal, M., Ihsanullah, I., Younas, M., & Shah, M. U. H. (2021). Recent advances in applications of low-cost adsorbents for the removal of heavy metals from water: A critical review. *Separation and Purification Technology, 278*, 119510. https://doi.org/10.1016/j.seppur.2021.119510

Biswal, B. K., & Balasubramanian, R. (2023). Use of biochar as a low-cost adsorbent for removal of heavy metals from water and wastewater: A review. *Journal of Environmental Chemical Engineering, 11*(5), 110986. https://doi.org/10.1016/j.jece.2023.110986

Chen, Q., Zheng, J., Wen, L., Yang, C., & Zhang, L. (2019). A multi-functional-group modified cellulose for enhanced heavy metal cadmium adsorption: Performance and quantum chemical mechanism. *Chemosphere, 224*, 509–518. https://doi.org/10.1016/j.chemosphere.2019.02.138

Chowdhury, M. S., Oliullah, M. S., Islam, R. T., Hurayra, M. A., Al Mahmud, M. Z., & Nazm. (2025). Biomaterials for energy storage: Synthesis, properties, and performance. *Green Technology and Sustainability, 3*, 100152. https://doi.org/10.1016/j.grets.2024.100152

Darmenbayeva, A., Rajasekharan, R., Massalimova, B., Bektenov, N., Taubayeva, R., Bazarbaeva, K., & Ungarbayeva, A. (2024). Cellulose-based sorbents: A comprehensive review of current advances in water remediation and future prospects. *Molecules, 29*(24), 5969. https://doi.org/10.3390/molecules29245969

de Morais Teixeira, E., Bondancia, T. J., Teodoro, K. B. R., Corrêa, A. C., Marconcini, J. M., & Mattoso, L. H. C. (2011). Sugarcane bagasse whiskers: Extraction and characterizations. *Industrial Crops and Products, 33*(1), 63–66. https://doi.org/10.1016/j.indcrop.2010.08.009

Egbueri, J. C., & Enyigwe, M. T. (2020). Pollution and ecological risk assessment of potentially toxic elements in natural waters from the Ameka metallogenic district in southeastern Nigeria. *Analytical Letters, 53*(17), 2812–2839. https://doi.org/10.1080/00032719.2020.1759616

Elbasiouny, H., Darwesh, M., Elbeltagy, H., Abo-Alhamd, F. G., Amer, A. A., Elsegaiy, M. A., El-Sheikh, M. A., & Brevik, E. C. (2021). Ecofriendly remediation technologies for wastewater contaminated with heavy metals with special focus on using water hyacinth and black tea wastes: A review. *Environmental Monitoring and Assessment, 193*(7), 449. https://doi.org/10.1007/s10661-021-09236-2

Fomina, M., & Gadd, G. M. (2014). Biosorption: Current perspectives on concept, definition and application. *Bioresource Technology, 160*, 3–14. https://doi.org/10.1016/j.biortech.2013.12.102

Fujita, S., Sasa, R., Kinoshita, N., Kishimoto, R., & Kono, H. (2025). Nano-fibrillated bacterial cellulose nanofiber surface modification with EDTA for the effective removal of heavy metal ions in aqueous solutions. *Materials, 18*(2), 374. https://doi.org/10.3390/ma18020374

Grönwall, J., & Danert, K. (2020). Regarding groundwater and drinking water access through a human rights lens: Self-supply as a norm. *Water, 12*(2), 419. https://doi.org/10.3390/w12020419

Gupta, A., Sharma, V., Sharma, K., Kumar, V., Choudhary, S., Mankotia, P., Thakur, P., & Mishra, P. K. (2021). A review of adsorbents for heavy metal decontamination: Growing approach to wastewater treatment. *Materials, 14*(16), 4702. https://doi.org/10.3390/ma14164702

Gupta, V. K., Nayak, A., & Agarwal, S. (2015). Bioadsorbents for remediation of heavy metals: Current status and their future prospects. *Environmental Engineering Research, 20*(1), 1–18. https://doi.org/10.4491/eer.2015.018

Hama Aziz, K. H., Fatah, N. M., & Muhammad, K. T. (2024). Advancements in application of modified biochar as a green and low-cost adsorbent for wastewater

remediation from organic dyes. *Royal Society Open Science, 11*(5), 232033. https://doi.org/10.1098/rsos.232033

Hashim, M. A., Mukhopadhyay, S., Sahu, J. N., & Sengupta, B. (2011). Remediation technologies for heavy metal contaminated groundwater. *Journal of Environmental Management, 92*(10), 2355–2388. https://doi.org/10.1016/j.jenvman.2011.06.009

Ighalo, J. O., & Adeniyi, A. G. (2020). A comprehensive review of water quality monitoring and assessment in Nigeria. *Chemosphere, 260*, 127569. https://doi.org/10.1016/j.chemosphere.2020.127569

Kaur, A., Setia, H., & Wanchoo, P. R. (2018). Cellulose fiber extracted from Napier grass in PVA composites. *Indian Journal of Chemical Technology, 25*(1), 88–93. http://op.niscpr.res.in/index.php/IJCT/article/viewFile/7440/465464738

Kaur, J., Sengupta, P., & Mukhopadhyay, S. (2022). Critical review of bioadsorption on modified cellulose and removal of divalent heavy metals (Cd, Pb, and Cu). *Industrial & Engineering Chemistry Research, 61*(5), 1921–1954. https://doi.org/10.1021/acs.iecr.1c04583

Kenawy, I. M., Hafez, M. A. H., Ismail, M. A., & Hashem, M. A. (2018). Adsorption of Cu(II), Cd(II), Hg(II), Pb(II) and Zn(II) from aqueous single metal solutions by guanyl-modified cellulose. *International Journal of Biological Macromolecules, 107*, 1538–1549. https://doi.org/10.1016/j.ijbiomac.2017.10.017

Kumar, D., & Khan, E. A. (2021). Remediation and detection techniques for heavy metals in the environment. In *Heavy metals in the environment* (pp. 205–222). Elsevier. https://doi.org/10.1016/B978-0-12-821656-9.00012-2

Lailaty, I. Q., Astutik, S., & Surya, M. I. (2024). The growth response of Rendeu (*Staurogyne elongata* (Neese) Kuntze) to shoot pruning and its propagation by shoot cutting. *Journal of Tropical Biodiversity and Biotechnology, 9*(1), 77078. https://doi.org/10.22146/jtbb.77078

Morales-Herrera, V. A., Quintero-Álvarez, F. G., Mendoza-Castillo, D. I., Reynel-Ávila, H. E., Aguayo-Villarreal, I. A., Landin-Sandoval, V. J., & Bonilla-Petriciolet, A. (2024). Assessment and modeling of mercury adsorption on carbon-based adsorbents prepared from *Jacaranda mimosifolia* and guava biomass via pyrolysis and hydrothermal carbonization. *Water Practice & Technology, 19*(4), 1162–1176. https://doi.org/10.2166/wpt.2024.051

Motloung, M. T., Magagula, S. I., Kaleni, A., Sikhosana, T. S., Lebelo, K., & Mochane, M. J. (2023). Recent advances on chemically functionalized cellulose-based materials for arsenic removal in wastewater: A review. *Water, 15*(4), 793. https://doi.org/10.3390/w15040793

Nikiforova, T., Kozlov, V., Razgovorov, P., Politaeva, N., Velmozhina, K., Shinkevich, P., & Chelysheva, V. (2023). Heavy metal ions (II) sorption by a cellulose-based sorbent containing sulfogroups. *Polymers, 15*(21), 4212. https://doi.org/10.3390/polym15214212

Obasi, P. N., & Akudinobi, B. B. (2020). Potential health risk and levels of heavy metals in water resources of lead–zinc mining communities of Abakaliki, southeast Nigeria. *Applied Water Science, 10*(7), 1–23. https://doi.org/10.1007/s13201-020-01233-z

Okudo, C. C., Ekere, N. R., & Okoye, C. O. (2023). Quality assessment of non-roof harvested rainwater in industrial layouts of Enugu, South East Nigeria. *Applied Water Science, 13*(5), 116. https://doi.org/10.1007/s13201-023-01916-3

Oyewo, O. A., Elemike, E. E., Onwudiwe, D. C., & Onyango, M. S. (2020). Metal oxide-cellulose nanocomposites for the removal of toxic metals and dyes from wastewater. *International Journal of Biological Macromolecules, 164*, 2477–2496. https://doi.org/10.1016/j.ijbiomac.2020.08.074

Rehman, M. U., Taj, M. B., & Carabineiro, S. A. (2023). Biogenic adsorbents for removal of drugs and dyes: A comprehensive review on properties, modification and applications. *Chemosphere, 338*, 139477. https://doi.org/10.1016/j.chemosphere.2023.139477

Riccardi, D., Guo, H. B., Parks, J. M., Gu, B., Summers, A. O., Miller, S. M., & Smith, J. C. (2013). Why mercury prefers soft ligands. *The Journal of Physical Chemistry Letters, 4*(14), 2317–2322. https://doi.org/10.1021/jz400885f

Saha, P., & Paul, B. (2019). Assessment of heavy metal toxicity related with human health risk in the surface water of an industrialized area by a novel technique. *Human and Ecological Risk Assessment, 25*(4), 966–987. https://doi.org/10.1080/10807039.2018.1458595

Saravanan, P., Saravanan, V., Rajeshkannan, R., Arnica, G., Rajasimman, M., Baskar, G., & Pugazhendhi, A. (2024). Comprehensive review on toxic heavy metals in the aquatic system: Sources, identification, treatment strategies, and health risk assessment. *Environmental Research, 258*, 119440. https://doi.org/10.1016/j.envres.2024.119440

Sasan Narkesabad, Z., Rafiee, R., & Jalilnejad, E. (2023). Experimental study on evaluation and optimization of heavy metals adsorption on a novel amidoximated silane functionalized *Luffa cylindrica*. *Scientific Reports, 13*(1), 3670. https://doi.org/10.1038/s41598-023-30634-8

Shi, R. J., Wang, T., Lang, J. Q., Zhou, N., & Ma, M. G. (2022). Multifunctional cellulose and cellulose-based (nano)composite adsorbents. *Frontiers in Bioengineering and Biotechnology, 10*, 891034. https://doi.org/10.3389/fbioe.2022.891034

Srivastava, V. (2021). Grand challenges in chemical treatment of hazardous pollutants. *Frontiers in Environmental Chemistry, 2*, 792814. https://doi.org/10.3389/fenvc.2021.792814

Trifirò, F., & Zanirato, P. (2024). Water purification: Physical, mechanical, chemical and biological treatments. *Mathews Journal of Pharmaceutical Science, 8*, 42. https://doi.org/10.30654/MJPS.10042

Wang, R., Ren, J., Ren, H., Tao, L., Wu, C., Sun, X., & Lv, M. (2023). Enhanced adsorption of Cu^{2+} from aqueous solution by sludge biochar compounded with attapulgite-modified Fe. *Water, 15*(23), 4169. https://doi.org/10.3390/w15234169

Yuan, J., Liu, G., Liu, P., & Huang, R. (2024). Comprehensive assessment of elephant grass (*Pennisetum purpureum*) stalks at different growth stages as raw materials for nanocellulose production. *Tropical Plants, 3*(1), Article tp-0024-0013. https://doi.org/10.48130/tp-0024-0013

Trakya University Journal of Natural Sciences, 26(2), 182–194, 2025
DOI: 10.23902/trkjnat.543576
www.tujns.org

Research Article

Diversity of *Melanoleuca* Pat. (Basidiomycota, Agaricales) in Çanakkale, Türkiye: Morphological and molecular perspectives

İsmail Acar[1]*, Halide Karabıyık[2]

[1]*Van Yüzüncü Yıl University, Başkale Vocational School, Department of Organic Agriculture, Van, Türkiye*
[2]*Trakya University, Arda Vocational School, Department of Food Processing, Edirne, Türkiye*

Cite this article as: Acar, İ., & Karabıyık, H. (2025). Diversity of *Melanoleuca* Pat. (Basidiomycota, Agaricales) in Çanakkale, Türkiye: Morphological and molecular perspectives. *Trakya University Journal of Natural Sciences, 26*(2), 182–194. https://doi.org/10.23902/trkjnat.543576

Abstract

The genus *Melanoleuca* Pat. (Basidiomycota or Agaricales) is taxonomically complex due to its remarkable morphological similarities with other genera. Consequently, any reliable species identification method requires a holistic approach that includes molecular phylogenetic data. In this study, five taxa, namely *M. exscissa* (Fr.) Singer, *M.* cf. *graminicola*, *M. granadensis* Armada, *M. paedida* (Fr.) Kühner & Maire, and *M. stridula* (Fr.) Singer were identified from the Çanakkale province, T*ü*rkiye. These were described by integrating macro and micromorphological characters with phylogenetic analyses, which were based on Internal Transcribed Spacer rDNA sequences. *M. exscissa*, *M. graminicola*, *M. paedida*, and *M. stridula* have already been documented in Türkiye. This study updated the detailed macro- and microscopic descriptions. *M. granadensis*, first described in Spain in 2020 and reported from only the Czech Republic and Slovakia in Europe, was confirmed as a novel record of the Turkish mycobiota. It represents the first known non-European specimen. The detailed habitat characteristics, geographic coordinates, and collection dates of all specimens were documented. The microscopic characters were supported with drawings; the description of the new record was supplemented with scanning electron microscope images. These findings contribute novel data for understanding the *Melanoleuca* spp. diversity in Türkiye, underscoring the significance of molecular data in distinguishing morphologically similar species. They also suggest that certain records should be re-evaluated within the context of current phylogenetics.

Özet

Melanoleuca Pat., Basidiomycota veya Agaricales, cinsi önemli morfolojik benzerliklerin varlığı nedeniyle taksonomik olarak karmaşık bir gruptur. Bu sebeple, güvenilir tür tanımlaması, moleküler filogenetik verilerle desteklenen bütünsel bir yaklaşım gerektirir. Bu çalışmada, Türkiye'nin Çanakkale ilinden tanımlanan beş takson, yani *M. exscissa* (Fr.) Singer, *M.* cf. *graminicola*, *M. granadensis* Armada, *M. paedida* (Fr.) Kühner & Maire ve *M. stridula* (Fr.) Singer incelenmiştir. Bu türler, makro- ve mikromorfolojik karakterlerin İçsel Transkribe Edilmiş Aralık rDNA dizilerine dayalı filogenetik analizlerle entegre edilmesiyle tanımlanmıştır. *M. exscissa, M. graminicola, M. paedida* ve *M. stridula* daha önce Türkiye'de belgelenmiştir; bu çalışmada, ayrıntılı makro- ve mikroskobik tanımlamalar güncellenmiş ve yeniden sunulmuştur. *M. granadensis*, ilk olarak 2020 yılında İspanya'da tanımlanmış ve Avrupa'da sadece Çek Cumhuriyeti ve Slovakya'da rapor edilmiştir. Bu tür, Türkiye mikobiyotası için güvenilir bir şekilde doğrulanmış yeni bir kayıt olup, Avrupa dışından bilinen ilk örnek olarak kabul edilmektedir. Tüm örneklerin habitat gözlemleri, coğrafi koordinatları ve toplama tarihleri ayrıntılı olarak belgelenmiştir; mikroskobik karakterler çizimlerle desteklenmiştir ve yeni kaydın tanımı taramalı elektron mikroskobu görüntüleri ile desteklenmiştir. Bu bulgular, Türkiye'deki *Melanoleuca* türlerinin çeşitliliğinin anlaşılmasına yeni veriler katmakta, morfolojik olarak benzer türleri ayırt etmede moleküler verilerin kritik önemini vurgulamakta ve literatürdeki bazı kayıtların mevcut filogenetik bağlamda yeniden değerlendirilmesi gerektiğini göstermektedir.

Keywords: DNA, Internal Transcribed Spacer, new record, molecular taxonomy, *Melanoleucaceae*

Edited by: *Boris Assyov*
***Corresponding Author:** İsmail Acar, **E-mail:** ismailacar@yyu.edu.tr*
***ORCID iDs of the authors:** İA. 0000-0002-6049-4896, HK. 0000-0002-1778-2200*

Received: 22 April 2025, **Accepted:** 28 August 2025, **Online First**: 16 September 2025, **Published:** 15 October 2025

Introduction

The genus *Melanoleuca* Pat. was first described in 1897 by Patouillard. It comprises > 440 species worldwide (Antonín et al., 2023). For a long time, the classification of the genus was ambiguous and was included in Tricholomataceae. Vizzini et al. (2024) placed five families into Pluteineae (a suborder of Agaricales): Amanitaceae (including *Leucocortinarius*), Limnoperdaceae, Melanoleucaceae, Pluteaceae, and Volvariellaceae. No clear, morphological synapomorphy unites the members of this suborder. The basidiomata are variously shaped: agaricoid, with open or closed hymenophore, or gasteroid/sequestrate. They are mostly fleshy; the way the lamellae attach to the stipe may vary (Vizzini et al., 2024).

For the first time, molecular analyses supported a monophyletic origin of *Giacomia* and *Melanoleuca* within Pluteineae (Vizzini et al., 2024). Thus, they were positioned within a novel family, Melanoleucaceae. Its members have pileostipitate basidiomata, mostly collybioid to tricholomatoid in structure, with subregular hymenophoral trama and monomitic hyphae.

Melanoleuca (Basidiomycota, Agaricales) comprises species with a diversity of stalked agarics, which are ecologically characterized as having a saprotrophic lifestyle. The genus can be distinguished by numerous morphological features, including basidiomata of collybioid–tricholomatoid habit, dull-colored tones, white–pale yellowish lamellae, and pale–whitish stipe bases. At the macroscopic level, these features comprise warty basidiospores with a robust amyloid reaction, prominent and variously shaped cheilocystidia, and the absence or rare presence of clamp connections, depending on the species (Vesterholt, 2008; Acar et al., 2017). However, the morphological classification of *Melanoleuca* spp. is cumbersome, especially due to overlapping macroscopic and microscopic characters and the blurring of interspecific boundaries. Indeed, many species are morphologically very similar, and the interspecific variations are often based on only a few microscopic features (Vizzini et al., 2011). This situation highlights the inadequacies of traditional identification methods, which lead to taxonomic confusion (Kalmer et al., 2022).

Over the last few decades, the application of molecular data has emerged as an essential approach to solving such taxonomic ambiguities. In particular, the nuclear ribosomal internal transcribed spacer (nrITS) region has been proposed as the most reliable DNA barcode region for the molecular identification of Basidiomycota members due to its high variability and easy amplification with universal primers (Schoch et al., 2012). The use of this region has thus become common. However, studies on the diversity of *Melanoleuca* spp. in Türkiye are limited, and most records are based only on morphological data.

This study aims to reveal the morphological characteristics of certain *Melanoleuca* spp. from Çanakkale, *Türkiye*, in detail and confirm their identity with molecular data from the nrITS region. Thus, it aims to clarify the taxonomic position of related species and contribute to the knowledge of the macrofungal diversity of Türkiye.

Materials and Methods

Sampling

The macrofungus samples analyzed in this study were collected between 2023 and 2025 from the Çanakkale province, Türkiye (Figure 1). *Melanoleuca* samples collected from their natural habitat were identified and classified using an integrated approach that combined traditional methods and advanced molecular techniques. Macro and micromorphological characteristics of the specimens were examined in detail. Additionally, the nrITS sequences were compared and phylogenetically analyzed.

Morphological Studies

The study materials comprised macrofungus samples collected from various regions of the Çanakkale province, Türkiye. The macroscopic characteristics were recorded during field studies, and the specimens were photographed in their natural habitat with an EOS 60D digital camera (Canon). Ecological data, like the location and date of collection, and substrate type, were meticulously recorded in the field notebook. After field studies, the samples were transported to the laboratory, dried under controlled conditions at room temperature (~25°C), stored in polyethylene bags, and labeled. Color descriptions were based on the classification system developed by Kornerup and Wanscher (1978). The microscopic characters were analyzed with a DM500 light microscope (Leica), and the basidia, basidiospores, cystidia, and pileipellis were structurally evaluated in detail. To ensure that each character was within a reliable range, it was measured ≥ 30 times utilizing the Leica Application Suite (v3.4.0) software. Drawings of the microscopic structures were created

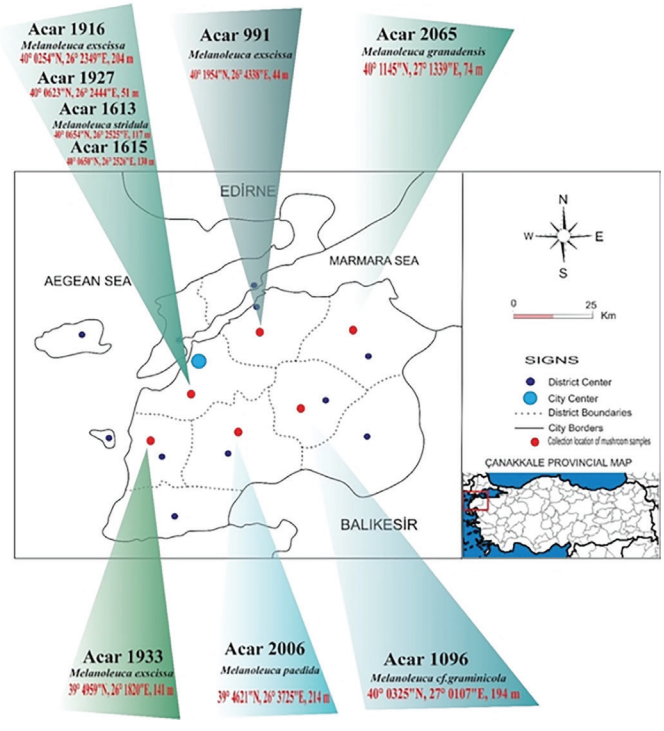

Figure 1. A map of the research area (Çanakkale, Türkiye).

using CorelDRAW (64-bit) (Corel Corporation, ON, Canada). Morphological identification was based on the literature, including Breitenbach and Kränzlin (1991), Kalmer et al. (2018), Xu et al. (2019), Acar et al. (2020), Armada (2020), and Antonín et al. (2022, 2023). After identification, the specimens were transformed into fungarium materials and stored under appropriate conditions in the Fungarium of the Department of Biology, Faculty of Science, Van Yüzüncü Yıl University, Van, Türkiye.

Sequencing of the ITS rDNA

Genomic DNA was isolated from the macrofungal samples by employing the CTAB method and following the protocols described by Rogers and Bendich (1994), Dizkırıcı et al. (2019), and Akata et al. (2024a, 2024b). The DNA purity and concentration were determined with a NanoDrop 2000c ultraviolet-visible spectrophotometer (Thermo Fisher Scientific Inc., MA, USA). The DNA was stored at −20°C. Polymerase chain reaction (PCR) amplification of the ITS rDNA region was performed in a 25 µL reaction mix, containing 10 µM primers (forward and reverse), 5 U/µL Taq polymerase, 10 ng/µL genomic DNA, 10X PCR buffer, 25 mM $MgCl_2$, 10 mM dNTP, and sterile water to make up the volume. The universal ITS1 and ITS4 primers were used; their respective sequences were 5'-TCCGTAGGTGAACCTGCGG-3' and 5'-TCCTCCGCTTTATTGATATATGC-3'. The PCR products were separated by agar gel electrophoresis at 100 V for 90 min, and an amplicon of ~700 bp was obtained; this single band confirmed amplification. The PCR products were purified using the HighPrep™ PCR Clean-up System kit (AC60005, MagBio Genomics, MD, USA), following the manufacturer's protocol. They were then sequenced at Macrogen Europe BV, Amsterdam, Netherlands. An ABI 3730XL Sanger sequencer and the BigDye Terminator v3.1 Cycle Sequencing Kit (Applied Biosystems, CA, USA) were used (Chen et al., 2014; Akata et al., 2024c, 2024d).

Molecular Phylogeny

The Sanger sequencing data obtained were assembled using the DNAMAN software v.10 (Lynnon Biosoft, CA, USA). The consensus sequences were analyzed with BLASTn (https://blast.ncbi.nlm.nih.gov/) to determine the species identity ratios. Based on the results, *Pluteus cervinus* (Schaeff.) P. Kumm. and *P. brunneidiscus* Murrill were selected as the ingroup and outgroup members, respectively, for further phylogenetic analyses. The related sequences were obtained from the NCBI GenBank (http://www.ncbi.nlm.nih.gov/) and are listed in Table 1.

Table 1. Sequences used for the phylogenetic analysis. Examples of direct submissions are indicated with an "–."

Species	Specimen Voucher	Country	IST (NCBI number)	Source
Melanoleuca aff. *graminicola*	AMB:19613	Italy	OR863461	Vizzini et al. (2024)
M. acystidiata	RR22.020	Switzerland	PV074842	-
M. acystidiata	BRNM 772203	Italy	MW491319	Antonín et al. (2021)
M. albomarginata	BRNM 817818	Italy	NR_198097	Antonín et al. (2022)
M. albomarginata	BRNM 817818	Italy	MT270938	Antonín et al. (2022)
M. albomarginata	BRNM 817817	Czech Republic	MT270939	Antonín et al. (2022)
M. angelesiana	HAY-F-005291	USA	PV791591	-
M. angelesiana	OMDL iNat# 118476394	USA	OR802136	Canan et al. (2024)
M. angelesiana	FDS-CA-04464	USA	PV273201	-
M. angelesiana	FDS-CA-05212	USA	PV019524	-
M. angelesiana	Acar 971	Türkiye	MG989682	Kalmer et al. (2018)
M. brachyspora	SLO 1565	Slovakia	OP394189	Antonín et al. (2023)
M. brachyspora	BRNM 829071	Slovakia	OP394188	Antonín et al. (2023)
M. brachyspora	BRNM 772200	Czech Republic	OP394187	Antonín et al. (2023)
M. cinereifolia	QHU20156	China	MZ453083	-
M. cinereifolia	QHU20156	China	OM970925	-
M. communis	FCME3445	Mexico	JX429148	-
M. communis	HMJAU59694	China	OR468700	-
M. exscissa	Acar 991	Türkiye	PV459218	This study
M. exscissa	Acar 1916	Türkiye	PV459219	This study
M. exscissa	Acar 1927	Türkiye	PV459220	This study
M. exscissa	Acar 1933	Türkiye	PV459217	This study
M. exscissa	JAC11654	New Zeland	MN738640	-

Table 1. Continued.

Species	Specimen Voucher	Country	IST (NCBI number)	Source
M. exscissa	GB65476	Sweden	JX429121	-
M. exscissa	GB 65455	Sweden	NR_154163	Sanchez-Garcia et al. 2013
M. exscissa	GB65455	Sweden	JX429192	Sanchez-Garcia et al. 2013
M. exscissa	ML14	Türkiye	PV065669	-
M. exscissa	FBT1465	Australia	OL771712	-
M. fontenlae	H89	Tunisia	PP533056	-
M. fontenlae	BRNM 772194	Italy	MW491326	Antonín et al. (2021)
M. fontenlae	BRNM 772194	Italy	NR_172809	Antonín et al. (2021)
M. graminicola	Acar 1096	Türkiye	PV459221	This study
M. graminicola	ANC M0201	Italy	JN616438	Vizzini et al. (2011)
M. graminicola	BRNM 829064	Czech Republic	OP394192	Antonín et al. (2023)
M. graminicola	BRNM 829062	Slovakia	OP394193	Antonín et al. (2023)
M. graminicola	SLO 1523	Slovakia	OP394194	Antonín et al. (2023)
M. graminicola	SLO 1532	Slovakia	OP394195	Antonín et al. (2023)
M. graminicola	SLO 1623	Slovakia	OP394196	Antonín et al. (2023)
M. graminicola	SLO 1527	Slovakia	OP394197	Antonín et al. (2023)
M. granadensis	Acar 2065	Türkiye	PV459222	This study
M. granadensis	AC20220508	France	PV089839	-
M. granadensis	FR2018040	Spain: Granada	MW289911	Armada (2020)
M. granadensis	PRM 955782	Czech Republic	PQ098927	-
M. luteolosperma	SB051123A	France	PP111921	-
M. luteolosperma	M 0139486	Germany	MW491330	Antonín et al. (2021)
M. luteolosperma	SLO 1632	Slovakia	MW491331	Antonín et al. (2021)
M. luteolosperma	BRNM 817820	Czech Republic	MW491329	Antonín et al. (2021)
M. melaleuca	NSK 1014679	Russia	OQ216539	-
M. melaleuca	ANC M0161	Italy	MT270919	Antonín et al. (2022)
M. melaleuca	BRNM 807677	Slovakia	MT270918	Antonín et al. (2022)
M. microcephala	HMJAS00133	China	MK659987	-
M. microcephala	HMJAS00132	China	MK659986	-
M. microcephala	ANC M0196	Italy	JN616449	Vizzini et al. (2011)
M. paedida	Acar 2006	Türkiye	PV459223	This study
M. paedida	ANC M0190	Italy	JN616453	Vizzini et al. (2011)
M. paedida	ANC M0189	Italy	JN616452	Vizzini et al. (2011)
M. paedida	SB0521	Canada	OM338006	-
M. paedida	R. Para 010907-02	Italy	MW491337	Antonín et al. (2021)
M. romanensis	BRNM 772193	Italy	NR_198286	Antonín et al. (2023)
M. romanensis	BRNM 829060	Italy	OP394204	Antonín et al. (2023)
Melanoleuca sp.	HFRG_LG2304152	United Kingdom	OR907161	-
M. stridula	Acar 1615	Türkiye	PV459224	This study
M. stridula	Acar 1613	Türkiye	PV459225	This study
M. stridula	F-3760	Sweden	PQ639185	-
M. stridula	BRNM 825716	Slovakia	MW491340	Antonín et al. (2021)

Table 1. Continued.

Species	Specimen Voucher	Country	IST (NCBI number)	Source
M. stridula	SLO 1543	Slovakia	MW491339	Antonín et al. (2021)
M. stridula	F-3756	Sweden	PQ639184	-
M. striimarginata	ANC M0202	Italy	JN616468	Vizzini et al. (2011)
M. subcinereiformis	CA FUNDIS	USA	PP975555	-
M. subcinereiformis	ONT WCMB23	USA	*OR167957*	-
M. subpulverulenta	ANC M0178	Italy	JN616473	Vizzini et al. (2011)
M. subpulverulenta	ANC M0004	Italy	JN616472	Vizzini et al. (2011)
M. subpulverulenta	MCVE:9821	Italy	JN392453	-
M. cf. subpulverulenta	SOMF30862	Bulgaria	OQ398593	Assyov and Slavova (2023)
Pluteus brunneidiscus	HMJAU 602011 i	China	OM991893	-
P. brunneidiscus	HMJAU 60206	China	OM943513	-
P. cervinus	REG 13641	Germany	HM562152	Justo et al. (2011)

The assembled sequences were aligned with those of the ingroup and outgroup members for phylogenetic analyses. Bayesian inference was performed employing the Markov Chain Monte Carlo (MCMC) + MC³ algorithm in the MrBayes v3.2.7a software (Ronquist et al., 2012). It allowed an exploration of the posterior probability distributions and uncertainty in the tree topologies. Such information is particularly relevant given the limited sequence divergence within the dataset. In this model, Dirichlet priors were used to calculate the rates of change: uniform (0.00 and 1.00) for the fixed regions and exponential (1.00) for the γ-shaped parameter. Independent MCMC runs were conducted twice, each with four chains. The analyses were run for 3,000,000 generations and sampled every 1,000 generations. The phylogenetic analyses performed in this study provided valuable insights into the evolutionary history of the *Melanoleuca* spp. in Türkiye. ITS-based phylogeny distinguished *M. granadensis* from closely related species such as *M. albomarginata*, supporting their recognition as distinct evolutionary lineages by Antonín et al. (2022). Furthermore, grouping the Turkish *M. granadensis* specimens with their European counterparts suggests a recent common ancestry, highlighting the potential significance of historical biogeographic connections across the Mediterranean. These evolutionary insights were corroborated by the posterior probability distributions, enabling a robust sampling of the phylogenetic tree space and bolstering the reliability of the evolutionary relationships inferred. These results emphasize the importance of incorporating molecular data into taxonomic and evolutionary research, particularly in genera where morphological characteristics demonstrate a high overlap and plasticity.

The General Time Reversible model + I + Γ model with uniform ratios was applied for nucleotide substitution during phylogenetic analyses (Höhna et al., 2017; Barba-Montoya et al., 2020). The bootstrap method (Felsenstein, 1985) was used, and 1,000 bootstrap replications were performed, to assess the reliability of the findings.

Results

The phylogenetic and morphological identification of the collected macrofungal specimens as *M. excissa, M.* cf. *graminicola, M. granadensis*, *M. paedida*, and *M. stridula* based on the methodology described in the literature is presented. It includes descriptions of the specimens, macromorphological illustrations, micromorphological drawings, locations and dates of collection, scanning electron microscopy images of the new spore records, ITS rDNA sequences, and phylogenetic analyses.

Morphological Taxonomy

Melanoleuca exscissa (Fr.) Singer (Figure 2)

Description. Pileus: 25–80 mm, convex when young, semi-convex, flattening as it matures, sometimes curving outwards in mature specimens, with a small, broad umbo, pale white to creamy white, grayish brown to gray, light brown to dark brown, usually darker in the center, finely tomentose, shiny when moist. **Context:** white and unchanging throughout, becoming slightly darker and more compact at the stipe base. **Lamellae:** white to cream, margin slightly undulating to crenate. **Stipe:** 20–70 × 3–8 mm, cylindrical, somewhat enlarged toward the pileus, surface fibrillose, dirty white to creamy white, with a white-pruinous apex, dark brown toward the base. **Basidia:** 25–38 × 6–10 (apex) × 5–8 (base) µm, cylindric, cylindric-clavate, clavate to sub–clavate, hyaline, guttulate, without clamp connections and with four sterigmata. **Spores:** 7–11 × 4.5–7 µm, ellipsoid to cylindric or subovoid, verrucose, hyaline, amyloid. **Cheilocystidia:** 30/35–55 × 5–10 µm, fusiform to lageniform, mostly transversely septate, often with crystals at the apex; both macrocystidia and urticoid cystidia (exscissa-type) present. **Pleurocystidia:** similar to cheilocystidia and very sparse. **Caulocystidia:** similar to cheilocystidia but narrower, extending up to 90 µm. **Pileipellis:** 20–50(–100) µm thick trichoderm, irregular hyphae up to 10 µm long, sometimes slightly gelatinized, somewhat ascending hyphae with obtuse or clavate terminal cells, occasionally at the apex encrusted with crystals, septa without clamp connections.

Figure 2. *Melanoleuca excissa.* (a–b) basidiomata (a: in meadows; b: in forest clearings); (c) spores; (d) basidia; (e) pleurocystidia; and (f) cheilocystidia. Scale bar = 10 µm.

Specimens examined: Türkiye, Çanakkale, Lapseki, around the Yeniceköy village, 40°19′54”N and 26°43′38”E, 44 m, in meadows, 05.IV.2023, Acar 991; above Çınarlı village, around Sefer Bozkurt Fountain, 40°02′54”N and 26°23′49”E, 204 m, under *Pinus brutia* L., in meadows, 08.V.2025, Acar 1916; Çanakkale Onsekiz Mart University (ÇOMÜ), Hasan Mevsuf sports hall vicinity, 40°06′23”N and 26 24′44”E, 51 m, under *P. brutia*, in meadows, 09.I.2025, Acar 1927; Ezine, around the Çamköy village, 39°49′59”N and 26°18′20”E, 141 m, in meadows, 10.I.2025, Acar 1933.

Melanoleuca cf. *graminicola* (Figure 3)

Description. Pileus: 20–65 mm, convex to campanulate when young, then flat, usually in mature specimens, the edges are curved outward, the center becomes more flattened, usually with a shallow central umbo, smooth, dull, grayish-brown, light brown to dark brown, with a darker center. **Context:** white, brownish under the cuticle, stipe base somewhat white tomentose. **Lamellae:** white when young, then cream to whitish cream, sometimes developing slightly pinkish hues, crowded, notched, and slightly uncinate, margin smooth. **Stipe:** 40–55 × 3–6 mm, more or less cylindrical, sometimes thicker near the pileus, slightly clavate toward the base, occasionally longitudinally white fibrillose, firm, powdery near the apex, whitish to light brown, grayish brown to dark brown, sometimes white tomentose at the base. **Basidia:** (18–)21–32(–37) × 7–10 (apex) × 5–7 (base) µm, cylindric to cylindric-clavate, hyaline, guttulate, without a clamp connection and with four sterigmata. **Spores:** 6–8(–9) × 4.7–6(–6.5) µm, fusoid-ellipsoid to subcylindrical or subovoid, hyaline, with verrucose ornamentation, guttulate. **Cheilocystidia:** 20–55 × 4.8–10 × 3–5.3 µm, urticoid, scattered, lageniform, often irregular, with a subulate, obtuse apex and thin walls. **Marginal cells:** 15–40 × 5–11 µm, sometimes irregular, clavate, subcylindrical, or subutriform, with thin walls. **Pleurocystidia:** absent. **Pileipellis:** initially appears in the form of an ixocutis, which develops into an ixotrichoderm structure in the center, composed of thin-walled, cylindrical, non-dextrinoid hyphae up to 10 µm in width; terminal cells are usually flattened to erect, cylindrical, subclavate, or rarely branched in shape, ca 65 × 8 µm, yellowish-gray colored in KOH.

Figure 3. *Melanoleuca graminicola.* (a–b) basidiomata; (c) spores; (d) basidia; and (e) cheilocystidia. Scale bar = 10 µm.

Specimens examined: Türkiye, Çanakkale, Çan, around Mallı village, 40°03'25"N and 27°01'07"E, 194 m, near *Pinus* spp. trees, in meadows, 25.I.2024, Acar 1096.

***Melanoleuca granadensis* Armada (Figures 4–6)**

Description. Pileus: 35–85 mm, campanulate when young, then plano–convex with a vaguely broad umbonate margin, surface smooth and dull, margin white, light brown to dark brown or yellowish brown when young, with equal colors or slightly darker in the center. **Context:** white to hyaline gray, fragile, thin or thick, becoming yellowish-gray toward the stipe base. **Lamellae:** white, fairly close, thin, fragile, greasy to the touch, interveined in the sinuses, notched to slightly decurrent on a narrow base; margin very irregular to eroded, paler. **Stipe:** 30–75 × 4–11 mm, 14 mm at the base, very fragile and brittle, hollow, longitudinally fibrous, whitish near the apex and base, cylindrical, slightly swollen at base, whitish at first, then dirty white to yellowish-gray, brown to grayish-brown. **Basidia:** 22–35 × 7–11 (apex) × 5–7 (base) µm, hyaline, guttulate, cylindrical to clavate, without a basal clamp and with four sterigmata. **Spores:** 7.5–10 × 4.8–6 µm, ellipsoid, slightly or moderately ornamented, with relatively small warts, occasionally with rough, truncate, or blunt warts, amyloid. **Cheilocystidia:** 50–80 × 10–16 µm, lageniform to fusiform, urticoid, some metuloid or plain, with a pointed or blunt apex, hyaline, and non-guttulate. **Pleurocystidia:** 43–75 × 13–17(–19) µm, lageniform to fusiform, sometimes cylindrical, urticoid, occasionally non-crystalliferous, some with tomentose apices, and a pointed or blunt apex, hyaline, and non-guttulate. **Caulocystidia:** 40–80 × 10–15 µm, mainly lageniform to fusiform, sometimes ventricose to cylindrical, occasionally 1 or 2-septate, urticoid, with some metuloid or plain, and a pointed or blunt apex, hyaline, non-guttulate. **Hairs:** 20–32 × 8–11, clavate, occasionally 1 or 2-septate, mostly among caulocystidia and sometimes in clusters near them. **Pileipellis:** develops on the surface of long and relatively smooth hyphae, sometimes quite elongated at the tip or short and blunt in morphology (× 4–16.5 µm). It is characterized by a yellowish coating with slight parietal pigmentation, or in some cases, it may show a thin encrustation, particularly evident when stained with Congo red. The substrate is characterized by sausage or sausage-like structures, which may reach 22 µm in diameter and consist of densely intertwined hyphae of homogeneous size.

Specimens examined: Türkiye, Çanakkale, Biga, Around Sarıkaya village, 40°11′45"N and 27°13′39"E, 74 m, under *P. brutia* trees, 02.II.2025, Acar 2065.

***Melanoleuca paedida* (Fr.) Kühner & Maire (Figure 7)**

Description. Pileus: 30–60 mm, initially almost hemispherical but soon flattening with an irregularly wavy margin and a broad, low umbo; cuticle slightly hygrophanous, smooth, grayish-brown, lighter toward the margin and darker toward the center. **Lamellae:** numerous, dense, lobed, white, becoming creamy with age, with an entire to slightly fimbriate edge. **Stipe:** 35–70 × 6–10 mm, cylindric, sometimes with a bulbous base or enlarged apex, surface longitudinally fibrillose, densely pruinose, cream to gray-brown. **Context:** white on the pileus, slightly hygrophanous on the lamellae, cream to ocher, thick in the center and thinning toward the margin, becoming slightly darker toward the stipe base. **Spores:** (6–)7–9.3 × 4.5–7 µm, subglobose to ellipsoid, hyaline, with drops, rounded tubercles, and strongly amyloid. **Cheilocystidia:** 37–52 × 4.5–8.3 µm, more or less frequent, urticoid to hair-shaped, typical or fusiform. Pluerocystidia:not seen. **Pileipellis:** hyphae 2–5 µm, arranged into cutis, with more/less interwoven hyphae from which some clavate tips emerge, which may give the impression of a trichodermium. **Stipitipellis:** of the middle zone without differentiated elements.

Specimens examined: Türkiye, Çanakkale, Bayramiç, Around Ören village, 39°46′21"N and 26°37′25"E, 214 m, garden area, in meadows, 25.I.2025, Acar 2006.

***Melanoleuca stridula* (Fr.) Singer (Figure 8)**

Description. Pileus: 25–50(–70) mm diameter, campanulate to convex when young, later flattening and sometimes curling outwards or wavy at the margin in mature specimens, and also somewhat obtusely umbonate; surface smooth, dull, with shades of brown ranging from light to dark, usually darker in the center

Figure 4. *Melanoleuca granadensis.* (a–b) basidiomata.

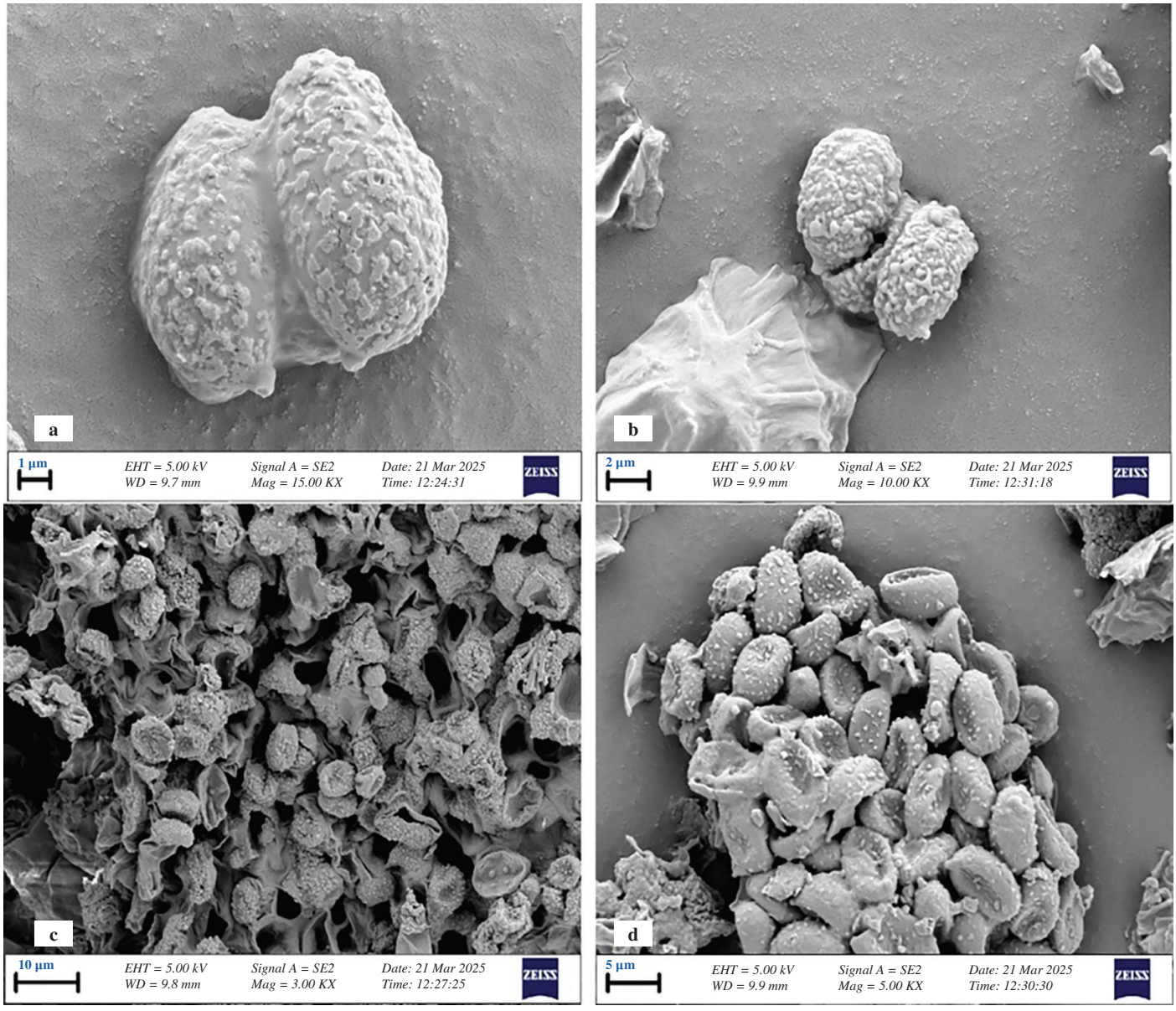

Figure 5. SEM images of basidiospores of *Melanoleuca granadensis*. (a) individual spores with verrucose ornamentation (scale bar = 1 µm); (b) paired spores with surface ornamentation (scale bar = 2 µm); (c) clustered spores (scale bar = 10 µm); and (d) aggregated spores showing surface sculpture (scale bar = 5 µm).

and occasionally with a white margin. **Context:** white to whitish cream, thin, becoming pale brownish in the stipe cortex and hollow interior. **Lamellae:** white, off-white to cream, broadly adnate to adnexed, occasionally notched. **Stipe:** 40–80 × 4–7 mm, cylindrical, bulbous, and white tomentose at the base, fragile with a longitudinally fibrillose white surface on an ocher-brown background. **Spores:** 7–8.2 × 4.5–5.5 µm, ellipsoid, hyaline, verrucose or slightly verrucose, with one or two drops. **Basidia:** 24–35 × 7–10 (apex) × 5–8 µm (base), cylindrical to clavate, with (1–2) 4 sterigmata, and without clamp connections. **Cystidia**: not seen. **Pileipellis:** composed of parallel to slightly irregularly arranged, brownish pigmented hyphae up to 10 µm in diameter, lacking clamp connections; the overall structure corresponds to a cutis.

Specimens examined: Türkiye, Çanakkale, ÇOMÜ, Opposite the Sports Faculty, 40°06′54”N and 26°25′25”E, 117 m, under *P. brutia*, 24.XII.2023, Acar 1613; behind Campus AVM, 40°06′50”N and 26°25′26”E, 130 m, under *P. brutia*, 24.XII.2023, Acar 1615.

Phylogenetic Results

The ITS rDNA sequences were amplified and used for the molecular identification of the nine *Melanoleuca* samples included in this study. After trimming the termini of the aligned forward and reverse sequences, the lengths of the newly generated sequences indicated efficiency (Acar 991 = 654 bp, Acar 1916 = 678 bp, Acar 1927 = 694 bp, Acar 1933 = 697 bp, Acar 1096 = 482 bp, Acar 2065 = 670 bp, Acar 2006 = 632 bp, Acar 1515 = 758 bp,

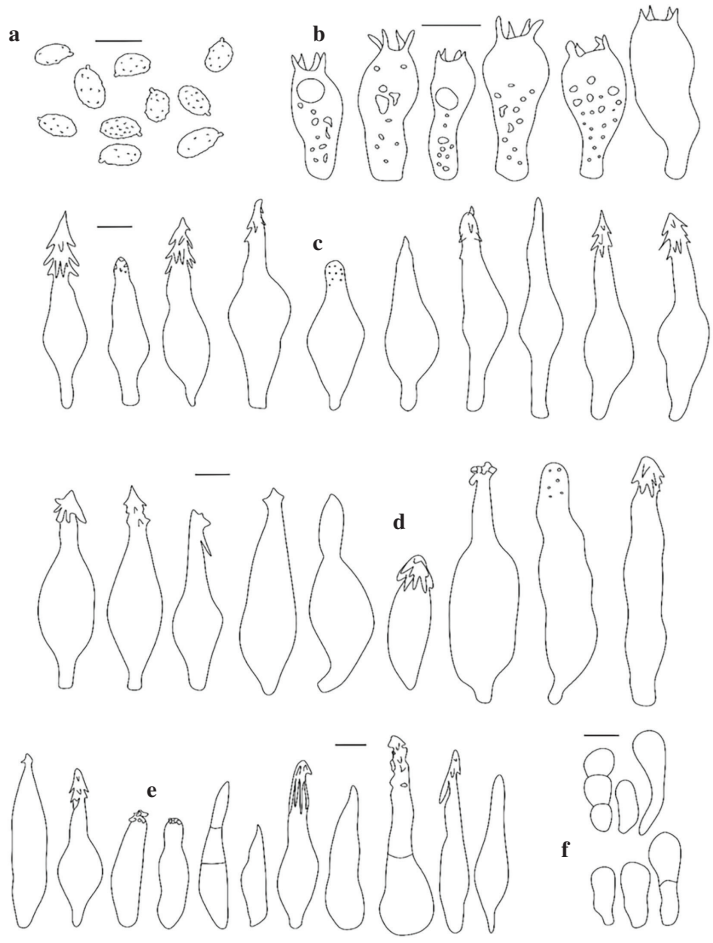

Figure 6. *Melanoleuca granadensis.* (a) spores; (b) basidia; (c) cheilocystidia; (d) pleurocystidia; (e) caulocystidia; and (f) hairs of stipe. Scale bar = 10 µm.

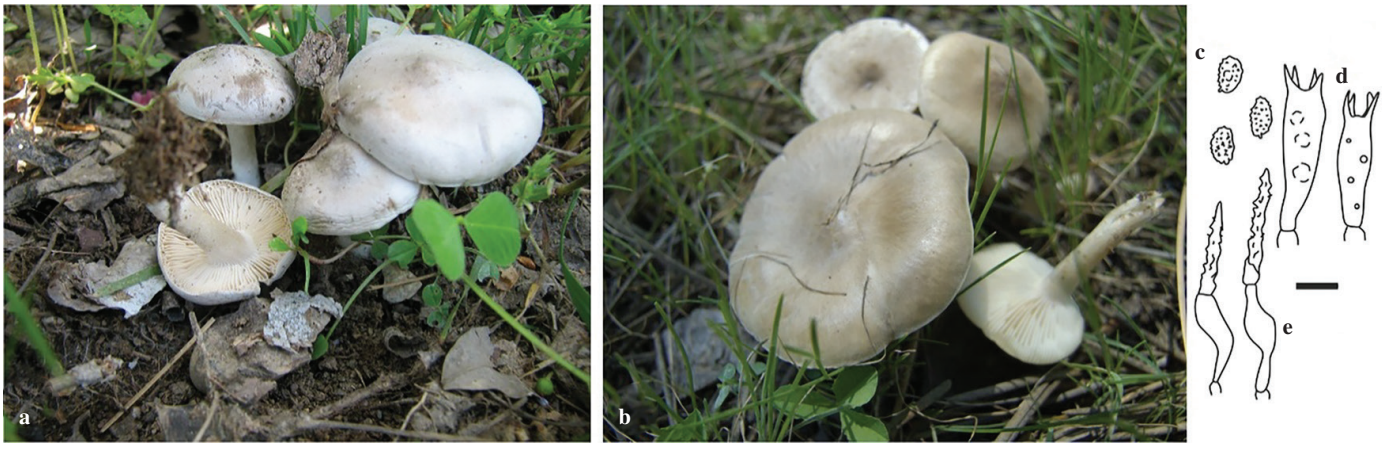

Figure 7. *Melanoleuca paedida.* (a–b) basidiomata; (c) spores; (d) basidia; and (e) cheilocystidia. Scale bar = 10 µm.

Acar 1613 = 543 bp, and Acar 1615 = 715). In addition to the sequences generated in this study (GenBank accession numbers: PV459217, PV459218, PV459219, PV459220, PV459221, PV459222, PV459223, PV459224, and PV459225), 68 sequences (including 3 outgroups) were obtained from GenBank; a total of 77 sequences were analyzed (Table 1). The sequences obtained from NCBI ranged from 380 (MW491330) to 1,624 (PQ639184) bp. The rediscovered *Melanoleuca* specimens were in the appropriate clades of the phylogenetic tree (Figure 9). In addition, the ITS region sequence obtained from the possibly new record "Acar 2065" was compared with those in the NCBI GenBank database using the BLASTn algorithm. The highest similarity was observed with *M. granadensis* (PVO98839). In total, 713 bp of the 855 bp sequence were aligned, with 99.55% similarity (667/670 matched

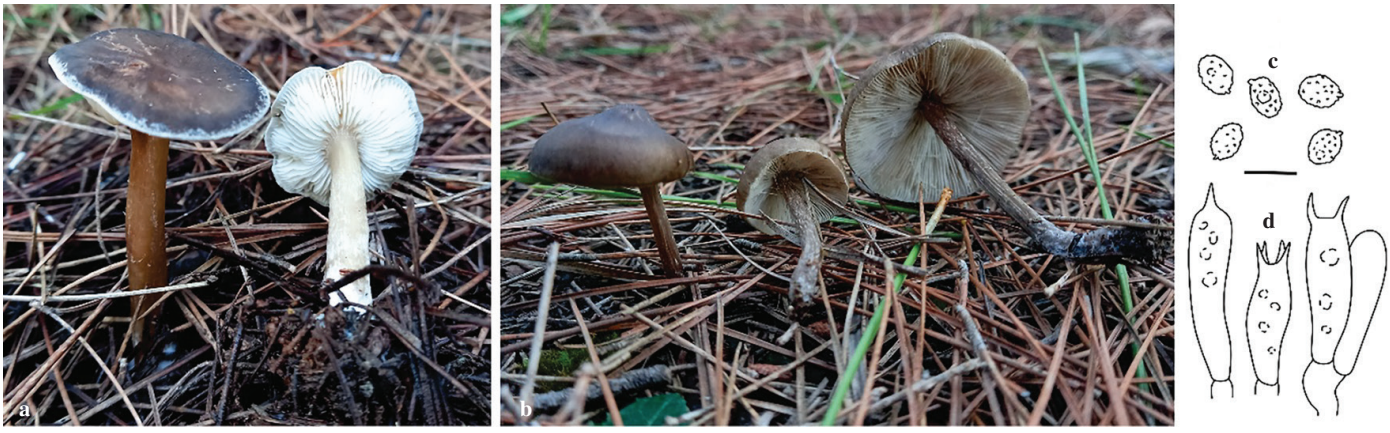

Figure 8. *Melanoleuca stridula.* (a–b) basidiomata (under *Pinus brutia*); (c) spores; and (d) basidia. Scale bar = 10 µm.

bases) and no gaps, indicating a high level of homology. This result demonstrates that our specimen was most likely *M. granadensis*. The high similarity rate (99%) and gap-free matching obtained through BLASTn analysis were over the threshold values (usually > 97–98%) commonly applied for the molecular identification of species. Along with morphological findings, the molecular data support the identification of the sample as *M. granadensis*.

Discussion

The present study unequivocally demonstrates that the taxonomic boundaries within the genus *Melanoleuca* cannot be reliably delineated using only morphology-based approaches, and that integrating molecular data is decisive for species-level identification (Vizzini et al., 2011; Kalmer et al., 2022). The findings obtained were of scientific significance for two principal reasons. The reliable documentation of *M. granadensis* from Türkiye for the first time indicates an expansion of its known ecological and diagnostic scope. Second, the phylogenetic separation of the Acar1096–OR863461–JN616438 lineage from the *M. graminicola* s. str. core suggests its independence.

Notably, the identification of the *Melanoleuca* specimen Acar 2065, collected from Çanakkale, as *M. granadensis* is supported by the high congruence between detailed morphological assessments and ITS-based molecular data. This specimen was recorded at a low elevation (~74 m) under a *P. brutia* tree, significantly extending the known altitudinal range of the species compared to the holotype and other records from higher elevations (Armada, 2020; Assyov & Slavova, 2023). Furthermore, it provides a novel ecological context in terms of habitat associations. The high degree of DNA sequence similarity and the absence of gaps with the reference sequences serve to reinforce the molecular-level identification.

The phylogenetic tree reaffirms the reported affinity with M. albomarginata. Additionally, the expanded measurement ranges of the diagnostic microcharacters (e.g., pleurocystidia and stipe hairs) support this relationship, enabling the inclusion of M. granadensis as an emended description (Table 2). In parallel, the placement of the specimen OQ398593, reported as M. cf. subpulverulenta by Assyov and Slavova (2023), within the M. granadensis clade and its separation from the *M. subpulverulenta* specimens in our phylogenetic tree strongly indicate the likelihood of a misidentification (Figure 9 and Table 2).

Table 2. A comparison of *Melanoleuca granadensis* and its holotype (Armada, 2020).

***Melanoleuca* granadensis**	**Armada (2020)**	**Current study**
Pileus	37–43 mm	35–85 mm
Stipe	42–51 × 7–9 mm	30–75 × 4–11 mm, at the base 14 mm
Basidia	23–34 × 9.5–13 µm	22–35 × 7–11 (apex) × 5–7 (base) µm
Spores	8–9 (9.5) × 4.75–5.5 (6) µm	7.5–10 × 4.8–6 µm
Cheilocystidia	50–82 × 11–17 µm	40–80 × 10–15 µm
Pleurocystidia	Similar or more lageniform with an obtuse apex	43–75 × 13–17(–19) µm
Caulocystidia	50–82 × 11– 17 µm	40–80 × 10–15 µm
Hairs on the stipe	Size unspecified	20–32 × 8–11, clavate, occasionally 1 or 2-septate
Habitat	Among several Cistaceae, under *Pinus pinaster*, *P. halepensis,* with rare *Quercus ilex*, very young, 1250–1300 m, November	Under *P. brutia* trees, 74 m, February

Second, although the Acar1096 sequence clustered within the same clade as M. aff. graminicola (OR863461) and *M. graminicola* (JN616438), it was markedly distant from the *M. graminicola* s. str. core (see Figure 9 for topology). Full-length ITS comparisons revealed only 74–75% identity between Acar1096 and the M. graminicola s.str. core specimens (OP394192–OP394197). These values fall well below the commonly accepted 97–99% threshold for species-level delimitation in Basidiomycota. OR863461 was collected in Italy (Emilia-Romagna, Imola) under *Cedrus deodara* (voucher AMB:19613, coll. S. Morini, 01 Jan 2021) and assessed recently via multi-locus phylogenies; JN616438 represents a classical record from Piedmont, Italy (voucher ANC M0201).

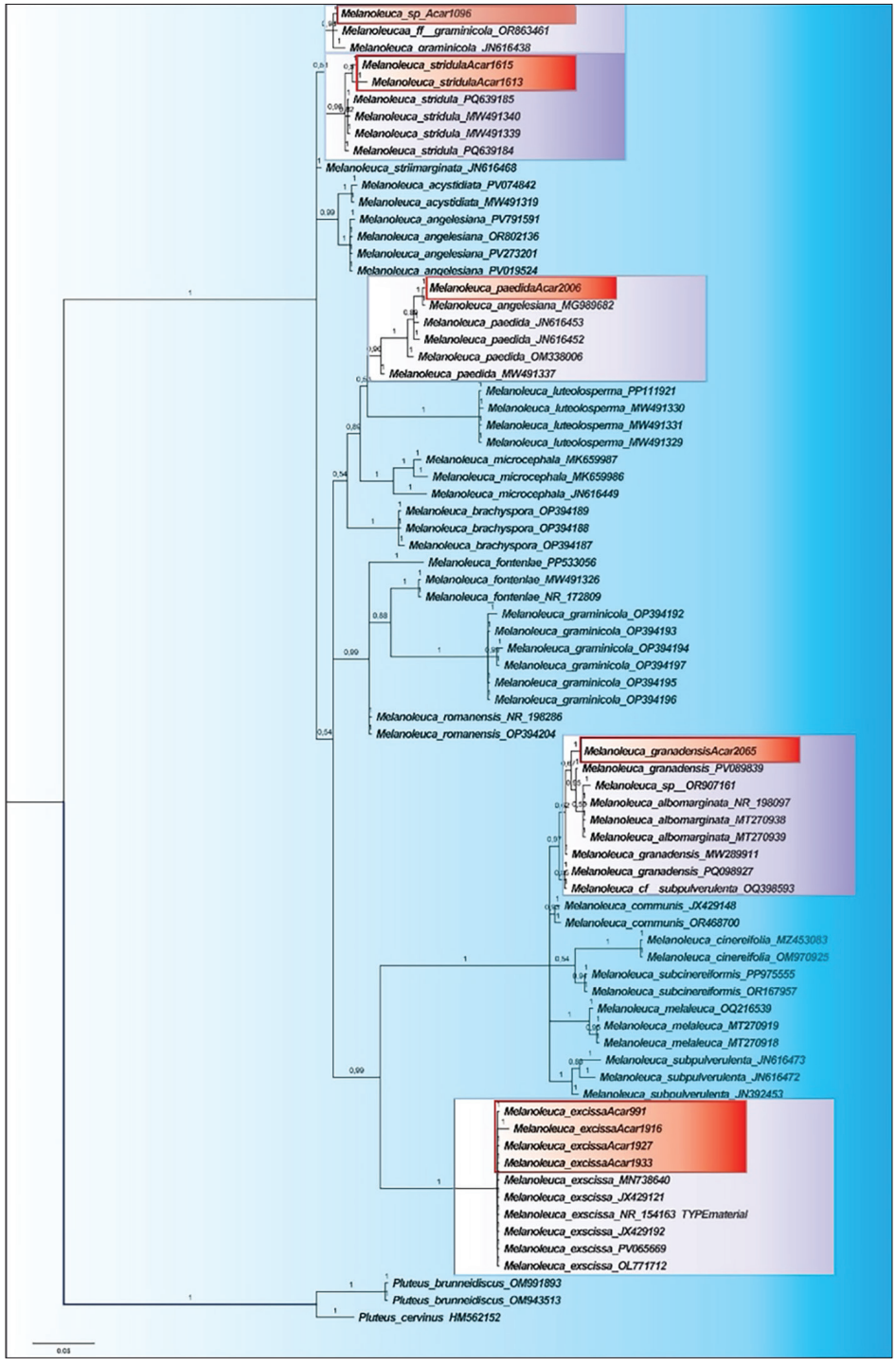

Figure 9. Bayesian 50% majority rule-based consensus tree constructed for *Melanoleuca* using ITS sequence data. The taxa recorded are indicated in the red boxes. Bayesian posterior probabilities are shown above the branches. *Pluteus cervinus* and *P. brunneidiscus* were the outgroups.

The findings suggest that this lineage may represent a Europe-derived variation line. However, the affinity observed does not imply a direct equivalence with *M. graminicola* s. str. Rather, it indicates that the Acar1096–OR863461–JN616438 trio forms a lineage closely related to, yet distinct from, the graminicola complex. In this context, the broad interpretations in certain studies, such as Antonín et al. (2023), and early GenBank annotations require a re-evaluation in light of updated sampling and analyses.

Technically, the high local similarity values (99–100%) observed in BLASTn searches may reflect matches within the conserved ITS subregions, potentially masking full-length variations. Therefore, species-level interpretations should be based on the alignment of complete sequences within a robust phylogenetic framework. Regarding the taxonomic designation of Acar1096, as the current dataset is ITS-based, its placement is best assessed in conjunction with other specimens within the same clade whenever available. Until then, it is recommended that Acar1096 be reported cautiously as *M.* cf. *graminicola*.

In conclusion, the present study not only confirms *M. granadensis* as a new record for Türkiye, but also suggests that the Acar1096–OR863461–JN616438 lineage should be regarded as a distinct and isolated clade, separate from *M. graminicola* s. str. based on robust morphological and molecular evidence. It also expands the known distribution, altitude, and habitat range of *M. granadensis*. These dual findings emphasize the pivotal role of integrating morphological and molecular data in establishing species limits within *Melanoleuca*. They underscore the need to re-evaluate specific records, notably early GenBank annotations, within a revised phylogenetic framework.

Ethics

Ethics Committee Approval: Since the article does not contain any studies with human or animal subject, its approval to the ethics committee was not required.

Data Sharing Statement: All data are available within the study.

Footnotes

Authorship Contributions: Conceptualization: İ.A., and H.K.; Design/methodology: İ.A., and H.K.; Execution/investigation: İ.A., and H.K.; Resources/materials: İ.A., and H.K.; Data acquisition: İ.A., and H.K.; Data analysis/interpretation: İ.A., and H.K.; Writing – original draft: İ.A., and H.K.; Writing – review & editing/critical revision: İ.A., and H.K.

Conflict of Interest: The authors have no conflicts of interest to declare.

Funding: The study was supported by the Scientific Research Projects Coordination Unit at Van Yüzüncü Yıl University under project number FBA-2024-11179.

References

Acar, İ., Dizkırıcı Tekpınar, A., Kalmer, A., & Uzun, Y. (2017). Phylogenetic relationships and taxonomical positions of two new records *Melanoleuca* species from Hakkari province, Turkey. *Biological Diversity and Conservation, 10*(3), 85–93.

Acar, İ., Uzun, Y., & Akata, İ. (2020). Some macrofungi determined in Şemdinli and Yüksekova districts (Hakkari-Turkey). *Kahramanmaraş Sütçü İmam Üniversitesi Tarım ve Doğa Dergisi, 23*(1), 157–167. https://doi.org/10.18016/ksutarimdoga.vi.588237

Akata, İ., Ediş, G., Kumru, E., Acar, İ., & Şahin, E. (2024b). Taxonomic studies on *Rhodocybe asyae* specimens discovered in a new location. *Kahramanmaraş Sütçü İmam Üniversitesi Tarım ve Doğa Dergisi, 27*(Suppl 1), 124–132. https://doi.org/10.18016/ksutarimdoga.vi.1507554

Akata, İ., Ediş, G., Kumru, E., Acar, İ., & Şahin, E. (2024c). Initial report of *Inocybe costinitii* in Türkiye with morphological and molecular data. *Kahramanmaraş Sütçü İmam Üniversitesi Tarım ve Doğa Dergisi, 27*(6), 1304–1312. https://doi.org/10.18016/ksutarimdoga.vi.1467628

Akata, İ., Kumru, E., Ediş, G., Acar, İ., & Şahin, E. (2024d). Two newly reported *Agaricales* species from Türkiye with morphological and molecular data. *Kastamonu University Journal of Forestry Faculty, 24*(3), 260–280. https://doi.org/10.17475/kastorman.1599952

Akata, İ., Kumru, E., Şahin, E., Acar, İ., & Kaya, E. (2024a). *Amanita vidua*: A new record for Turkish *Amanita* section *Phalloideae* based on morphological and molecular data. *Trakya University Journal of Natural Sciences, 25*(1), 97–110. https://doi.org/10.23902/trkjnat.1446327

Antonín, V., Ďuriška, O., Jančovičová, S., Kudláček, T., Para, R., Ševčíková, H., & Tomšovský, M. (2023). Two new European species of *Melanoleuca* (Fungi, Agaricales) with comments on the *M. graminicola* group. *Systematics and Biodiversity, 21*(1), 2218375. https://doi.org/10.1080/14772000.2023.221837

Antonín, V., Ďuriška, O., Jančovičová, S., Para, R., Kudláček, T., & Tomšovský, M. (2022). Multilocus phylogeny and taxonomy of European *Melanoleuca* subgenus *Melanoleuca*. *Mycologia, 114*(1), 114–143. https://doi.org/10.1080/00275514.2021.1966246

Antonín, V., Ševčíková, H., Para, R., Ďuriška, O., Kudláček, T., & Tomšovský, M. (2021). *Melanoleuca galbuserae, M. fontenlae* and *M. acystidiata*: Three new species in subgenus *Urticocystis* (Pluteaceae, Basidiomycota) with comments on *M. castaneofusca* and related species. *Journal of Fungi, 7*(3), 191. https://doi.org/10.3390/jof7030191

Armada, F. (2020). Quelques basidiomycètes nouveaux ou rares pour l'Andalousie, découverts près de Grenade dans la Sierra Nevada (Espagne). *Bulletin Mycologique et Botanique Dauphiné-Savoie, 239*, 67–78.

Assyov, B., & Slavova, M. (2023). Macrofungi in stands of the endemic pine *Pinus peuce* as inferred from morphological and molecular data. *Proceedings of the Bulgarian Academy of Sciences, 76*(5), 707–715. https://doi.org/10.7546/CRABS.2023.05.06

Barba-Montoya, J., Tao, Q., & Kumar, S. (2020). Using a GTR+Γ substitution model for dating sequence divergence when stationarity and time-reversibility assumptions are violated. *Bioinformatics, 36*(Suppl 1), i884–i894. https://doi.org/10.1093/bioinformatics/btaa820

Breitenbach, J., & Kränzlin, F. (1991). *Fungi of Switzerland* (Vol. 3). Richmond Publishing Co., Ltd.

Canan, K., Quark, M., Russell, S., Ostuni, S., Rockefeller, A., Williams, J., Culliton, S., Geurin, Z., & Birkebak, J. (2024). Introducing the Ohio Mushroom DNA Lab: Early lessons and contributions from a new community-driven nanopore sequencing laboratory. *McIlvainea, 33*, 2024.

Chen, L., Cai, Y., Zhou, G., Shi, X., Su, J., Chen, G., & Lin, K. (2014). Rapid Sanger sequencing of the 16S rRNA gene for identification of some common pathogens. *PLOS ONE, 9*(2), e88886. https://doi.org/10.1371/journal.pone.0088886

Dizkırıcı, A., Kalmer, A., & Acar, İ. (2019). Morphologic and molecular diagnosis of some *Leucoagaricus* species and revealing a new record from Turkey. *Mantar Dergisi, 10*(2), 143–150. https://doi.org/10.30708/mantar.590274

Felsenstein, J. (1985). Phylogenies and the comparative method. *The American Naturalist, 125*(1), 1–15.

He, M. Q., Zhao, R. L., Hyde, K. D., Begerow, D., Kemler, M., Yurkov, A., McKenzie, E. H. C., Raspe, O., Makoto, K., Sanchez-Ramirez, S., Vellinga, E. C., Halling, R., Papp, V., Zmitrovich, I. V., Buyck, B., Ertz, D., Wijayawardene, N. N., Bao-Kai, C., Schoutteten, N., Liu, X. Z., Li, T. H., Yao, Y. J., Zhu, X. Y., Liu, A. Q., Li, G. J., Zhang, M. Z., Ling, Z. L., Cao, B., Antonín, V., Boekhout, T., da Silva, B. D. B., De Crop, E., Decock, C., Dima, B., Dutta, A. K., Fell, J. W., Geml, J., Ghobad-Nejhad, M., Giachini, A. J., Gibertoni, T. B., Gorjon, S. P., Haelewaters, D., He, S. H., Hodkinson, B. P., Horak, E., Hoshino, T., Justo, A., Lim, Y. W., Menolli, N., Mešić, A., Moncalvo, J. M., Mueller, G. M., Nagy, L. G., Nilsson, R. H., Noordeloos, M., Nuytinck, J., Orihara, T., Ratchadawan, C., Rajchenberg, M., Silva-Filho, A. G. S., Sulzbacher, M. A., Tkalčec, Z., Valenzuela, R., Verbeken, A., Vizzini, A., Wartchow, F., Wei, T. Z., Weis, M., Zhao, C. L., & Kirk, P. M. (2019). Notes, outline and divergence times of Basidiomycota. *Fungal Diversity, 99*(1), 105–367. https://doi.org/10.1007/s13225-019-00435-4

Höhna, S., Landis, M. J., & Heath, T. A. (2017). Phylogenetic inference using RevBayes. *Current Protocols in Bioinformatics, 57*(1), 6.16.1–6.16.34. https://doi.org/10.1002/cpbi.2

Justo, A., Vizzini, A., Minnis, A. M., Menolli, N., Capelari, M., Rodriguez, O., Malysheva, E., Contu, M., Ghignone, S., & Hibbett, D. S. (2011). Phylogeny of the Pluteaceae (Agaricales, Basidiomycota): Taxonomy and character evolution. *Fungal Biology, 115*(1), 1–20. https://doi.org/10.1016/j.funbio.2010.09.012

Kalmer, A., Acar, İ., & Dizkırıcı, A. (2018). Phylogeny of some *Melanoleuca* species (Fungi: Basidiomycota) in Turkey and identification of *Melanoleuca angelesiana* A. H. Sm. as a first record. *Kastamonu University Journal of Forestry Faculty, 18*(3), 314–326. https://doi.org/10.17475/kastorman.499076

Kalmer, A., Dizkırıcı, A., & Acar, İ. (2022). Molecular and morphological identification of *Melanoleuca cinereifolia* from Türkiye. *Mantar Dergisi, 13*(2), 134–140. https://doi.org/10.30708/mantar.1125768

Kaşık, G., Alkan, S., Aktaş, S., Öztürk, C., & Akgül, H. E. (2022). Macrofungi of Yenice (Karabük) district and new records for Turkey. *Kahramanmaraş Sütçü İmam Üniversitesi Tarım ve Doğa Dergisi, 25*(6), 1264–1278. https://doi.org/10.18016/ksutarimdoga.vi.889463

Knudsen, H., & Vesterholt, J. (2008). *Funga Nordica: Agaricoid, boletoid and cyphelloid genera*. Nordsvamp.

Kornerup, A., & Wanscher, J. H. (1978). *Methuen handbook of colour* (3rd ed.). Eyre Methuen.

Patouillard, N. T. (1897). *Fungi: Catalogue raisonné des plantes cellulaires de la Tunisie*. Imprimerie Nationale.

Rogers, S. O., & Bendich, A. J. (1994). Extraction of total cellular DNA from plants, algae and fungi. In S. B. Gelvin & R. A. Schilperoort (Eds.), *Plant molecular biology manual* (pp. 183–190). Springer.

Ronquist, F., Teslenko, M., Van Der Mark, P., Ayres, D. L., Darling, A., Höhna, S., Larget, B., Liu, L., Suchard, M. A., & Huelsenbeck, J. P. (2012). MrBayes 3.2: Efficient Bayesian phylogenetic inference and model choice across a large model space. *Systematic Biology, 61*(3), 539–542. https://doi.org/10.1093/sysbio/sys029

Sanchez-Garcia, M., Cifuentes-Blanco, J., & Matheny, P. B. (2013). Taxonomic revision of the genus *Melanoleuca* in Mexico and description of new species. *Revista Mexicana de Biodiversidad, 84*(Suppl 1), S111–S127. https://doi.org/10.7550/rmb.31569

Schoch, C. L., Seifert, K. A., Huhndorf, S., Robert, V., Spouge, J. L., Levesque, C. A., Chen, W., & Fungal Barcoding Consortium. (2012). Nuclear ribosomal internal transcribed spacer (ITS) region as a universal DNA barcode marker for fungi. *Proceedings of the National Academy of Sciences, 109*(16), 6241–6246. https://doi.org/10.1073/pnas.1117018109

Uzun, Y., Kaya, A., Keleş, A., Akçay, M. E., & Acar, İ. (2009). Macromycetes of Genç district (Bingöl-Turkey). *International Journal of Botany, 5*(4), 301–306. https://doi.org/10.3923/ijb.2009.301.306

Vesterholt, J. (2008). *Melanoleuca* Pat. In H. Knudsen & J. Vesterholt (Eds.), *Funga Nordica: Agaricoid, boletoid and cyphelloid genera* (pp. 347–352). Nordsvamp.

Vizzini, A., Alvarado, P., Consiglio, G., Marchetti, M., & Xu, J. (2024). Family matters inside the order Agaricales: Systematic reorganization and classification of incertae sedis clitocyboid, pleurotoid and tricholomatoid taxa based on an updated 6-gene phylogeny. *Studies in Mycology, 107*(1), 67–148. https://doi.org/10.3114/sim.2024.107.02

Vizzini, A., Para, R., Fontenla, R., Ghignone, S., & Ercole, E. (2011). A preliminary ITS phylogeny of *Melanoleuca* (Agaricales), with special reference to European taxa. *Mycotaxon, 118*(1), 361–381. https://doi.org/10.5248/118.361

Xu, J., Yu, X., Lu, M., Hu, J., Moodley, O., Zhang, C., Gong, L., & Li, Y. (2019). Phylogenetic analyses of some *Melanoleuca* species (Agaricales, Tricholomataceae) in Northern China, with descriptions of two new species and the identification of seven species as a first record. *Frontiers in Microbiology, 10*, 2167. https://doi.org/10.3389/fmicb.2019.02167

Trakya University Journal of Natural Sciences, 26(2), 195–202, 2025
DOI: 10.23902/trkjnat.58745277
www.tujns.org

Research Article

Identification and phylogenetic analysis of two newly recorded *Hebeloma* species (Basidiomycota) from Türkiye

Ayşenur Kalmer[1], Sedat Kesici[2]* Ayten Tekpınar[1], Yusuf Uzun[3]

[1]*Van Yüzüncü Yıl University, Department of Molecular Biology and Genetics, Van, Türkiye*
[2]*Hakkâri University, Department of Plant and Animal Production, Hakkâri, Türkiye*
[3]*Van Yüzüncü Yıl University, Faculty of Pharmacy, Department of Pharmaceutical Sciences, Van, Türkiye*

Cite this article as: Kalmer, A., Kesici, S., Tekpınar, A., & Uzun Y. (2025). Identification and phylogenetic analysis of two newly recorded *Hebeloma* species (Basidiomycota) from Türkiye. *Trakya University Journal of Natural Sciences, 26*(2), 195–202. https://doi.org/10.23902/trkjnat.58745277

Abstract

Hebeloma species are ectomycorrhizal fungi that are widely distributed in nature and grow in a wide variety of habitats. *Hebeloma* spp. are difficult to identify and distinguish due to high morphological similarity between species. In this study, two newly recorded *Hebeloma* (Fr.) P. Kumm. species (*H. minus* Bruchet and *H. rostratum* Beker, Vesterh. & U. Eberh.) from Türkiye were described and photographed. Specimens were identified using morphological and molecular methods. Phylogenies based on the internal transcribed spacer (ITS) and translation elongation factor 1-alpha (TEF1-α) regions of the genome were constructed employing the Maximum-Likelihood method. In conclusion, a technique that combines morphological and molecular data provides a robust approach to assessing the taxonomic status of *Hebeloma* spp. Descriptions and photographs of the species are also presented.

Özet

Hebeloma türleri doğada geniş yayılım gösteren ektomikorizal mantarlardır ve çok çeşitli habitatlarda yetişirler**.** *Hebeloma* türleri, türler arasındaki yüksek morfolojik benzerlik nedeniyle tanımlanması ve ayırt edilmesi zordur. Bu çalışmada, Türkiye'den iki *Hebeloma* (Fr.) P. Kumm. türü (*H. minus* Bruchet ve *H. rostratum* Beker, Vesterh. & U. Eberh.) tanımlanmış ve fotoğraflanmıştır. Örnekler, moleküler ve morfolojik yöntemler kullanılarak belirlenmiştir. İç transkripsiyon aralayıcı (ITS) ve translasyon uzatma faktörü 1-alfa (TEF1-α) bölgelerinin filogenisi Maksimum Olasılık yöntemi kullanılarak oluşturulmuştur. Sonuç olarak, moleküler veriler ve morfolojinin birleşimi, *Hebeloma* türlerinin taksonomik durumunu değerlendirmek için sağlam bir yaklaşım sunmuştur. Türlerin ayrıntılı açıklamaları ve çizimleri verilmiştir.

Keywords: fungal systematics, ITS, molecular taxonomy, phylogeny, TEF1-α

Introduction

Hebeloma (Fr.) P. Kumm. (Basidiomycota, Hymenogastraceae) is a fungal genus growing widely over varying habitats and forming symbiotic relationships with various tree species (Cripps et al., 2019). Currently, more than 500 *Hebeloma* species have been recognized globally (https://www.indexfungorum.org), including a few undocumented ones. Beker et al. (2016) conducted a worldwide study and documented this genus comprehensively. In the *Hebeloma* monograph published by Beker et al. (2016), 84 species were recognized based on morphological and molecular characters. Additionally, 51 species were identified in other studies conducted by the Beker group (Cripps et al., 2019; Eberhardt et al., 2020; Eberhardt et al., 2021a, 2021b; Eberhardt et al., 2022a, 2022b, 2022c). In total, 135 species have been recorded globally

Edited by: *Boris Assyov*
***Corresponding Author:** Sedat Kesici, **E-mail:** sedatkesici@hakkari.edu.tr*
***ORCID iDs of the authors:** AK. 0000-0001-6176-8812, SK. 0000-0002-0284-1247, AT. 0000-0002-0578-5092, YU. 0000-0002-0537-4517*

Received: 13 March 2025, **Accepted:** 02 September 2025, **Online First**: 30 September 2025, **Published:** 15 October 2025

using morpho–molecular analysis, of which 35 have been identified in Türkiye (Dizkırıcı et al., 2019, 2022; Sesli et al., 2020; Acar et al., 2021, 2022, 2024; Solak & Türkoğlu, 2022; Lambert et al., 2024). Among them, only eight have been studied using molecular data (Dizkırıcı et al., 2019, 2022; Acar et al., 2021, 2022, 2024; Lambert et al., 2024).

Hebeloma species are morphologically characterized by a bicolored convex pileus, mostly yellowish–brown lamellae, a veil, and abundant cheilocystidia (Eberhardt et al., 2015, 2021b, 2022b; Beker et al., 2016). However, as identifying the species within this genus remains challenging, infrageneric classification requires both morphological and molecular data (Beker et al., 2016). The internal transcribed spacer (ITS) region is considered one of the most vital DNA barcodes applicable for species-level identification in fungal taxonomy (Schoch et al., 2012). It is commonly used in phylogenetic studies due to easy amplification, the availability of vast amounts of related data in the GenBank database, and a distinct barcode gap for species determination (Schoch et al., 2012). It can be utilized alone or in combination with protein-coding genes like the translation elongation factor 1-alpha (TEF1-α) to improve precision in the molecular identification of fungi (Tekpinar & Kalmer, 2019).

This study aimed to report and document two new records, *H. minus* Bruchet and *H. rostratum* Beker, Vesterh. & U. Eberh. from Türkiye, identified based on morphological features and molecular data. It also evaluates the phylogenetic affinities of the two species.

Materials and Methods

Fungal Materials and Morphological Observations

The *Hebeloma* specimens were collected from Hakkâri province of Türkiye. The samples were photographed in the field using an EOS 60D camera (Canon, Tokyo, Japan) equipped with an AT-X 100 mm macro lens (Tokina, Tokyo, Japan). The macroscopic characteristics were determined based on field notes and photographs. For microscopic examinations, thin cuttings from the lamellae and basidiomata surfaces were obtained with razor blades. They were then treated with distilled water and Melzer's reagent. The material was microscopically examined underwater to count basidiospores, cystidia, and basidia, and to determine other vital features, but in Melzer's solution to assay the dextrinoid reactions (Vesterholt, 2005; Beker et al., 2016). At least 50 spores, 40 basidia, and cheilocystidia were measured from each specimen of each recorded species. Observations were made using a DM500 research microscope (Leica Microsystems), and images were captured utilizing the Leica Application Suite (version 3.4.0). The length–width ratio of the basidiospores is referred to as "Q" in the text. The dextrinoid reaction of spores in the Melzer's reagent (Atom scientific) is mentioned as "D." The loosening of the spore perisporium in Melzer's reagent is noted as "P." The ornamentation of the spore is recorded as "O." All materials studied were preserved in the Fungarium of the Van Yüzüncü Yıl University, Van, Türkiye.

DNA Isolation and Sequencing

CTAB Doyle & Doyle, 1987). The ITS and TEF1-α regions were polymerase chain reaction (PCR)-amplified using the primer sets N-nc18S10/C26A (Wen & Zimmer, 1996) and EF1-983F/EF1-1567R (Rehner & Buckley, 2005). PCR was performed in a total volume of 25 µL, containing genomic DNA (10 ng/µL), 10X Buffer, $MgCl_2$ (25 mM), dNTP mix (10 mM), primer pair (10 µM), Taq Pol (5U/µL), and sterile water. The thermocycling conditions included, an initial denaturation at 94°C for 3 min, followed by 35 cycles of denaturation at 95°C for 1 min, annealing at 51°C (52°C for TEF1-α) for 35 s, and extension at 72°C for 40 s, with a final extension at 72°C for 5 min. The amplicons were separated using 1% TAE agarose gel and stained with Gelred dye. The positive reactions were bidirectionally sequenced using the same primer pairs on an ABI 3730XL automated sequencer at BM Labosis Inc., Ankara, Türkiye. The sequences generated were submitted to the GenBank, and their accession numbers are listed in Table 1.

Phylogenetic Analysis

The chromatograms were visualized using Finch TV (http://www.geospiza.com). Consensus sequences were generated and utilized for BLAST alignment against the sequences available in the National Center for Biotechnology Information (NCBI) database (https://www.ncbi.nlm.nih.gov/). The novel sequences were submitted to the NCBI and related taxa identified were downloaded to establish the phylogenetic relationships (Table 1). *H. mesophaeum* (Pers.) Quél. and *H. sacchariolens* Quél. were chosen as the outgroup taxa. All sequences were aligned using CLUSTALW (Thompson et al., 1994) and refined with the Mesquite v3.70 software (Maddison & Maddison, 2021).

Phylogenetic analyses utilized a concatenated ITS/TEF1-α dataset, and the Maximum-Likelihood (ML) method was applied. The best substitution model for each partition was calculated via the Modelfinder algorithm (Kalyaanamoorthy et al., 2017). ML analysis was performed with IQ-TREE v.1.6.12 (Nguyen et al., 2015) employing the K2P + R2 model. Branch support was assessed through 1,000 replicates of the ultrafast bootstrap (Hoang et al., 2018) and Shimodaira–Hasegawa-like approximate likelihood ratio tests (Guindon et al., 2010). The phylograms were visualized using Figtree v1.4.3 (Rambaut 2016).

Results

Taxonomy

Descriptions, locations, collection dates, fungarium numbers, and illustrations of the identified taxa are provided below.

***Hymenogastraceae* Vittad.**

Hebeloma* sect. *Denudata* subsect. *Crustliniformia

***H. minus* Bruchet, *Bull. Mens. Soc. Linn. Lyon* 39 (suppl. 6): 126 (1970), (Figure 1)**

Description: Pileus: 10–25(30) mm, shape convex to umbonate; generally bicolored, yellow–brown or dark brown in center, margin

Table 1. The species studied, along with their NCBI accession numbers, country of origin, voucher numbers, and citations.

Taxa	NCBI accession number (ITS)	NCBI accession number (TEF1-α)	Country/Voucher	References
Hebeloma ammophilum	KT217509	MZ782958	Hungary/HJB12374	Eberhardt et al. (2016)
Hebeloma alpinum	KM390654	KT216819	Switzerland/HJB12502	Eberhardt et al. (2015)
Hebeloma alpinum	MW445565	KT216820	Greenland/CF106775	Eberhardt et al. (2021b)
Hebeloma arcticum	MW445588	MW452585	Greenland/HJB17680	
Hebeloma aurantioumbrinum	MW445900	MW452577	Greenland/CF137117	
Hebeloma cavipes	KX905028	KT216780	Germany/KRM0044143	Direct submission
Hebeloma cavipes	KT217555	KT216799	United Kingdom/HJB13725	Eberhardt et al. (2016)
Hebeloma cinnamomeum	MZ782134	MZ782965	Japan/HJB16245	Eberhardt et al. (2022a)
Hebeloma crustuliniforme	KF309409	KT216854	England/HJB11215	Eberhardt et al. (2015)
Hebeloma crustuliniforme	KF309417	KT216824	Cyprus/HJB13430	
Hebeloma eburneum	JN943863	KT216777	Belgium/HJB11687	Direct submission
Hebeloma eburneum	KM390744	KT216853	Macedonia/HJB12772	Eberhardt et al. (2015)
Hebeloma geminatum	KM390554	KT216769	United Kingdom/HJB10766	
Hebeloma geminatum	KM390584	KT216815	Belgium/BRBELVJ03073	
Hebeloma helodes	MW445873	KT216810	Greenland/HJB15780	Eberhardt et al. (2021b)
Hebeloma hiemale	GQ869521	KT216848	Norway/HJB11964	Direct submission
Hebeloma lutense	KM390631	KT216798	United Kingdom/HJB12917	Eberhardt et al. (2015)
Hebeloma mesophaeum	MK961995	ON167781	Iceland/HJB11050	Eberhardt et al. (2020)
Hebeloma minus	KM390751	KT216842	France/LYBR6915	Eberhardt et al. (2015)
Hebeloma minus	JN943872	KT216818	Iceland/ue3984	Direct submission
Hebeloma minus	KM390664	KT216816	France/LWBS9630	Eberhardt et al. (2015)
Hebeloma minus	PV124179	PV156016	Türkiye/16SDT	This study
Hebeloma minus	PV124180	PV156017	Türkiye/4SDT	
Hebeloma minus	PV124181	PV156018	Türkiye/5SDT	
Hebeloma pallidolabiatum	KM390703	KT216840	Norway/HJB11992	Eberhardt et al. (2015)
Hebeloma pallidolabiatum	KM390713	KT216846	Norway/HJB12059	
Hebeloma populinum	KT217560	KT216861	United Kingdom/HJB13758	Eberhardt et al. (2016)
Hebeloma populinum	KT217563	KT216862	Greece/HJB14114	
Hebeloma pusillum	KM390665	KT216835	France/HJB12515	Eberhardt et al. (2015)
Hebeloma rostratum	KT217532	KT216829	Germany/HJB13009	Eberhardt et al. (2016)
Hebeloma rostratum	KT217534	KT216855	Italy/TUR177056	
Hebeloma rostratum	KT217535	KT216774	France/HJB13139	
Hebeloma rostratum	PV124182	PV156019	Türkiye/50SDT	This study
Hebeloma rostratum	PV124183	PV156020	Türkiye/178SDT	
Hebeloma sacchariolens	KT218266	KT217618	Italy/HJB10321	Grilli et al. (2016)
Hebeloma salicicola	KM390682	KT216788	Netherlands/HJB12533	Eberhardt et al. (2015)
Hebeloma vaccinum	MF039237	MZ782984	Belgium/HJB11578	Eberhardt et al. (2018)
Hebeloma vaccinum	MW445835	MZ782985	Greenland/HJB17076	Eberhardt et al. (2021b)

ITS = internal transcribed spacer; NCBI = National Center for Biotechnology Information; TEF1-α = translation elongation factor 1-alpha

smooth, sometimes curly. **Lamellae:** emarginate, occasionally adnate, L = 26–40. Cortina absent. **Stipe:** 10–30(40) × 2–8 mm, generally cylindrical, clavate, often pruinose. **Odor:** absent or slightly radish-like. **Basidiospores:** (8.6)9–15 × 5–7(7.9) µm (n = 50), on average 12.8 × 6.4 ± 0.9 (length), ± 0.4 (width); Q = 1.6–1.91, amygdaliform, brown or yellow–brown, ornamentation distinct (O2–O3), no loosening perispore (P0–P1), slightly dextrinoid (D1–D2). **Basidia:** 27–40 × 7–15 µm (n = 40), four-

Figure 1. *Hebeloma minus.* (a–c) basidiomata; (d) basidia; (e) spores (H_2O); (f) spores (Melzer); (g–h) cheilocystidia.

spored. **Cheilocystidia:** 35–70(80) × 7(8)–10(14) × 3–7 × 2–7(8) µm (n = 40), on average 40–62 × 7–10 (apex) × 3–5 (middle) × 3–6 (base) µm, usually clavate–stipitate, often capitate–stipitate, contents yellow. **Caulocystidia:** like cheilocystidia, up to 100 µm.

Specimen examined: Hakkâri, Yüksekova, Adaklı Village, meadow area, 37°31′34″N and 44°10′12″E, elev. 1,870 m a.s.l., 03.11.2012; VANF4, leg. S. Kesici. 37°31′39″N and 44°10′04″E, elev. 1,872 m a.s.l., 03.11.2012; VANF5, leg. S. Kesici. 37°31′35″N and 44°10′11″E, elev. 1,868 m a.s.l., 03.11.2012; VANF16, leg. S. Kesici.

Notes: *H. minus* is classified within the *Denudata* section with its clavate cheilocystidia (Beker et al., 2016). The species is distinguished from other members of the section by its mostly ornamented basidiospores. The monograph by Beker et al. (2016) states that the species prefers Arctic tundra habitats with mossy soils. Eastern Anatolia and its environs are included in the Irano–Turanian phytogeographical region of Türkiye. The Irano–Anatolian region is a mountainous area, and Parolly (2004) classified it as high mountain grasslands. *H. minus* specimens have also been found in the high mountain grassland areas of Türkiye.

Hebeloma sect. *Denudata* subsect. *Echinospora*

H. rostratum Beker, Vesterh. & U. Eberh., *Fungal Biol.* 120: 96 (2015), (Figure 2)

Description: Pileus: 16–35(40) mm, shape convex, sometimes umbonate, generally bicolored; yellow–brown, cream-brown, cream, dark brown in center, margin curly, sometimes smooth. **Lamellae:** generally emarginate, adnate, L = 30–65. Cortina absent. **Stipe:** 20–45(50) × 2–6 mm, cylindrical at the base, clavate, floccose at the apex. **Odor:** absent or slightly radish-like. **Basidiospores:** 6–13(14.6) × (5.5)6–8(8.7) µm (n = 50), on average 11.2 × 6.7 ± 0.7 (length), ± 0.33 (width); Q = 1.62–1.95, amygdaliform, yellow–brown; strongly ornamented (O3–O4), loosening perisporium (P2–P3), strongly dextrinoid (D3–D4). **Basidia:** 24−45 × 6−10 µm (n = 40), four-spored. **Cheilocystidia:** 40–60(90) × 3(4)–7 × 3–6(8) × 4–10(12) µm (n = 40), on average 44–65 × 5–7 (apex) × 4–6 (middle) × 6–9 (base) µm, often clavate–lageniform or clavate–ventricose, bifurcate, rostrate, contents yellow. **Caulocystidia:** like cheilocystidia, larger, up to 120 µm.

Specimen examined: Hakkâri, Yüksekova, Gürdere Village, under *Populus* spp., 37°29′48″N and 44°12′53″E, elev. 1,962 m a.s.l., 06.11.2012; VANF50, leg. S. Kesici. 37°30′08″N and

Figure 2. *Hebeloma rostratum*. (a–b) basidiomata; (c) basidia; (d) spores (H_2O); (e) spores (Melzer); (f) cheilocystidia.

44°12′50″E, elev. 1,894 m a.s.l., 03.11.2013; VANF178, leg. S. Kesici.

Notes: This species of the *Denudata* section is distinguished from other members by its rostrate-shaped cheilocystidia and cheilocystidia apex measuring up to 98 µm (Beker et al., 2016). According to the monograph of Beker et al. (2016), *H. rostratum* prefers grassy or marshy soils. The most recorded associations of this species were with *Populus* spp. (Beker et al., 2016). Turkish specimens have also been found under *Populus* spp.

Phylogenetic Analyses

The DNA sequences of the ITS and TEF1-α genomic regions of *H. minus and H. rostratum* specimens were deposited in the GenBank database. After removing the missing data and ambiguous regions, the final ITS and TEF1-α datasets were 567 and 524 bp long, respectively. In total, 127 and 89 variable sites were identified in the ITS and TEF1-α datasets, respectively. The length of the concatenated sequence was ~1,158 bp, comprising 176 variable sites.

The combined dataset consisting of 38 sequences, including the five studied here and two outgroups, was utilized to construct the phylogenetic tree. It illustrated the phylogenetic relations and taxonomic positions of the species studied (Figure 3). Members of the *Denudata* section formed a monophyletic clade with robust support (100%). The section was subdivided into two main clusters: the newly recorded *H. minus* species clustered within clade A (subsect. *Crustuliniformia*) with reference sequences of the same species with robust support (99%), and *H. rostratum* grouped closely with its representatives in clade B (subsect. *Echinospora*) with high support (99%). These results provide strong evidence for the taxonomic classification of both species within the section *Denudata* with high bootstrap values.

Discussion

The present study provided morphological descriptions of two newly recorded species of the *Hebeloma* genus from Türkiye. They were identified based on morphological features and then verified using molecular data. After confirmation, the phylogenetic relationships of these species with close relatives within the genus were established.

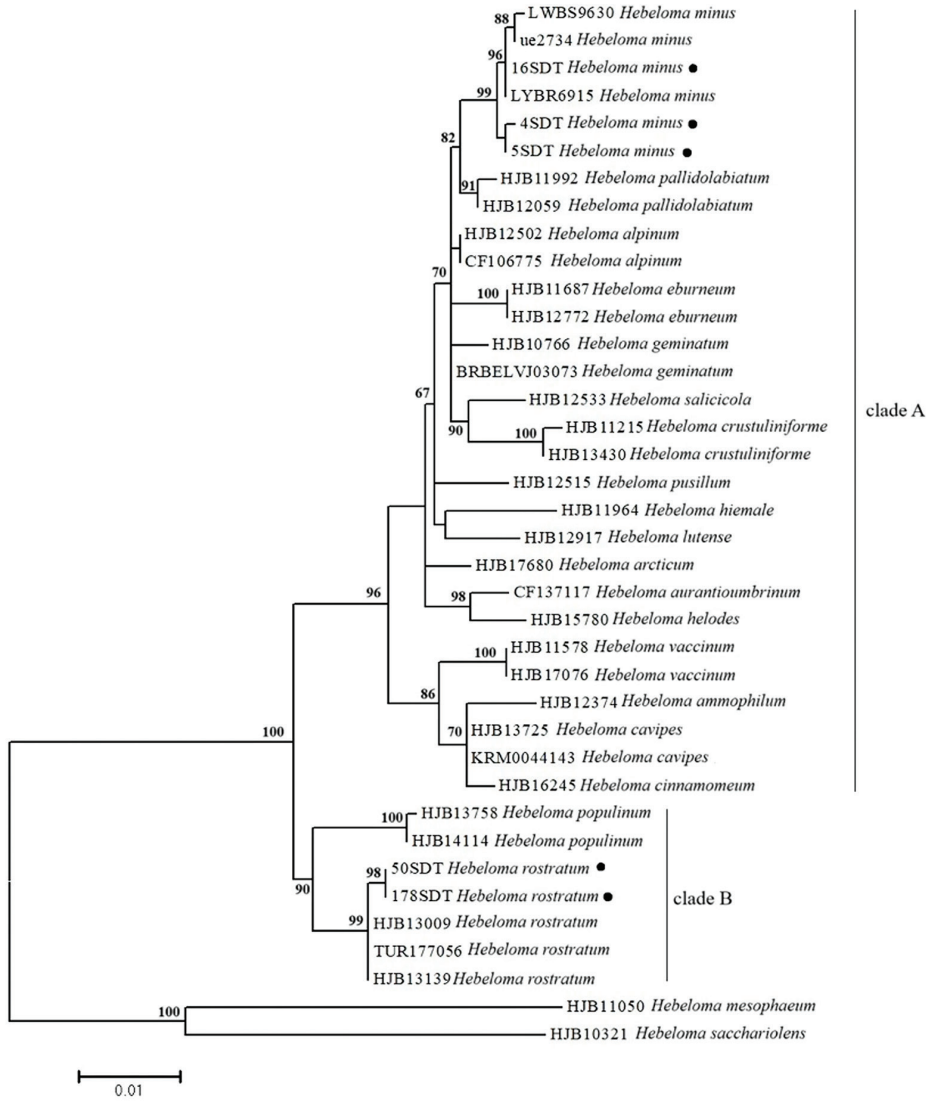

Figure 3. Phylogram of the Maximum-Likelihood analysis using the combined ITS + TEF1-α dataset. The newly generated sequences were marked with black circles. The numbers representing the likelihood bootstrap support (≥ 60%) are shown above the nodes.

The species presented in this study were included in the *Denudata* section, which is the largest within the *Hebeloma* genus. The most important feature of this section is the cheilocystidia morphology, with swollen apices and constricted midsections. Members of this section generally lack a cortina, and their odor is usually described as radish-like. The lamellae typically have clear droplets. Basidiospores are usually almond-shaped. The spore codes were O1–3; P0–2; and D1–3, on an average. The average spore size was 9−12 × 5−7.5 µm, and the mean Q value was 1.60−2.10. The average length of the cheilocystidia was between 40 and 75 µm (Beker et al., 2016). Eberhardt et al. (2016) recognized four subsections: *Crustuliniformia*, *Clepsydroida*, *Hiemalia*, and *Echinospora* within this section. *Crustuliniformia* is characterized by clavate–stipitate and clavate–capitate cheilocystidia. Clavate–stipitate to clavate–ventricose cheilocystidia indicate that a species is from *Echinospora* (Beker et al., 2016; Eberhardt et al., 2016).

The phylogeny presented in this work confirmed that *H. minus* belongs to *Crustuliniformia*. It can be distinguished from other members by its highly ornamented spores (Eberhardt et al., 2016). *H. minus* occupied a clearly distinct position in the phylogenetic tree and was closely related to *H. pallidolabiatum* Beker & U. Eberh. These two species resembled one another, but could be distinguished microscopically based on the shape of cheilocystidia and ornamentation of the spores, which were often capitate–stipitate and O2–3 for *H. minus* but clavate–lageniform and O2 for *H. pallidolabiatum* (Beker et al., 2016). *H. minus* was also macroscopically similar to *H. alpinum* (J. Favre) Bruchet. However, detailed examinations revealed that *H. minus* had smaller basidiomes with a darker coloration and fewer full-length lamellae, with counts < 40. This was in contrast to *H. alpinum,* which consistently exhibited ≥ 40 full-length lamellae (Cripps et al., 2019; Eberhardt et al., 2021b).

H. rostratum belongs to *Echinospora* and is characterized by clavate–ventricose cheilocystidia and amygdaliform-shaped spores (Eberhardt et al., 2016). It draws attention via its rostrate cheilocystidia that distinguish it from other species within the section when examined microscopically. The species was first collected in Italy by Eberhardt et al. (2016) and reported to grow under *Salix* and *Populus* spp. *H. rostratum* occupied a clearly distinct position in the phylogram and was closely related to *H. populinum* Romagn. The *H. rostratum* specimens studied can be differentiated based on highly warty spores and cheilocystidia apex with dimensions averaging < 7.5 µm.

Conclusion

Türkiye harbors a noticeable climatic and phytogeographical diversity, supporting a wide variety of vegetation. It is hypothesized that many fungal species are yet to be discovered in this country. The fact that species belonging to *Hebeloma* have been studied extensively across the globe has enabled the construction of a comprehensive database. It allows us to cluster a newly discovered species into collections with similar characteristics and to compare the collection parameters within the same phylogenetic clade. Considering such a situation, the lack of data for this genus in Türkiye is a serious scientific lacuna. Being aware of this deficiency, we performed diagnostic studies on the samples collected during every field study and accumulated data for *Hebeloma*. Based on the data collected in the present work, we report two new species from Türkiye and present them to the scientific community.

Ethics

Ethics Committee Approval: Since the article does not contain any studies with human or animal subject, its approval to the ethics committee was not required.

Data Sharing Statement: Data available on reasonable request.

Footnotes

Author Contributions: Conceptualization: A.K.; Design/methodology: A.K.; Execution/investigation: A.K.; Resources/materials: S.K., and Y.U.; Data acquisition: A.K.; Data analysis/interpretation: A.K.; Writing – original draft: A.K., and A.T.; Writing – review & editing/critical revision: A.T.

Conflict of Interest: The authors have no conflicts of interest to declare.

Funding: The authors declared that this study has received no financial support.

References

Acar, I., Dizkırıcı, A., Kalmer, A., & Uzun, Y. (2022). Hebeloma bingolense, a new species in section Hebeloma (Basidiomycota) from Turkey. Nova Hedwigia, 114(1–2), 55–68. https://doi.org/10.1127/nova_hedwigia/2022/0673

Acar, İ., Kalmer, A., & Dizkırıcı, A. (2024). Confirmation of Hebeloma salicicola (Basidiomycota) from Türkiye. Austrian Journal of Mycology, 31, 89–97.

Acar, I., Uzun, Y., Kalmer, A., Dizkırıcı, T. A., & Öğün, Y. (2021). A new record for Turkish mycobiota from Selim (Kars) district. The Journal of Fungus, 12(1), 65–70. https://doi.org/10.30708/mantar.820871

Beker, H. J., Eberhardt, U., & Vesterholt, J. (2016). Fungi Europaei 14, Hebeloma (Fr.) P. Kumm. Edizioni Candusso.

Cripps, C. L., Eberhardt, U., Schütz, N., Beker, H. J., Evenson, V. S., & Horak, E. (2019). The genus Hebeloma in the Rocky Mountain alpine zone. MycoKeys, 46, 1–54. https://doi.org/10.3897/mycokeys.46.32823

Dizkırıcı, A., Acar, I., Kalmer, A., & Uzun, Y. (2019). Morphological and molecular characterization of Hebeloma subtortum (Hymenogastraceae), a new record macrofungus from Bingöl Province, Turkey. Kastamonu University Journal of Forestry Faculty, 19(1), 1–10. https://doi.org/10.17475/kastorman.543375

Dizkırıcı, A., Kalmer, A., & Acar, I. (2022). New Turkish records of Hebeloma excedens and H. geminatum, and confirmation of H. celatum. Mycotaxon, 137, 123–134. https://doi.org/10.5248/137.123

Doyle, J. J., & Doyle, J. L. (1987). A rapid DNA isolation procedure for small quantities of fresh leaf tissue. Phytochemical Bulletin, 19, 11–15.

Eberhardt, U., Beker, H. J., & Vesterholt, J. (2015). Decrypting the Hebeloma crustuliniforme complex: European species of Hebeloma section Denudata subsection Denudata (Agaricales). Persoonia, 35, 101–147. https://doi.org/10.3767/003158515X687704

Eberhardt, U., Beker, H. J., Borgen, T., Knudsen, H., Schütz, N., & Elborne, S. A. (2021b). A survey of Hebeloma (Hymenogastraceae) in Greenland. MycoKeys, 79, 17–118. https://doi.org/10.3897/mycokeys.79.63363

Eberhardt, U., Beker, H. J., Schütz, N., Pedersen, O. S., Sysouphanthong, P., & Læssøe, T. (2020). Adventurous cuisine in Laos: Hebeloma parvisporum, a new species in Hebeloma section Porphyrospora. Mycologia, 112(1), 172–184. https://doi.org/10.1080/00275514.2019.1680220

Eberhardt, U., Beker, H. J., Vesterholt, J., & Schütz, N. (2016). The taxonomy of the European species of Hebeloma section Denudata subsections Hiemalia, Echinospora subsect. nov. and Clepsydroida subsect. nov. and five new species. Fungal Biology, 120, 72–103. https://doi.org/10.1016/j.funbio.2015.09.014

Eberhardt, U., Kong, A., Montoya, A., Schütz, N., Bartlett, P., & Beker, H. J. (2022b). Not (only) poison pies – Hebeloma (Agaricales, Hymenogastraceae) in Mexico. MycoKeys, 90, 163–202. https://doi.org/10.3897/mycokeys.90.85267

Eberhardt, U., Schütz, N., Bartlett, P., & Beker, H. J. (2022c). 96 North American taxa sorted – Peck's Hebeloma revisited. Mycologia, 114(2), 337–387. https://doi.org/10.1080/00275514.2021.2012063

Eberhardt, U., Schütz, N., Bartlett, P., Hosaka, K., Kasuya, T., & Beker, H. J. (2022a). Revisiting Hebeloma (Hymenogastraceae, Agaricales) in Japan: Four species recombined into other genera but three new species discovered. Mycological Progress, 21, 447–472. https://doi.org/10.1007/s11557-021-01757-x

Eberhardt, U., Schütz, N., Beker, H. J., Lee, S. S., & Horak, E. (2021a). Hebeloma in the Malay Peninsula: Masquerading within Psathyrella. MycoKeys, 77, 117–141. https://doi.org/10.3897/mycokeys.77.57394

Eberhardt, U., Schütz, N., Krause, C., & Beker, H. J. (2018). Hebelomina (Agaricales) revisited and abandoned. Plant Ecology and Evolution, 151(1), 96–109. https://doi.org/10.5091/plecevo.2018.1361

FinchTV (2025). Geospiza. http://www.geospiza.com (Accessed February 17, 2025).

Grilli, E., Beker, H. J., Eberhardt, U., Schütz, N., Leonardi, M., & Vizzini, A. (2016). Unexpected species diversity and contrasting evolutionary hypotheses in Hebeloma (Agaricales) sections Sinapizantia and Velutipes in Europe. Mycological Progress, 15(5), 1–15. https://doi.org/10.1007/s11557-015-1148-6

Guindon, S., Dufayard, J. F., Lefort, V., Anisimova, M., Hordijk, W., & Gascuel, O. (2010). New algorithms and methods to estimate maximum-likelihood phylogenies: Assessing the performance of PhyML 3.0. Systematic Biology, 59(3), 307–321. https://doi.org/10.1093/sysbio/syq010

Hoang, D. T., Chernomor, O., von Haeseler, A., Minh, B. Q., & Vinh, L. S. (2018). UFBoot2: Improving the ultrafast bootstrap approximation. Molecular Biology and Evolution, 35, 518–522. https://doi.org/10.1093/molbev/msx281

Index Fungorum. (2025). Index Fungorum. https://www.indexfungorum.org (Accessed May 12, 2025).

Kalyaanamoorthy, S., Minh, B. Q., Wong, T. K. F., von Haeseler, A., & Jermiin, L. S. (2017). ModelFinder: Fast model selection for accurate phylogenetic estimates. Nature Methods, 14, 587–589. https://doi.org/10.1038/nmeth.4285

Lambert, H., Acar, I., Dizkirici Tekpinar, A., Fortin, G., Ivanushkina, N., Jacobs, K., Lamoureux, Y., Landry, J., Lebeuf, R., Kachalkin, A., Kalmer, A., Moncalvo, J. M., Paul, A., Van der Merwe, B., Williams, J., Zervakis, G. I., Kochkina, G., Vainshtein, M., Dima, B., Dovana, F., Ferisin, G., Malysheva, E., Papp, V., Ševčíková, H., Krisai-Greilhuber, I., & Haelewaters, D. (2024). Fungal systematics and evolution: FUSE 10. Sydowia, 76, 297–365. https://doi.org/10.12905/0380.sydowia76-2024-0297

Maddison, W. P., & Maddison, D. R. (2021). Mesquite: A modular system for evolutionary analysis (Version 3.7.0). http://www.mesquiteproject.org

National Center for Biotechnology Information (NCBI). (2025). National Center for Biotechnology Information. Bethesda, MD: National Library of Medicine (US). https://www.ncbi.nlm.nih.gov/

Nguyen, L. T., Schmidt, H. A., von Haeseler, A., & Minh, B. Q. (2015). IQ-TREE: A fast and effective stochastic algorithm for estimating maximum likelihood phylogenies. Molecular Biology and Evolution, 32, 268–274. https://doi.org/10.1093/molbev/msu300

Parolly, G. (2004). The high mountain vegetation of Turkey: A state-of-the-art report, including a first annotated conspectus of the major syntaxa. Turkish Journal of Botany, 28, 39–63.

Rambaut, A. (2016). FigTree: Tree figure drawing tool (Version 1.4.3). http://tree.bio.ed.ac.uk/

Rehner, S. A., & Buckley, E. (2005). A Beauveria phylogeny inferred from nuclear ITS and EF1-α sequences: Evidence for cryptic diversification and links to Cordyceps teleomorphs. Mycologia, 97, 84–89. https://doi.org/10.1080/15572536.2006.11832842

Schoch, C. L., Seifert, K. A., Huhndorf, S., Robert, V., Spouge, J. L., Levesque, C. A., & Chen, W. (2012). Nuclear ribosomal internal transcribed spacer (ITS) region as a universal DNA barcode marker for fungi. Proceedings of the National Academy of Sciences, 109, 6241–6246. https://doi.org/10.1073/pnas.1117018109

Sesli, E., Asan, A., Selçuk, F., Abacı Günyar, Ö., Akata, I., Akgül, H., Aktaş, S., Alkan, S., Allı, H., Aydoğdu, H., Berikten, D., Demirel, K., Demirel, R., Doğan, H. H., Erdoğdu, M., Ergül, C. C., Eroğlu, G., Giray, G., Halikî Uztan, A., Kabaktepe, Ş., Kadaifçiler, D., Kalyoncu, F., Karaltı, İ., Kaşık, G., Kaya, A., Keleş, A., Kırbağ, S., Kıvanç, M., Ocak, İ., Ökten, S., Özkale, E., Öztürk, C., Sevindik, M., Şen, B., Şen, İ., Türkekul, İ., Ulukapı, M., Uzun, Y., & Yoltaş, A. (2020). Türkiye mantarları listesi (The checklist of fungi of Türkiye). Ali Nihat Gökyiğit Vakfı Yayını.

Solak, M., & Türkoğlu, A. (2022). Macrofungi of Turkey, checklist (Vol. 3). Kanyılmaz Matbaacılık.

Tekpinar, A. D., & Kalmer, A. (2019). Utility of various molecular markers in fungal identification and phylogeny. Nova Hedwigia, 109(1–2), 187–224. https://doi.org/10.1127/nova_hedwigia/2019/0528

Thompson, J. D., Higgins, D. G., & Gibson, T. J. (1994). CLUSTAL W: Improving the sensitivity of progressive multiple sequence alignment through sequence weighting, position-specific gap penalties and weight matrix choice. Nucleic Acids Research, 22, 4673–4680. https://doi.org/10.1093/nar/22.22.4673

Vesterholt, J. (2005). The genus Hebeloma (Fungi of Northern Europe, Vol. 3). Danish Mycological Society.

Wen, J., & Zimmer, E. A. (1996). Phylogeny and biogeography of Panax L. (the ginseng genus, Araliaceae): Inferences from ITS sequences of nuclear ribosomal DNA. Molecular Phylogenetics and Evolution, 6, 167–177. https://doi.org/10.1006/mpev.1996.0069

Trakya University Journal of Natural Sciences, 26(2), 203–212, 2025
DOI: 10.23902/trkjnat.59587078
www.tujns.org

Research Article

Advanced deep learning approaches for the automated classification of macrofungal species in biodiversity monitoring

Şifa Özsarı[1,2], Eda Kumru[3], Fatih Ekinci[4], Mehmet Serdar Güzel[1], Koray Açıcı[5], Tunç Aşuroğlu[6], Ilgaz Akata[7]*

[1]*Ankara University, Faculty of Engineering, Department of Computer Engineering, Ankara, Türkiye*
[2]*Ankara University, Faculty of Engineering, Department of Computer Sciences, Ankara, Türkiye*
[3]*Ankara University, Graduate School of Natural and Applied Sciences, Ankara, Türkiye*
[4]*Ankara University, Institute of Artificial Intelligence, Ankara, Türkiye*
[5]*Ankara University, Faculty of Engineering, Department of Artificial Intelligence and Data Engineering, Ankara, Türkiye*
[6]*Tampere University, Faculty of Medicine and Health Technology, Tampere, Finland*
[7]*Ankara University, Faculty of Science, Department of Biology, Ankara, Türkiye*

Cite this article as: Özsarı, Ş., Kumru, E., Ekinci F., Güzel, M. S., Açıcı K., Aşuroğlu T., & Akata, I. (2025). Advanced deep learning approaches for the automated classification of macrofungal species in biodiversity monitoring. *Trakya University Journal of Natural Sciences, 26*(2), 203–212. https://doi.org/10.23902/trkjnat.59587078

Abstract

Macrofungal species attract significant attention due to their critical roles in ecosystems and widespread industrial applications. Traditional species identification methods are expertise-intensive and time-consuming processes. Artificial intelligence (AI) techniques, especially, deep learning (DL), have been employed to accelerate these processes and improve result accuracy. This article aimed to classify five macrofungi using AI, specifically DL. The study focuses on classifying *Amanita muscaria*, *A. phalloides*, *Lepista nuda*, *Macrolepiota procera*, and *Craterellus cornucopioides*, utilizing various DL models, including DenseNet121, InceptionV3, MobileNetV2, Xception, VGG16, and ResNet101. The dataset comprised 683 images across five classes. The data were collected in a balanced manner, and the model's effectiveness was evaluated based on accuracy, precision, recall, and F1-score metrics. Additionally, Grad-CAM visualizations were utilized to analyze the regions of focus. The best-performing model achieved 93% accuracy (7% error), outperforming a simple Convolutional Neural Network baseline with 70% accuracy (30% error). Overall, all transfer-learning models achieved accuracies of ≥ 90%. In particular, the DenseNet121 and Xception models achieved the maximum success by correctly

Özet

Makromantar türleri, ekosistemlerdeki kritik rolleri ve geniş endüstriyel uygulamaları nedeniyle dikkat çekmektedir. Geleneksel tür teşhis yöntemleri uzmanlık gerektiren ve zaman alıcı süreçlerdir; bu nedenle yapay zekâ (YZ), özellikle derin öğrenme (DÖ) teknikleri, bu süreçleri hızlandırmak ve doğruluğu artırmak amacıyla kullanılmaktadır. Bu makale, beş farklı makromantar türünü YZ, özelde DÖ teknikleri kullanarak otomatik olarak sınıflandırmayı amaçlamaktadır. Çalışma kapsamında *Amanita muscaria, A. phalloides, Lepista nuda, Macrolepiota procera* ve *Craterellus cornucopioides* türleri ele alınmış; bu türlerin sınıflandırılmasında DenseNet121, InceptionV3, MobileNetV2, Xception, VGG16 ve ResNet101 gibi çeşitli derin öğrenme modelleri kullanılmıştır. Veri kümesi, 5 sınıfta toplam 683 görüntüden oluşmaktadır. Veriler dengeli bir şekilde toplanmış ve modellerin etkinliği doğruluk, kesinlik (precision), duyarlılık (recall) ve F1-skoru gibi metrikler üzerinden değerlendirilmiştir. Ayrıca modellerin hangi bölgelere odaklandığını analiz etmek amacıyla Grad-CAM görselleştirmeleri kullanılmıştır. En iyi performansı gösteren model %93 doğruluk (%7 hata) elde etmiş, %70 doğruluk (%30 hata) sağlayan basit bir Evrimsel Katmanlı Sinir Ağı temel modelini belirgin biçimde geride bırakmıştır; genel olarak, tüm transfer öğrenimi modelleri %90 ve üzeri doğruluklara ulaşmıştır.

Edited by: *Kadri Kıran*

***Corresponding Author:** Ilgaz Akata, **E-mail:** akata@science.ankara.edu.tr*

***ORCID iDs of the authors:** ŞÖ. 0000-0002-0531-4645; EK. 0009-0000-7417-6197; FE. 0000-0002-1011-1105; MSG. 0000-0002-3408-0083; KA. 0000-0002-3821-6419; TA. 0000-0003-4153-0764; IA. 0000-0002-1731-1302*

Received: 29 May 2025, **Accepted:** 14 September 2025, **Online First**: 30 September 2025, **Published:** 15 October 2025

identifying relevant regions of these species. The study demonstrates that AI, particularly DL-based techniques, can be effectively applied in species identification. Expanding datasets could further enhance their performance. The novelty of this study is the use of a combination of transfer-learning and Grad-CAM explainability to provide an interpretable and biologically meaningful framework for macrofungi identification.

Özellikle DenseNet121 ve Xception modelleri, makromantar türlerine ait ilgili bölgeleri doğru şekilde tespit ederek en yüksek başarıyı sağlamıştır. Bu çalışma, biyolojik tür teşhisinde YZ, özellikle DÖ tekniklerinin etkin bir şekilde kullanılabileceğini ortaya koymakta ve veri setlerinin genişletilmesinin bu tekniklerin başarısını daha da artırabileceğini göstermektedir. Bu çalışmanın yeniliği, transfer öğrenmeyi Grad-CAM açıklanabilirliği ile birleştirerek makrofungusların tanımlanmasına yönelik yorumlanabilir ve biyolojik açıdan anlamlı bir çerçeve sunmasıdır.

Keywords: deep learning, macrofungi classification, artificial ıntelligence, Grad-CAM visualization, biodiversity monitoring

Introduction

Fungi play vital roles in ecosystems and have significant industrial and medicinal applications (Chugh et al., 2022; Llanaj et al., 2023). Macrofungi, primarily belonging to the *Basidiomycota* and *Ascomycota* phyla, are notable for their large fruiting bodies and comprise ~41,000 known species, with > 2,000 being edible (Priyamvada et al., 2017; Li et al., 2021; Ekinci et al., 2025). They contribute to forest health management through symbiotic relationships with trees, breaking down organic matter and recycling nutrients (de Mattos-Shipley et al., 2016; Ye et al., 2019; Ozsari et al., 2024). In addition to their ecological roles, macrofungi are valued for their bioactive compounds, which are utilized in medicine and explored for their potential applicability in biodegradation and as renewable resources (Cheong et al., 2018; Hyde et al., 2019; El-Ramady et al., 2022).

Integrating ML and computer vision into mycological research and citizen science is revolutionizing macrofungal identification and classification (Picek et al., 2022; Ozsari et al., 2024; Korkmaz et al., 2025). Traditional identification methods, which require extensive expertise and are often time-consuming, are being superseded by artificial intelligence (AI)-based systems capable of rapidly analyzing large datasets and distinguishing minute variations in shape, color, and texture (Yan et al., 2023). AI democratises this process by providing intuitive mobile applications, enabling individuals who are not experts to identify macrofungi from photographs, thereby substantially mitigating the risk of misidentification (Chathurika et al., 2023; Ekinci et al., 2025; Kumru et al., 2025). These AI models evolve by incorporating community-contributed data, ensuring their relevance to new findings (Bartlett et al., 2022). Moreover, the ability of AI to analyze environmental variables along with visual characteristics enhances ecological research and conservation efforts. By engaging scientists and the general public in collaborative biodiversity monitoring, AI helps generate more precise and comprehensive datasets, which are crucial for informed conservation strategies (Yan et al., 2023). The application of AI in mycology markedly advances macrofungal identification by offering speed, precision, accessibility, and robust data handling, thereby benefiting from scientific research and public involvement in research on fungal biodiversity (Picek et al., 2022). Although these studies demonstrate the potential of AI, they have not meaningfully integrated performance with interpretability, highlighting a gap that the present study seeks to address.

This study aims to classify five species of macrofungi: *Amanita muscaria*, *A. phalloides*, *Lepista nuda*, *Macrolepiota procera*, and *Craterellus cornucopioides* using deep learning (DL). The five macrofungal species were specifically chosen because they represent both toxic and edible taxa with high ecological and societal importance. Their morphological similarities often led to frequent misidentifications in the field. These were selected for their ecological significance and morphological diversity. The objective was to develop a model that can quickly and accurately identify these species based on their visual characteristics.

The novelty of this study lies in the application of DL techniques to achieve high-accuracy classification. Its contributions may represent a significant advancement in the *in silico* identification of macrofungal species, supporting the conservation of natural habitats and biodiversity monitoring. The technical contributions of this study include a systematic comparison of six transfer-learning architectures, the integration of Grad-CAM to ensure biologically meaningful interpretability, and benchmarking against a Convolutional Neural Network (CNN) baseline to demonstrate methodological advances. AI-based approaches have been applied in mycology, systematic research combining multiple DL architectures with interpretability-associated analyses, such as Grad-CAM, remains limited (Raghavan et al., 2024). Addressing these challenges, this study not only provides a performance benchmark applicable to varied state-of-the-art DL architectures but also an interpretable framework through Grad-CAM, thereby extending beyond the available DL-based biodiversity monitoring works that mainly emphasized accuracy. This study, therefore, contributes to taxonomy by providing a more comprehensive evaluation that highlights the significance of model performance and interpretability in macrofungal classification. In this context, the models DenseNet121 (Huang et al., 2017), InceptionV3 (Szegedy et al., 2016), MobileNetV2 (Sandler et al., 2018), Xception (Chollet, 2017), VGG16 (Simonyan & Zisserman, 2014), and ResNet101 (He et al., 2016), which have demonstrated considerable efficacy in classification, were employed.

Materials and Methods

Dataset

For this study, some macrofungal images were sourced from publicly accessible website primarily the Global Biodiversity Information Facility (www.gbif.org). We photographed the other specimens. Before their use, the publicly available images were modified, and all sources have been cited. The number of photographs taken by the authors was lower than that acquired from the websites (GBIF.org). The primary reason for this difference was the difficulty in locating all species simultaneously. Furthermore, obtaining the required quantity of data for each species was time-consuming and costly. Figure 1 displays a sample image for each macrofungal species. The dataset comprised 683 original images across five classes. Online data augmentation (horizontal flipping and 0.2° rotation) was applied during training; the augmented images were not stored offline, and all reported counts referred to the original images. Ensuring a balanced dataset is crucial for DL models; therefore, data were collected for all macrofungi species. An imbalance in data quantity can lead to models having an inherent majority bias.

Application of DL Methods

Training and testing procedures employed an equal number of data samples for each species. Table 1 illustrates the distribution of data samples across the training, validation, and testing phases. The images employed for each phase were entirely distinct. Specifically, the images used for training did not include any photos that were used for verification or testing. The validation images did not contain any test data.

Table 1. Data distribution.

Species	Training	Validation	Test
Amanita muscaria	120	10	10
A. phalloides	117	10	10
Lepista nuda	115	10	10
Macrolepiota procera	111	10	10
Craterellus cornucopioides	120	10	10

Metrics

The effectiveness of all the methods employed was assessed based on the parameters of accuracy, precision, recall, and F1-score.

- Accuracy is the ratio between the correctly predicted and the total number of instances within each dataset.
- Precision is the proportion of instances with accurate positive predictions among all those predicted as positive.
- Recall is the ratio between the instances with accurate positive predictions and the total number of actual positive instances.
- F1-score is the harmonic mean of precision and recall, offering a single metric that balances both.

Figure 1. A sample image for each macrofungi species. (a) *Amanita muscaria*; (b) *A. phalloides*; (c) *Lepista nuda*; (d) *Macrolepiota procera*; (e) *Craterellus cornucopioides*.

The formulae used for these metrics are given in Equations 1, 2, 3, and 4, respectively.

$$\text{Accuracy} = \frac{(TP + TN)}{(TP + TN + FP + FN)} \quad \text{(Equation 1)}$$

$$\text{Precision} = \frac{TP}{(TN + FP)} \quad \text{(Equation 2)}$$

$$\text{Recall} = \frac{TP}{(TP + FN)} \quad \text{(Equation 3)}$$

$$\text{F1-score} = \frac{2*(\text{Precision}*\text{Recall})}{\text{Precision} + \text{Recall}} \quad \text{(Equation 4)}$$

For Equations 1, 2, and 3, the terms True Positive (TP), False Positive (FP), True Negative (TN), and False Negative (FN) were defined. TPs refers to cases where the test sample is actually diseased and is correctly predicted as such. FPs denotes cases where the sample is healthy but is incorrectly classified as diseased. TNs indicates samples that are healthy and correctly identified as such. FNs represents samples that are diseased but are mistakenly classified as healthy (Ozsari et al., 2024).

In addition, the Grad-CAM approach was employed to examine specific regions of the images prioritized by the models during inference. Neural networks consist of interconnected layers where numerous parameters are adjusted during training to process the input data. However, the mechanisms by which the outputs are generated based on the inputs remain unclear, diminishing model confidence. Grad-CAM is a visualization technique used to interpret and understand the decision-making processes behind CNNs. It is particularly popular in image classification tasks, aiding in identifying the regions of an input image that are significant for accurate prediction by a model. The red regions in the Grad-CAM images indicate the areas where the model focused the most, signifying that the network makes its inferences by examining these regions. The blue regions indicate the least important regions, denoting areas on which the network does not concentrate.

Model Architectures and Training Hyperparameters

We evaluated six transfer-learning backbones: DenseNet121, InceptionV3, MobileNetV2, Xception, VGG16, and ResNet101, which were initialized with ImageNet (https://www.image-net.org/index.php) weights. In each model, the original classification head was replaced with a global average pooling layer followed by a fully connected softmax layer with five outputs corresponding to the target species. All layers were fine-tuned end-to-end.

The images were resized to 224 × 224 pixels for DenseNet121, MobileNetV2, VGG16, and ResNet101, and to 299 × 299 pixels for InceptionV3 and Xception. Preprocessing used the dedicated preprocess_input function of each model. During training, we applied horizontal flipping and a 0.2° rotation as data augmentation.

Training employed the Adaptive Moment Estimation (Adam) optimizer with an initial learning rate of 1×10^{-4} and a categorical cross-entropy loss. We trained with a batch size of 32 for 50 epochs, selecting the best checkpoint based on validation loss. We employed the ReduceLROnPlateau scheduling technique (factor 0.1, patience 5, and minimum learning rate 1×10^{-6}) and early stopping (patience 10 and restore_best_weights=True). Experiments were conducted in a GPU-enabled Google Colab environment (Python 3.x; TensorFlow/Keras), with fixed random seeds to enhance reproducibility (Ozsari et al., 2024).

Methodological Overview and Contributions

This study implements a standardized transfer-learning pipeline for macrofungi identification that (i) benchmarks six widely used backbones (DenseNet121, InceptionV3, MobileNetV2, Xception, VGG16, and ResNet101) under identical data splits and a unified training protocol; (ii) employs on-the-fly augmentation (horizontal flip and 0.2° rotation) to mitigate limited data without artificially inflating the sample counts; (iii) integrates Grad-CAM–based visual explanations to verify the attention on morphologically relevant regions; and (iv) establishes a simple CNN baseline for contextual comparison. All experimental settings, including input resolutions and preprocessing, fine-tuning strategy, optimizer, learning rate schedule, batch size, epochs, early stopping, and the hardware/software environments, facilitate reproducibility (Ekinci et al., 2025; Kumru et al., 2025).

Results

Due to the limited number of images, data augmentation preceded training. This technique involves increasing the quantity of available data through minor transformations, such as rotation and brightness adjustment, without altering the image content. In the present study, data were augmented using horizontal flipping and a 0.2-degree rotation. Augmented samples were not stored offline; therefore, all dataset counts reported refer to the original images, while augmentation only enhances the effective number of training instances per epoch. Figure 2 presents a sample output for *A. muscaria*.

With on-the-fly augmentation, a series of experiments was conducted to evaluate and confirm the performance of various transfer-learning based models, including DenseNet121, InceptionV3, MobileNetV2, Xception, VGG16, and ResNet101, for automatically predicting five different macrofungi species. Table 2 presents the results for the models.

A CNN model built with basic layers yields average results (Table 2). Given the limited number of available images, this outcome is expected and highlights the rationale for utilizing pre-trained networks. All fine-tuned models demonstrated substantial effectiveness, achieving results > 90%. Among all metrics, the MobileNetV2 network attained the maximum values, with the InceptionV3 architecture also producing comparable results.

Figure 2. A sample output for data augmentation.

Table 2. Experimental results.

Model	Accuracy	Precision	Recall	F1-score
CNN	0.70	0.68	0.65	0.67
DenseNet121	0.90	0.90	0.90	0.90
InceptionV3	0.93	0.93	0.93	0.93
MobileNetV2	0.93	0.93	0.93	0.93
Xception	0.90	0.90	0.90	0.90
VGG16	0.89	0.93	0.90	0.91
ResNet101	0.90	0.90	0.90	0.90

The ResNet101 network produced lower accuracy values when compared to the other models. Notably, the high performance of these networks does not guarantee that the inferences made were from the correct regions. Therefore, Grad-CAM visualizations were generated to analyse the areas that the models focused on for predictions.

Specifically, Figure 3 illustrates the macrofungi for which Grad-CAM visualizations were conducted. Figure 4 displays the Grad-CAM images for DenseNet121, Figure 5 for InceptionV3, Figure 6 for MobileNetV2, Figure 7 for Xception, Figure 8 for VGG16, and Figure 9 for ResNet101.

Figure 3. Original images (without Grad-CAM visualization).

Figure 4. Grad-CAM images of DenseNet121.

Analysis of the Grad-CAM images of the DenseNet architecture reveals that it derives inferences from the correct regions for all three macrofungi species. The blue areas denote regions unrelated to the macrofungi. Although its metric values were high, it is evident that the InceptionV3 network concentrates on the entire image (Figure 5), suggesting that the network makes incorrect predictions. The Grad-CAM images for the MobileNetV2 network demonstrate that it focuses on the correct regions for the for the central macrofungus (second image) and partially correct ones for the first and third macrofungi images. The heatmap indicates that the Xception network, just like DenseNet121, concentrates on macrofungi-related areas (Figure 7). The VGG16 network made accurate predictions for the second and third images,but shifted to areas in the first image that were unrelated to macrofungi. The ResNet101 model, apart from InceptionV3, focused on the correct regions in the second image, considering the stem part in the third macrofungi, and shifting to the knife-related area in the first macrofungi. Thus, it can be concluded that DenseNet121 was the most successful model based on the Grad-CAM visualizations and metric values.

Figure 5. Grad-CAM images of InceptionV3.

Figure 6. Grad-CAM images of MobileNetV2.

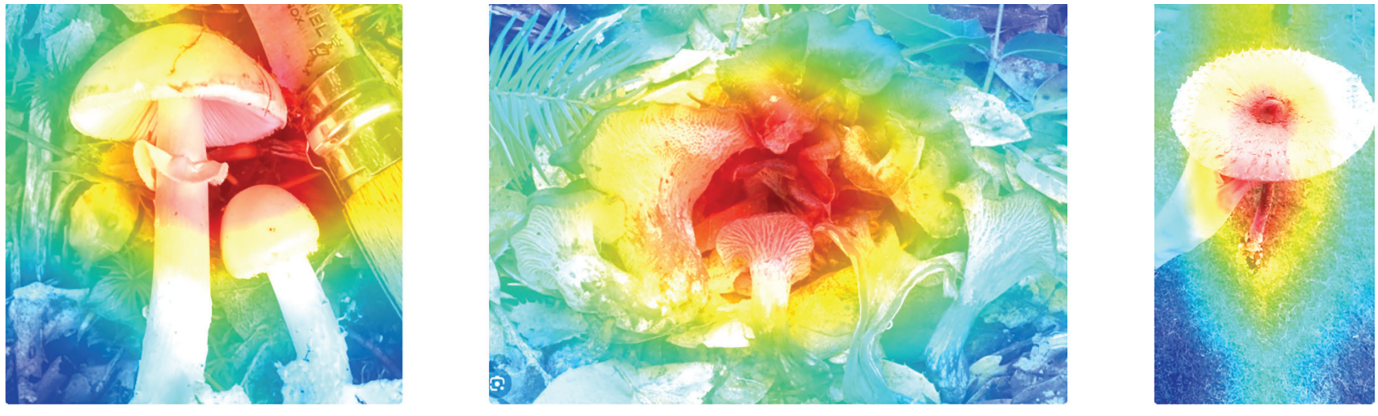

Figure 7. Grad-CAM images of Xception.

Figure 8. Grad-CAM images of VGG16.

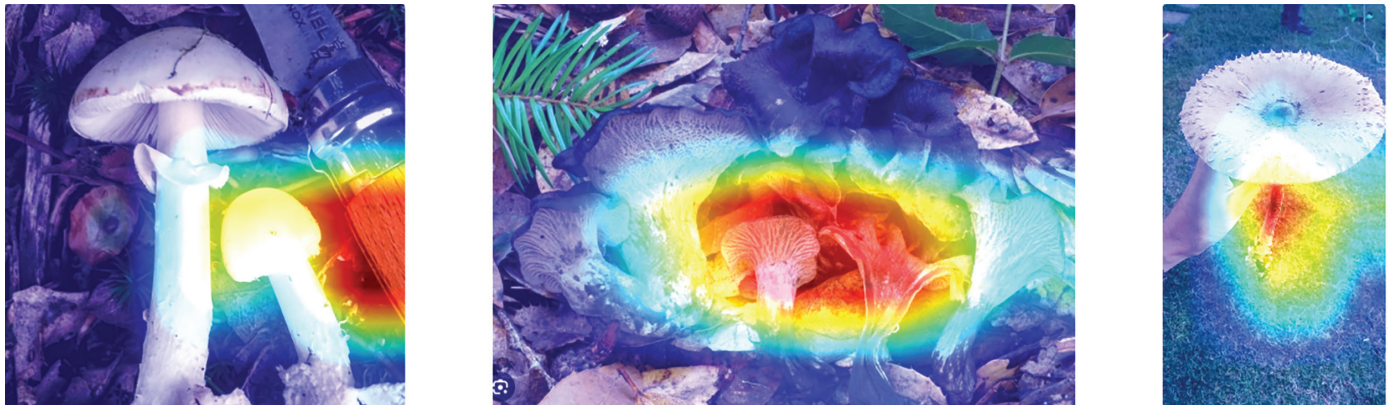

Figure 9. Grad-CAM images of ResNet101.

Discussion

Fungi represent a diverse kingdom of organisms, including yeasts, moulds, and macrofungi. They are essential components of various ecosystems, serving as decomposers, symbionts, and pathogens. Recently, DL applications in mycology have gained significant popularity, particularly for image classification, species identification, and disease diagnosis. This study employed the models DenseNet121, InceptionV3, MobileNetV2, Xception, VGG16, and ResNet101 to assess the effectiveness of DL techniques in autonomously detecting five distinct macrofungal species. The results, with values ≥ 0.9, demonstrate that these networks are highly efficient in distinguishing between these species. However, high-performance metrics do not necessarily ensure that the architectures operate with the appropriate regions. Consequently, Grad-CAM visualizations were also employed. Analysis of the Grad-CAM outputs revealed that the networks generally drew inferences from the correct areas. The Grad-CAM images for the DenseNet121 model demonstrated that it drew inferences from the correct regions for all macrofungal species. This result aligns with the findings of Van Horn et al. (2018), who observed that DL models accurately identify the regions relevant to species classification tasks. Conversely, the InceptionV3 network focused on entire images and, despite high metric values, made incorrect inferences. This outcome was consistent with the findings of Wah et al. (2011), who noted that DL models can sometimes derive inferences from the irrelevant regions. The MobileNetV2 network focused on the correct regions applicable to the middle macrofungi and partially correct areas for *A. phalloides* and *M. procera*. The Xception network, similar to DenseNet-121, focused on areas related to macrofungi. The VGG16 network made accurate predictions using the second and third images, but shifted to regions irrelevant to macrofungi in the first image. The ResNet101 model, apart from InceptionV3, focused on the correct areas of the second image, considering the stem part in the third macrofungi, and shifting to the knife-related area in the first macrofungi.

The application of DL techniques in classifying macrofungal species, as demonstrated in this study, has shown significant promise. By leveraging advanced architectures such as DenseNet121, InceptionV3, MobileNetV2, Xception, VGG16, and ResNet101, we achieved accuracy rates > 90%, indicating the efficacy of these models in identifying and classifying species based on their visual characteristics. The use of Grad-CAM visualizations provided further insights into those regions of the images that the models focused on. This observation confirmed that DenseNet121 and Xception, in particular, were highly effective in identifying the areas relevant to the species.

The performance of these architectures was assessed based on accuracy, precision, recall, and F1-score metrics. Additionally, Grad-CAM visualizations were generated to pinpoint the regions that the models concentrated on during inference. These results indicated that the networks achieved high effectiveness, with scores ≥ 0.9. The Grad-CAM images demonstrated that the DenseNet121 and Xception architectures focused accurately on the macrofungi.

Despite these positive outcomes, several challenges persist, particularly concerning data availability and diversity. The current dataset, while effective, is limited in size, which restricts the ability of the model to realize its potential fully. This limitation underscores the need to expand datasets to encompass a broader range of species and more diverse image sets. Larger and more varied datasets would not only enhance model performance but also improve the generalizability of the results, rendering the models more robust across different ecological contexts. Our results were consistent with findings from previous studies on image-based fungal classification, which reported that DL architectures outperform traditional ML approaches (Picek et al., 2022; Yan et al., 2023). However, unlike prior studies that mostly evaluated single CNN models, this study systematically compared six state-of-the-art transfer-learning architectures on macrofungi. Moreover, while earlier research focused only on accuracy-associated metrics, performance evaluation in this study was complemented with Grad-CAM visualizations, thereby adding interpretability and biological relevance to the results.

The main contribution of this study lies in the systematic comparison of six transfer-learning architectures for macrofungi classification, which was combined with the Grad-CAM visualizations to validate the model's focus on biologically relevant regions. In addition, benchmarking against a simple CNN baseline highlighted the methodological advantage of advanced DL models. These contributions together provide a reproducible and interpretable framework that can be adapted to future biodiversity monitoring studies.

Future research should focus on addressing these data limitations by developing and utilizing more comprehensive and diverse datasets. Furthermore, integrating DL models with other computational techniques, such as computer vision, could further enhance the efficiency and accuracy of species classification, particularly in identifying poisonous macrofungi and supporting mechanized harvesting processes. Such a line of research could be further strengthened by incorporating additional data types, including spore prints and relevant environmental variables. In conclusion, while this study adds significant amounts of data to the automated classification of macrofungi species, it also underscores the necessity for continued research and development. Future studies should aim to build upon these findings by expanding data resources, refining model architectures, and exploring new applications of AI in mycology, ultimately contributing to more effective biodiversity conservation efforts.

Conclusion

This study addresses the core challenge of reliable macrofungal identification with limited datasets, in a context where traditional methods remain inadequate and the existing AI-based approaches seldom integrate performance with interpretability. Through a systematic comparison of six state-of-the-art transfer-learning architectures and the integration of Grad-CAM visualization, this study demonstrated high accuracy and biologically meaningful interpretability, providing a methodological framework that advances beyond previous works. Importantly, by highlighting the diagnostic image regions used by the models, this framework not only advances methodological development but also offers practical ease in the identification of the fungal species included in the study, thereby supporting both taxonomic accuracy and applied usability.Future research should focus on scaling up this framework by employing larger and more diverse datasets and enhancing generalizability under data-scarce conditions through advanced approaches such as transformer-based architectures and semi-supervised learning. Moreover, applying these models to field-based contexts, particularly for the reliable identification of poisonous species and for ecological monitoring, would provide significant practical contributions.

Ethics

Ethics Committee Approval: Since the article does not contain any studies with human or animal subject, its approval to the ethics committee was not required.

Data Sharing Statement: All data are available within the study.

Footnotes

Authorship Contributions: Conceptualization: Ş.Ö., E.K., F.E., and I.A.; Design/methodology: Ş.Ö., E.K., F.E., and T.A.; Execution/investigation: F.E., M.S.G., K.A., and T.A.; Resources/materials: Ş.Ö., E.K., and F.E.; Data acquisition: Ş.Ö. and E.K.; Data analysis/interpretation: Ş.Ö., F.E., and K.A.; Writing – original draft: Ş.Ö. and I.A.; Writing – review & editing/critical revision: E.K., F.E., M.S.G., K.A., and T.A.

Conflict of Interest: The authors have no conflicts of interest to declare.

Funding: The authors declared that this study has received no financial support.

Editor-in-Chief's Note: Fatih Ekinci is a member of the editorial board of the Trakya University Journal of Natural Sciences. He was not involved in the editorial evaluation or decision-making process for this manuscript.

References

Bartlett, P., Eberhardt, U., Schütz, N., & Beker, H. J. (2022). Species determination using AI machine-learning algorithms: Hebeloma as a case study. *IMA Fungus, 13*(1), 13. https://doi.org/10.1186/s43008-022-00099-x

Chathurika, K., Siriwardena, E., Bandara, H., Perera, G., & Dilshanka, K. (2023). Developing an identification system for different types of edible mushrooms in Sri Lanka using machine learning and image processing. *International Journal of Engineering and Management Research, 13*(5), 54–59. https://doi.org/10.31033/ijemr.13.5.9

Cheong, P. C. H., Tan, C. S., & Fung, S. Y. (2018). Medicinal mushrooms: Cultivation and pharmaceutical impact. In Biology of macrofungi (pp. 287–304). Springer. https://doi.org/10.1007/978-3-030-02622-6_14

Chollet, F. (2017). Xception: Deep learning with depthwise separable convolutions. In *Proceedings of the IEEE Conference on Computer Vision and Pattern Recognition* (pp. 1800–1807). Honolulu, HI, USA. https://doi.org/10.1109/CVPR.2017.195

Chugh, R. M., Mittal, P., Mp, N., Arora, T., Bhattacharya, T., Chopra, H., Cavalu, S., & Gautam, R. K. (2022). Fungal mushrooms: A natural compound with therapeutic applications. *Frontiers in Pharmacology, 13,* 925387. https://doi.org/10.3389/fphar.2022.925387

Das, A. K., Nanda, P. K., Dandapat, P., Bandyopadhyay, S., Gullón, P., Sivaraman, G. K., McClements, D. J., Gullón, B., & Lorenzo, J. M. (2021). Edible mushrooms as functional ingredients for development of healthier and more sustainable muscle foods: A flexitarian approach. *Molecules, 26*(9), 2463. https://doi.org/10.3390/molecules26092463

de Mattos-Shipley, K. M., Ford, K. L., Alberti, F., Banks, A., Bailey, A. M., & Foster, G. (2016). The good, the bad and the tasty: The many roles of mushrooms. *Studies in Mycology, 85*(1), 125–157. https://doi.org/10.1016/j.simyco.2016.11.002

De, J., Nandi, S., & Acharya, K. (2022). A review on Blewit mushroom (*Lepista* sp.) transition from farm to pharm. *Journal of Food Processing and Preservation, 46*(11), e17028. https://doi.org/10.1111/jfpp.17028

Ekinci, F., Ugurlu, G., Ozcan, G. S., Acici, K., Asuroglu, T., Kumru, E., Guzel, M. S., & Akata, I. (2025). Classification of *Mycena* and *Marasmius* species using deep learning models: An ecological and taxonomic approach. *Sensors, 25*(6), 1642. https://doi.org/10.3390/s25061642

El-Ramady, H., Abdalla, N., Badgar, K., Llanaj, X., Törős, G., Hajdú, P., Eid, Y., & Prokisch, J. (2022). Edible mushrooms for sustainable and healthy human food: Nutritional and medicinal attributes. *Sustainability, 14*(9), 4941. https://doi.org/10.3390/su14094941

GBIF Secretariat. (2023). GBIF backbone taxonomy [Checklist dataset]. GBIF.org. https://doi.org/10.15468/39omei (Accessed July 21, 2024)

Google Colab. (n.d.). Retrieved August 14, 2024, from https://research.google.com/colaboratory/faq.html

He, K., Zhang, X., Ren, S., & Sun, J. (2016). Deep residual learning for image recognition. In *Proceedings of the IEEE Conference on Computer Vision and Pattern Recognition* (pp. 770–778). Las Vegas, NV, USA. https://doi.org/10.1109/CVPR.2016.90

Huang, G., Liu, Z., Van Der Maaten, L., & Weinberger, K. Q. (2017). Densely connected convolutional networks. In *Proceedings of the IEEE Conference on Computer Vision and Pattern Recognition* (pp. 2261–2269). Honolulu, HI, USA. https://doi.org/10.1109/CVPR.2017.243

Hyde, K. D., Xu, J., Rapior, S., Jeewon, R., Lumyong, S., Niego, A. G. T., Abeywickrama, P. D., Aluthmuhandiram, J. V., Brahamanage, R. S., & Brooks, S. (2019). The amazing potential of fungi: 50 ways we can exploit fungi industrially. *Fungal Diversity, 97,* 1–136. https://doi.org/10.1007/s13225-019-00430-9

Jančo, I., Šnirc, M., Hauptvogl, M., Demková, L., Franková, H., Kunca, V., Lošák, T., & Árvay, J. (2021). Mercury in *Macrolepiota procera* (Scop.) Singer and its underlying substrate—Environmental and health risks assessment. *Journal of Fungi, 7*(9), 772. https://doi.org/10.3390/jof7090772

Kingma, D. P., & Ba, J. (2014). Adam: A method for stochastic optimization. *arXiv Preprint,* arXiv:1412.6980. https://doi.org/10.48550/arXiv.1412.6980

Korkmaz, A. F., Ekinci, F., Altaş, Ş., Kumru, E., Güzel, M. S., & Akata, I. (2025). A deep learning and explainable AI-based approach for the classification of Discomycetes species. *Biology, 14*(6), 719. https://doi.org/10.3390/biology14060719

Kumru, E., Ugurlu, G., Sevindik, M., Ekinci, F., Güzel, M. S., Acici, K., & Akata, I. (2025). Hybrid deep learning framework for high-accuracy classification of morphologically similar puffball species using CNN and transformer architectures. *Biology, 14*(7), 816. https://doi.org/10.3390/biology14070816

Li, H., Tian, Y., Menolli Jr, N., Ye, L., Karunarathna, S. C., Perez-Moreno, J., Rahman, M. M., Rashid, M. H., Phengsintham, P., & Rizal, L. (2021). Reviewing the world's edible macrofungi species: A new evidence-based classification system. *Comprehensive Reviews in Food Science and Food Safety, 20*(2), 1982–2014. https://doi.org/10.1111/1541-4337.12708

Llanaj, X., Törős, G., Hajdú, P., Abdalla, N., El-Ramady, H., Kiss, A., Solberg, S. Ø., & Prokisch, J. (2023). Biotechnological applications of mushroom under the water-energy-food nexus: Crucial aspects and prospects from farm to pharmacy. *Foods, 12*(14), 2671. https://doi.org/10.3390/foods12142671

Niego, A. G. T., Lambert, C., Mortimer, P., Thongklang, N., Rapior, S., Grosse, M., Schrey, H., Charria-Girón, E., Walker, A., & Hyde, K. D. (2023). The contribution of fungi to the global economy. *Fungal Diversity, 121*(1), 95–137. https://doi.org/10.1007/s13225-023-00520-9

Niego, A. G. T., Rapior, S., Thongklang, N., Raspé, O., Hyde, K. D., & Mortimer, P. (2023). Reviewing the contributions of macrofungi to forest ecosystem processes and services. *Fungal Biology Reviews, 44,* 100294. https://doi.org/10.1016/j.fbr.2022.11.002

Niego, A. G., Rapior, S., Thongklang, N., Raspé, O., Jaidee, W., Lumyong, S., & Hyde, K. D. (2021). Macrofungi as a nutraceutical source: Promising bioactive compounds and market value. *Journal of Fungi, 7*(5), 397. https://doi.org/10.3390/jof7050397

Ozsari, S., Kumru, E., Ekinci, F., Akata, I., Guzel, M. S., Acici, K., Ozcan, E., & Asuroglu, T. (2024). Deep learning-based classification of macrofungi: Comparative analysis of advanced models for accurate fungi identification. *Sensors, 24*(22), 7189. https://doi.org/10.3390/s24227189

Picek, L., Šulc, M., Matas, J., Heilmann-Clausen, J., Jeppesen, T. S., & Lind, E. (2022). Automatic fungi recognition: Deep learning meets mycology. *Sensors, 22*(2), 633. https://doi.org/10.3390/s22020633

Pilz, D., Norvell, L., Danell, E., & Molina, R. (2003). Ecology and management of commercially harvested mushrooms. *United States Department of Agriculture, Forest Service, Pacific Northwest Research Station, General Technical Report.* https://doi.org/10.2737/PNW-GTR-576

Pinto, S., Barros, L., Sousa, M. J., & Ferreira, I. C. (2013). Chemical characterization and antioxidant properties of *Lepista nuda* fruiting bodies and mycelia obtained by in vitro culture: Effects of collection habitat and culture media. *Food Research International, 51*(2), 496–502. https://doi.org/10.1016/j.foodres.2012.12.009

Priyamvada, H., Akila, M., Singh, R. K., Ravikrishna, R., Verma, R., Philip, L., Marathe, R., Sahu, L., Sudheer, K., & Gunthe, S. (2017). Terrestrial macrofungal diversity from the tropical dry evergreen biome of southern India and its potential role in aerobiology. *PLoS One, 12*(1), e0169333. https://doi.org/10.1371/journal.pone.0169333

Raghavan, K. B. S., & Veezhinathan, K. (2024). Attention guided grad-CAM: An improved explainable artificial intelligence model for infrared breast cancer detection. *Multimedia Tools and Applications, 83,* 57551–57578. https://doi.org/10.1007/s11042-023-17776-7

Roncero-Ramos, I., & Delgado-Andrade, C. (2017). The beneficial role of edible mushrooms in human health. *Current Opinion in Food Science, 14,* 122–128. https://doi.org/10.1016/j.cofs.2017.04.002

Sandler, M., Howard, A., Zhu, M., Zhmoginov, A., & Chen, L.-C. (2018). Mobilenetv2: Inverted residuals and linear bottlenecks. In *Proceedings of the IEEE Conference on Computer Vision and Pattern Recognition* (pp. 4510–4520). Salt Lake City, UT, USA. https://doi.org/10.1109/CVPR.2018.00474

Selvaraju, R. R., Cogswell, M., Das, A., Vedantam, R., Parikh, D., & Batra, D. (2017). Grad-CAM: Visual explanations from deep networks via gradient-based localization. In *Proceedings of the IEEE International Conference on Computer Vision* (pp. 618–626). Venice, Italy. https://doi.org/10.1109/ICCV.2017.74

Simonyan, K., & Zisserman, A. (2014). Very deep convolutional networks for large-scale image recognition. *arXiv Preprint,* arXiv:1409.1556. https://doi.org/10.48550/arXiv.1409.1556

Szegedy, C., Vanhoucke, V., Ioffe, S., Shlens, J., & Wojna, Z. (2016). Rethinking the inception architecture for computer vision. In *Proceedings of the IEEE Conference on Computer Vision and Pattern Recognition* (pp. 2818–2826). Las Vegas, NV, USA. https://doi.org/10.1109/CVPR.2016.308

Van Horn, G., Mac Aodha, O., Song, Y., Cui, Y., Sun, C., Shepard, A., Adam, H., Perona, P., & Belongie, S. (2018). The iNaturalist species classification and detection dataset. In *Proceedings of the IEEE Conference on Computer Vision and Pattern Recognition.* https://doi.org/10.48550/arXiv.1707.06642

Wah, C., Branson, S., Welinder, P., Perona, P., & Belongie, S. (2011). The Caltech-UCSD birds-200-2011 dataset. *California Institute of Technology.* https://doi.org/10.22002/D1.20092

Yan, Z., Liu, H., Li, J., & Wang, Y. (2023). Application of identification and evaluation techniques for edible mushrooms: A review. *Critical Reviews in Analytical Chemistry, 53*(3), 634–654. https://doi.org/10.1080/10408347.2021.1969886

Ye, F., Yu, X.-D., Wang, Q., & Zhao, P. (2016). Identification of SNPs in a nonmodel macrofungus (*Lepista nuda,* Basidiomycota) through RAD sequencing. *SpringerPlus, 5,* 1–7. https://doi.org/10.1186/s40064-016-3459-8

Ye, L., Li, H., Mortimer, P. E., Xu, J., Gui, H., Karunarathna, S. C., Kumar, A., Hyde, K. D., & Shi, L. (2019). Substrate preference determines macrofungal biogeography in the Greater Mekong sub-region. *Forests, 10*(10), 824. https://doi.org/10.3390/f10100824

Yilmaz, I., Ermis, F., Akata, I., & Kaya, E. (2015). A case study: What doses of *Amanita phalloides* and amatoxins are lethal to humans? *Wilderness & Environmental Medicine, 26*(4), 491–496. https://doi.org/10.1016/j.wem.2015.08.003

Trakya University Journal of Natural Sciences, 26(2), 213–222, 2025
DOI: 10.23902/trkjnat.574355887
www.tujns.org

Research Article

Toll-like receptor 3-mediated modulation of umbilical cord mesenchymal stem cell phenotype and pancreatic cancer cell responses during coculture

Ayşegül Yılmaz[1], Demet Kaçaroğlu[2]

[1]*Lokman Hekim University, Faculty of Medicine, Department of Medical Microbiology, Ankara, Türkiye*
[2]*Lokman Hekim University, Faculty of Medicine, Department of Medical Biology, Ankara, Türkiye*

Cite this article as: Yılmaz, A., & Kaçaroğlu, D. (2025). Toll-like receptor 3-mediated modulation of umbilical cord mesenchymal stem cell phenotype and pancreatic cancer cell responses during coculture. *Trakya University Journal of Natural Sciences, 26*(2), 213–222. https://doi.org/10.23902/trkjnat.574355887

Abstract

Mesenchymal stem cells (MSCs) are progenitor cells isolated from various tissues and are crucial for tissue repair, immune support, and anticancer therapies. MSC functions such as migration, immunomodulation, and regeneration are regulated through Toll-like receptors (TLRs). In particular, TLR3 activation enhances the immunosuppressive and therapeutic capabilities of MSCs. This research employed human umbilical cord-derived MSCs (UCMSCs) and investigated the effects of TLR3 stimulation on their viability, phenotype-associated gene expression, and during co-culture with *Panc-1* pancreatic cancer cells. UCMSCs were cultured and characterized for mesenchymal markers by flow cytometry. TLR3-based signaling was modulated using Poly(A:U) (an agonist) and CU-CPT4a (an antagonist). Cell viability was assessed using the 3-[4,5-dimethylthiazol-2-yl]-2,5 diphenyl tetrazolium bromide assay, and relative gene expression was measured employing quantitative reverse transcription polymerase chain reaction. *Panc-1* cells were co-cultured with UCMSCs to evaluate TLR3-mediated effects. Data are presented as the means ± standard error of the mean, with statistical significance determined by analysis of variance ($p \leq 0.05$). The TLR3 agonist improved cell viability, whereas the antagonist reduced it. Additionally, both regulated the expression of *CD44*, *CDH1*, and *VIMs*. When UCMSCs and *Panc-1* cells were cocultured at 10:1, TLR3 affected the expression of MSC-related genes, including *CD44*, *CDH1*, *CLDN1*, *VIM*, *ZEB*1, *MMP9*, *MMP2*, *TIMP1*, *VEGFR2*, and *PLAU*. Thus, TLR3-based signaling influenced the viability, maintenance of the mesenchymal phenotype, and *Panc-1* coculture-associated phenotype in UCMSCs. These results underscore the crucial role of TLR3-based signaling in modulating UCMSC function

Özet

Mezenkimal kök hücreler (MSC'ler), doku onarımı, bağışıklık desteği ve kanser karşıtı tedaviler açısından kritik öneme sahip progenitör hücrelerdir. Farklı dokulardan izole edilen MSC'lerin göç, immünomodülasyon ve rejenerasyon gibi fonksiyonları Toll-benzeri reseptörler (TLR'ler) aracılığıyla düzenlenmektedir. Özellikle, TLR3 aktivasyonu MSC'lerin immünosupresif ve terapötik özelliklerini artırmaktadır. Bu çalışmada, TLR3 uyarımının insan göbek kordonu kaynaklı MSC'lerin (UK-MSC'ler) canlılığı, fenotip ile ilişkili gen ekspresyonu üzerindeki etkileri ile bu hücrelerin *Panc-1* pankreas kanseri hücreleriyle ortak kültürdeki etkileri araştırılmıştır. UK-MSC'ler kültür ortamında çoğaltıldı ve mezenkimal yüzey belirteçleri açısından akım sitometrisi ile karakterize edildi. TLR3 sinyali, Poly(A:U) agonisti ve CU-CPT4a antagonisti ile modüle edildi. Hücre canlılığı 3-(4,5-dimetiltiazol-2-il)-2,5-difeniltetrazolyum bromür testi ile değerlendirildi ve gen ekspresyonu gliseraldehit-3-fosfat dehidrogenaz referans geni kullanılarak kantitatif gerçek zamanlı ters transkripsiyon polimeraz zincir reaksiyonu ile ölçüldü. *Panc-1* pankreas kanseri hücreleri UK-MSC'lerle ko-kültüre edilerek TLR3 aracılı etkiler analiz edildi. Tüm veriler ortalama ± ortalamanın standart hatası olarak sunuldu ve istatistiksel analiz varyans analizi veya t-test ile yapıldı ($p \leq 0{,}05$). TLR3 agonistlerinin hücre canlılığını artırdığı, TLR3 antagonistlerinin ise azalttığı gözlemlenmiştir. Ayrıca, hem agonist hem de antagonistlerin CD44, CDH1 ve VIM genlerinin ekspresyonunu düzenlediği bulunmuştur. UK-MSC ve *Panc-1* hücreleri 10:1 oranında ortak kültüre alındığında, TLR3 aktivasyonu ve inhibisyonunun *CD44*, *CDH1*, *CLDN1*, *VIM*, *ZEB1*, *MMP9*, *MMP2*, *TIMP1*, *VEGFR2* ve *PLAU* gibi MSC ile ilişkili genlerin ekspresyon profillerini etkilediği gösterilmiştir. Sonuç

Edited by: *Reşat Ünal*
***Corresponding Author:** Demet Kaçaroğlu, **E-mail:** demetkacaroglu@gmail.com*
***ORCID iDs of the authors:** AY. 0000-0002-9541-9853, DK. 0000-0003-4920-0516*

Received: 31 May 2025, **Accepted:** 17 September 2025, **Online First**: 06 October 2025, **Published:** 15 October 2025

and suggest its potential utility in enhancing MSC-based therapeutic strategies. We believe that these results can help elucidate the role of TLR3-based signaling on UCMSC functions and provide a basis for future research.

olarak, TLR3 sinyal iletiminin UK-MSC'lerin canlılığını, mezenkimal fenotipin korunmasını ve *Panc-1* kanser hücrelerine yanıtla ilişkili fenotipini etkilediği gözlemlenmiştir. Bu bulgular, TLR3 sinyal iletiminin UK-MSC fonksiyonlarını modüle etmedeki önemini vurgulamakta ve özellikle tümörle ilişkili uygulamalarda MSC tabanlı tedavi stratejilerini geliştirmede potansiyel bir araç olabileceğini düşündürmektedir. Bu çalışmanın, TLR3 sinyal iletiminin UK-MSC'lerin biyolojik işlevleri üzerindeki etkilerini aydınlatmaya yardımcı olacağına ve gelecekteki araştırmalara temel oluşturacağına inanmaktayız.

Keywords: mesenchymal stem cell, TLR3, UCMSC, pancreatic ductal adenocarcinoma, cancer biology

Introduction

Mesenchymal stem cells (MSCs), essential for maintaining tissue homeostasis, constitute the cell-level foundation of the stromal microenvironment (Zhang et al., 2024). Within biological systems, MSCs exert a variety of beneficial effects, including supporting antiviral immune responses, promoting tissue repair through antifibrotic activity, and secreting proangiogenic growth factors (Golchin et al., 2020). These cells can be isolated from embryonic and adult tissues and comprise a heterogeneous population with unique regenerative and immunomodulatory properties, making them highly valuable for therapeutic applications (Chandrasekar et al., 2023; El Omar et al., 2014; Gholizadeh-Ghaleh Aziz et al., 2021). MSCs have potential in cancer therapy due to their ability to target tumor sites, modulate immune responses, and serve as carriers for anticancer agents. They can be polarized through different toll-like receptors (TLRs), creating tumor-suppressing and -promoting effects (Chandrasekar et al., 2023).

TLRs are pattern recognition receptors that detect microbe-associated molecular patterns. Their expression in MSCs varies with tissue origin, including umbilical cord, adipose tissue, and dental pulp (Liu et al., 2023; Raicevic et al., 2011). Human umbilical cord-derived MSCs (UCMSCs) play crucial roles in tissue repair due to their higher regenerative and immunomodulatory capacities compared to MSCs from other sources. Thus, they attract considerable interest in experimental and clinical studies as they are used as carrier cells in cancer treatment. Notably, MSCs express various TLRs and are capable of targeted migration to inflammation sites, demonstrating anticancer responses, and secrete immunomodulatory molecules in response to TLR activation (Tomchuck et al., 2008). Therefore, the regulation of MSC responses via TLRs is of great importance in tumor therapies, by modulating immune cells to affect the tumor microenvironment (TME) and directly impact tumor cells.

TLR signaling modulates MSC behavior: TLR2 maintains the undifferentiated state of bone marrow MSCs, while TLR3 and TLR4 influence stress responses, migration, and immunoregulation, especially with activated T cells (Hwang et al., 2023; Najar et al., 2017, 2019). TLR3-primed MSCs facilitate the suppression of NK cell activity by reducing the susceptibility of infected/damaged cells to NKs and increasing immunosuppressive capacity of MSCs (Hwang et al., 2023; Najar et al., 2019). TLR3 signaling shapes MSC phenotype and affects tumor cell responses. Activation by dsRNA analogs, such as Poly(I:C), triggers the NF-κB and IRF3 pathways, altering cytokine secretion, adhesion molecule expression, and extracellular matrix (ECM) remodeling (Najar et al., 2017). Importantly, several downstream genes regulated by TLR3 signaling play pivotal roles in determining MSC phenotype and influencing tumor biology. Claudin-1 (CLDN1) is a tight junction protein involved in maintaining epithelial barrier integrity; its dysregulation is linked to epithelial–mesenchymal transition (EMT) and metastasis in various cancers, including gastric, pancreatic, colon, and hepatocellular carcinoma (Bhat et al., 2020). Zinc finger E-box-binding homeobox 1 (ZEB1) is a transcription factor (TF) that represses E-cadherin expression but promotes EMT and invasiveness. Matrix metalloproteinase-9 (MMP9) degrades ECM components, aiding MSC migration and tumor invasion/angiogenesis (Zheng & Ma, 2022). These proteins collectively link TLR3-mediated MSC behavior to the modulation of the TME; the MSC phenotype alters during this process. Determining the role of MSCs is particularly critical in aggressive tumors such as pancreatic cancer, which have a microenvironment dense in immune cells and MSCs.

A literature review indicated that TLR3 activation regulates migration, regeneration responses, immunomodulation capacity, differentiation, and inflammation-related responses in MSCs. Understanding the mechanisms by which TLR activation influences MSC characteristics and the responses of tumor cells is critical for optimizing their therapeutic use. This study investigated whether TLR3 stimulation affects viability and the expression of phenotype-associated genes in UCMSCs. It also examined the effect of these genes during coculture with *Panc-1* cells.

Materials and Methods

UCMSC Cell Culture and Immunophenotyping

UCMSCs were purchased from STEMBIO, İstanbul, Türkiye, and cultured in T-75 flasks at 37 °C in a humidified atmosphere containing 5% CO_2. The cells were maintained in Dulbecco's Modified Eagle Medium (DMEM)/F12 medium (Capricorn Scientific GmbH,

Ebsdorfergrund, Germany) supplemented with 20% fetal bovine serum (Capricorn Scientific GmbH, Ebsdorfergrund, Germany), 1% L-glutamine (Sigma-Aldrich, Milan, Italy), and 1% penicillin + streptomycin (Biological Industries, Kibbutz Beit Haemek, Israel). The culture medium was renewed every 2–3 days until the cells reached 70–80% confluence. These optimized culture conditions supported UCMSC proliferation while preserving their characteristics, useful for subsequent analysis. To evaluate the expression of the mesenchymal cell surface markers cluster of differentiation 73 (CD73), CD90, CD44, and CD105, 50,000 cells at passage 3 were used. An MSC Marker Validation Kit (Catalog # FMC020; R&D Systems, MN, USA) was used for phenotypic characterization.

The cells were incubated with 10 µL of a cocktail containing 10 µL each of anti-CD73, anti-CD90, anti-CD44, and anti-CD105 positive marker antibodies + 10 µL of a cocktail containing 10 µL each of anti-CD45, anti-CD34, anti-CD11b, anti-HLA-DR, and anti-CD79 negative marker antibodies + 10 µL of an isotype control antibody. Staining was performed in the dark at incubated at 37 ℃ for 30–45 min. After incubation, the cells were washed with a staining buffer, and the pellet was resuspended in 100 µL of the staining buffer for flow cytometry. Cell debris was excluded utilizing forward scatter and side scatter dot plots. Fluorescence data were analyzed using CellQuest Pro software (BD Biosciences, CA, USA), and the marker expression proportion was determined relative to the isotype-matched controls.

Method of Preparing TLR3 and TLR3 Solutions

The TLR3 agonist, polyadenylic-polyuridylic acid Poly(A:U) (Cat No: tlrl-pau) was obtained from InVivogen, CA, USA[18]. The TLR3 antagonist, CU-CPT4a (Cas No: 1279713-77-7), was obtained from Cayman Chemical Company Inc., MI, USA. The antagonist was dissolved in dimethyl sulfoxide (DMSO) (Serva, Germany) to achieve a 1 mg/mL stock solution. The agonist was dissolved in the physiological water provided along with it to obtain a 1 mg/mL stock solution. The agonist and antagonist stocks were diluted to 0.01, 0.1, 1, 10, and 100 µg/mL, according to the manufacturer's protocol. For viability analysis, these concentrations were applied for 24 and 48 h. For gene expression analysis, the cells were seeded in 24-well plates at a density of 50,000 cells/well. They were treated with 0.1, 1, 5, and 10 µg/mL of TLR3 or 0.01, 0.1, 0.5, and 1 µg/mL of CU-CPT4a for 24 h. Each experimental group consisted of six wells, the contents of which were later pooled for analysis. For co-culture experiments, 1 µg/mL of TLR3 and 0.5 µg/mL of CU-CPT4a were added. After 24 h of polarization, the coculture experiments were started.

Cell Viability Analysis

To determine the role of TLR3 signaling in cell viability, UCMSCs were seeded in 96-well plates at 3,000 cells per well. TLR3 agonist and antagonist solutions were prepared in a new medium to obtain concentrations of 0.01, 0.1, 1, 10, and 100 µg/mL; each concentration was added to a separate well. Each concentration group included three replicates. After 24 and 48 h of incubation, cell viability was assessed using the 3-(4,5-dimethylthiazol-2-yl)-2,5-diphenyl tetrazolium bromide (MTT) assay. To each well, 10 µL of 0.5 mg/mL MTT solution (Biotium, CA, USA) and 90 µL of DMEM were added. The plates were then dark-incubated for 4 h at 37℃ in a humidified 5% CO_2 atmosphere to allow the formation of formazan crystals. Next, 100 µL of DMSO was added to each well to dissolve the crystals. OD_{570} was measured using a Synergy H1 microplate reader (BioTek Instruments, Inc., VT, USA). The OD of the untreated control group was considered to represent 100% viability, and those of the experimental groups were calculated relative to the control.

Panc-1 Cell Culture and Coculture Design

Panc-1 cells (ATCC:CRL-1469™) were purchased and cultured in high-glucose DMEM medium supplemented with 10% serum, 1% antibiotics, and 1% L-glutamine. The cells were seeded into the lower chamber of a 24-well plate at a density of 30,000 cells/well, in a 1:10 *Panc-1*:UCMSC ratio, and incubated at 37℃ under 5% CO_2 for 24 h to allow cell adhesion. In parallel, UCMSCs were also seeded in transwell inserts (0.4 µm pore size) at 300,000 cells/insert. The control UCMSCs were cultured in standard DMEM/F-12 medium, while the experimental UCMSCs were cultured in the same medium supplemented with either TLR3 agonist or antagonist. The inserts were then placed above the *Panc-1* cells containing wells to establish the coculture conditions; six wells/experimental group were used to ensure replicates. The UCMSCs were incubated for 24 h, washed with phosphate-buffered saline, and then placed on the *Panc-1* cells. After 72 h, the cells in the insert were collected, and DNA was isolated with Trizol, which was used for polymerase chain reaction (PCR).

Gene Expression Analysis

The expression of glyceraldehyde-3-phosphate dehydrogenase *(GAPDH)*, *CD44,* cadherin 1 *(CDH1)*, and vimentin *(VIM)* was evaluated in TLR3 agonist and antagonist-treated UCMSCs. The expression of *GAPDH, CD44, CDH1, CLDN1, VIM, ZEB1, MMP9,* matrix metalloproteinase-2 *(MMP2),* tissue inhibitor of metalloproteinase-1 *(TIMP1),* vascular endothelial growth factor receptor 2 *(VEGFR2)* and plasminogen activator urokinase *(PLAU)* was ascertained in UCMSCs co-cultured with *Panc-1* cells. For gene expression analysis, the Lightcycler® 96 system (Roche Diagnostics GmbH, Penzberg, Germany) and its compatible software were used. For the one-step PCR reactions, ABT™ 2X qPCR SYBR-Green Master Mix (ATLAS Biotechnology, Ankara, Türkiye) was used. Primers specific to *GAPDH, CD44*, *VIM*, and *CDH1* were employed for one set of analyses. Primers for a broader panel of genes, including *GAPDH, CD44, VIM, CDH1*, *CLDN1*, *ZEB1*, *MMP2*, *MMP9*, *PLAU*, *VEGFR2*, and *TIMP1* were used for the other set. The sequences of the primers and ENSEMBL transcript IDs are presented in Table 1. The reaction mix for each sample comprised 10 µL of master mix, 45 ng/mL of RNA, 3 µL of H_20, 10 mM each of sense and antisense primers; 20 µL of the mix was pipetted into each octet strip well. The octuplicate strips were centrifuged at 1000 ×*g* for 30 s. The Lightcycler® 96 system was run employing the program recommended by the

Table 1. Primers used for qRT-PCR expression analysis.

Gene name	Forward sequences	Reverse sequences	ENSEMBL transcript IDs
GAPDH	5′-GTCTCCTCTGACTTCAACAGCG-3′	5′-ACCACCCTGTTGCTGTAGCCAA -3′	ENST00000229239.10
MMP2	5′- TTCATTTGGCGGACTGTGAC -3′	5′-GTGCTGGCTGAGTAGATCCA -3′	ENST00000219070.9
PLAU	5′-GCCACACACTGCTTCATTGA-3′	5′-TATACATCGAGGGCAGGCAG-3′	ENST00000372764.4
VEGFR2	5′- ATCTGTGACTTTGGCTTGGC -3′	5′-TCCCACAGCAAAACACCAAA-3′	ENST00000263923.4
MMP9	5′-GACGAGGGCCTGGAGTGT-3′	5′-TGTGCTGTAGGAAGCTCATCTC-3′	ENST00000372330.3
TIMP1	5′-ACCCCTGGAGCACGGCT-3′	5′-CCCACCTTCCAAGTTAGTGACA-3′	ENST00000218388.9
CD44	5′- CACACGAAGGAAAGCAGGAC -3′	5′- CCAGAGGTTGTGTTTGCTCC -3′	ENST00000263398.11
CDH1	5′-TTAGAGGTCAGCGTGTGTGA-3′	5′- CTTCTCCGCCTCCTTCTTCA -3′	ENST00000261769.10
VIM	5′-CTGCCAACCGGAACAATGAC-3′	5′- TAGTTAGCAGCTTCAACGGC-3′	ENST00000544301
ZEB1	5′-AGGAGCCACAAAAGGACAGT- 3′	5′- TGGGGAATCAGAATCGTTTGC-3′	ENST00000318451.11
CLDN1	5′- TGCTTGGAAGACGATGAGGT- 3′	5′- GAGCCTGACCAAATTCGTACC-3′	ENST00000358432.9

manufacturer. The threshold cycle (C_t) value of *GAPDH* was used for data normalization, and the relative gene expression levels were calculated utilizing the $2^{-\Delta\Delta Ct}$ method. All samples were analyzed in triplicate.

Statistical Analysis

All data are expressed as the mean ± standard error of the mean (SEM). Graphs were created using GraphPad Prism version 8.1 (GraphPad Software, CA, USA). Statistical evaluations of cell viability were conducted via one-way analysis of variance using the same software. The untreated cells served as the control group in all experiments. The changes in *CDH1*, *VIM*, and *CD44* expression levels were analyzed utilizing two-tailed t-tests. The *Panc-1* and UCMSC coculture data were also examined using two-tailed t-tests by comparing with untreated groups. A $*p \leq 0.05$ was considered statistically significant. Additional levels were $*p \leq 0.05$, $**p < 0.01$, $***p < 0.001$, and $****p < 0.0001$.

Results

Characterization of Umbilical Cord MSCs

The cultured cells were characterized morphologically for surface markers. Flow cytometry results of UCMSCs are shown in Figure 1a as staining-based histogram plots. Specifically, 43,155/50,000 stained cells were included, and the passage interval was 86.3%. Of the stained cells within the passage range, 99.7% expressed CD73, 99.9% CD90, 99.3% CD44, and 99.8% CD105, confirming their identity as MSCs. The cultured cells exhibited a characteristic fibroblast-like morphology (Figure 1b).

TLR3 Agonist and Antagonist Affect the Viability of UCMSCs in a Dose-dependent Manner

Treatment with the TLR3 agonist resulted in statistically significant variations in viability at all doses. In the 24-hour group, treatment with 0.01 µg TLR3 agonist decreased cell viability by 15%, by 17% at 0.1 µg, 7% at 1 µg, but a 2% increase at 10 µg, compared to the control. However, at 100 µg, the cell viability declined by 17%. At 48 h, the cell viability was reduced by 23% at 0.01 µg, by 30% at 0.1 µg, by 14% at 1 µg, and by 25% at 100 µg, demonstrating a dose-dependent cytotoxic effect (Figure 2a).

At 24 h treatment with 0.01 µg of the TLR3 antagonist increased viability by 15% and by 20% at 0.1 µg. However, the viability decreased by 24% at 1 µg, 30% at 10 µg, and by 44% at 100 µg, re-affirming a dose-dependent response. At 48 h, the antagonist suppressed the viability by 16% at 0.01 µg, by 35% at 0.1 µg, by 30% at 1 µg, by 25% at 10 µg, and by the most pronounced effect of 80% reduction with 100 µg (Figure 2b). Thus, the TLR3 agonist and antagonist affect the viability of UCMSCs in a dose- and time-dependent manner.

TLR3 Agonist and Antagonist Influence the Expression of Phenotypic Markers in UCMSCs

The treatment of UCMSCs with a TLR3 agonist markedly suppressed *CDH1* expression (RQ: 0.79) but significantly increased *VIM* expression (RQ: 0.04) (Figure 3a, c). With *CD44*, expression was enhanced up to a 5 µg dose (RQ: 0.009), whereas it was reduced at 10 µg (RQ: 0.001) (Figure 3e, f). Following TLR3 antagonist treatment, *CDH1* (RQ: 24.82) and *VIM* (RQ: 0.75) expression elevated significantly at 1 µg (Figure 3b, d). However, the expression levels of both markers declined markedly at other concentrations. *CD44* expression was markedly downregulated at 0.1 (RQ: 0.01) and 10 µg (RQ: 0.014) of antagonist compared to the control. Thus, it can be concluded that an enhancement in TLR3 signaling improves the maintenance of the mesenchymal phenotype, whereas its inhibition alters cell responses in a dose-dependent manner. Overall, these results highlight the critical role of TLR3 in modulating the UCMSC phenotype and underline its potential as a target for regulating stem cell behavior in therapeutic applications.

TLR3-Modulated the Influence of UCMSCs During Co-culture with *Panc-1* Cells

Panc-1 and UCMSCs were cocultured at a 1:10 ratio, and the gene expression profiles in *Panc-1* cells were analyzed following

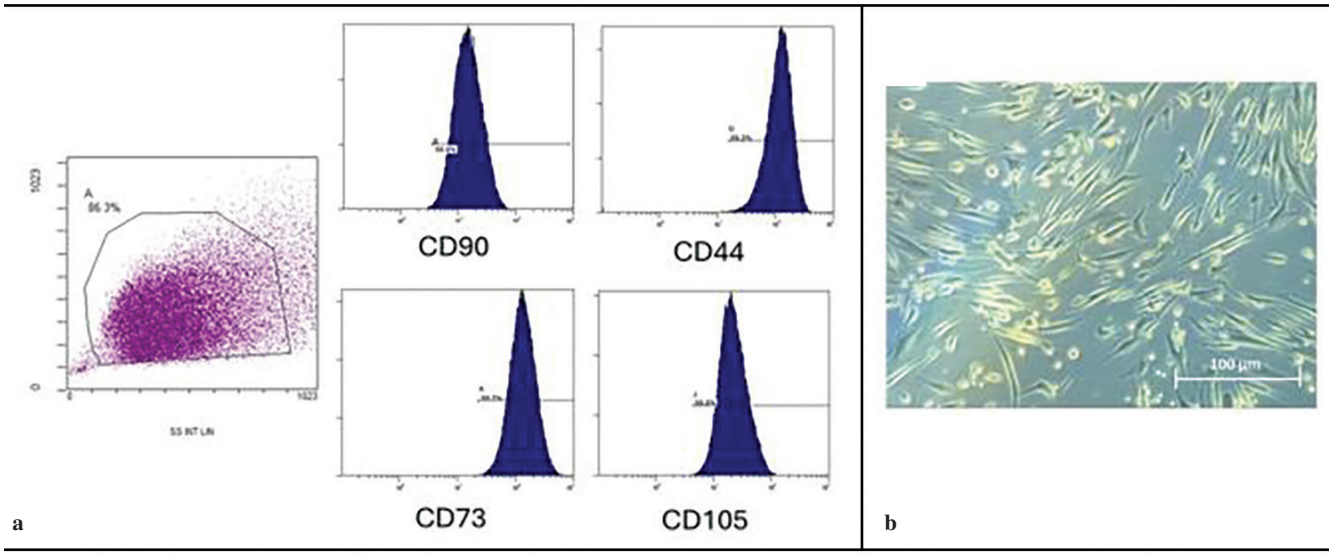

Figure 1. Morphological and immunophenotypic characterization of UCMSCs during culture. (a) Representative gate dot plot and flow cytometry histograms showing the expression levels of MSC surface markers CD90, CD73, CD44, and CD105; (b) fibroblast-like morphology of UCMSCs was observed under light microscopy. MSC = mesenchymal stem cells; UCMSCs = umbilical cord-derived MSCs.

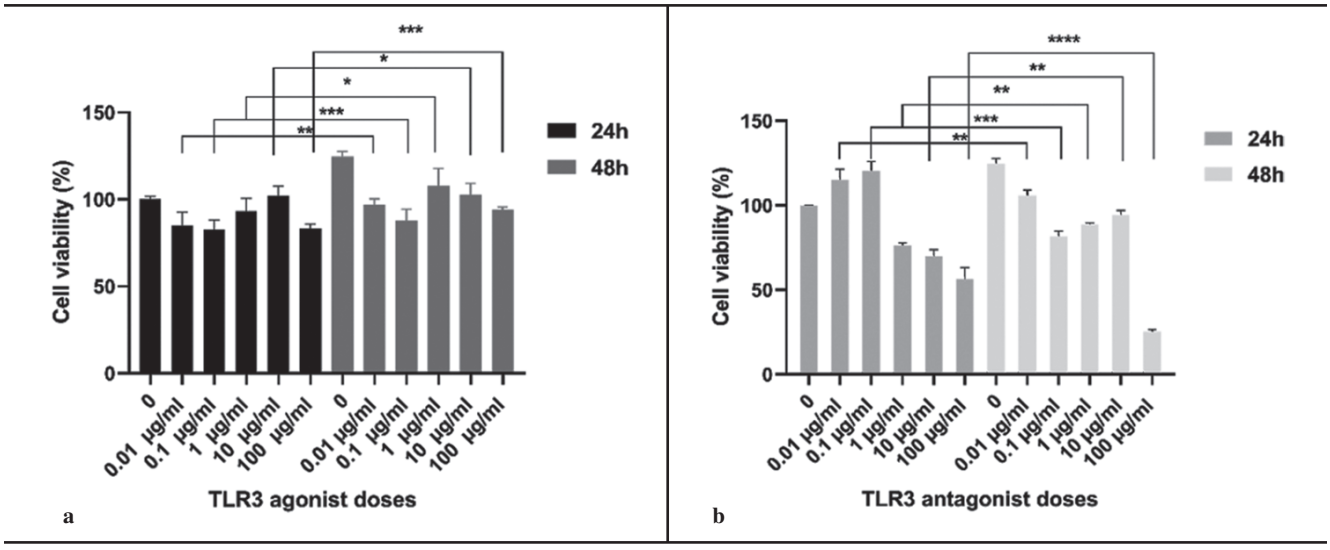

Figure 2. Viability changes in UCMSCs following 24 h and 48 h of treatment with different doses of a TLR3 agonist or antagonist. (a) Graph illustrating the viability changes of TLR3 agonists UCMSCs after 24 h of treatment; (b) graph illustrating the viability changes of TLR3 antagonists UCMSCs after 48 h of treatment. Data are displayed as the mean ± SEM. $*p \leq 0.05$, $**p < 0.01$, $***p < 0.001$, and $****p < 0.0001$ were considered statistically significant. MSC = mesenchymal stem cells; UCMSCs = umbilical cord-derived MSCs; TLR = Toll-like receptors; SEM = standard error of the mean.

the treatment of UCMSCs with the TLR3 agonist or antagonist. In such co-cultures, a significant increase in the expression of *CD44* (RQ: 6.46), *CDH1* (RQ: 2.86), and *ZEB1* (RQ: 0.03) was observed, while *CLDN1* expression (RQ: 4.42) was markedly decreased (Figure 4a–e). In contrast, the expression levels of *CD44* (RQ: 3.62), *VIM* (RQ: 0.004), and *MMP9* (RQ: 0.0001) were elevated, suggesting that activation and inhibition of TLR3 modulate the expression profiles of tumor-associated genes in distinct ways (Figure 4a, d, f). During UCMSCs and *Panc-1* co-culture, TLR3 activation and inhibition affected the expression profiles of UCMSC phenotype- and function-relevant genes, including *CD44, CDH1, CLDN1, VIM, ZEB1, MMP9, MMP2, TIMP1, VEGFR2,* and *PLAU (Figure 4g, h, i, j).* These results underscore the dual regulatory role of TLR3 signaling in shaping pancreatic cancer cells through its impact on UCMSC-mediated gene expression dynamics.

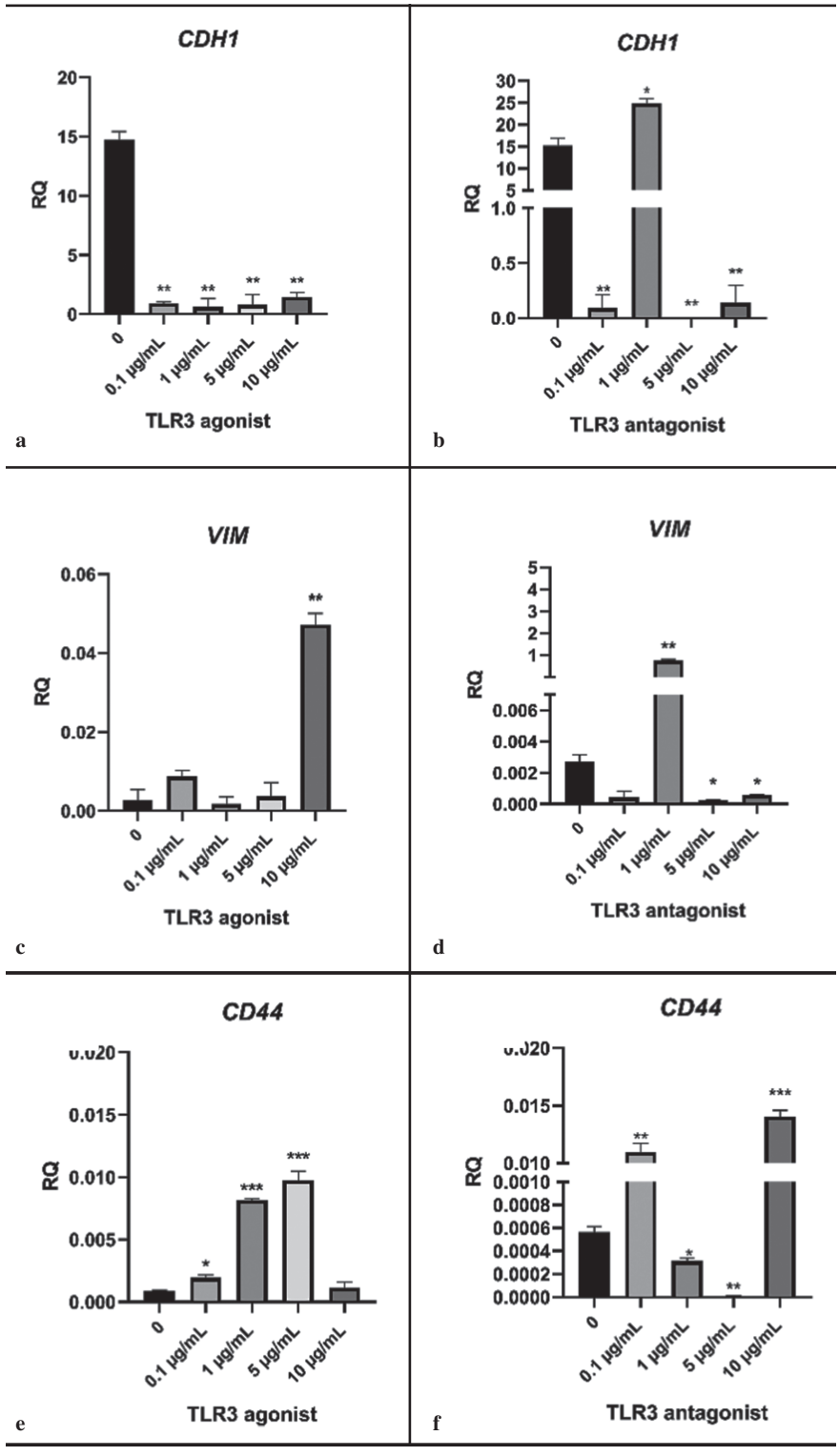

Figure 3. Changes in *CDH1*, *VIM*, and *CD44* expression in UCMSCs following TLR3 agonist and antagonist treatment. Expression changes following TLR3 agonist treatment at doses of 0.1–10 µg/mL (a, c, e); (b) expression changes following TLR3 agonist treatment at doses of 0.1–10 µg/mL (b, d, e). Data are presented as mean ± SEM, and RQ values were normalized using *GAPDH*. In statistical tests, the significance level was accepted as $p \leq 0.05$ and this was represented by an asterisk (*) sign. The significance levels are presented by ranking as follows: *$p \leq 0.05$, **$p < 0.01$, ***$p < 0.001$ and ****$p < 0.0001$. RQ: Represents relative quantification. MSC = mesenchymal stem cells; UCMSCs = umbilical cord-derived MSCs; TLR = Toll-like receptors; SEM = standard error of the mean.

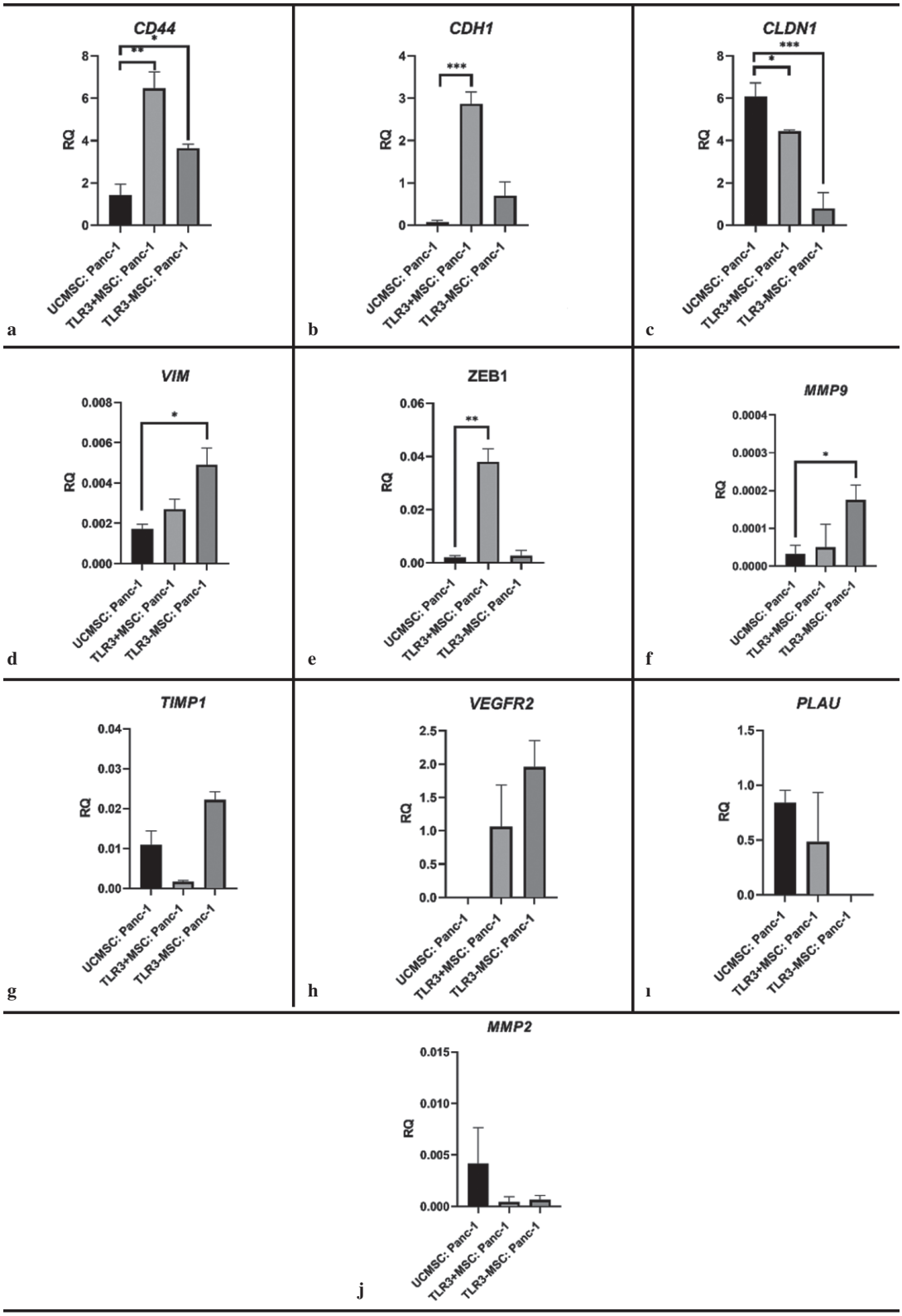

Figure 4. Gene expression changes in UCMSC and *Panc-1* cocultures (1:10 *Panc-1*:UCMSC ratio) after 72 hours. Experimental groups included: *Panc-1* + untreated UCMSC, *Panc-1* + TLR3-activated UCMSC, and *Panc-1* + TLR3-inhibited UCMSC. Genes analyzed: *CD44, CDH1, CLDN1, VIM, ZEB1, MMP9, MMP2, TIMP1, VEGFR2*, and *PLAU* (a–j). Data are presented as mean ± SEM, and RQ values were normalized using *GAPDH*. p-value ≤ 0.05 was considered statistically significant and represented by an asterisk (*). Levels of statistical significance were also described as follows: *$p \leq 0.05$, **$p < 0.01$, ***$p < 0.001$ and ****$p < 0.0001$. MSC = mesenchymal stem cells; UCMSCs = umbilical cord-derived MSCs; TLR = Toll-like receptors; SEM = standard error of the mean.

Discussion

MSCs are essential for regeneration, tissue homeostasis, and anti-tumor responses. This study examined the effects of TLR3 activation/inhibition on the viability and phenotype-associated gene expression in UCMSCs, as well as their impact during coculture with *Panc-1* pancreatic cancer cells. UCMSC viability is modulated by the TLR3 agonist and antagonist in a dose- and time-dependent manner. Both regulated the expression of mesenchymal phenotype-related genes. During co-culture, TLR3 modulation influenced the expression profiles of various UCMSC phenotype- and function-associated genes. These findings suggest that TLR3 signaling not only governs intrinsic UCMSC functions but also dynamically alters their interactions with tumor cells, highlighting a bidirectional crosstalk between the stromal and cancer cell compartments.

Numerous studies have demonstrated that MSCs express various TLRs. Evidence from mesenchymal and hematopoietic stem cell research suggests that TLR activation may play a critical role in modulating stem cell functions, particularly by enhancing their migratory capacity. MSC phenotype is substantially impacted by their diverse functions, such as multilineage differentiation potential, hematopoietic supporting capacity, and immunomodulatory properties. Furthermore, TLR activation plays a vital role in the pathogenesis of various inflammatory diseases such as rheumatoid arthritis and inflammatory bowel disease. The underlying reason is that sustained exposure to TLR ligands can either initiate or sustain chronic inflammation (Huang & Chen, 2016; Ishihara et al., 2006; Yamamoto-Furusho & Podolsky, 2007). Our data are consistent with such a view, as in this study, prolonged TLR3 activation promoted EMT-like changes in the UCMSCs, which may create a pro-inflammatory and pro-tumorigenic niche.

Understanding the impacts of TLR activation on MSC immunobiology is essential for optimizing their therapeutic potential. Among various MSCs, UCMSCs have gained considerable attention in regenerative medicine owing to a non-invasive isolation procedure, robust proliferative capacity, and pronounced immunomodulatory functions (El Omar et al., 2014). In comparison to MSCs obtained from adult tissues, UCMSCs exhibit a more primitive phenotype and enhanced differentiation potential, positioning them as a highly advantageous cell population for clinical applications. This study investigated the dose-dependent effects of a TLR3 agonist and antagonist on UCMSC viability, phenotype-associated gene expression, and tumor-related gene profiles during coculture with *Panc-1* pancreatic cancer cells. Our findings indicate that the modulation of TLR3 signaling not only affects MSC survival but also significantly alters the expression of EMT markers and TME-associated genes. These results align with those of a previous study, demonstrating that TLR3 activates NF-κB in response to dsRNA, supporting its broader role in regulating cell fate and the expression of inflammation-related genes (Alexopoulou et al., 2001).

The results of the viability assays indicated a biphasic response to the TLR3 agonist, where low doses reduced the viability, while intermediate doses had minimal or slightly proliferative effects. However, high concentrations, especially 100 µg, consistently suppressed viability at 24 and 48 h of treatment. This dose-dependent cytotoxicity is in line with prior studies, which reported TLR3-mediated apoptosis in various cell types through the activation of downstream pathways such as TRIF- and caspase-based signaling (Salaun et al., 2006; Eskandari et al., 2023). In contrast, the TLR3 antagonist enhanced viability at lower doses but demonstrated cytotoxicity at higher concentrations, suggesting that delicately balanced TLR3 signaling may regulate stem cell survival (Eskandari et al., 2023).

In terms of gene expression, TLR3 activation markedly downregulated *CDH1* but upregulated *VIM* in UCMSCs. These alterations may reflect changes in cell plasticity or shifts in migratory, adhesive, or differentiation-related properties rather than a phenotypic transition. Additionally, *CD44* expression increased at lower doses of the agonist but declined at elevated concentrations, suggesting a dose-dependent effect on cell-surface-marker encoding genes. These findings imply that TLR3 activation modulates the mesenchymal features of UCMSCs, potentially enhancing their responsiveness to microenvironmental cues (Waterman et al., 2010). Conversely, TLR3 inhibition exhibited a variable effect: while low doses slightly increased *CDH1* and *VIM* expression, higher doses generally suppressed them, indicating an altered regulation of cell characteristics under TLR3-suppressed conditions (Eskandari et al., 2023; Zhao et al., 2015). Overall, TLR3 signaling appears to influence the phenotypic dynamics of UCMSCs in a dose-dependent manner, which could impact their behavior in therapeutic or pathological contexts.

MSCs have been extensively studied as potential vectors for targeted anti-cancer therapy, primarily due to their intrinsic tendency to migrate toward tumors (Fayyad-Kazan et al., 2016; Chulpanova et al., 2018; Hmadcha et al., 2020). The TME, often likened to a "non-healing wound," mimics the inflamed and damaged states of injured tissues, thereby facilitating MSC recruitment and migration. This homing behavior is typically induced in response to stress-induced conditions, including mechanical trauma, inflammation, infection, or neoplastic processes (Huerta et al., 2023; Nwabo Kamdje et al., 2020; Monguió-Tortajada et al., 2021). While the precise molecular mechanisms governing MSC tumor tropism remain to be fully elucidated, it is widely believed that their transendothelial migration resembles that of leukocytes, encompassing steps such as rolling, adhesion, and transvascular migration. Our results build upon this concept by indicating that TLR3 modulation alters the expression of adhesion molecules (e.g., CD44 and CLDN1) and EMT-associated TFs (e.g., ZEB1), thereby potentially redefining MSC migratory behavior in tumor contexts.

This study has several limitations that should be acknowledged. First, the interpretations regarding potential changes in migration or differentiation capacities are based solely on gene expression data, but no functional assays were performed to directly assess and confirm these behaviors. Second, the absence of *in vivo*

validation limits the translational relevance of the findings, as the observed *in vitro* effects may not fully reflect UCMSC behavior within a particular physiological microenvironment. Third, donor-dependent variability in UCMSC populations could influence gene expression responses, potentially affecting the reproducibility and generalizability of the results. Lastly, although levels of key markers such as E-cadherin, vimentin, and CD44 were assessed, the evaluation of a more comprehensive panel of mesenchymal and epithelial markers would be necessary to more robustly characterize the phenotypic changes observed. Future studies incorporating functional, *in vivo*, and broader molecular analyses are needed to more definitively elucidate the impacts of TLR3 modulation on UCMSC biology.

Collectively, our findings highlight the dual and context-dependent roles of TLR3 signaling in MSCs, particularly in shaping their interactions with cancer cells. These results contribute to a growing body of evidence suggesting that TLR3 is not only an immune sensor but also a modulator of stem cell phenotype and TME dynamics. By integrating gene expression profiles and functional outcomes in a co-culture model, our study provides novel insights into the mechanisms by which TLR3 acts as a molecular switch—modulating UCMSC plasticity and tumor-modulatory capacity. Further studies are warranted to elucidate the downstream pathways involved and to determine whether the targeting of TLR3 signaling can offer therapeutic benefits in pancreatic cancer or other malignancies involving the stromal compartment.

Ethics

Ethics Committee Approval: Since the article does not contain any studies with human or animal subject, its approval to the ethics committee was not required.

Data Sharing Statement: Data are available on reasonable request.

Footnotes

Authorship Contributions: Conceptualization: A.Y. and D.K.; Design/methodology: D.K.; Execution/investigation: A.Y.; Resources/materials: D.K.; Data acquisition: A.Y.; Data analysis/interpretation: A.Y. and D.K.; Writing – original draft: A.Y.; Writing – review & editing/critical revision: D.K.

Conflict of Interest: The authors have no conflicts of interest to declare.

Funding: The study was supported by the Scientific and Technological Research Council of Türkiye (TÜBİTAK) with project number 1245740.

References

Alexopoulou, L., Holt, A. C., Medzhitov, R., & Flavell, R. A. (2001). Recognition of double-stranded RNA and activation of NF-κB by toll-like receptor 3. *Nature, 413*(6857), 732–738. https://doi.org/10.1038/35099560

Bhat, A. A., Syed, N., Therachiyil, L., Nisar, S., Hashem, S., Macha, M. A., Yadav, S. K., Krishnankutty, R., Muralitharan, S., Al-Naemi, H., Bagga, P., Reddy, R., Dhawan, P., Akobeng, A., Uddin, S., Frenneaux, M. P., El-Rifai, W., & Haris, M. (2020). Claudin-1, a double-edged sword in cancer. *International Journal of Molecular Sciences, 21*(2), 569. https://doi.org/10.3390/ijms21020569

Bhat, A. A., Uppada, S., Achkar, I. W., Hashem, S., Yadav, S. K., Shanmugakonar, M., Al-Naemi, H. A., Haris, M., & Uddin, S. (2019). Tight junction proteins and signaling pathways in cancer and inflammation: A functional crosstalk. *Frontiers in Physiology, 10,* 1942. https://doi.org/10.3389/fphys.2018.01942

Chandrasekar, S. A., Palaniyandi, T., Parthasarathy, U., Surendran, H., Viswanathan, S., Wahab, M. R. A., Baskar, G., Natarajan, S., & Ranjan, K. (2023). Implications of toll-like receptors (TLRs) and their signaling mechanisms in human cancers. *Pathology, Research and Practice, 248,* 154673. https://doi.org/10.1016/j.prp.2023.154673

Chen, X., Zhang, Z. Y., Zhou, H., & Zhou, G. W. (2014). Characterization of mesenchymal stem cells under the stimulation of toll-like receptor agonists. *Development, Growth & Differentiation, 56*(3), 233–244. https://doi.org/10.1111/dgd.12124

Chulpanova, D. S., Kitaeva, K. V., Tazetdinova, L. G., James, V., Rizvanov, A. A., & Solovyeva, V. V. (2018). Application of mesenchymal stem cells for therapeutic agent delivery in anti-tumor treatment. *Frontiers in Pharmacology, 9,* 259. https://doi.org/10.3389/fphar.2018.00259

El Omar, R., Beroud, J., Stoltz, J. F., Menu, P., Velot, E., & Decot, V. (2014). Umbilical cord mesenchymal stem cells: The new gold standard for mesenchymal stem cell-based therapies? *Tissue Engineering Part B: Reviews, 20*(6), 523–544. https://doi.org/10.1089/ten.TEB.2013.0664

Eskandari, F., Zolfaghari, S., Yazdanpanah, A., Shabestari, R. M., Fomeshi, M. R., Milan, P. B., Kiani, J., Zomorrod, M. S., & Safa, M. (2023). TLR3 stimulation improves the migratory potency of adipose-derived mesenchymal stem cells through the stress response pathway in the melanoma mouse model. *Molecular Biology Reports, 50*(3), 2293–2304. https://doi.org/10.1007/s11033-022-08111-8

Fayyad-Kazan, M., Fayyad-Kazan, H., Lagneaux, L., & Najar, M. (2016). The potential of mesenchymal stromal cells in immunotherapy. *Immunotherapy, 8*(7), 839–842. https://doi.org/10.2217/imt-2016-0037

Gholizadeh-Ghaleh Aziz, S., Alipour, S., Ranjbarvan, P., Azari, A., Babaei, G., & Golchin, A. (2021). Critical roles of TLRs on the polarization of mesenchymal stem cells for cell therapy of viral infections: A notice for COVID-19 treatment. *Comparative Clinical Pathology, 30*(1), 119–128. https://doi.org/10.1007/s00580-021-03209-0

Golchin, A., Seyedjafari, E., & Ardeshirylajimi, A. (2020). Mesenchymal stem cell therapy for COVID-19: Present or future. *Stem Cell Reviews and Reports, 16*(3), 427–433. https://doi.org/10.1007/s12015-020-09973-w

Hmadcha, A., Martin-Montalvo, A., Gauthier, B. R., Soria, B., & Capilla-Gonzalez, V. (2020). Therapeutic potential of mesenchymal stem cells for cancer therapy. *Frontiers in Bioengineering and Biotechnology, 8,* 43. https://doi.org/10.3389/fbioe.2020.00043

Huang, Y., & Chen, Z. (2016). Inflammatory bowel disease related innate immunity and adaptive immunity. *American Journal of Translational Research, 8*(6), 2490–2497.

Hwang, S., Sung, D. K., Kim, Y. E., Yang, M., Ahn, S. Y., Sung, S. I., & Chang, Y. S. (2023). Mesenchymal stromal cells primed by toll-like receptors 3 and 4 enhanced anti-inflammatory effects against LPS-induced macrophages via extracellular vesicles. *International Journal of Molecular Sciences, 24*(22), 16264. https://doi.org/10.3390/ijms242216264

Huerta, C. T., Voza, F. A., Ortiz, Y. Y., Liu, Z. J., & Velazquez, O. C. (2023). Mesenchymal stem cell-based therapy for non-healing wounds due to chronic limb-threatening ischemia: A review of preclinical and clinical studies. *Frontiers in Cardiovascular Medicine, 10,* 1113982. https://doi.org/10.3389/fcvm.2023.1113982

Ishihara, S., Rumi, M. A., Ortega-Cava, C. F., Kazumori, H., Kadowaki, Y., Ishimura, N., & Kinoshita, Y. (2006). Therapeutic targeting of toll-like receptors in gastrointestinal inflammation. *Current Pharmaceutical Design, 12*(33), 4215–4228. https://doi.org/10.2174/138161206778743448

Liu, X., Zhou, Z., Zeng, W. N., Zeng, Q., & Zhang, X. (2023). The role of toll-like receptors in orchestrating osteogenic differentiation of mesenchymal stromal cells and osteoimmunology. *Frontiers in Cell and Developmental Biology, 11,* 1277686. https://doi.org/10.3389/fcell.2023.1277686

Monguió-Tortajada, M., Bayes-Genis, A., Rosell, A., & Roura, S. (2021). Are mesenchymal stem cells and derived extracellular vesicles valuable to halt the COVID-19 inflammatory cascade? Current evidence and future perspectives. *Thorax, 76*(2), 196–200. https://doi.org/10.1136/thoraxjnl-2020-215717

Najar, M., Fayyad-Kazan, M., Merimi, M., Burny, A., Bron, D., Fayyad-Kazan, H., Meuleman, N., & Lagneaux, L. (2019). Mesenchymal stromal cells and natural killer cells: A complex story of love and hate. *Current Stem Cell Research & Therapy, 14*(1), 14–21. https://doi.org/10.2174/1574888X13666180912125736

Najar, M., Krayem, M., Meuleman, N., Bron, D., & Lagneaux, L. (2017). Mesenchymal stromal cells and toll-like receptor priming: A critical review. *Immune Network, 17*(2), 89–102. https://doi.org/10.4110/in.2017.17.2.89

Nwabo Kamdje, A. H., Seke Etet, P. F., Simo Tagne, R., Vecchio, L., Lukong, K. E., & Krampera, M. (2020). Tumor microenvironment uses a reversible reprogramming of mesenchymal stromal cells to mediate pro-tumorigenic effects. *Frontiers in Cell and Developmental Biology, 8,* 545126. https://doi.org/10.3389/fcell.2020.545126

Raicevic, G., Najar, M., Stamatopoulos, B., De Bruyn, C., Meuleman, N., Bron, D., Toungouz, M., & Lagneaux, L. (2011). The source of human mesenchymal stromal cells influences their TLR profile as well as their functional properties. *Cellular Immunology, 270*(2), 207–216. https://doi.org/10.1016/j.cellimm.2011.05.010

Salaun, B., Coste, I., Rissoan, M.-C., Lebecque, S. J., & Renno, T. (2006). TLR3 can directly trigger apoptosis in human cancer cells. *Journal of Immunology, 176*(8), 4894–4901. https://doi.org/10.4049/jimmunol.176.8.4894

Tolstova, T., Dotsenko, E., Kozhin, P., Novikova, S., Zgoda, V., Rusanov, A., & Luzgina, N. (2023). The effect of TLR3 priming conditions on MSC immunosuppressive properties. *Stem Cell Research & Therapy, 14,* 344. https://doi.org/10.1186/s13287-023-03579-y

Tomchuck, S. L., Zwezdaryk, K. J., Coffelt, S. B., Waterman, R. S., Danka, E. S., & Scandurro, A. B. (2008). Toll-like receptors on human mesenchymal stem cells drive their migration and immunomodulating responses. *Stem Cells, 26*(1), 99–107. https://doi.org/10.1634/stemcells.2007-0563

Waterman, R. S., Tomchuck, S. L., Henkle, S. L., & Betancourt, A. M. (2010). A new mesenchymal stem cell (MSC) paradigm: Polarization into a pro-inflammatory MSC1 or an immunosuppressive MSC2 phenotype. *PLoS One, 5*(4), e10088. https://doi.org/10.1371/journal.pone.0010088

Yamamoto-Furusho, J. K., & Podolsky, D. K. (2007). Innate immunity in inflammatory bowel disease. *World Journal of Gastroenterology, 13*(42), 5577–5580. https://doi.org/10.3748/wjg.v13.i42.5577

Zhang, H., Jin, C., Hua, J., Chen, Z., Gao, W., Xu, W., Zhou, L., & Shan, L. (2024). Roles of microenvironment on mesenchymal stem cells therapy for osteoarthritis. *Journal of Inflammation Research, 17,* 7069–7079. https://doi.org/10.2147/JIR.S475617

Zhao, C., Zhang, L., Kong, W., Liang, J., Xu, X., Wu, H., Feng, X., Hua, B., Wang, H., & Sun, L. (2015). Umbilical cord-derived mesenchymal stem cells inhibit cadherin-11 expression by fibroblast-like synoviocytes in rheumatoid arthritis. *Journal of Immunology Research, 2015,* 137695. https://doi.org/10.1155/2015/137695

Zheng, R., & Ma, J. (2022). Immunotherapeutic implications of toll-like receptors activation in tumor microenvironment. *Pharmaceutics, 14*(11), 2285. https://doi.org/10.3390/pharmaceutics14112285